

# **STUDY OF DOPING IN ZINC OXIDE THIN FILMS GROWN BY SPRAY PYROLYSIS TECHNIQUE**

Thesis

Submitted in partial fulfillment of the requirements for the degree of

**DOCTOR OF PHILOSOPHY**

by

**SADANANDA KUMAR N.**



**DEPARTMENT OF PHYSICS**

**NATIONAL INSTITUTE OF TECHNOLOGY KARNATAKA,**

**SURATHKAL, MANGALORE – 575025.**

**SEPTEMBER, 2014**

## **DECLARATION**

*by the Ph.D. Research Scholar*

I hereby *declare* that the Research Thesis entitled  
**“STUDY OF DOPING IN ZINC OXIDE IN THIN FILMS GROWN BY SPRAY  
PYROLYSIS TECHNIQUE”** Which is being submitted to the **National Institute of  
Technology Karnataka, Surathkal** in partial fulfillment of the requirements for the  
award of the Degree of **Doctor of Philosophy** in **PHYSICS** is a *bonafide report of the  
research work carried out by me*. The material contained in this Research Thesis has  
not been submitted to any University or Institution for the award of any degree.

**PH09F04,      Sadananda Kumar N.**

(Register Number, Name & Signature of the Research Scholar)

**Department of Physics**

Place: NITK-Surathkal

Date:

## CERTIFICATE

This is to *certify* that the Research Thesis entitled “**STUDY OF DOPING IN ZINC OXIDE IN THIN FILMS GROWN BY SPRAY PYROLYSIS TECHNIQUE**”

Submitted by **Mr. Sadananda Kumar N. (Register Number: PH09F04)** as the record of the research work carried out by him, is *accepted as the Research Thesis submission* in partial fulfillment of the requirements for the award of degree of **Doctor of Philosophy**.

Prof. (Mrs.) Kasturi V. Bangera  
Research Guide

Prof. G.K. Shivakumar  
Additional Research Guide

Prof. N.K.Udayashankar  
Chairman - DRPC

*Dedicated to*

*Parents & Family*



## **Acknowledgement**

I would like to express my sincere gratitude to my esteemed guides Prof. Kasturi V. Bangera and Prof. G. K. Shivakumar for considering me as their research student. The research work presented here would have been impossible without the able guidance of my research guides. I heartily acknowledge their kindness, generous help and valuable suggestions I received from them during the course of my research work.

I sincerely thank the members of RPAC: Prof. A. Nithyananda Shetty and Prof. Jagannath Nayak for their valuable suggestions and excellent advice in accomplishing this work.

I heartily thank my research colleagues; Dr. Prakash Shenoy, Dr. Gowrish Rao and Dr. Sowmya Palimar, Mr. Shashidar, Mr. Santhosh T.C.M. and Ms. Veena E. for their help, encouragement and best wishes. It was great pleasure to work with them.

The help received by Dr. Anandan C., Scientist-F, National Aerospace Laboratories (CSIR), Bangalore in my research work is greatly acknowledged.

I am thankful to Dr. Vikas Shelar and Mr. Hidayath Ulla, Department of Physics, for their help and encouragement during the course of work.

I thank all faculty members, staff and research students of the Department of Physics, for their kind and sincere support throughout my work.

I am grateful to The Head, Department of Physics for supporting me to attend various conferences and workshops, which in turn helped me to understand the current research trends.

I also express my sincere thanks to Mr. Chandrayya achar and Mr. Jagadish, skilled mechanic, Department of mechanical engineering, for helping me in fabricating the unit.

I offer my heartfelt gratitude to institute, the National Institute of Technology Karnataka, for providing financial assistance and wonderful work environment.

Last but most important are my parents and family. I wish to express special thanks and appreciation to my parents Janardhana Bangera and Umavathi, Brothers Mr. Harish and Mr. Ravi, Sisters Mrs. Savitha and Mrs. Latha for their unflinching support, encouragement and patience. I also thank my wife Mrs. Sukhalatha for her support and wish to complete this doctoral thesis.

There are many more whom I must remember with gratitude. Their names, though I might have failed to mention here, shall never be forgotten.

## ABSTRACT

The main objective of present work is to study the effect of doping on the optical and electrical properties of spray deposited zinc oxide (ZnO) thin films. The optimum conditions required to obtain quality of ZnO thin films is determined initially by varying the deposition parameters such as substrate temperature, spray rate and precursor molarity. Later film thickness and annealing temperature is fixed by considering the transmittance and conductivity of the films. ZnO thin films obtained under optimum conditions were found to be crystalline in nature with the combination of visible region transmittance of 78 % and room temperature conductivity of 0.156 S/cm. XPS analysis has been shown that the *as-deposited* film is oxygen deficient and annealed films are oxygen rich. Further, ZnO films were doped with group V and group III dopants to improve their conductivity. Investigation has been carried out to know the optimum percentage of dopant to be added to retain the transmittance of the films by varying dopant concentration from 0 to 5%. The effect of group V elements as dopants in the form of pure metals has been studied by doping the film with antimony and bismuth separately. A slight improvement in the conductivity of the films was observed with antimony and bismuth doping without changing optical transmittance in the visible region. ZnO film doped with Sb (3% and above) shows p-type conductivity. Role of group III elements as n-type dopants in the form of pure metals is studied by doping the film with aluminium, indium and gallium separately. It has been observed that all the doped films possess transparent and highly conducting properties. The 3% doping concentration and annealing at 450°C for 4hr is the optimum condition to achieve transparent and high conductive ZnO films doped with Al, In and Ga. From the structural, optical and electrical properties of these doped ZnO films it is found that all films have smooth surface with visible region transparency of 80% and significantly high electrical conductivity of the order of  $10^2$  S/cm at room temperatures, which are well suited for the transparent electrodes application.

Keywords: Zinc Oxide, Thin Film, Spray Pyrolysis, Doping, Conductivity,

Transmittance

# Contents

<b>1 Introduction</b>	<b>1</b>
1.1 Thin film preparation	1
1.1.1 Physical methods	4
1.1.2 Chemical methods	6
1.2 Properties and preparation of zinc oxide	8
1.2.1 Importance of zinc oxide	8
1.2.2 Deposition techniques for ZnO films	12
1.3 Literature survey	14
1.4 Scope and objectives of the present work	21
<b>Chapter 2 Experimental techniques</b>	<b>23</b>
2.1 Growth technique	23
2.1.1 Spray pyrolysis	24
2.1.2 Principle of spray pyrolysis	25
2.1.3 Importance of process parameter on the formation of thin films	26
2.1.4 Description of spray set up	28
2.2 Thickness measurement	31
2.2.1 Stylus method	31
2.2.2 Multiple beam Fizeau fringes method	31
2.2.3 Gravimetric method	32
2.3 Characterization techniques	33
2.3.1 Structural characterization	33
a. X-ray diffraction technique	34
b. Scanning electron microscopy (SEM)	38
2.3.2 Compositional analysis	39
a. Energy dispersive X-ray analysis (EDS/EDAX)	39
b. X-ray photoelectron spectroscopy (XPS)	43
2.3.3 Optical characterization	46

2.3.4	Electrical characterization	52
<b>Chapter 3 Undoped ZnO thin films</b>		<b>61</b>
3.1	Preparation of ZnO thin films using zinc acetate precursor	61
3.1.1	Experimental details	62
3.2	Effect of deposition parameters	63
3.2.1	Substrate temperature	63
3.2.2	Spray rate	66
3.2.3	Precursor molarity	68
3.3	Effect of film thickness	70
3.4	Effect of annealing temperature	75
3.5	ZnO films prepared using zinc nitrate precursor	83
3.5.1	Experimental details	83
3.5.2	Results & Discussions	84
<b>Chapter 4 ZnO thin films doped with group V elements</b>		<b>89</b>
4.1	Introduction	89
4.2	Antimony doped ZnO thin films	94
4.2.1	Effect of doping concentration	94
4.2.2	Effect of annealing temperature	101
4.3	Bismuth doped ZnO films	106
4.3.1	Effect of doping concentration	106
4.3.2	Effect of annealing temperature	113
<b>Chapter 5 ZnO thin films doped with group III elements</b>		<b>118</b>
5.1	Introduction	118
5.2	Aluminium doped ZnO thin films	119
5.2.1	Effect of doping concentration	120
5.2.2	Effect of annealing temperature	125
5.3	Indium doped ZnO thin films	130

5.3.1	Effect of doping concentration	130
5.3.2	Effect of annealing temperature	136
5.4	Gallium doped ZnO thin films	140
5.4.1	Effect of doping concentration	140
5.4.2	Effect of annealing temperature	146
<b>Chapter 6 Summary and conclusions</b>		<b>150</b>
6.1	Summary of the present work	150
6.2	Conclusions of the present work	154
6.3	Scope for the future work	155

## List of Tables

Table 3.1: XRD data of ZnO films deposited with different substrate temperature.	67
Table 3.2: XRD data of ZnO thin films deposited at different spray rate.	70
Table 3.3: XRD data of ZnO films deposited with different precursor molarity.	72
Table 3.4: The optimum deposition parameters to prepare ZnO thin films.	73
Table 3.5: XRD data of ZnO films with different thickness.	75
Table 3.6: Optical and electrical data of ZnO films with different thickness.	77
Table 3.7: XRD data of ZnO films annealed at different temperatures for 4 hr.	79
Table 3.8 : Composition analysis of ZnO films using EDAX technique.	81
Table 3.9: Optical and electrical data of ZnO films annealed at different temperatures.	86
Table 3.10: Optical and electrical data of ZnO films annealed at different temperatures.	91
Table 4.1: XRD data of Sb doped ZnO thin films.	100
Table 4.2: Optical and electrical data of Sb doped ZnO thin films.	105
Table 4.3: XRD data of ZnO: 3% Sb films annealed at different temperatures for 4hr.	107
Table 4.4: Optical and electrical data of ZnO: 3% Sb films annealed at different temperatures for 4 hr.	108
Table 4.5: XRD data of Bi doped ZnO thin films.	112
Table 4.6: Optical and electrical data of Bi doped ZnO thin films.	117
Table 4.7: XRD data of annealed 3% Bi doped ZnO films.	118
Table 4.8: Optical and electrical data of ZnO: 3% Bi films annealed at different temperatures for 4 hr.	121

Table 5.1: XRD data Al doped ZnO thin films.	125
Table 5.2: Optical and electrical data of Al doped ZnO thin films.	128
Table 5.3: XRD data of ZnO: 3% Al film annealed at different temperatures for 4 hr.	130
Table 5.4: Optical and electrical data of ZnO: 3% Al films annealed at different temperatures for 4hr.	133
Table 5.5: XRD data of indium doped ZnO thin films.	135
Table 5.6: Optical and electrical data of In doped ZnO thin films.	139
Table 5.7: XRD data of ZnO: 3%In thin films annealed at different temperatures for 4 hr.	141
Table 5.8: Optical and electrical data of ZnO: 3% In films annealed at different temperatures for 4 hr.	143
Table 5.9: XRD data of Ga doped ZnO thin films.	145
Table 5.10: Optical and electrical data Ga doped ZnO thin films.	148
Table 5.11: XRD data of ZnO: 3% Ga films annealed at different temperature for 4hr.	150
Table 5.12: Optical and electrical data of ZnO: 3% Ga films annealed at different temperatures for 4 hr.	153



## List of Figures

Figure 1.1: Crystal structure of ZnO	22
Figure 2.1: Spray pyrolysis unit used to deposit the ZnO thin films.	30
Figure 2.2: Schematic representation of X-Ray diffractometers: a) $\theta$ - $\theta$ type (b) $\theta$ - $2\theta$ type	37
Figure 2.3: Schematic diagram of scanning electron microscope.	41
Figure 2.4: Scanning Electron Microscope (Model: JEOL JSM-6380LA)	42
Figure 2.5 Schematic representation of X-ray photoelectron spectroscope.	45
Figure 2.6: The optical absorption phenomenon: (a) Conservation of Energy and Momentum, and Transition in (b) Direct bandgap material (c) indirect bandgap material.	50
Figure 2.7: The schematic diagram of a typical spectrophotometer.	51
Figure 2.8: Three different structures used for making contacts to thin films. (a) Bridge structure, (b) Planar structure and (c) sandwich Structure.	58
Figure 2.9: The schematic diagram of the experimental setup for hot probe technique.	59
Figure 2.10: The contacts in Van der Paw setup for (a) a sample of arbitrary shape and (b) for a sample with a line of symmetry (MO). (c) The experimental setup for Hall effect analysis of a sample by der Paw method.	60
Figure 2.11: Vacuum coating unit (Hind High Vacuum Ltd, Model 12A4D).	61
Figure 2.12: Keithley 2400 source meter and multimeter 2002.	62
Figure 3.13: XRD pattern of ZnO films deposited at different	

substrate temperature.	66
Figure 3.2: (a) Transmittance spectra and (b) Tauc's plot for ZnO thin films deposited at different substrate temperature.	67
Figure 3.3: I-V characteristics of ZnO films deposited at different substrate temperature.	68
Figure 3.4: XRD pattern of ZnO thin films deposited at different spray rate.	69
Figure 3.5: (a) Transmittance spectra and (b) Tauc's plot for ZnO thin films deposited at different spray rate.	70
Figure 3.6: I-V characteristics of ZnO thin films deposited at different spray rate.	71
Figure 3.7: XRD pattern of ZnO thin films deposited at different precursor molarity.	72
Figure 3.8: (a) Transmittance spectra and (b) Tauc's plot for ZnO thin films deposited at different precursor molarity.	73
Figure 3.9: XRD pattern of ZnO films of different thickness.	74
Figure 3.10: SEM image of ZnO films with thickness (a) 600 nm and (b) 1.2 $\mu\text{m}$ .	75
Figure 3.11: (a) Transmittance spectra and (b) Tauc's plot for ZnO films with different thickness.	76
Figure 3.12 : I-V characteristics of ZnO films of different thickness.	77
Figure 3.13: Plot of $\log R$ vs. $1/T$ of undoped ZnO thin film.	78
Figure 3.14: XRD pattern of ZnO thin films annealed at different temperatures.	79
Figure 3.15: Strain and grain size evaluation of as deposited and annealed ZnO films.	80
Figure 3.16: SEM image of ZnO thin films (a) as deposited and (b) annealed at 450°C.	80
Figure 3.17: EDAX analysis of (a) as deposited and (b) annealed ZnO thin films	81

Figure 3.18: Survey scan of ZnO films (a) as deposited and (b) annealed at 450° C for 4hr.	82
Figure 3.19: XPS spectra of as deposited ZnO thin films (a) Zn2p and (b) O1s spectrum.	82
Figure 3.20: XPS spectra of annealed ZnO thin films (a) Zn2p and (b) O1s spectrum.	83
Figure 3.21: (a) Transmittance spectra and (b) Tauc's plot for ZnO thin films annealed at different temperatures for 4 hr	84
Figure 3.22: I-V characteristics of ZnO films annealed at different temperatures.	85
Figure 3.23: XRD pattern of ZnO film annealed at 450°C for 4hr.	88
Figure 3.24: SEM image of ZnO films annealed at 450°C for 4 hr.	89
Figure 3.25: Zn2p and O1s spectra of annealed ZnO films.	90
Figure 3.26: (a) Optical transmittance spectra and (b) Tauc's plot for ZnO films annealed at different temperatures.	91
Figure 3.27: I-V characterization of ZnO films annealed at different temperatures	92
Figure 3.28: Variation of logR with 1/T of ZnO films annealed at 450°C.	92
Figure 4.1: XRD pattern of Sb doped ZnO thin films.	100
Figure 4.2: SEM image of (a) undoped film and (b) 1% Sb, (b) 3% Sb, (c) 5% Sb doped ZnO films.	101
Figure 4.3: EDAX spectrum of Sb doped ZnO thin films.	101
Figure 4.4: XPS spectra of ZnO: 3% Sb thin films annealed at 450°C (a) Survey scan,(b) Zn2p spectrum and (c) Sb3d, O1s spectrum.	102
Figure 4.5: (a) Transmittance spectra and (b) Tauc's plot for Sb doped	

ZnO thin films	103
Figure 4.6: I-V characteristics of Sb doped ZnO thin films.	104
Figure 4.7: Variation of logR as a function of 1/T of 3% Sb doped films.	105
Figure 4.8: XRD pattern of as deposited and annealed ZnO: 3% Sb films.	106
Figure 4.9: SEM image of ZnO: 3% Sb films (a) as deposited and annealed at (b) 450°C, (c) 500°C, (d) 550°C.	107
Figure 4.10: (a) Transmittance spectra and (b) Tauc's plot for ZnO: 3% Sb films annealed at different temperatures.	108
Figure 4.11: I-V characteristics of annealed ZnO: 3% Sb thin films.	109
Figure 4.12: XRD pattern of Bi doped ZnO thin films.	111
Figure 4.13: SEM image of (a) undoped, (b) 1%, (c) 3% and (d) 5% Bi doped ZnO films.	113
Figure 4.14: EDAX spectrum of Bi doped ZnO thin film.	113
Figure 4.15: XPS spectra of annealed ZnO: 3% Bi films; (a) Zn2p, (b) O1s, and (c) Bi4f spectra.	114
Figure 4.16: (a) Transmittance spectra and (b) Tauc's plot for Bi doped ZnO thin films	115
Figure 4.17 : I-V characteristics of Bi doped ZnO thin films.	116
Figure 4.18: Variation of logR vs. reciprocal temperature of 3% Bi doped thin films.	117
Figure 4.19 : XRD spectra of ZnO:3% Bi films annealed at different temperatures for 4hr.	118
Figure 4.20: SEM image of ZnO: 3%Bi films (a) as deposited and annealed at (b) 450°C, (c) 500°C, (d) 550°C.	119
Figure 4.21: (a) Transmittance spectra and (b) Tauc's plot for ZnO: 3% Bi	

films annealed at different temperatures.	120
Figure 4.22: I-V characteristics of annealed ZnO: 3% Bi thin films.	121
Figure 5.1: XRD spectra of undoped and Al doped ZnO films.	124
Figure 5.2: SEM image of (a) undoped, (b) 1% ,(c) 3% & (d) 5% Al doped ZnO films.	125
Figure 5.3: EDAX spectrum of 3% Al doped ZnO films.	126
Figure 5.4: (a) Transmittance spectra and (b) Tauc's plot for Al doped ZnO thin films.	127
Figure 5.5: I-V characteristics of Al doped ZnO films.	128
Figure 5.6: Variation of logR vs. 1/T for 3% Al doped ZnO thin films.	129
Figure 5.7: XRD pattern of ZnO: 3% Al thin films.	130
Figure 5.8: SEM image of ZnO: 3% Al thin films (a) as deposited, (b) annealed at 450°C, (c) annealed at 500°C and (d) at 550°C.	131
Figure 5.9: (a) Transmittance spectra and (b) Tauc's plot for as deposited and annealed ZnO: 3% Al thin films.	132
Figure 5.10: I-V characteristics of ZnO: 3% Al thin films.	132
Figure 5.11: XRD pattern of In doped ZnO films.	134
Figure 5.12: SEM image of (a) undoped (b) 1% (c) 3% and (d) 5% In doped ZnO films.	135
Figure 5.13: EDAX spectrum of 3% In doped ZnO thin films.	136
Figure 5.14: XPS spectra of ZnO: 3% In films annealed at 450°C (a) Survey scan, (b) Zn2p spectra, (c) O1s spectra and (d) In3d spectra	136
Figure 5.15: (a) Transmittance spectra and (b) Tauc's plot for In doped ZnO thin films.	137
Figure 5.16: I-V characteristics of In doped ZnO thin films.	138

Figure 5.17: Variation of logR vs. 1/T of 3% In doped ZnO thin film.	139
Figure 5.18: XRD pattern of ZnO: 3% In thin films.	140
Figure 5.19: SEM image of ZnO: 3% In films (a) as deposited, (b) annealed at 450°C, (c) annealed at 500°C, (d) annealed at 550°C.	141
Figure 5.20: (a) Transmittance spectra and (b) Tauc's plot for as deposited and annealed ZnO: 3% In thin films.	142
Figure 5.21: I-V characteristics of ZnO: 3% In thin films.	143
Figure 5.22: XRD pattern of Ga doped ZnO thin films.	144
Figure 5.23: SEM image of (a) undoped, (b) 1% (c) 3% and (d) 5% Ga doped ZnO films	145
Figure 5.24: EDAX spectrum of 3% Ga doped ZnO thin films.	146
Figure 5.25: XPS spectra of ZnO: 3%Ga thin films annealed at 450°C (a) Survey scan, (b) Zn2p spectra, (c) O1s spectra and (d) Ga2p spectra	147
Figure 5.26: (a) Transmittance spectra and (b) Tauc's plot for Ga doped ZnO thin films.	148
Figure 5.27: I-V characteristics of Ga doped ZnO thin films.	149
Figure 5.28: Variation of logR vs. reciprocal temperature of ZnO: 3% Ga thin film.	149
Figure 5.29 :XRD pattern of ZnO: 3% Ga thin films.	150
Figure 5.30: SEM image of ZnO: 3% Ga films (a) as deposited, (b) annealed at 450°C, (c) annealed at 500°C and (d) annealed at 550°C.	151
Figure 5.31: (a) Transmittance spectra and (b) Tauc's plot for ZnO: 3% Ga thin films	152
Figure 5.32: I-V characteristics of ZnO: 3% Ga thin films.	152

## NOMENCLATURE

### ABBREVIATIONS

ZnO	Zinc oxide
RF	Radio frequency
D C	Direct current
SP	Spray pyrolysis
VPE	Vapour phase epitaxy
MBE	Molecular beam epitaxy
PLD	Pulsed laser deposition
Si	Silicon
C.C.	Carrier concentration
GZO	Gallium doped zinc oxide
AZO	Aluminium doped zinc oxide
IZO	Indium doped zinc oxide
AGZO	Aluminium gallium co doped zinc oxide
DFT	Density functional theory
TFT	Thin film transistor
XRD	X-ray diffractometer
SEM	Scanning electron microscope
EDAX	Energy dispersive analysis of X-rays
PID	Proportional-integral-derivative controller

### SYMBOLS & UNITS

eV	electron volt
meV	milli-electron volt

$\mu\text{m}$	micrometer
nm	nanometer
ml/min	millilitre/ minute
M	molarity
h	hour
D	crystallite size
$\sigma$	conductivity
n	carrier concentration /cm <sup>3</sup>
R	resistance
T (K)	temperature (Kelvin)
$E_g$	energy band gap
$E_a$	activation energy
at. %	atomic percent
I-V	Current – Voltage
h $\nu$	photon energy
$\mu$	mobility
Å	angstrom
°C	degree Celsius
$\alpha$	Alpha
A	ampere
min	minute
$\lambda$	lamda
$\Omega$	Ohm
S/cm	Seimen/centimeter
T	Tesla
$\theta$	theta



# CHAPTER 1

## INTRODUCTION

### 1.1 THIN FILM PREPARATION

The physical properties of solid bulk materials are almost independent of their thickness. However drastic reduction in the thickness may change the properties of the solid materials. When the thickness is much less than a micrometer, or so, the properties of the material may become dependent on its thickness. Such materials whose properties change as a function of their thickness are called thin films. Thin films are thin material layers ranging from fractions of a nanometer to several micrometers in thickness. Because of the highly reduced thickness, materials in thin film form have very large surface to volume ratio. Most of the mechanical properties of thin films can be attributed to this large surface to volume ratio.

The physical properties of solid bulk materials because of its potential technical value and scientific curiosity in the properties of a two dimensional solid, thin films have been extensively studied. Physical phenomena peculiar to thin films and basis for their study are generally the consequence of their planar geometry, size and unique structure. Epitaxial growth, occurrence of metastable structures, size-limited electron and phonon transport process's in metals, insulators and semiconductors, quantum mechanical tunnelling through normal and superconducting metal-insulator junctions, micromagnetics and plasma resonance absorption are some of the noteworthy contributions of thin film phenomenon to solid state physics. The technical interests which stimulated these studies have also rewarded in the form of useful inventions such as a variety of active and passive microminiaturized components and devices, solar cells, radiation sources and detectors, magnetic memory devices, bolometer and anti reflection coatings.

In thin films, deviation from the properties of the corresponding bulk materials arise because of their small thickness, large surface to volume ratio, and unique physical structure, which is the direct consequence of growth process. The mechanical

properties of thin films are quite different from those of the bulk material. For example, the strengths exhibited by some films appear to be as much as 200 times as great as for well annealed bulk samples, and are usually several times as great as the strengths of severely cold worked bulk material. This behavior has been explained in two ways ; first, the polycrystalline film structure is more disordered (smaller crystallites or grains) than can be achieved by cold working, and second, if the films are sufficiently thin , the dislocations could extend throughout the entire thickness of the film and thus locked in place, giving no mechanism for yielding.

An electronic effect of thinness is observed in very thin dielectric films as an abrupt change in the conductance at constant field as the thickness is reduced below some finite dimension. With dielectric films thicker than about  $100\text{\AA}$ , the field required to cause a given current to flow is generally independent of film thickness. Thinner films, however, exhibit a large increase in current density due to “tunnelling”. This is because the probability of an electron with a given energy penetrating the potential barrier presented the dielectric increases exponentially with decreasing thickness. Thinness also results in a marked change in the conductivity of metallic films as film thickness of the same order as, or smaller than the electron mean free path. When this occurs, scattering of the electrons at the film surface becomes a significant factor, and the effective conductivity is reduced.

Observations of film resistivity as a function of thickness thus provide one means of estimating the mean free path. This method has been found difficult in practice, since films of a high degree of perfection are required. The resistivity of metal films may be separated into two portions, one caused by electrons being scattered by atoms in thermal motion, and another caused by scattering at lattice imperfections. The imperfections in deposited metal films results in resistivities higher than those observed for bulk metals. The effect of temperature on two modes of scattering is not the same, and these results in differences between the temperature coefficients of resistance of bulk metals and those of polycrystalline metallic films. The magnitude of this difference may be used to infer the degree of imperfection in films.

Ceramic thin films are widely used for different applications. The relatively high hardness and inertness of ceramic materials make this type of thin coating of interest for protection of substrate materials against corrosion, oxidation and wear. In particular, the use of such coatings on cutting tools can extend the life of these items by several orders of magnitude.

The emerging technology requires different types of thin films for variety of applications. Because of the potential technical value and scientific curiosity of thin film properties different materials have been prepared in the form of thin films. Properties of thin film differ significantly from those of bulk which is due to surface and interface effects; this strongly influences overall behavior of the thin films. Thin films have very wide range of applications and extend from the micrometer dots in microelectronic, photo electronic, thermo electronic, superconductivity, information storage media, fuel cells, and bio-compatible coatings. Thin film semiconductor science is the expanding field and studies on thin film semiconductor are becoming interesting.

The various methods have been employed to deposit the thin films. The required properties and versatility can be obtained by choosing proper method of thin films deposition. Thin film preparation techniques can be broadly classified as either physical or chemical. Under physical methods, sputtering, vacuum evaporation, pulsed laser evaporation and molecular beam epitaxy, where the deposition takes place after the material to be deposited has been transferred to a gaseous state either by evaporation or an impact process. Under chemical methods, Liquid phase chemical methods include spray pyrolysis technique, electrodeposition, chemical bath deposition (CBD), modified chemical bath deposition (M-CBD), electroless deposition, and anodization. The gas phase chemical method includes chemical vapor deposition (CVD), metal organo-chemical vapor deposition (MOCVD), Plasma enhanced chemical vapour deposition (PECVD).

### 1.1.1 Physical methods

Physical deposition uses thermal or mechanical means to form a thin film. The material to be deposited is placed in a vacuum and energetic environment so that the particle of the material escapes from its surface. The substrate draws energy from these particles to travel as freely as possible. Since particles tend to follow a straight path in the vacuum, films deposited by physical means are usually directional rather than conformal. Some of the widely used physical deposition techniques are as follows.

#### i. Sputtering

Sputtering is one of the versatile techniques used for the deposition ZnO thin films. Compared to the chemical methods, samples will have better-controlled composition and homogeneity; also this permits to have better control of film thickness. Sputtering is a momentum transfer process. In sputtering, the incident particles (ions) are accelerated by an applied electrical potential. If the kinetic energy with which they strike the surface is less than about 5 eV, they can be reflected or absorbed on the surface. When the kinetic energy crosses the surface atom binding energy, surface damage will occur as atoms are forced into new lattice positions. At incident ion kinetic energies above a threshold, typically 10 to 30 eV, atoms may be dislodged or sputtered from the surface. These sputtered atoms and ions can be condensed on a substrate to form a thin film coating.

Sputtering is normally performed at a pressure of  $10^{-2}$  to  $10^{-3}$  Torr. For conducting targets, DC voltage is applied between cathode and anode (DC Sputtering) and for non-conducting samples (insulators) a high frequency generator is connected between the electrodes (RF Sputtering). Magnetron sputtering is useful for high deposition rates and low substrate temperatures are required. In magnetron sputtering, a magnetic field is applied to enhance the sputtering rate, which in turns, enhances the deposition rate also.

## ii. Thermal evaporation technique

The vacuum evaporation method basically involves evaporation of the material in vacuum environment. The two main variations are possible depending upon the technique used to evaporate the material, namely thermal evaporation and electron-beam evaporation. In thermal evaporation technique the material to be evaporated is heated resistively in a vacuum enclosure to such a temperature that large numbers of atoms or molecules escape the surface of the material and deposit on the substrate to form a thin film. Most of the evaporated molecules suffer no collisions with residual gas molecules due to the low pressure in the vacuum system; hence follow the straight path to reach the substrate. Only the materials with a much higher vapor pressure than the heating element can be deposited without contamination of the film.

## iii. Pulsed laser deposition

Pulsed laser deposition (PLD) is one of the sophisticated techniques for depositing transparent semiconducting oxides. In PLD technique high-energy laser pulses are used to vaporise target material in a high vacuum/ultra high vacuum chamber. Cylindrical tablets made from pressed powder material are usually used as targets. A pulsed laser beam vaporizes the surface of the target, and the vapour condenses on the substrate, producing a film with the same composition as the target. This is the result of the extremely high heating rate of the target surface ( $10^8$  K/s) due to pulsed laser irradiation.

Because of high heating rate of the ablated materials, laser deposition of crystalline film demands a much lower substrate temperature than other film growth techniques. For this reason, the semiconductor and the underlying integrated circuit are not damaged from thermal degradation. It is quite easy to produce multi-layered films of different materials by sequential ablation of assorted targets. Besides, by controlling the number of pulses, a fine control of film thickness down to even atomic monolayer can be achieved.

#### iv. Molecular beam epitaxy (MBE)

Molecular beam epitaxy is a modified and sophisticated form of thermal evaporation technique. In MBE, slow streams of an element can be directed at the substrate, so that material deposits one atomic layer at a time. The beam of material can be generated by either physical means or by a chemical reaction (chemical beam epitaxy). Molecular beam epitaxy takes place in high or ultra high vacuum. The most important aspect of MBE is the slow deposition rate which allows the films to grow epitaxially.

In solid-source MBE, ultra-pure elements are heated in separate effusion cells until they begin to slowly sublimate. The gaseous elements then condense on the wafer, where they may react with each other. The deposited films are usually highly crystalline. The term "beam" means that evaporated atoms do not interact with each other or with the residual gases in the vacuum chamber until they reach the wafer, due to the long mean free paths of the atoms.

Molecular beam epitaxy is also used for the deposition of some types of organic semiconductors. In this case, molecules, rather than atoms, are evaporated and deposited onto the wafer. Other variations include gas-source MBE, which resembles chemical vapor deposition. The main advantage of molecular beam epitaxy is its precise control over the deposition parameter and insitu diagnostic capabilities.

#### **1.1.1 Chemical methods**

In chemical deposition a fluid precursor undergoes chemical change on the solid surface, leaving a solid layer. Since the fluid surrounds the solid object, deposition happens on every surface, with little regard to direction. Hence the films prepared by chemical deposition techniques tend to be conformal, rather than directional. Chemical deposition is further categorized as follows.

i. Chemical vapor deposition (CVD)

Chemical vapor deposition technique is particularly interesting, because it gives rise to high quality films and it is applicable to large scale production. This method involves reaction of one or more gaseous species reacting on a solid surface (substrate). The metallic oxides are generally grown through the vaporisation of the organo-metallic compounds by this process. The vapours of condensate material are transported to a substrate surface where it is decomposed by the heterogeneous process. The decomposition process varies according to the composition of the volatile transporting species. The decomposition condition should be such that the reaction occurs only at or near the substrate surface and not in the gaseous state to avoid formation of the powdery deposits which may result in haziness in the films. Depending on precursors used the several modifications in the methods were made. When the metal-organic precursors are used the technique is called MOCVD. The plasma enhanced CVD (PECVD) uses an ionized vapor, or plasma, as a precursor. Commercial PECVD relies on electromagnetic means (electric current, microwave excitation), rather than a chemical reaction, to produce a plasma.

ii. Chemical solution deposition (CSD)

This technique uses a liquid precursor, usually a solution of organometallic powders dissolved in an organic solvent. This is a relatively inexpensive, simple thin film process that is able to produce stoichiometrically accurate crystalline phases.

iii. Plating

Plating relies on liquid precursors, often a solution of water with a salt of the metal to be deposited. Some plating processes are driven entirely by reagents in the solution (usually for noble metals), but by far the most commercially important process is electroplating. It was not commonly used in semiconductor processing for many years, but has seen resurgence with more widespread use of chemical-mechanical polishing techniques.

#### iv. Spray pyrolysis

Spray pyrolysis (SP) technique was used as early as 1910 to obtain transparent oxide films. It is one of the chemical methods widely used for the preparation of variety thin films. In case of spray deposition of ZnO thin films, the aqueous or alcoholic solution of zinc nitrate, zinc chloride or zinc acetate is used to spray on the hotter substrate using air as the carrier gas. The sprayed aerosols reaching the hot substrate undergo pyrolytic reaction and form a single crystalline or cluster of crystallites of ZnO thin films. The substrate provides thermal energy for decomposition reaction and subsequent recombination of the consequent species followed by sintering and recrystallization of clusters of crystallites giving rise to coherent films. The other volatile by-product escapes in the vapor phase through exhaust. In SP, doping process is relatively easy; just by varying the dopant concentration in the solution; one can vary the dopant percentage in the sample. A major drawback of this technique is that it cannot be used for the deposition of very thin films. Further since it is a high temperature process selection of substrate is restricted.

The higher-end techniques like molecular beam epitaxy produce high quality films but at the same time they prove to be very expensive. The methods such as spray pyrolysis, on the other hand, are simple, inexpensive and versatile technique to deposit the oxide material hence they are preferred for mass production in the industries.

## **1.2 PROPERTIES AND PREPARATION OF ZINC OXIDE**

### **1.2.1 Importance of zinc oxide**

Zinc oxide (ZnO) is an II - VI compound semiconductor. Most of the group II–VI binary compound semiconductors crystallize in either cubic zinc blende or hexagonal wurtzite structure where each anion is surrounded by four cations at the corners of a tetrahedron, and vice versa. This tetrahedral coordination is typical of  $sp^3$  covalent bonding nature; but these materials also have substantial ionic character that tends to increase the band gap beyond the one expected from the covalent bonding. ZnO is a



compound semiconductor whose ‘ionicity’ resides at the borderline between the covalent and ionic semiconductors. The crystal structures shared by ZnO are hexagonal wurtzite, zinc blende, and rock salt (or Rochelle salt). The crystal structure of hexagonal wurtzite ZnO is schematically shown in figure 1.1. At room temperature, thermodynamically stable phase is hexagonal wurtzite. The zinc-blende structure can be stabilized only by the growth on cubic structure while rock salt (NaCl) structure may be obtained at relatively high pressure.

Zinc oxide is a very promising material for semiconductor device applications. Over the past three decades we have witnessed a significant improvement in the ZnO single crystal and epitaxial films. The prospects of ZnO as a complement in optoelectronics have driven many research groups worldwide to focus on its semiconductor properties. This in turn has led to the revival of the idea of using ZnO as optoelectronic or dielectric applications in its own right. The wide range of useful properties displayed by ZnO has been recognized for a long time. What has captured most of the attention in recent years is that ZnO is a semiconductor of band gap 3.37 eV which in principle enables the optoelectronic applications in blue and UV region of the spectrum. The prospectus of such application is fueled by impressive progress in bulk crystals as well as in thin films over past few years. A partial list of the properties of ZnO that distinguish it from other semiconductors or oxides or render it useful for applications is given below.

i. Direct and wide band gap

The band gap of ZnO is 3.44 eV at low temperatures and 3.37 eV at room temperature (Janotti, 2009). For comparison, the respective values for wurtzite GaN are 3.50 eV and 3.44 eV (Ozgur et al. 2005). As mentioned above, this enables applications in optoelectronics in the blue/UV region, including light-emitting diodes, laser diodes and photo detectors (Look et al. 2001). Optically pumped lasing has been reported in ZnO platelets (Reynolds et al. 1996), thin films (Bagnall et al. 1997), clusters consisting of ZnO nanocrystals (Cao et al. 1999) and ZnO nanowires (Haung et al. 2001).

ii. Large exciton binding energy

The free-exciton binding energy in ZnO is 60 meV, which could lead to lasing action based on exciton recombination even above room temperature. Since the oscillator strength of excitons is typically much larger than that of direct electron hole transition in direct band gap semiconductors (Ozgur et al. 2005), the large exciton binding energy makes ZnO a promising material for optical devices that are based on excitonic effects.

iii. Large piezoelectric constants

In piezoelectric materials, deformation in the crystal caused by an applied voltage and vice versa. The low symmetry of the wurtzite crystal structure combined with a large electromechanical coupling in ZnO gives rise to strong piezoelectric and pyroelectric properties. Piezoelectric ZnO film with uniform thickness and orientation have been grown on a variety of substrates using different deposition techniques including sol-gel process, chemical vapor deposition, spray pyrolysis and sputtering (Janotti et al. 2009).

iv. Radiation hardness

Radiation hardness is important for applications at high altitude or in space. It has been observed that ZnO is very resistive to high energy radiation, making it a very suitable candidate for space applications (Ozgur et al. 2005; Janotti et al. 2009).

v. High thermal conductivity

This property makes ZnO useful as an additive. It also increases the appeal of ZnO as a substrate for homo-epitaxy and hetero-epitaxy. High thermal conductivity translates into high efficiency of heat removal during device operation (Florescu et al. 2002).

vi. Strong luminescence

ZnO is also a suitable material for phosphor applications due to its strong luminescence in the green-white region of the spectrum. The emission spectrum has a peak at 495 nm which is broad [half-width of 0.4 eV] (Vossen 1977). The n-type

conductivity of ZnO makes it appropriate for applications in vacuum fluorescent displays and field emission displays. Origin of the luminescence center and luminescence mechanism is not really understood, being frequently attributed to oxygen vacancies or zinc interstitials, without any clear evidence (Vossen 1977). It has been suggested that zinc vacancies are more likely the cause of green luminescence.

vii. Amenability to wet chemical etching

Semiconductor device fabrication process generally benefit from the amenability to low temperature chemical etching. It has been reported that ZnO thin films can be etched with acidic, alkaline, as well as mixture of solutions (Ozgur et al. 2005; Janotti et al. 2009). This possibility of low temperature chemical etching adds great exibility in the processing, designing and integration of electronic and optoelectronic devices.

viii. Strong sensitivity of surface conductivity to the presence of adsorbed species

The conductivity of ZnO thin films is very sensitive to the exposure of the surface to various gases. It can be used as a ‘cheap smell sensor’ capable of detecting the freshness of foods and drinks, due to the high sensitivity to trimethylamine present in the odour. Mechanisms of the sensor action are poorly understood. Recent experiments reveal the existence of a surface electron accumulation layer in vacuum-annealed single crystals, which disappears upon exposure to ambient air (Exarhos and Zhou 2007; Calnan and Tiwari 2010). This layer may play a role in sensor action, as well. Presence of this conducting surface channel has been suggested to be related to some puzzling type-conversion effects observed when attempting to obtain p-type ZnO.

In addition to the above mentioned properties and applications ZnO has recently found other niche applications as well, such as, since ZnO based transistors are insensitive to visible light, hence used as protective layer preventing light exposure in the fabrication of transparent thin film transistors . Also up to  $2 \times 10^{21} \text{ cm}^{-3}$  charge carriers can be introduced by heavy substitutional doping into ZnO. By controlling the doping level in ZnO its electrical properties can be changed from insulator through n-

type semiconductor to metal while maintaining optical transparency that makes it useful for transparent electrodes in at panel displays and solar cells. ZnO is also a promising candidate for spintronics applications.

### **1.2.2 Deposition techniques for ZnO films**

Most of the current technological applications of ZnO, such as varistors, transparent conductive electrodes for solar cells, piezoelectric devices and gas sensors, have made use of thin films that are grown by a variety of deposition techniques, mostly on glass substrates. Some of the commonly used deposition techniques of ZnO thin films include,

#### **i. Sputtering**

One of the most popular growth techniques for early ZnO investigations was sputtering (DC sputtering, RF magnetron sputtering and reactive sputtering). The magnetron sputtering was a preferred method because of its low cost, simplicity, and low operating temperature. In this method ZnO films can be grown at a certain substrate temperature by sputtering from a high-purity ZnO target using a RF magnetron sputter system. The growth is usually carried out in the growth ambient with O<sub>2</sub> / Ar+ O<sub>2</sub> ratios ranging from 0 to 1 at a pressure of 10<sup>3</sup>-10<sup>2</sup> torr. O<sub>2</sub> serves as the reactive gas and Ar acts as the sputtering enhancing gas. ZnO can also be grown by DC sputtering from a Zn target in an Ar + O<sub>2</sub> gas mixture. The RF power applied to the plasma is tuned to regulate the sputtering yield rate from the ZnO target (Bachari et al. 1999; Ozgur et al. 2005; Gong et al. 2002).

#### **ii. Thermal evaporation**

It is a one of the physics methods used to deposit the zinc oxide thin films. Evaporation can be done by fixing a definite source to substrate distance in chamber. The high purity zinc oxide powder can be evaporated by resistive heating using tungsten boats. Usually the deposition is carried out under the residual pressure less than 10<sup>-5</sup> torr. In this system substrates can be maintained at room temperature or particular substrate temperature during the process of deposition (Park et al. 2008).

iii. Pulsed laser deposition (PLD)

For the growth of ZnO by PLD technique, usually UV excimer lasers KrF:  $\lambda = 248$  nm and ArF:  $\lambda = 193$  nm and Nd: yttrium aluminum garnet YAG pulsed lasers  $\lambda = 355$  nm are used for ablation of the ZnO target in an oxygen environment. In some cases, Cu-vapor laser emitting at  $\lambda = 510 - 578$  nm was also used for the same purpose. Cylindrical ZnO tablets made from pressed ZnO powder are usually used as targets. Single-crystal ZnO has been used to grow high-quality ZnO thin films very recently. A pure Zn metal is used only in rare cases. The properties of the grown ZnO films depend mainly on the substrate temperature, ambient oxygen pressure, and laser intensity (Ozgun et al. 2005; Craciun et al. 1994).

iv. Molecular beam epitaxy (MBE)

For ZnO thin film deposition by MBE, Zn metal and O<sub>2</sub> are usually used as the source materials. High-purity Zn metal is evaporated from an effusion cell, where the cell temperature can be varied to examine the effect of the Zn flux on the growth rate and material properties. The oxygen radical beam, which can be generated by an ECR or a RF plasma source, is directed on the film surface to obtain high-oxidation efficiency. When the O plasma is used, the chamber pressure during growth is in the 10<sup>-5</sup> torr range (Ozgun et al. 2005).

v. Chemical vapor deposition (CVD)

In the CVD method, ZnO deposition occurs as a result of chemical reactions of vapor-phase precursors on the substrate, which are delivered into the growth zone by the carrier gas. The reactions take place in a reactor where a necessary temperature profile is created in the gas flow direction. For hydride vapor phase epitaxy (VPE) growth of ZnO, hydrogen will be employed as a carrier gas and targets made using pure ZnO powder will be placed in the evaporation zone maintained at high temperature (Funakubo et al. 1999; Ozgun et al. 2005).

The growth techniques mentioned here to produce ZnO thin film that is highly n-type. This high level n-type conductivity is very useful for some applications, such as

transparent conductors and gas sensors but in general it would be desirable to have a better control over the conductivity. In particular, the ability to reduce the n-type background and to achieve p-type doping would open up tremendous possibilities for semiconductor device applications in general and for light emitting diodes and laser diodes.

### **1.3 LITERATURE SURVEY**

The ZnO thin films have coexisting properties like high transparency and conductivity due to this it has gained substantial interest in the research community. There has been a great deal of interest in zinc oxide thin films as seen from the surge of a relevant number of publications in the past two decades. The various research groups have been used different physical and chemical method to deposit the good quality of ZnO thin films. During the period of present research work the research papers referred and briefly explained as follows.

Heerden and Swanepoel (1997) were prepared the ZnO thin films by spray pyrolysis technique. The study was mainly focused on the changes in structural properties with varying molarity and substrate temperature. Reported that films deposited below the temperature of 420°C are crystalline with (002) growth orientation, increase in molarity increases the peak intensity.

Kang and Joung (2004) prepared ZnO thin films on quartz substrate by using RF magnetron sputtering. In this study the influence of substrate temperature on the structural, optical and piezoelectric properties of grown ZnO thin films were studied. The high quality of ZnO thin films with good crystallinity and smooth surface was obtained at the deposition temperature 200°C and also reported that these films were highly transparent in the visible region and have better piezoelectric properties.

Liu et al. (2007) prepared the ZnO thin films deposited on Si (100) substrate at room temperature and 750°C using RF magnetron sputtering. The study was mainly focused on the morphological and interface characteristics. The structural and

morphological studies show that the ZnO film has crystallographic orientation relationship with Si.

Structural, optical and electrical properties of sputtered ZnO films are studied by Bachari et al. (1999). In this study ZnO thin films were deposited by RF magnetron sputtering. In the reported results of this study it has been shown that the crystallinity of the films is found to increase with kinetic energy of sputtered particles. Infrared investigations have shown that zinc atoms stay tetrahedrally co-ordinated even though oxygen zinc atomic ratio changes from 0.95- 1.06.

Lokhande et al. (2003) studied the structural, optical and electrical properties of ZnO thin films deposited on glass substrate by spray pyrolysis technique. In the reported results of this study it has been shown that all films exhibit polycrystalline hexagonal structure. Optically transparent on the visible region and electrical conductivity was found to vary from  $10^2$  to  $10^{-3}$  S/cm.

The influence of thickness on the structural, optical and electrical properties of nanostructured ZnO thin films have been studied by Prasada and Santhosh (2009). In the reported results it has been shown that with increasing film thickness crystal quality of the films gets better, tensile strain decreases and electrical conductivity increases and also reported the improvement in the electrical conductivity with heat treatment.

Varnamkhasti et al. (2011) studied the influence of annealing treatment on the structural, morphological, optical and electrical properties of nanocrystalline zinc oxide films grown on glass substrate by electron beam evaporation method. In this study it was shown that annealing temperature increases the crystallinity and optical transmittance, whereas annealing temperature decreases the optical band gap and electrical conductivity.

Venkatachalam and Kanno (2009) reported the preparation and characterization of micro and nano crystalline ZnO thin films grown by PLD technique. In this case films were deposited on glass substrate. It was shown that the incorporation of Zn

with oxygen is greatly increased; optical band gap decreased and hydrated oxide content reduced with increasing laser power density.

Alver et al. (2007) prepared the micro sized zinc oxide on glass substrate using ultrasonic spray pyrolysis technique. It has been reported that the ZnO rods exhibit excellent crystalline structure with (002) growth orientation, hexagonal rods are uniformly aligned and shows 80% optical transparency.

Tsay et al. (2010) deposited the ZnO thin films on alkali free glass substrates by sol-gel method and spin-coating technique. This study showed that the obtained ZnO thin films were conducting and highly transparent in the visible region. The films annealed at 500°C for 1 h showed an improvement in the transparency, reduction the surface roughness and reduced the strain.

Ratheesh et al. (2007) studied the origin of blue green luminescence in spray deposited ZnO thin films by irradiating ion fluences of 120meV Au and 80 MeV Ni. In this paper reported that the mechanism of blue green emission was strongly associated with the antisite oxygen and the emission resulted from the transition from conduction band to the acceptor level corresponding to antisite oxygen.

Characterization of sputtered ZnO thin film as sensor and actuator for diamond AFM probe is studied by Shibata et al. (2002). In order to develop a diamond atomic force microscopy (AFM) probes with a piezoelectric sensor and actuator. The research group fabricated piezoelectric ZnO thin film and measured its piezoelectric constant. Finally in this study they achieved ZnO thin film with high piezoelectric constant of -3.5 pC/N, using this value, properties of the diamond cantilever AFM probes of various dimensions and of 5 mm in thickness with a ZnO sensor and actuator of 1 mm in thickness is calculated.

Tellier et al. (2010) obtained transparent, amorphous and organics free ZnO thin film by chemical solution deposition method. In this case the films were deposited on soda-lime glass and polymer substrates. It was shown that the films coated on glass and polymer substrates were amorphous in nature, but films coated on glass substrates



which were then additionally heated at 450°C found to be crystalline consisting of randomly oriented grains.

In recent years researchers are very much interested in doping of ZnO thin films to improve its electrical conductivity without changing its transparency in the visible region. ZnO thin film can be doped by using different techniques either as p-type or n-type. Obtaining n-type conductivity in ZnO thin films with stable and reproducible properties relatively easier since ZnO is basically an n-type conductivity. Various research groups have been succeeded in doping ZnO thin films with n-type donors using different deposition techniques.

Venkatachalam et al. (2011) prepared the Al doped ZnO thin films on silicon (100) substrate using pulsed laser deposition and studied the structural, Optical and electrical properties by varying the Al percentage from 1 to 6. In this paper it was reported that all the films were crystalline in nature with decreasing particle size with increasing dopant concentration. The incorporation of Al in the ZnO film was confirmed by XPS analysis. The films doped with 1% Al showed high optical transparency and electrical properties.

Zhang et al. (2011) studied the influence of deposition temperature on the crystallinity of Al-doped ZnO thin films deposited on glass substrates prepared by RF magnetron sputtering method. In this study the ZnO films were deposited from 50°C to 350°C. It was reported that the films deposited at 100°C showed better crystallinity. All the films showed high transparency in the visible region. The lowest resistivity of  $3.6 \times 10^{-4} \Omega\text{-cm}$  was obtained for films prepared at the substrate temperature of 100°C.

Rozati and Akesteh (2007) prepared the Al doped ZnO thin films on soda lime glass substrates by spray pyrolysis technique. The doping concentration is varied from 0 to 0.6%. It was reported that all the films showed polycrystalline structure with (002) orientation. All the films were transparent and lowest sheet resistance obtained for 0.125% Al doped films. Films annealed at 400°C showed a decrease in the sheet resistance.

Ma et al. (2007) deposited the transparent and conducting Ga doped ZnO thin films on glass substrate by DC reactive magnetron sputtering. The effect of deposition pressure on the structural and optical properties of Ga: ZnO films were reported. It has been shown that Ga doped ZnO thin films are polycrystalline with (001) growth orientation. The deposition pressure has a great influence on the film surface structure. All the films are optically transparent.

Nam et al. (2010) studied the anode material properties of Ga-doped ZnO thin films by pulsed DC magnetron sputtering method for organic light emitting diodes. In this study electrical and structural property of GZO films as a function of substrate temperature from room temperature to 400°C was examined. The GZO films deposited at 200 °C showed excellent electrical properties, such as a low resistivity, high mobility and high work function of  $5.3 \times 10^{-4} \Omega\text{-cm}$ ,  $9.9 \text{ cm}^2/\text{Vs}$  and 4.37 eV, respectively.

Shin et al. (2011) studied the properties of multilayer gallium and aluminum doped ZnO transparent thin films deposited on glass substrate by pulsed laser deposition process. The 2 % GZO and 2% AZO thin films were deposited using GZO and AZO targets. In this study properties of multilayer's were studied by varying the substrate temperature and it has been shown that GZO/AZO thin films begin to crystallize at 100 °C and crystallized phase was obtained at 300 °C. The GZO/AZO thin films show 85% optical transmittance and thin films prepared at 400 °C show minimum electrical resistivity of  $4.18 \times 10^{-4} \Omega\text{-cm}$  with electron concentration of  $7.5 \times 10^{20} \text{ cm}^{-3}$ , and carrier mobility  $25.4 \text{ cm}^2/(\text{V}\cdot\text{s})$ .

Tiburcio et al. (1998) studied the properties of gallium doped ZnO thin films on glass substrate by spray pyrolysis technique. The properties of the Ga doped ZnO thin films were studied by varying substrate temperature from 350°C to 500°C and doping concentration from 2% to 6%. It was reported that all the films were transparent in the visible region. It was concluded that 6% Ga doped ZnO deposited at 500°C had high electrical conductivity with carrier concentration of  $1.14 \times 10^{20} \text{ m}^{-3}$  among the other combination. Hence this transparent and conducting Ga doped ZnO films are suitable for photovoltaic applications.

Tsay et al. (2012) deposited the gallium-doped ZnO (GZO) thin films on glass substrate by sol-gel spin coating technique. The microstructure, optical, electrical and photoluminescence properties of ZnO films were studied by varying gallium concentration from 0 to 5%. It has been reported that the optimum microstructure characteristics, transparency, and resistivity of ZnO films obtained with 2% Ga dopant concentration.

Indium doped ZnO thin films were obtained by Joseph et al. (2005) using spray pyrolysis technique. In this study indium chloride is used as source of dopant. The study was carried out by varying the dopant concentration from 0 to 1.6%. It was reported that all the films are polycrystalline hexagonal wurzite structure and the optical band gap increases with indium doping. The highly transparent and conducting ZnO thin films obtained with the 0.8% In.

Fang and Kang (2010) deposited the indium doped ZnO nano rods on SiO<sub>2</sub> substrate by using RF magnetron sputtering. The structural, optical, electrical and mechanical properties of IZO films were studied. It was reported that the IZO films crystalline in nature with (002) growth orientation, highly transparent and conducting.

Kim et al. (2012) studied the structural and optical properties of sol-gel derived indium doped ZnO (IZO) thin films by varying indium concentration from 0 to 5%. This study reports that crystal quality of ZnO films improved with indium concentration, especially up to 3% In but the surface morphology is affected by the In incorporation. The IZO films are transparent in the visible region.

You (2013) reported that effects of indium doping concentration on the fabrication of zinc-oxide thin-film transistors (TFT). The semiconducting layer of IZO was spin coated onto the p-type Si wafer. The study was mainly focused on characteristics of ZnO TFT. The ZnO TFT achieved a  $10^5$  on/off current ratio and had a large threshold voltage of 15.6 V. The doping concentration of indium was found to influence the electrical characteristics of the IZO transistor.

The difficulties in obtaining p-type ZnO films may arise from variety of causes like compensation by native point defects or dopant atoms that locate on interstitial

sites. The defect compensates for the substitutional impurity level through the formation of a deep level trap. The low solubility of the dopant limits the accessible extrinsic carrier density. In spite of these problems number of research groups have been reported the p-type conductivity in ZnO thin films.

Kim et al. (2003) obtained p-type ZnO thin films by phosphorus doping. In this method ZnO films were prepared on a sapphire substrate using P<sub>2</sub>O<sub>5</sub> as a phosphorus dopant. Phosphorus was doped in ZnO thin films using the ZnO target mixed with 1 wt% P<sub>2</sub>O<sub>5</sub>.

Kumar et al. (2010) reported the p-type ZnO: As thin films were grown on sapphire substrate by R. F. magnetron sputtering. In this method the p-type doping was done using ZnO: Zn<sub>3</sub>As<sub>2</sub> target as source material. The structural, optical and electrical properties of p-type ZnO films were studied. The XPS analysis suggested as an As<sub>Zn</sub>-2V<sub>Zn</sub> complex doping mechanism and Hall measurement showed the good p-type conductivity in the ZnO: As films.

Pan et al. (2012) obtained the p-type ZnO thin films by pulsed laser deposition. In this method p-type ZnO thin films were deposited on a quartz substrate high-purity ZnO–Sb<sub>2</sub>O<sub>3</sub> ceramic disk with 2% Sb. In this paper reported that XPS confirmed the incorporation of Sb in the film as Sb<sub>Zn</sub>. The p-type conduction is achieved at the growth temperature of 550 °C with a resistivity of 3 Ω cm, a carrier concentration of  $2.3 \times 10^{18} \text{ cm}^{-3}$  and a Hall mobility of  $1.23 \text{ cm}^2\text{V}^{-1}\text{s}^{-1}$ .

Dhara and Giri (2012) reported the stable p-type conductivity in nitrogen doped ZnO thin films grown by RF magnetron sputtering method. In this work very low resistivity and a moderately high mobility p-type conduction ZnO:N films grown on Si substrate and it was shown that annealed p-type ZnO films were more stable, this stability was discussed on the basis of morphology and structural improvement which prevents the diffusion of impurities. The suitability in the application of p-type film was checked and suitable for photodetection applications.

Liu et al. (2012) prepared ZnO thin films on the sapphire substrate using plasma enhanced molecular beam epitaxy and on the surface of ZnO films Na layer was

deposited by pulsed laser deposition technique using NaF as target. The ZnO: Na film was annealed at 850°C for 2 minutes in nitrogen atmosphere showed p-type conductivity. Hence diffusion temperature and time are important parameters in determining the conduction type in Na-diffused ZnO thin films. XPS confirmed incorporation of Na in ZnO films by diffusion. Hall measurement demonstrated the firm p-type conductivity in Na-diffused ZnO films.

#### **1.4 SCOPE AND OBJECTIVES OF THE PRESENT WORK**

From the literature survey it is observed that the ZnO thin films have been deposited by using different physical and chemical methods. It is possible to tailor the properties of ZnO thin films by controlling the deposition parameters, which in turn make these films suitable for particular applications. Therefore the deposition techniques play a vital role. It is possible to employ an appropriate deposition technique depending on the type of devices, geometry and expected performance.

Spray pyrolysis is one of versatile technique used to deposit the thin films of oxide materials. The research work presented in this thesis aims at optimizing the deposition conditions for obtaining good quality ZnO films by spray pyrolysis technique. Most of the previous studies on ZnO thin films deposited by spray pyrolysis technique concentrated on doping of fourth and third group elements. More over not many reports have been observed on the study of electrical, optical and structural properties of Sb, Bi doped spray deposited ZnO thin films. Also not much study has been reported the effect of annealing of Al, Ga, In doped ZnO films on its properties.

Spray pyrolysis is simple and inexpensive technique to obtain ZnO thin film. This method involves a simple chemical decomposition at certain temperature. Control over the deposition parameters in this method is relatively easy and it does not require vacuum environment. The temperature of annealing for further oxidation of these films is also moderate enough to be easily applied in thin film technology. The doping of any element in any proportions is relatively easy in this method. The method is useful for the large area surface coatings.

The main objectives of the present research work are as follows

1. Deposition of good quality of ZnO thin films on glass substrates with zinc acetate and zinc nitrate as precursor solution using spray pyrolysis technique.
2. Study of structure, morphology and chemical composition using XRD, SEM, EDAX and XPS. Optical evaluations of the films using UV-Visible spectrophotometer and electrical characterization with the help of computer assisted Keithley instruments.
3. Doping of ZnO films with group V dopants (Sb, Bi) and group III dopants (Al, Ga, In) to study the modulations in the structural, morphological, optical and electrical properties by varying dopant concentration from 0 to 5%.
4. Effect of annealing on the properties of undoped and doped ZnO thin films.

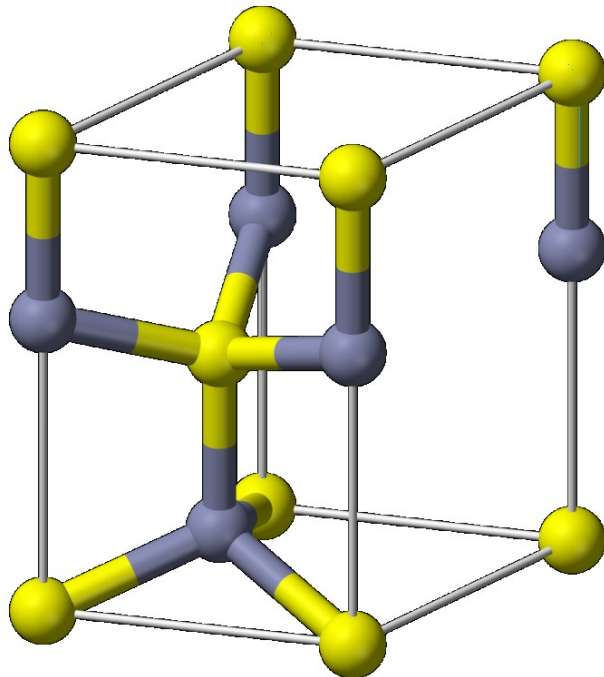


Figure 1.1: Crystal structure of ZnO (Hexagonal wurtzite)

## CHAPTER 2

# EXPERIMENTAL TECHNIQUES

### 2.1 GROWTH TECHNIQUE

Zinc oxide thin films can be prepared by different and almost all well-known deposition methods. The selection of a particular deposition method depends on various factors such as quality of films produced by the method, operation and maintenance, cost of production, etc.

Liang et al. (2005), Yang et al. (2008), Wang et al. (2009), Pan et al. (2012) and many others adopted the higher end techniques like molecular beam epitaxy (MBE) to deposit the ZnO thin films on glass, sapphire and other substrates. The films prepared from the MBE were found to be highly crystalline and free from impurities. The device quality films were usually produced by MBE technique. However technique is very costly for mass production.

Chemical techniques are usually less expensive and are suitable for mass production. Reports are available on ZnO thin films prepared by various chemical deposition methods. Ilican et al. (2008) reported the successful deposition of ZnO films on glass substrates by sol-gel spin coating method using zinc acetate dehydrate, 2-methoxyethanol and monoethanolamine solutions as precursors. These researchers claim that spin coating is simple and inexpensive method to prepare the transparent ZnO films. However the films obtained by this method have poor crystallinity and high electrical resistivity which renders them useless for device fabrication.

Lokhande et al. (2002), Dedova et al. (2007), Nese and Sertap (2008), Ergin et al. (2009), Prasada et al. (2010) and many others have used spray pyrolysis technique to deposit good quality polycrystalline ZnO thin films and nano rods on different substrates. Most of these researchers have used zinc acetate dehydrate precursor. A limitation of spray pyrolysis technique is preparation of very thin films with stable properties. However highly transparent, conducting and stable ZnO thin films can be

prepared using this simple and inexpensive technique. Hence all these researchers opine that spray pyrolysis method is a simple and effective method to obtain good quality ZnO films.

Apart from the above method, other methods are such as chemical vapour deposition (Labeau et al. 1992; Polley et al. 1999; Fay et al. 2006; Kondo et al. 2008; Christian et al. 2012), sputtering (Song et al. 2004; Tvarozeka et al. 2008; Lim et al. 2008; Gong et al. 2011), pulsed laser evaporation (Yolanda et al. 2006; Sun and Tsui 2007; Tsoutsouva et al. 2011) and thermal evaporation (Fouad et al. 2006; Aida et al. 2006; Senthilkumar and Vickraman 2010) have also been employed to deposit the good quality ZnO thin films.

In the present research work, spray pyrolysis technique has been used to deposit ZnO thin films. Spray pyrolysis technique has proved to be one of the simplest and economical techniques for producing good quality ZnO thin films.

### **2.1.1 Spray pyrolysis**

The spray pyrolysis technique is basically a chemical deposition technique in which, solutions of the required materials are sprayed onto a hot substrate. Pyrolytic process occurs, when the aerosol droplets reaches near to the hot substrate resulting the formation of continuous and adherent films. Films deposited by such a technique are generally polycrystalline in structure and their properties are highly influenced by the deposition parameters. In particular, spray pyrolysis is a versatile technique used to deposit oxide semiconductor thin films of desired stoichiometry on large surface areas. This technique is particularly attractive because of its simplicity in comparison with methods requiring vacuum conditions or complex equipments. It has a few advantages over the other thin film deposition techniques such as

- i. Simple and inexpensive technique.
- ii. Does not require vacuum environment.
- iii. It is easy to dope films, by adding required dopant in any proportion to spray solution.
- iv. By controlling the spray parameters, rate of deposition and thickness of the



films can be controlled over a wider range. It can produce films on less robust materials as the operating temperatures are moderate (100- 600°C).

- v. There are no restrictions on substrate material, dimensions or its surface profile.

Compound thin films have been prepared by spray pyrolysis technique on a variety of substrates like glass, quartz, mica, ceramic and metals. The mechanism of thin film formation and influence of variables on the film formation process has been comprehensively reviewed in the literature (Pamplin 1979).

### **2.1.2 Principle of spray pyrolysis**

Thin film formation by spray pyrolysis is a thermally stimulated reaction between clusters of atoms or molecules of different chemical species in the precursor solution. The process involves spraying a solution containing soluble salts of the constituent atoms or molecules of the desired compound onto a substrate maintained at higher temperatures. The sprayed droplets, on reaching the hot substrate, undergo pyrolytic decomposition and form deposits of the product. The other volatile by-products and excess solvent escape in the form of vapour. The substrate provides thermal energy not only for the thermal decomposition, but also for the subsequent recombination of the species followed by sintering and recrystallization of clusters of crystallites giving rise to a coherent film. The atomization of the chemical solution into a spray of fine droplets is effected by the spray nozzle with the help of filtered carrier gas. The carrier gas and spraying solutions are fed into the spray nozzle at a predetermined constant flow rate and pressure. The nature of the carrier gas also has its effect on the properties of the deposited films. The substrate temperature is maintained at the deserved level with the help of feedback circuit and heater power supply. Uniform coverage of large area of the substrate can be achieved by scanning either or both the spray head and the substrate using mechanical or electromagnetic arrangements.

The necessary criteria for the choice of chemicals used for spray pyrolysis are as follows: (a) In thermal decomposition, the chemicals in the solution must provide the species or complexes that would undergo a thermally activated chemical reaction to yield the required thin film material. (b) The remainder of the constituents of the

chemicals, including the carrier gas or liquid should be volatile at that substrate temperature.

For a given thin film material, these conditions are met in a number of combinations of chemicals. Since each combination has its own thermodynamic and kinetic considerations under the prevailing spray conditions, different deposition parameters are required to obtain films of comparable quality. The spray parameters that decide the growth and quality of the deposited layers are

- Chemical nature and concentration of spray solution
- Substrate temperature
- Spray head geometry
- Carrier gas and solvent used
- Spray pattern and spray rate
- Droplet velocity, size and geometry
- Kinetics and thermodynamics of pyrolytic reactions

The spray deposited films are usually strongly adherent, mechanically hard, pin-hole free and stable with time and temperature. The surface topography of the spray deposited film is normally rough and roughness depending on the substrate temperature and spray conditions. Depending on the chemical reactivity, droplet size and mobility of various chemical constituents, the microstructure of the spray deposited films ranges from amorphous to polycrystalline.

### **2.1.3 Importance of process parameter on the formation of thin films**

In spray pyrolysis the process parameters like precursor solution, evaporation period, thermolysis and atomization are very important in the study of structure and morphology of the thin films. These process parameters are discussed below.

#### **i. Precursors**

A precursor solution plays an important role in the formation of thin film of various compounds. Aqueous solutions are used due to ease of handling safely and availability of a wide range of water-soluble metal salts. The solute must have a high

solubility which increases in particle yield of the process. Increasingly, organic and alcoholic solutions have been studied due to the interest in the synthesis of inorganic materials from metal organic complexes that undergo thermal decomposition, gelation or polymerization and also for the synthesis of non-oxide ceramic materials.

ii. Atomization

A variety of atomization techniques have been used for solution aerosol formation, including pneumatic, ultrasonic and electrostatic. These atomizers differ in droplet size, rate of atomization and droplet velocity. The velocity of the droplet when it leaves the atomizer is important because it can determine the heating rate and the residence time of the droplet during spray pyrolysis. The size of the droplets produced with pneumatic or pressure nozzles decreases when the pressure difference across the nozzle is increased. For a specific atomizer the droplet characteristics depend on the solution density, viscosity and surface tension.

iii. Evaporation

Solvent evaporation from the surface of the droplet, diffusion of the solvent vapour away from the droplet in the gas phase, shrinkage of the droplet, change in droplet temperature and diffusion of solute towards the centre of the droplet are different stages in pyrolytic decomposition. The factors controlling the particle growth and ultimately film formation are

- Evaporation of liquid droplets
- Temperature of liquid droplets
- Solute diffusion in a droplet
- Solute condensation etc.

The various steps involved during pyrolysis of aerosols are summarized below.

- Precursor solution is converted into aerosols by spray nozzle.
- Solvent evaporation takes place.
- Vaporization of solvent leads to precipitate formation as droplets / aerosols reaches the substrate.

- Pyrolysis of the precipitate occurs in succession before the precipitate reaches the substrates.
- When precipitate reaches the substrates, nucleation and growth of thin film on the substrate takes place. Finally, growth of the nuclei leads to the formation of continuous thin layer of films.

#### **2.1.4 Description of spray set up**

The schematic diagram of the spray pyrolysis unit used in the present study for the preparation of the ZnO thin films is shown in figure 2.1. It consists of following parts

i. Spray nozzle

It is a specially designed nozzle made of glass consisting of different ports such as outer air port, inner liquid port and cylinder port. The outer air port is connected to an air compressor through an air flow meter. The inner liquid port is connected to the solution reservoir through a flow meter. The solution reservoir is placed well above the nozzle head level. The solution is fed to the liquid port by gravity and solution flow rate can be monitored by a valve. When the valve is activated, compressed air lifts a pneumatically operated air cylinder inside the nozzle allowing solution to be atomized. This arrangement prevents the solution flow out of the nozzle before atomizing air is admitted.

ii. Motor for nozzle movement with speed controller

Mechanically adjustable motor is used for linear simple harmonic motion of the spray nozzle over the required length of the substrates. Spray nozzle is attached to two stainless steel rods, which in turn are fixed to motion assembly.

iii. Hot plate with temperature controller

Hot plate with temperature controller (M/s Heatron India Ltd, Mangalore) consists of an iron disc, with diameter 20 cm and thickness 3 cm supported on the electric heater (2000 W). In this arrangement the maximum temperature up to 600°C can be obtained. Chromel-alumel thermocouple was used to measure the temperature

of the substrates and is fixed at the centre of the iron disc. The temperature of the hot plate was monitored with PID temperature controller (Precision  $\pm 5^{\circ}\text{C}$ ).

iv. Air compressor

Compressed filtered air was used as the carrier gas. It was provided by a compressor with a starter and pressure cut-off switch. The pressure in the tank can be limited to any desired value. The pressure regulator is fitted with a gauge to record the outlet pressure of air sent to the spray nozzle. The solution and air flow rates were monitored by using the flow meters and valves.

v. Metallic chamber

During the thermal decomposition of sprayed solution a number of toxic vapours may evolve and it is necessary to fix the spraying system inside a metallic chamber. An exhaust fan is fixed at the top of the metallic chamber. It exhausts the vapours produced during pyrolytic decomposition of reactants. A metallic chamber of the size 2' x 2' x 2.5' having a glass window and a bulb inside for illumination was used.

The selection of substrate for depositing the films is very important. Substrate materials such as glass, quartz, silicon, alumina etc. are used for spray deposition. Glass substrates are chemically inert and provide good mechanical support to the films. They can also bear reasonably high deposition temperatures. Since glass is amorphous it normally does not influence the crystal structure of the films deposited on it. Adhesion of the deposited films to the glass substrates depend on the film material. Glass substrates are sometimes treated with chemicals such as chromic acid, prior to the deposition, in order to improve adhesion of films. Treating with chromic acid increases the surface roughness of the glass surface and improves adhesion.



Figure 2.1 Spray pyrolysis unit used to deposit the ZnO thin films.

## **2.2 THICKNESS MEASUREMENT**

Thickness is an important parameter on which many properties of films depend. The light transmittance and resistivity of the films which are very relevant to ZnO films depend on film thickness. Thus it is often necessary to measure the thickness to characterize the films. Many techniques are available for the thickness measurements of the films. Some of these techniques are destructive and some require special sample preparation. The precision and range of measurement vary from method to method. The measurement techniques described in this section are applicable to post-deposition evaluation.

### **2.2.1 Stylus method**

In principle this method consists only of measuring the mechanical movement of stylus as it traverses film substrate step. The stylus traverses a substrate film step, and the vertical motion of the stylus relative to the reference plane is converted to the electrical signal which is amplified and recorded on rectilinear paper. Thus, a profile graph is produced which represents a cross section of the film step as well as substrate surface irregularities.

Factors which limit the usefulness and accuracy of this instrument are:

- The diamond stylus may penetrate and scratch a groove in soft films. This will destroy the films or introduce large error.
- Substrate roughness may introduce "noise" which causes uncertainty in the measured thickness.

### **2.2.2 Multiple beam Fizeau fringes method**

This method, developed by Tolansky (1950), requires a sharp step in the film down to the substrate plane which can be made either by using a mechanical mask during deposition or by etching the film after deposition. Both the film and substrate surfaces must be highly reflective. This is accomplished by evaporating a metal such as silver or aluminium over both film and substrate. Interference fringes are generated by placing a reflective, but semitransparent, optically flat reference plate very close to the step region. At small distance between the two plates, multiple beam interference

fringes appear with a spacing  $x$ . In the region of sharp step, fringes are shifted by a distance  $\Delta x$ . The thickness  $t$  of the film is then given by,

$$t = \left( \frac{\Delta x}{x} \right) \frac{\lambda}{2} \quad (2.2.1)$$

where  $\lambda$  is the wavelength of the light used.

### 2.2.3 Gravimetric method

In this method the mass of the film is determined by weighing. The thickness is then calculated, usually assuming the bulk density. If  $A$  is the area,  $t$  is the thickness,  $\rho$  is the density and  $m$  is the mass of the film then,

$$tA\rho = m, \quad (2.2.2)$$

$$t = \frac{m}{A\rho} \quad (2.2.3)$$

Then  $m$  can be determined by weight difference in the substrate before and after deposition and  $A$  can be measured. By considering the bulk density thickness of the film can be calculated with the help of equation 2.2.3. The limitation of weighing method is that determination of thickness distribution on a single substrate is not possible, since an average thickness is obtained for entire area weighed. This was found to be a convenient method for measuring film thickness in the course of this study.

In the present study, the depositions were carried out using a starting solution of 0.5M concentration of zinc acetate anhydrous (Aldrich, 99.99%) in methanol. The glass substrates were kept in concentrated nitric acid for 24 hrs to remove the surface impurities present on it. After removing the glass substrate, it is thoroughly washed with soap solution (Laboline), further it is cleaned with acetone, Isopropyl alcohol and finally with deionised water using ultrasonic bath and dried. During deposition the temperature was maintained at  $450 \pm 5^\circ \text{C}$ , the spray nozzle is fixed at a distance of 26 cms from the substrate, the solution is sprayed at the rate of 2 ml/min. Air is used as carrier gas at the pressure of 2 bar. Pyrolytic process occurs, when the aerosol droplets reach the hot glass substrate and adherent ZnO thin films were produced. The deposited ZnO thin films were annealed at different temperatures for 4 hrs in air.



Films with thickness ranging from 400 nm to 1200 nm were prepared for various characterizations.

## **2.3 CHARACTERIZATION TECHNIQUES**

The spray deposited zinc oxide thin films grown in the present investigations were characterized using appropriate techniques to evaluate the physical properties such as structure, composition, optical and electrical properties. The details of the different instruments, techniques and procedures used for this purpose are given in the following sections.

### **2.3.1 Structural characterization**

The structural information of thin films is vital in research, process development and reliability analysis. Parameters such as uniformity of thickness, surface topography and morphology, including grain size and shape, existence of different compound phases, hillocks and whiskers, evidence of voids, micro-cracking or lack of adhesion are of concern for any device application. Also in micro-electronic and opto-electronic devices, the structure of grain boundaries, identification of phases, direct imaging of atoms at interfaces, interfacial quality and defects, cross-sectional views are very crucial in evaluating the performance of the device. The crystal structure of thin films largely depends on the deposition conditions. The structure and composition of the films affect their optical and electrical properties. Hence it is also necessary to understand the influence of various deposition parameters on the structure and composition of the films. Besides crystal structure and composition, the study of surface topography of the films is also of considerable interest. High magnification images of the film surface may provide information about the presence of any impurities or holes in the film. In order to determine the structural features of the deposited films, the present investigation employs the X-ray diffractometer (XRD) and Scanning electron microscope (SEM).

### **a. X-ray diffraction technique**

For most of the solids, crystalline state is the natural one since the energy of a regular arrangement of atoms is less than that of an irregular packing of atoms. However when atoms are not given an opportunity to properly arrange themselves by inhibiting their mobility, amorphous materials may be formed. This situation is frequently encountered during the deposition of thin films. Due to the finite rate of deposition and limited mobility of the atoms impinging on the substrate, the resultant film may often become polycrystalline or amorphous. In the polycrystalline state the film contains a large number of small crystals which are often referred as grains. These grains are randomly oriented. The size of the grains may be controlled, to some extent, by varying the deposition parameters and by post deposition heat treatments. Except for epitaxial techniques, almost all deposition techniques produce either polycrystalline or amorphous films.

When it comes to structural characterization, X-ray diffraction (XRD) is a versatile and non-destructive technique used for studying the crystallographic structure of materials and hence chemical composition of natural and manufactured materials. This method requires minimum sample preparation and provides valuable information about the crystal structure and orientation. The method relies on measuring the intensity of X-rays scattered by the sample as a function of incident and scattered angle. This technique can also be used to detect the presence of a material in the film, since the X-ray diffraction patterns are characteristic of a material (Cullity 1956).

When a monochromatic X-ray beams with wavelength ' $\lambda$ ' is incident onto a crystalline material at an angle ' $\theta$ ', diffraction occurs only when the distance travelled by the rays reflected from successive planes differ by a complete number ' $n$ ' of wavelengths. Then Bragg's law for X-ray diffraction is given by

$$2d \sin\theta = n\lambda \quad (2.3.1)$$

where ‘ $\lambda$ ’ is wavelength of incident X-rays, ‘ $\theta$ ’ is diffraction angle, ‘ $d$ ’ is interplaner spacing can be measured for different set of planes and ‘ $n$ ’ is an integer. The intensity of the diffracted beams is related to the strength of the diffraction in the sample.

In X-ray powder diffractometer, X-rays are generated within a sealed vacuum tube containing a filament and a target. A current is applied to the filament to emit electrons. Higher the current applied the greater is the number of electrons emitted from the filament. A high voltage, typically 30 kV, is applied between the filament and the target material. This high voltage accelerates the electrons emitted from the filament, which then hit the target, and produce X-rays. The wavelength of the X-rays generated is characteristic of the target. X-ray tubes with copper (Cu) targets are most commonly used for X-ray diffraction of inorganic materials. The X-rays generated are collimated and directed onto the sample which could be a thin film or powdered crystal. The X-ray data obtained is compared with JCPDS (Joint Committee for Powder Diffraction Standards) data card to verify the compound. This diffraction data is used to determine dimensions of unit cell, crystal structure, standard deviation and crystallinity. The lattice constants ‘ $a$ ’ and ‘ $c$ ’ for hexagonal phase of ZnO thin films were calculated using the following equation (Cullity 1956)

$$\frac{1}{d^2} = \frac{4}{3} \left( \frac{h^2 + hk + k^2}{a^2} \right) + \frac{l^2}{c^2} \quad (2.3.2)$$

where h, k, l are miller indices.

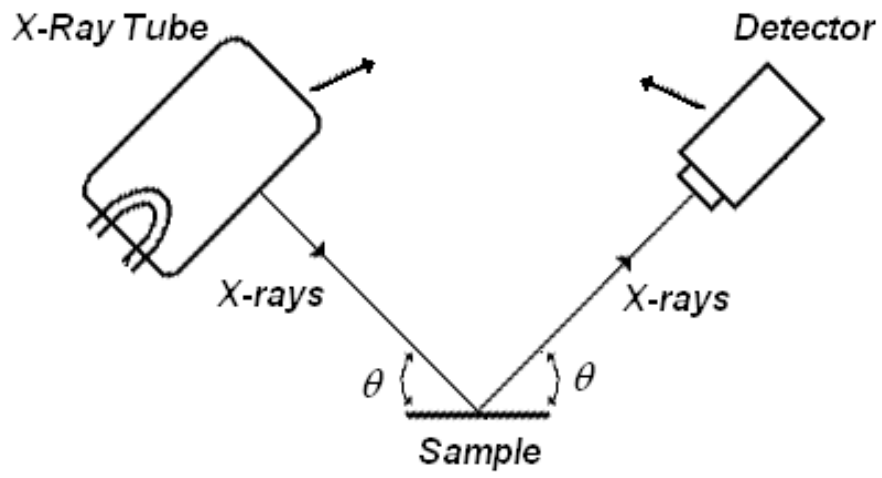
In addition to the effect of grain size, peak broadening may also be caused by other reasons, such as inhomogeneous strains, lattice bending, twinned structure, or other point defects that may be present in the films, hence Scherrer’s equation may produce results that are different from the actual size. In order to calculate the strain ( $\epsilon$ ) and the grain size (D) of the deposited films, the Williamson and Hall (1953) equation can be used.

$$\frac{\beta \cos \theta}{\lambda} = \frac{1}{D} + \frac{4\epsilon \sin \theta}{\lambda} \quad (2.3.3)$$

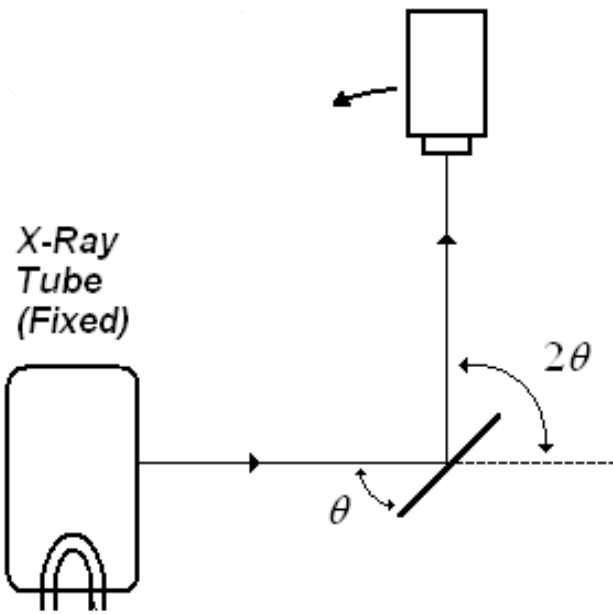
where  $\beta$  is the full width at half maximum (FWHM) of the diffraction peaks,  $\theta$  is the Bragg's angle and  $\lambda$  is the wavelength of X-ray used. A plot of  $(\beta \cos \theta)/\lambda$  versus  $(4\sin \theta)/\lambda$  is made. The reciprocal of intercept on the y-axis gives the average grain size, and the slope of the plot gives the amount of residual strain.

Figure 2.2 shows the X-ray diffraction arrangement, which consists of an X-ray tube and detector. These are positioned so that the focal spot of the source, the center of the orienter system and center of the detector aperture all lie in a plane accurately perpendicular to the  $2\theta$  axis. The detector mounted on  $2\theta$  circular scale, moves around the specimen at a speed of  $2\theta^\circ/\text{min}$ , while the sample moves  $\theta^\circ/\text{min}$ . In this way the incident and diffracted beams always make equal angles with the specimen surface. With the goniostat (orienter), the specimen could also be tilted through  $\phi$ ,  $\chi$  angles, to bring the diffracted beam into the horizontal plane. The axes of rotations  $\phi$  and  $\chi$  intersect at a known point. If the X-ray beam is made to strike the specimen at this point, the crystal will not be displaced from the beam during the tilting. The wavelength is controlled by using a combination of a characteristic line of the chosen target material and the absorption edge of a specific filter material.

In addition to the elements described above, the complete diffractometer normally includes a scalar for counting the pulses from the detector, and usually a rate meter, which smoothens the pulses to a steady current, so that the average intensity can be read on the meter or fed to a chart recorder for continuous scanning of a pattern. Observations thus made can be compared with tables of known spacing and the structural data of the sample can be determined. In the present investigation we have used JEOL X-ray diffractometer with Cu  $K_\alpha$  radiation (1.5406 Å) in  $2\theta^\circ$  range of  $20^\circ$  to  $65^\circ$ . The scanning rate was maintained at  $2^\circ/\text{min}$ .



(a)



(b)

Figure 2.2: Schematic representation of X-Ray diffractometers: (a)  $\theta$ -  $\theta$  type (b)  $\theta$ -  $2\theta$  type.

## b. Scanning electron microscopy (SEM)

SEM provides a convenient and versatile method for studying surface structures and exploring certain material vibrations. It is also capable of examining very small objects. The SEM images have resolution of the order of few tens of nanometers. The studies provide the nature of surface (about the uniformity, smoothness and cracks) and the nature of the grains (shape, particulate or interconnected crystallites and the grain size). It can be used for examining thick samples. Scanned images are particularly useful for examining the morphology of the metal alloys, thin film of metal and semiconductors and crystalline materials.

The high magnification and resolution required for the study of film surface cannot be met by the optical microscopy. Therefore electron microscopy is preferred for the surface characterization of thin films. Electron microscopes use electron beam rather than light. The use of electrons has two main advantages over optical microscopes: much larger magnifications are possible since electron wavelengths are much smaller than photon wavelengths and the depth of field is much higher. During the operation of an electron microscope, the electrons are accelerated through a very high voltage. The electron wavelength  $\lambda_e$  is related to the electron velocity  $v$  or the accelerating voltage  $V$  by de-Broglie's equation,

$$\lambda_e = \frac{h}{mv} = \frac{h}{\sqrt{2meV}} = \frac{1.22}{\sqrt{V}} \text{ nm} \quad (2.3.4)$$

An accelerating voltage of about 10,000 V can produce an electron beam of wavelength 0.012 nm which is far less than the wavelength of visible light. Thus very high resolution can be achieved by an electron beam.

The figures 2.3 and 2.4 show the schematic representation of a scanning electron microscope (SEM). The thermionically emitted electrons from a tungsten or LaB<sub>6</sub>-cathode filament are accelerated towards anode and focused by couple of successive condenser lenses into a beam with a very fine spot size ( $\sim 10 \text{ \AA}$  in diameter). Pairs of scanning coils located at the objective lens deflect the beam either linearly or in raster fashion over a rectangular area of the specimen surface. Electron beams having energies of 10 - 30 keV are impinging on the specimen; the primary electrons

decelerate and in losing energy, transfer it inelastically to other atomic electrons and to the lattice. The size of the interaction volume depends on the electrons landing energy, the atomic number of the specimen and the specimen's density. The energy exchange between the electron beam and the sample results in the reflection of high energy electrons by elastic scattering, emission of secondary electrons by inelastic scattering and the emission of electromagnetic radiation which can be detected with an Everhart-Thornley (ET) detector. The basic component of the detector is a scintillation material that emits light when struck by energetic electrons accelerated from the sample to the detector. The light from the scintillator is channeled through a light pipe to a photomultiplier, where the light incident on a photocathode produces electrons that are multiplied, creating the very high gain necessary to drive the CRT.

Magnifications over a range of about 5 orders of magnitude from 25X to 250,000X or more are possible in SEM. Unlike optical and transmission electron microscope, image magnification in the SEM is not function of the power of the objective lens. SEMs may have condenser and objective lenses but their function is to focus the beam to a spot, and not to image the specimen. SEM magnification results from the mapping process according to the ratio of the dimension scanned on the display to the dimension of the scanned sample. Assuming that the display screen has a fixed size, higher magnification results from reducing the size of the raster on the specimen, and vice versa. Magnification is therefore controlled by the changing current supplied to the x, y scanning coils, and not by changing objective lens power.

### **2.3.2 Composition analysis**

#### **a. Energy dispersive X-ray analysis (EDS/EDAX)**

The composition analysis of the thin films mainly focuses on the determination of composition of the elements. The energy dispersive X-ray analysis (EDAX) is usually preferred for the compositional analysis of the films. The EDAX can detect the presence of almost all elements having atomic number  $Z > 11$ . The technique of EDAX is based on the analysis of characteristic X-rays emitted by the matter when it is hit by the charged particles.

To stimulate the emission of characteristic X-rays from a specimen, a high energy beam of charged particles such as electrons is focused into the sample being studied. At rest, an atom within the sample contains ground state (or unexcited) electrons in discrete energy levels or electron shells bound to the nucleus. The incident beam may excite an electron in an inner shell, ejecting it from the shell while creating a hole. An electron from an outer, higher energy shell then fills the hole, and the difference in energy between the higher energy shell and the lower energy shell is released in the form of an X-ray. The number and energy of the X-rays emitted from a specimen can be measured by an energy dispersive spectrometer. As the energy of the X-rays is characteristic of the difference in energy between the two shells, and of the atomic structure of the element from which they were emitted, this allows the elemental composition of the specimen to be measured.

The set of X-rays emitted from these electron interactions is the characteristic with respect to both energy and wavelength for each element. The energy and wavelength are related by the equation

$$\lambda = \frac{12.396}{E} \quad (2.3.5)$$

where ' $\lambda$ ' is the wavelength in Angstroms and ' $E$ ' is the energy in keV.

There are two types of spectrometers used in electron microprobes, the wavelength dispersive or electron probe microanalysis spectrometer (WDS/EPMA) and the energy dispersive spectrometer (EDS/EDAX). The WDS is used for highly quantitative analysis. The EDAX utilizes a solid-state detector to analyse all X-ray photon energies simultaneously. Thus EDAX is a method of elemental analysis by scanning scattered X-rays from high voltage electron bombardment usually in SEM characteristic emission peaks which enable identification of most of elements. This can be made quantitative by comparing with standards.



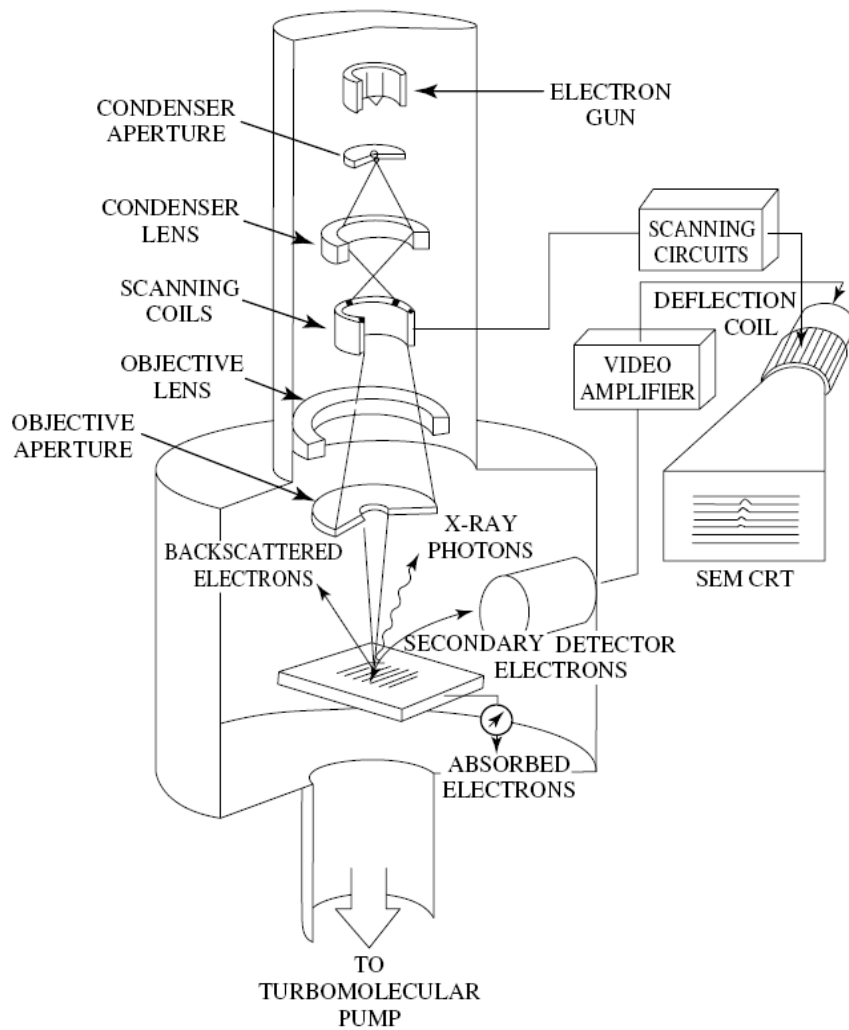


Figure 2.3: Schematic diagram of scanning electron microscope.  
 [Ref: Dieter K Schroder (2005), *Semiconductor Material and Device Characterization*, Wiley Inter Science, New Jersey]



Figure 2.4: Scanning Electron Microscope (Model: JEOL JSM-6380LA)

## **b. X-ray photoelectron spectroscopy (XPS)**

X-ray photoelectron spectroscopy is also called as electron spectroscopy for chemical analysis (ESCA). It is one of the surface analytical techniques that bombard the sample with photons, electrons or ions in order to excite the emission of photons, electrons or ions. The kinetic energy ( $E_k$ ) of these photoelectrons is determined from the experiment; as the energy of the X-ray beam ( $h\nu$ ) is already known, the electron binding energy ( $E_b$ ) can be calculated as,

$$E_k = h\nu - E_b \quad (2.3.6)$$

The electron binding energies are dependent on the chemical environment of the atom. XPS is hence useful tool to identify the oxidation and / or compound state of an atom. Binding energy of the valence electrons is affected by the chemical environment of the atom, when atomic environment of an atom changes, it alters the local charges surrounding the atom. This charge in turn, reflects itself as a variation in the binding energy of the valence electrons of the atom. Thus binding energies of valence electrons experience a characteristic shift and this can give important information regarding the valence states/compound formation of the atoms in the sample and one can use this technique to find out whether an element present in a sample is in pure or in compound form.

XPS is a quantitative technique in the sense that the number of electrons recorded for a given transition is proportional to the number of atoms at the surface. Instead of impinging the sample surface with an electron beam, XPS utilizes a monochromatic X-ray beam to cause electrons to be ejected, usually two to twenty atomic layers deep. In XPS, the sample is irradiated with low energy ( $\approx 1.5$  keV) X-rays, in order to provoke the photoelectric effect. The energy spectrum of the emitted photoelectrons is determined by means of a high resolution electron spectrometer. The sample analysis is conducted in a vacuum chamber, which facilitates the transmission of the photoelectrons to the analyzer but more importantly minimizes the recontamination rate of a freshly cleaned sample. This is crucial because XPS is surface sensitive, with a typical sampling depth of only a few nanometers.

In practice, however, finding accurate atomic concentrations from XPS spectra is not straight forward. The precision of the intensities measured using XPS is not in doubt; that is intensities measured from similar samples are repeatable to good precision. What may be doubtful are results reporting to be atomic concentrations for the elements at the surface. For specific carefully performed and characterized measurements better accuracy is possible, but for quantification based on standard relative sensitivity factors, precision is achieved not accuracy. Since many problems involve monitoring changes in samples, the precision of XPS makes the technique very powerful. The basic mechanism behind an XPS instrument is illustrated in figure 2.5. Photons of a specific energy are used to excite the electronic states of atoms below the surface of sample. Electrons ejected from the surface are energy filtered via a hemispherical analyzer (HSA) before the intensity for a defined energy is recorded by a detector. Since core level electrons in solid-state atoms are quantized, the resulting energy spectra exhibit resonance peaks characteristic of the electronic structure for atoms at the sample surface. While the X-rays may penetrate deep into the sample, the escape depth of the ejected electrons is limited. That is, for energies around 1400 eV, ejected electrons from depths greater than 10 nm have a low probability of leaving the surface without undergoing an energy loss event, and therefore contribute to the background signal rather than well defined primary photoelectric peaks.

In principle, the energies of the photoelectric lines are well defined in terms of the binding energy of the electronic states of atoms. Further, the chemical environment of the atoms at the surface results in well defined energy shifts to the peak energies. In the case of conducting samples, for which the detected electron energies can be referenced to the Fermi energy of the spectrometer, an absolute energy scale can be established, thus aiding the identification of species.

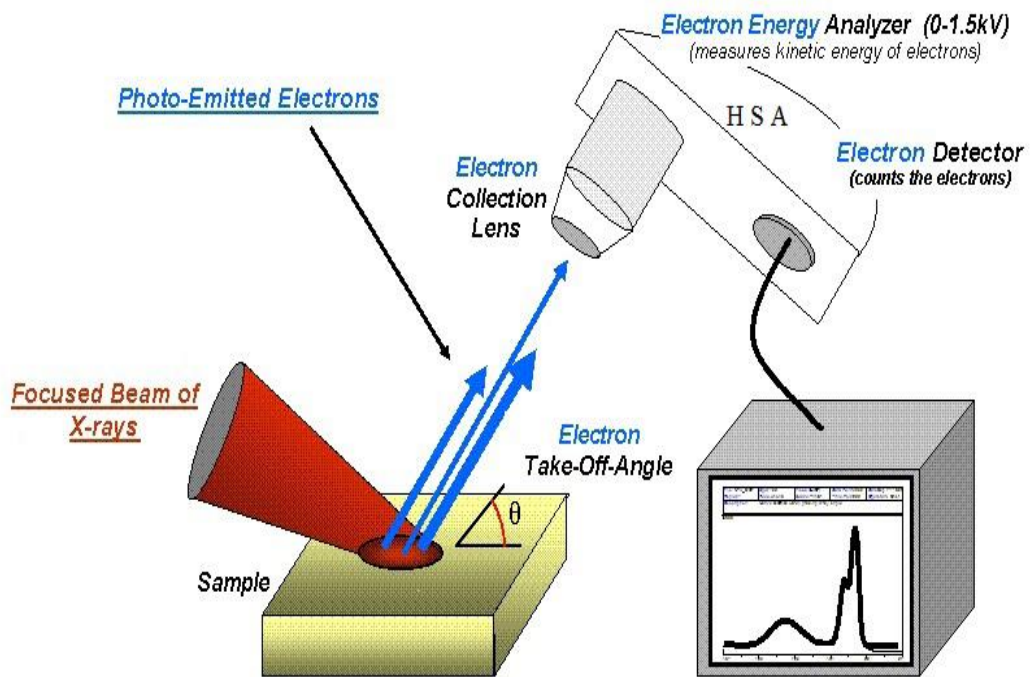


Figure 2.5 Schematic representation of X-ray photoelectron spectroscope.

### 2.3.3 Optical characterization

One of the simplest methods to analyze the band structure of semiconductor materials is the study of their interaction with light. When light falls on a material part of the incident light may get reflected, some part may get absorbed and the remaining part may get transmitted. The amount of reflected, transmitted or absorbed light energy depends on the energy of the incident photons and the band structure of the material. The transmission or absorption measurements would, therefore, reveal valuable information about the band structure of the material. Generally in a semiconductor optical absorption may take place due to various mechanisms and each contributes to the total absorption (Yacobi 2004; Mishra and Singh 2008).

#### a. Optical absorption

The fundamental absorption process resulting from band-to-band transition is very important among all the above mechanisms. The other mechanisms are significant only when the incident light energy is less than the bandgap energy of the material. In many semiconductors, the intraband transitions take place, due to the transitions between light-hole and heavy-hole bands in the valence band. The absorption due to dopants occurs because of the transitions from donor level to conduction band or valence band to acceptor level. These transitions usually result in the absorption in far-infrared region. Absorption may also occur due to the presence of impurities, point defects, grain boundaries, collectively called imperfections, which create localized energy levels in the energy gap of a semiconductor. In this case, transitions may occur from occupied imperfection levels to the conduction band or from the valence band to the unoccupied imperfection levels. The free carrier absorption results from the transitions to higher energy levels within the same energy band.

In the fundamental absorption process, the incident photon excites an electron from valence band to conduction band. During such transition both energy and momentum must be conserved. The conservation of energy implies that the final energy  $E_f$  of the electron must be equal to the sum of initial energy  $E_i$  and photon energy  $h\nu$ . i.e,

$$E_f = E_i + h\nu \quad (2.3.7)$$

Since the minimum energy difference between conduction band and the valence band is the bandgap energy  $E_g$ , the incident photon energy must be larger than the bandgap energy. The conservation of momentum requires the effective momentum  $\hbar k$  of the electron-photon system to be same before and after the transition. Since the  $k$ -value of the photon, given by,

$$k = \frac{2\pi}{\lambda} \quad (2.3.8)$$

is negligibly small compared to the  $k$ -value of the electron, the transition can take place only if the  $k$ -value of the electron remains same before and after the transition. Thus for the fundamental absorption process only transitions which are at same  $k$  are allowed as shown in figure 2.6 (a).

If the minimum of the conduction band and maximum of the valence band of a semiconductor occur at the same value of  $k$  [fig.2.6 (b)] then the semiconductor is said to be a direct bandgap semiconductor. In such semiconductors the most likely transitions are across the minimum-energy gap, between minimum of the conduction band and the maximum of the valence band. ZnO and many other II-VI compounds are direct bandgap semiconductors. If the minimum of the conduction band and maximum of the valence band do not occur at same  $k$ -value then the material is said to be indirect bandgap semiconductor [fig.2.6 (c)]. The most widely used semiconductors Si, Ge are indirect bandgap semiconductors. The band-to-band transitions in indirect bandgap semiconductors essentially require the participation of phonons in order to conserve momentum. The probability of such a transition is low and hence the optical transitions near the band edges are weak.

The process of absorption is characterized by absorption co-efficient  $\alpha$ , which can be defined as the relative decrease in the intensity  $I(h\nu)$  of the light in its path of propagation in the material.

$$\alpha = \frac{1}{I(h\nu)} \frac{d[I(h\nu)]}{dx} \quad (2.3.9)$$

The absorption co-efficient of a material can be determined by the transmission measurements. If  $I_0$  is the incident light intensity,  $I$  is the transmitted light intensity, and  $R$  is the reflectivity, then transmittance  $T= I/I_0$  is given by,

$$T = \frac{(1-R)^2}{1-R^2} \frac{\exp(-\alpha t)}{\exp(-2\alpha t)} \quad (2.3.10)$$

where  $t$  is the thickness of the material. For large values of  $\alpha t$  and negligible reflectance then equation (2.3.10) reduces to,

$$T = \frac{I}{I_0} = \exp(-\alpha t) \quad (2.3.11)$$

The transmittance  $T$  is related to absorbance  $A$  by the equation,

$$A = \ln(T) = \alpha t \quad (2.3.12)$$

Thus  $\alpha$  can also be defined as absorbance per unit thickness.

In the case of direct bandgap semiconductors,  $\alpha$  is related to bandgap energy  $E_g$  by the equation,

$$\alpha h\nu = B(h\nu - E_g)^{1/2} \quad (2.3.13)$$

where  $B$  is a constant ( $\sim 10^4$ ). A plot of  $(\alpha h\nu)^2$  against  $h\nu$ , called Tauc's plot, shows a linear portion, which, when extrapolated, meets the  $x$ -axis at  $h\nu = E_g$ . Hence the optical bandgap may be evaluated.

The phenomenon of optical transmission or absorption in a thin film can be studied by the help of a spectrophotometer (Schroder 2006). For wide-bandgap materials like ZnO, ZnSe, etc. the absorption edge is located in the UV or visible region of the electromagnetic spectrum. Hence a UV-Visible spectrophotometer is suitable for such materials. Although many variations of UV-Visible spectrophotometers are available, the basic setup and working principle are same for all of them. The schematic diagram of a typical UV-Visible spectrophotometer is shown in figure 2.7. The working of the instrument is relatively straight forward. A beam of light from a visible and/or UV light source is separated into its component wavelengths by a prism or diffraction grating. Each monochromatic beam in turn is split into two equal intensity beams by a half-mirrored device. One beam, the sample beam, passes through the film sample being studied. The other beam, the reference,



passes through a reference specimen of the substrate which is used to deposit the films. The intensities of these light beams are then measured by electronic detectors and compared. The intensity of the reference beam, which should have suffered little or no light absorption, is defined as  $I_0$ . The intensity of the sample beam is defined as  $I$ . Over a short period of time, the spectrometer automatically scans all the component wavelengths in the manner described. The ultraviolet (UV) region scanned is normally from 200 to 400 nm, and the visible portion is from 400 to 800 nm. If the sample compound does not absorb light of a given wavelength, then  $I = I_0$  for that wavelength. However, if the sample compound absorbs light then  $I$  is less than  $I_0$ . Absorption is usually presented as transmittance ( $T = I/ I_0$ ) or absorbance ( $A = \ln(I_0/I)$ ). If no absorption has occurred,  $T = 1.0$  and  $A = 0$ .

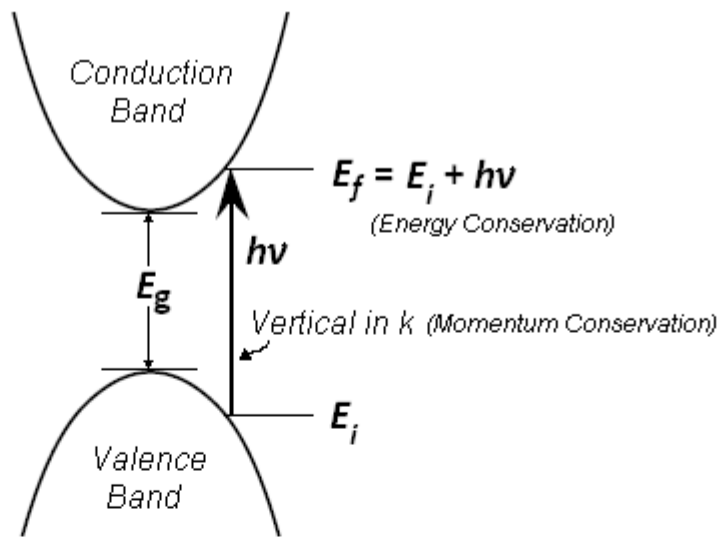
In the present research work priority is given to study the transmittance as well as the optical absorbance spectra of undoped and doped ZnO thin films deposited at 450°C and annealed at various temperatures. The optical bandgap of the ZnO thin films were evaluated using absorbance data. The films were prepared by spray pyrolysis technique as explained in previous section. Deposited films of thickness 600 nm are used for the study. The annealing temperature was varied from 450 °C to 550 °C. The absorbance spectra were recorded by a UV-Visible spectrophotometer (Ocean Optics). The bandgap calculated from the Tauc's plots of ZnO films annealed at various temperatures found to be decreased. This variation in bandgap energy can arise due to many factors such as deviation from stoichiometry, quantum size effect, defects etc. The effect of quantum confinement is usually reflected in the inverse-square relation between bandgap deviation  $\Delta E_g$  and the grain size  $D$  as given below (Cortes 2004),

$$\Delta E_g = E_g^{\text{observed}} - E_g^{\text{bulk}} = E_b \left( \frac{\pi a_B}{D} \right)^2 \quad (2.3.14)$$

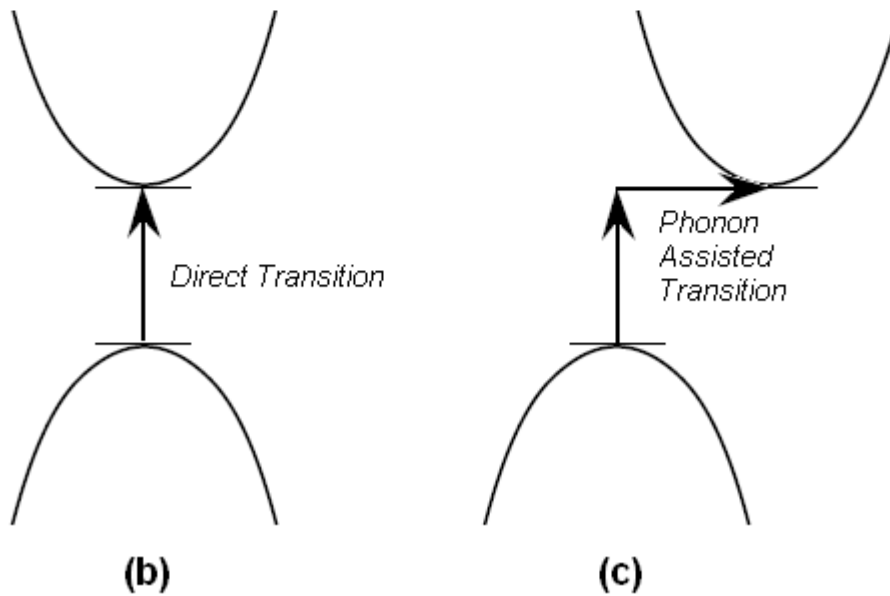
where  $E_b$  is the exciton binding energy and  $a_B$  is the exciton Bohr radius. This equation leads to a simple inverse-square relation between the observed bandgap energy and the grain size,

$$E_g^{\text{observed}} = A + \frac{B}{D^2} \quad (2.3.15)$$

where  $A$  and  $B$  are constants.



(a)



(b)

(c)

Figure 2.6: The optical absorption phenomenon: (a) Conservation of energy and momentum, (b) Transition in direct bandgap material (c) Transition in indirect bandgap material.

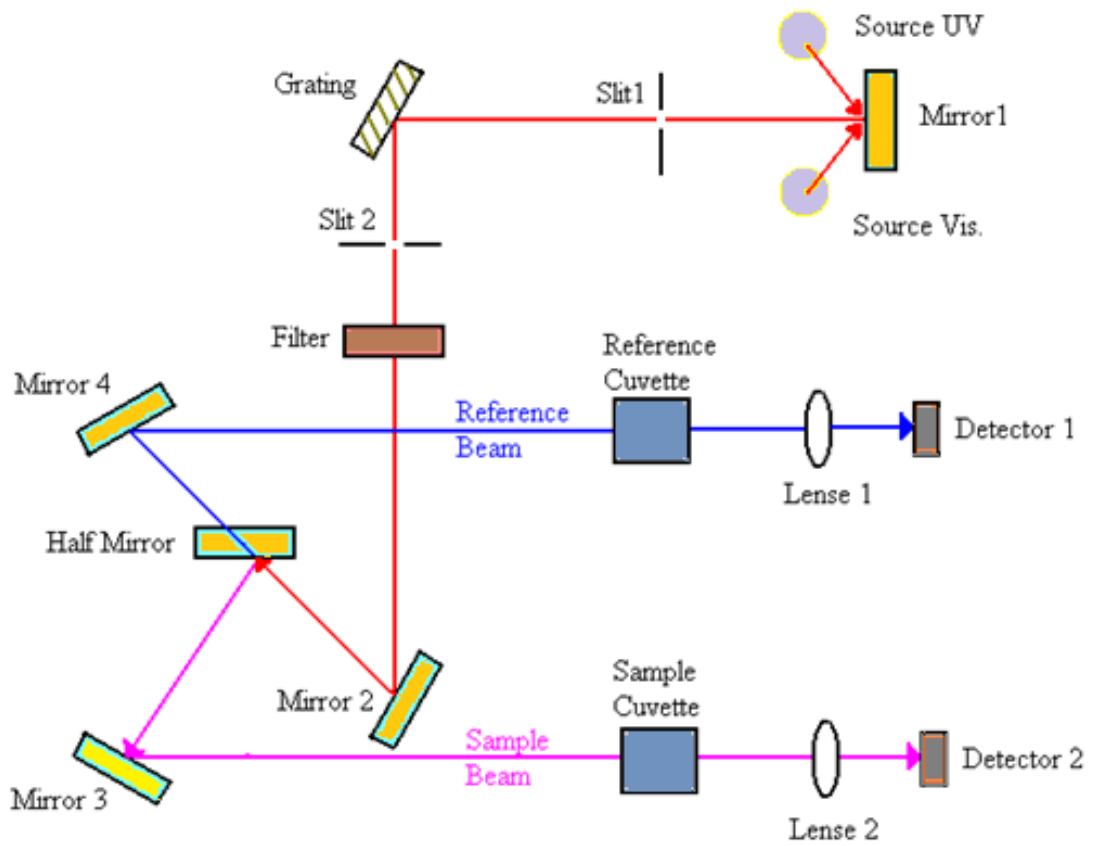


Figure 2.7: The schematic diagram of a typical spectrophotometer.

### 2.3.4 Electrical characterization

Measurement of electrical properties like resistivity, carrier type, carrier concentration, mobility and variation of resistance with temperature of a material is very much required before using the material in fabrication of electronic devices.

For electrical characterization, thin layer of silver used as a contact electrode which makes Ohmic contact with ZnO thin films. Silver electrodes were deposited on the films by thermal vacuum evaporation technique (Hind High Vacuum Ltd.) at vacuum better than  $10^{-5}$  mbar. Resistivity measurement for films of various composition was done using Keithley 2002 multimeter ( $8^{1/2}$  digit, 100 n $\Omega$  resolution) by D.C. two-point probe method in air. I-V characteristics were recorded with computer interfaced Keithley 2400 source meter (100 pA, 5  $\mu$ V resolution setup). I-V characteristics and variation of resistance with temperature were studied in bridge geometry. A copper-constantan thermocouple was placed behind the glass substrate for the measurement of ambient temperature. Resistance values were measured at different temperatures. Then logR was plotted against reciprocal of absolute temperature. The resulting Arrhenius plots were used to estimate the activation energies of the carriers in the samples under study.

Spray deposited thin films are usually polycrystalline in nature as it has been seen in the present case of ZnO films. Polycrystalline films can be generally treated as a group of crystallites joined together by the grain boundaries. In such a material the electrical conduction is largely controlled by the grain boundary phenomena (Maity et al. 1995). The grain boundary regions are disordered regions, characterized by the presence of a large number of defect states arising due to the non-stoichiometric nature of the films and incomplete atomic bonding. These defects can act as effective carrier traps which can trap charge carriers and become charged after trapping. This results in the appearance of a potential barrier which impedes the flow of carriers from one grain boundary to another and affects the electrical conductivity of the films.

In a semiconductor material, the donor or acceptor levels in the forbidden energy gap are formed due to the presence of donor or acceptor type impurities (Kittel 1996;

Sze 2006). The impurity concentration is usually very low and is scarcely distributed within the material. The donor levels are usually exists near the lower edge of the conduction band and acceptor levels near the upper edge of the valence band. Electrons having sufficient energy can jump from valence band to acceptor levels producing an equal number of holes in the valence band. Similarly, the electrons can jump from donor levels to conduction band. Both these processes are limited by the impurity ionization energies.

At very low temperatures even if it contains donor or acceptor impurities, conductivity of semiconductor material will be low. The increase in temperature results more and more donors or acceptors get ionized, contributing either electrons to the conduction band or holes to the valence band, which contributes to electrical conductivity. This electrical conduction which is largely due to the free carriers contributed by the impurities is referred as extrinsic conduction. If the temperature is increased further the intrinsic conduction, due to the electrons jumping from valence band to the conduction band, predominates. The intrinsic conduction is limited by the forbidden energy gap, which is far higher than the activation energy, and hence takes place at relatively high temperatures. Once the intrinsic conduction begins, the electrical conductivity increases sharply with the increase in temperature. The intrinsic and extrinsic conduction are not mutually exclusive, but can co-exist in the material. The extrinsic conduction dominates in the low temperature region and intrinsic conduction dominates in the high temperature region.

Electrical contacts are required to connect a semiconductor device to the other circuit elements such as voltage or current sources, other semiconductor devices etc. Low resistance, stable contacts are critical for the good, long term and reliable performance of a semiconductor device. The metal-semiconductor contacts are most common although semiconductor-semiconductor contacts are also used in some devices. In most of the semiconductor devices it is highly desirable for the metal-semiconductor contact to have a linear I-V behavior. Such type of contact is called Ohmic contact. If the I-V curve is non-linear and asymmetric then the contact is said to be blocking or rectifying contact. The contacts must be able to supply the necessary device current, and the voltage drop across the contact should be small compared to

the voltage drops across the active device regions. An Ohmic contact should not degrade the device to any significant extent, and it should not inject minority carriers.

The room temperature electrical conductivity of spray deposited ZnO thin films is measured by two probe method using silver as a metallic contact. In this technique two silver strips of thickness approximately 70 nm and a gap of 1mm were coated using the mask. The conductivity of the film is calculated by using the basic conductivity formula

$$\rho = \frac{RA}{l} \quad (2.3.16)$$

where, R is resistance of the film, l is length of the contact and A is the area between the contacts.

Area between the contacts can be again written as

$$A = t \times d \quad (2.3.17)$$

where, t is the film thickness and d is the gap between the contacts.

Another important aspect of the electrical characterization is determination of conductivity type of semiconductor materials. Usually two methods employed to accomplish this task are hot probe or thermoelectric probe technique and Hall Effect analysis. The hot probe technique is simple but very efficient (Sze 2000; Schroder 2006). In this method the conductivity type is determined by the sign of the thermal emf or Seebeck voltage generated by a temperature gradient. The hot and cold probes are attached to the semiconductor surface as shown in figure 2.9. The free ends of the probes are wired to a sensitive voltmeter. The hot probe is attached to the positive terminal while the cold probe is connected to the negative terminal. Thermal gradient generate current in the semiconductor. If the semiconductor is *n*-type then electrons diffuse from the hot to the cold region causing the hot probe to develop a positive potential with respect to the cold probe and setting up an electric field that opposes the diffusion. The electric field produces a potential detected by the voltmeter with the hot probe positive with respect to the cold probe. Analogous reasoning leads to the opposite potential for *p*-type samples.

The conductivity type of a semiconductor films can also be determined using Hall effect analysis. In addition to that the Hall effect analysis can reveal valuable

information about carrier concentration, mobility and resistivity of the semiconductor material. Hall effect analysis of a bulk material with a regular shape can be done by measuring the Hall voltage developed across the specimen carrying current in a direction perpendicular to a magnetic field. However in the case of a thin film, it is highly preferable to use the Van der Paw method (1958) to perform the Hall effect analysis.

The sample lamina must be free of holes, which is the primary requirement for Van der Paw method. Although the method can be applied to samples of any arbitrary shape [figure 2.10(a)], if the sample possesses a line of symmetry, then measurements will be particularly straightforward as shown in figure 2.10(b). The measurements require four ohmic contacts on the periphery of the sample; represented by points  $M$ ,  $N$ ,  $O$  and  $P$  in the figure 2.10(b). In the case of a sample of arbitrary shape, these contacts can be made at arbitrary places but if the sample possesses a line of symmetry then it is useful to place one pair of contacts, either  $M$  and  $O$  or  $N$  and  $P$ , on the line of symmetry. The other pair can then be positioned symmetrically with respect to the line. The contacts must be as small as possible.

The resistivity of a symmetrical sample can be determined by allowing a current  $I_{MN}$  to flow through the sample. The suffix  $MN$  denotes that the current enters the sample through the contact  $M$  and leaves the sample through  $N$ . Then the resistance  $R_{MN, OP}$  can be defined as,

$$R_{MN, OP} = \frac{V_P - V_O}{I_{MN}}, \quad (2.3.18)$$

where  $V_P - V_O$  is the potential difference between the contacts  $P$  and  $O$ . An analogous resistance  $R_{NO, PM}$  can be defined as,

$$R_{NO, PM} = \frac{V_M - V_P}{I_{NO}}, \quad (2.3.19)$$

$R_{MN, OP}$  and  $R_{NO, PM}$  are related by the expression,

$$\exp\left(-\frac{\pi d}{\rho}\right) R_{MN, OP} + \exp\left(-\frac{\pi d}{\rho}\right) R_{NO, PM} = 1 \quad (2.3.20)$$

For symmetrical samples the resistances given by equations (2.3.18) and (2.3.19) are equal.

$$\text{i.e., } R_{MN, OP} = R_{NO, PM} \quad (2.3.21)$$

Hence making use of the equations (2.3.20) and (2.3.21), the expression for resistivity  $\rho$  can be written as,

$$\rho = \frac{\pi d}{\ln 2} R_{MN, OP} \quad (2.3.22)$$

The Hall co-efficient too can be measured for the samples in figure 2.10 by applying a current through any one of the contacts, say  $M$ . This current should leave the sample through the contact following the succeeding one, i.e.  $O$ . Now a resistance  $R_{MO, NP}$  should be measured before and after applying a magnetic field  $B$  perpendicular to the surface of the sample. If  $\Delta R_{MO, NP}$  is the difference between the two resistances then the Hall co-efficient  $R_H$  of the sample is given by,

$$R_H = \frac{d}{B} R_{MN, OP} \quad (2.3.23)$$

From the determined value of  $R_H$  the carrier concentration can be found by the equation,

$$n = \frac{1}{R_H q} \quad (2.3.24)$$

where  $q$  is the elementary charge.

The mobility  $\mu$  is related to  $\rho$  and  $n$  by the equation,

$$\mu = \frac{1}{nq\rho} \quad (2.3.25)$$

The study of variation of film resistance with ambient temperature was performed by heating the film in a hot air oven and measuring the resistance at different temperatures. A copper-constantan thermocouple was placed behind the glass substrate for the measurement of ambient temperature. Resistance of the film was noted at different temperature. Then a plot of  $\log(R)$  verses reciprocal of the absolute temperature is used to estimate the activation energy of the carriers in the sample under study. Generally the low temperature region corresponds to the extrinsic



conduction where as the high temperature region corresponds to intrinsic conduction in the film. The thermal activation energy ( $E_a$ ) can be determined by the slope of the plots in the extrinsic region using following equation (Sze 2006),

$$E_a = \frac{2.303 \times k_b \times (\text{slope})}{e} \quad (2.3.26)$$

where  $k_b$  is Boltzmann constant and  $e$  is electronic charge.

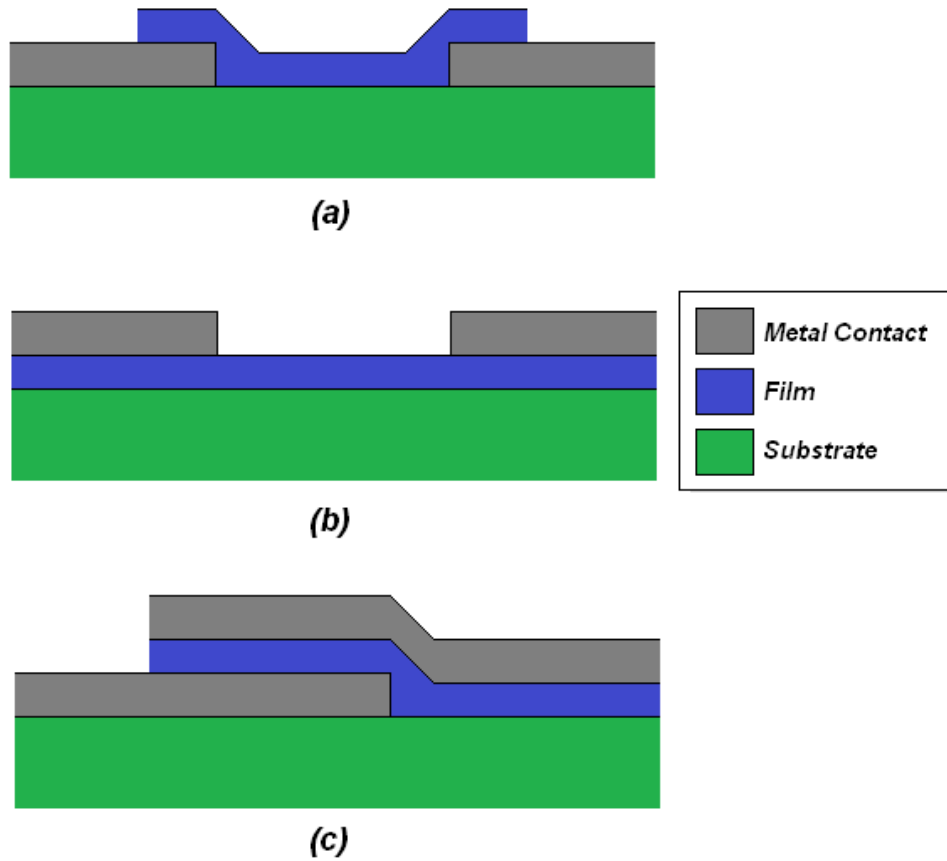


Figure 2.8: Three different structures used for making contacts to thin films. (a) Bridge structure, (b) Planar structure and (c) sandwich Structure.

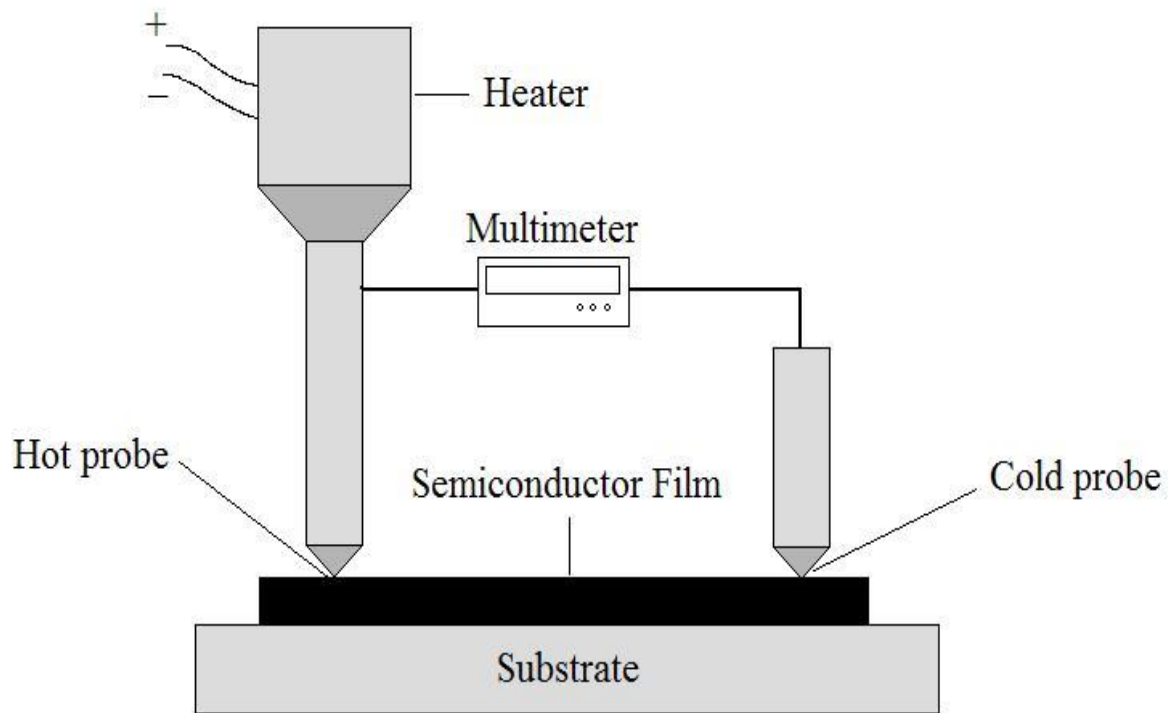


Figure 2.9: The schematic diagram of the experimental setup for hot probe technique.

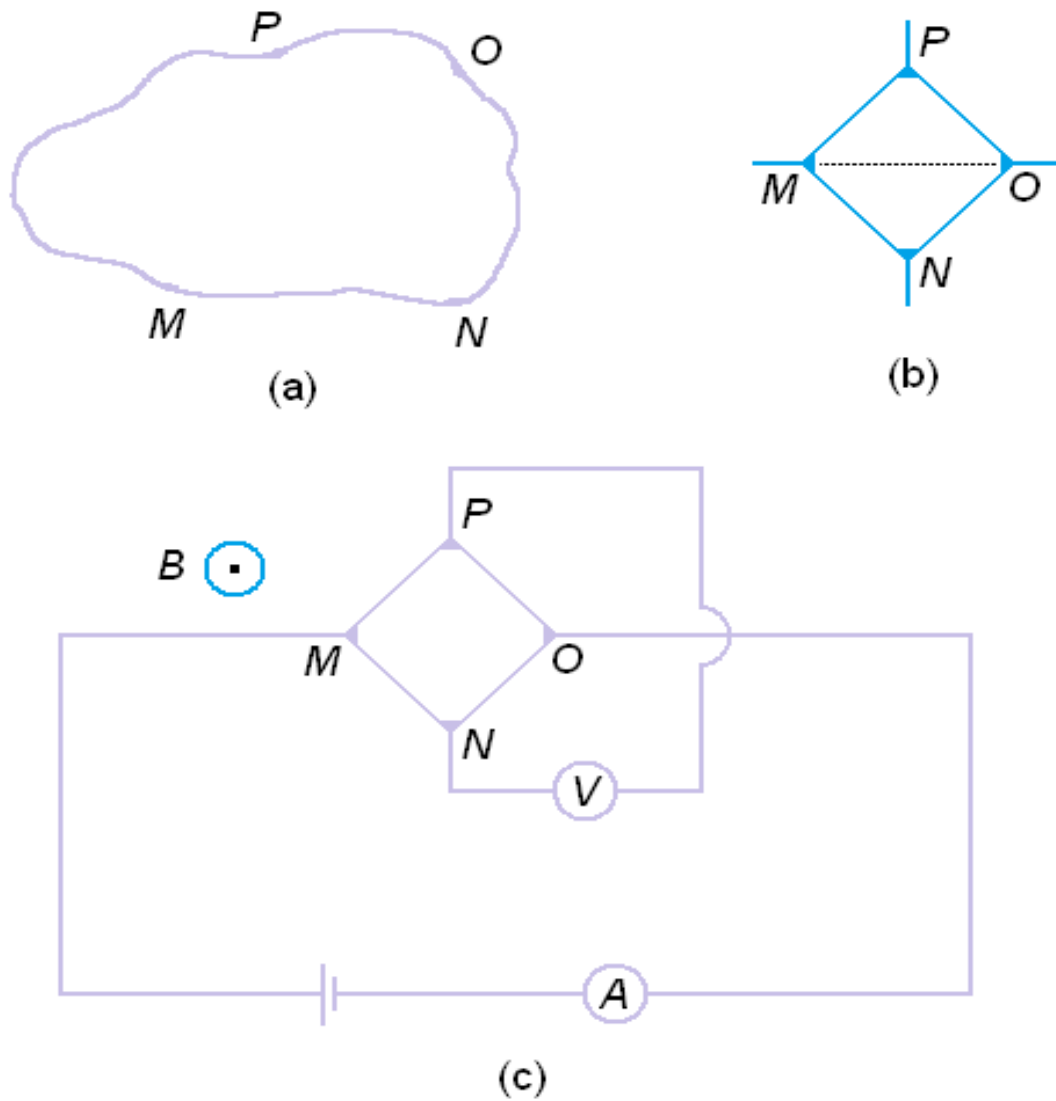


Figure 2.10: The contacts in Van der Pauw setup for (a) a sample of arbitrary shape and (b) for a sample with a line of symmetry (MO). (c) The experimental setup for Hall effect analysis of a sample by Van der Pauw method.



Figure 2.11: Vacuum coating unit (Hind High Vacuum Ltd, Model 12A4D).



Figure 2.12: Keithley 2400 source meter and multimeter 2002.

## **CHAPTER 3**

### **UNDOPED ZnO THIN FILMS**

#### **3.1 PREPARATION OF ZnO THIN FILMS USING ZINC ACETATE PRECURSOR**

Thin film preparation by spray pyrolysis technique, involves spraying a solution / mixture of solutions onto a hot substrate. The solution / mixture of solutions contain compounds of the elements, whose film is required. The droplets, after striking on the hot substrate surface, spread into a circular shaped structure and undergo thermal decomposition. The shape and size of the circular shape depends on the momentum and volume of the droplet. The precursor solution plays an important role in the film formation which includes type of salt (acetate, nitrate or halide) used, concentration of the salt, nature of the solvent and molar ratio of the required elements in the solution are all influencing film formation and its properties. The substrate temperature is another important factor affecting crystallinity and grain size / orientation of the films. Therefore the structure and properties of deposited film can be tailored by varying composition of precursor solution and substrate temperature. In the present work the effect of variation of these parameters on properties of ZnO films has been studied.

The nozzle dimension, precursor solution and carrier gas pressure strongly affect the spray pattern, spray rate, size distribution of droplets and angle at which droplets meet substrate surface which in turn, determine the growth kinetics and hence the quality of the films. Other factors like nature and temperature of the substrate, solution composition, gas and solution flow rates, deposition time and nozzle-to-substrate distance also affect film properties. In order to obtain films with good conductivity, it is essential that complex oxidation of the metal be avoided. This is usually achieved by adding an appropriate reducing agent such as propanol or ethyl alcohol.

Rideal-Elay mechanism and Langmuir - Hinshelwood mechanism explain the growth rate of ZnO thin films (Nakao et al. 1996). According to the former one, films

grow continuously with the molarity of Zn precursor and the formation of ZnO is through the reaction with absorbed water molecules. In spray pyrolysis the incorporation of O<sub>2</sub> into the film during the process of growth is quite difficult to control because the film is deposited in atmospheric condition. Hence in the spray deposited ZnO films, stoichiometry as well as growth rate of the film can be controlled only through Zn-concentration and oxidation in the atmosphere.

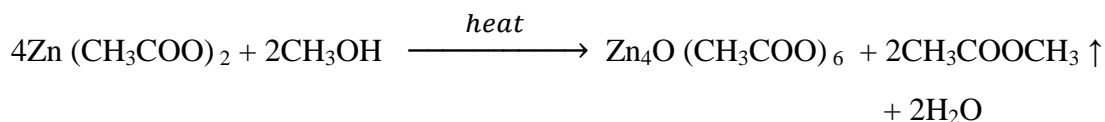
In the present study ZnO thin films have been prepared using two different precursor solutions namely zinc acetate and zinc nitrate. The preparation of ZnO thin films using zinc acetate precursor is discussed in the following section.

### **3.1.1 Experimental details**

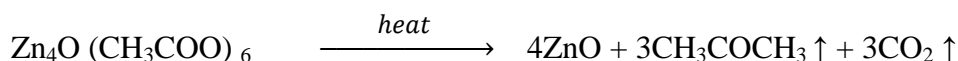
The glass substrates were first washed with the detergent solution 'labolene' and then with the distilled water. These substrates were kept in beaker containing concentrated nitric acid for 24 h. After removing from nitric acid beaker it is washed with distilled water and dried. These glass plates were then rinsed with acetone, isopropyl alcohol and dried. Finally glass plates were washed with distilled water, after drying the vapours of water the substrates were used for deposition. The above cleaning procedure ensured removal of acidic, basic and organic impurities, which may have otherwise adhered to the substrates.

ZnO thin films were prepared on cleaned glass substrate using spray pyrolysis technique. The starting solution was prepared using 0.05 M zinc acetate anhydrous Zn (CH<sub>3</sub>COO)<sub>2</sub> in methanol. The small quantity of acetic acid is added to avoid the formation of zinc hydroxide precipitate. The solution was sprayed on to the heated glass substrate at a constant pressure of 2bar. The deposition of ZnO thin films has been carried out at different temperatures, with air as the carrier gas. The separation between the substrate and nozzle was optimized to get the uniform film deposition. The following pyrolytic reaction takes place during the deposition.





Pyrolysis of basic zinc acetate occurs between 573 and 723 K by a decarboxylation



Gravimetric method was used to determine the thickness of the film and the film thickness is maintained around 600 nm throughout the study. The structural characterization of ZnO films was carried out using X-ray diffractometer with Cu K $\alpha$  radiation of wavelength  $\lambda = 1.5418 \text{ \AA}$ . Scanning electron microscope (SEM) has been used to study the surface morphology of the films. The compositional analysis of ZnO films has been studied using EDAX technique and XPS analysis. The optical transmittance spectra and band gap of ZnO films were studied using UV–Visible spectrophotometer. The electrical properties of the films were determined using computer assisted Keithley instruments.

## 3.2 EFFECT OF DEPOSITION PARAMETERS

ZnO thin films were deposited on glass substrate using zinc acetate precursor by spray pyrolysis technique. Different sets of experiments have been performed by changing the deposition parameter such as substrate temperature, spray rate, precursor concentration and source to substrate distance. Some of the important spray parameters which affect the film properties are discussed in this section.

### 3.2.1 Substrate temperature

In the present study the ZnO thin films were prepared at different substrate temperatures such as 400°C, 450°C and 500°C by maintaining the precursor concentration of 0.05M, spray rate of 2 ml/min, nozzle to substrate distance of 26 cm and compressed air pressure 2bar. Since the *as-deposited* film shows poor crystallinity and high resistivity, all the deposited films are annealed at its growth temperature in air for 4 h. The effect of substrate temperature on structural, optical and electrical properties of ZnO films was studied.

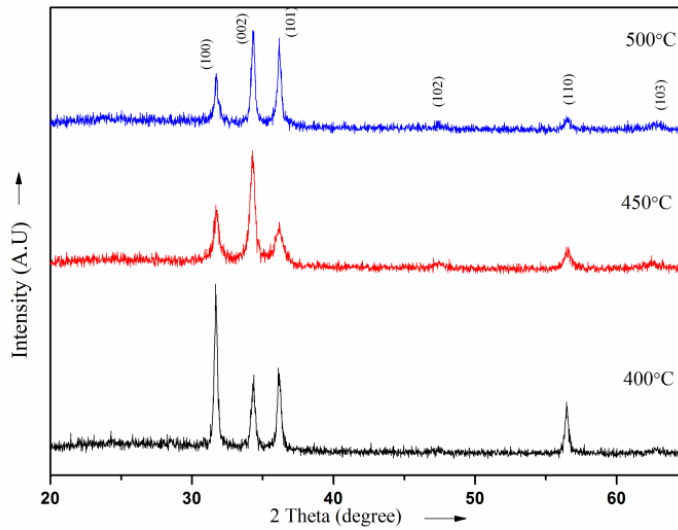


Figure 3.1: XRD pattern of ZnO films deposited at different substrate temperature.

In general, the films grown at substrate temperature less than 300°C are amorphous in nature, while at higher temperatures, polycrystalline films are formed. The XRD pattern of ZnO films deposited at different substrate temperatures are shown in figure 3.1. It is observed that films deposited at different substrate temperatures exhibit polycrystalline hexagonal wurtzite structure. The films deposited at 400°C show (100) texture whereas the films deposited at 450°C and 500°C show (002) texture. The strain ( $\epsilon$ ) and average grain size ( $D$ ) of wurtzite phase of ZnO thin films were calculated using equation 2.3.3.

The grain size of the thin films found to increase slightly with increasing substrate temperature which suggests the improvement in crystallinity of the films. In thin films, lattice mismatch between the deposited film and the substrate or difference in coefficients of thermal expansion of the film and the substrate forms strain in the films. The estimated residual strain in the films is shown in table 3.1. The lattice parameter  $a$  and  $c$  of thin films were calculated using the equation 2.3.2. The calculated values of ' $a$ ' and ' $c$ ' are shown in the table 3.1 and are almost matched with standard data [JCPDS file No. 080 - 0074].

Table 3.1: XRD data of ZnO thin films deposited with different substrate temperature.

Substrate temp. (°C)	Texture	Grain size (nm)	a (Å)	c (Å)	Strain
400	(100)	20.8	3.27	5.24	0.010
450	(002)	22.3	3.27	5.24	0.004
500	(002)	25.6	3.27	5.23	0.002

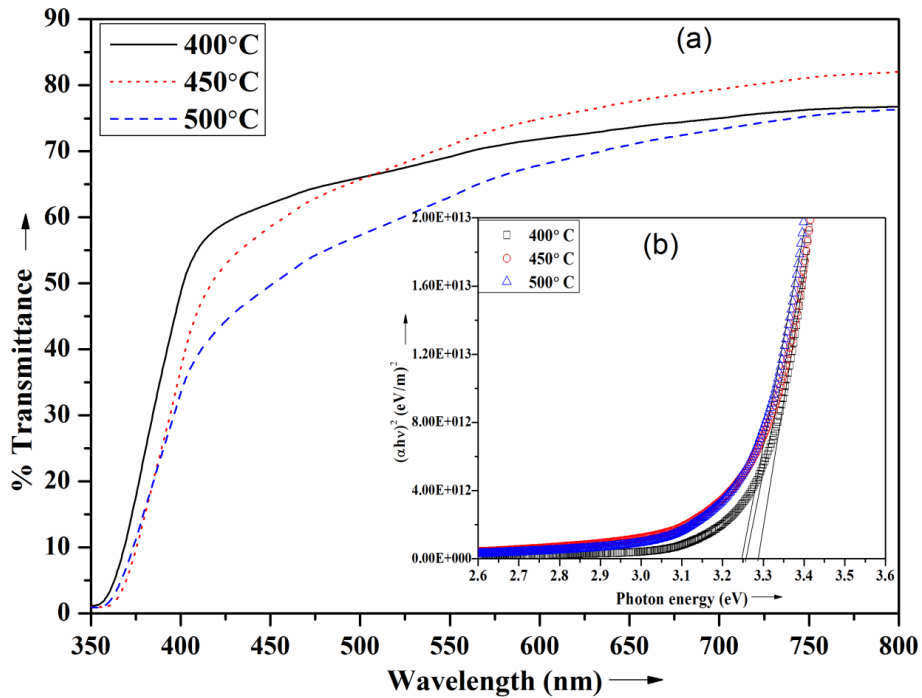


Figure 3.2: (a) Transmittance spectra and (b) Tauc's plot for ZnO thin films deposited at different substrate temperature.

Transmittance spectra of ZnO thin films deposited at different substrate temperatures are shown in figure 3.2(a). It is seen that, all the films show transmittance above 70 % in the visible region and sharp absorption edge in the UV region. The films deposited at 450°C show better optical transmittance in the visible region, reveal that films has less defects and better crystallinity (Rusop et al. 2006). Furthermore there are no interference effects in transmission spectra indicating the uniformity of film surface.

Absorption coefficient ( $\alpha$ ) was determined at the region of strong absorption from the transmittance (T) data, and calculated using the equation 2.3.12. ZnO thin films

have a direct band gap. For the direct allowed transition, the band gap ( $E_g$ ) of ZnO thin films can be determined using the equation 2.3.13.

Figure 3.2(b) shows the variation of  $(\alpha h\nu)^2$  with  $h\nu$  of ZnO thin films deposited at different substrate temperature. The extrapolation of linear part of  $(\alpha h\nu)^2$  verses  $h\nu$  plot to the x-axis gives the energy band gap ( $E_g$ ) of the film. The linear part in the plot indicates the direct allowed transition (Rusop et al. 2007). The measured band gap energy of ZnO thin films deposited at 400°C - 500°C is between 3.25 eV and 3.28 eV which shows no significant change in band gap energies with increasing substrate temperature. These values of optical band gap are in good agreement with literature (Mosbah et al. 2005).

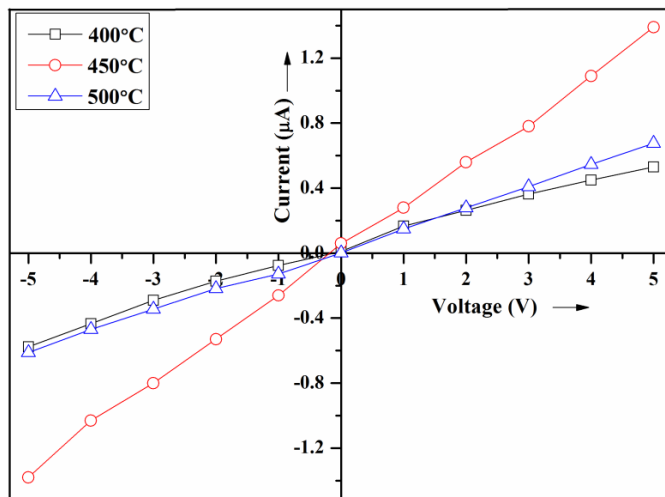


Figure 3.3: I-V characteristics of ZnO thin films deposited at different substrate temperature.

The electrical resistivity measurements of all the ZnO films prepared at different substrate temperatures were carried out using two-probe method. The variation in the electrical conductivity ( $\sigma$ ) of ZnO thin films deposited at different substrate temperatures has been shown in figure 3.3. It is seen that all the films show linear I-V characteristics satisfying Ohmic conduction mechanism. It is also observed that the thin films deposited at 450°C show better electrical conductivity compared with films deposited at 400°C and 500°C.

### 3.2.2 Spray rate

ZnO films were deposited by varying spray rate from 1 ml/min to 6 ml/min keeping substrate temperature at 450°C and other process parameter constant as mentioned earlier. The structural, optical and electrical properties of the obtained films were studied.

The XRD pattern of ZnO films deposited at 450°C for different spray rate has been shown in the figure 3.4. It is observed that films deposited with different spray rate exhibit polycrystalline hexagonal wurtzite structure. The films deposited at 1ml/min to 3 ml/min show (002) texture whereas the films prepared with spray rate 4 ml/min and 6 ml/min show (100) texture. The strain and average grain size of the wurtzite phase of ZnO thin films were calculated using equation 2.3.3 and results are shown in the table 3.2.

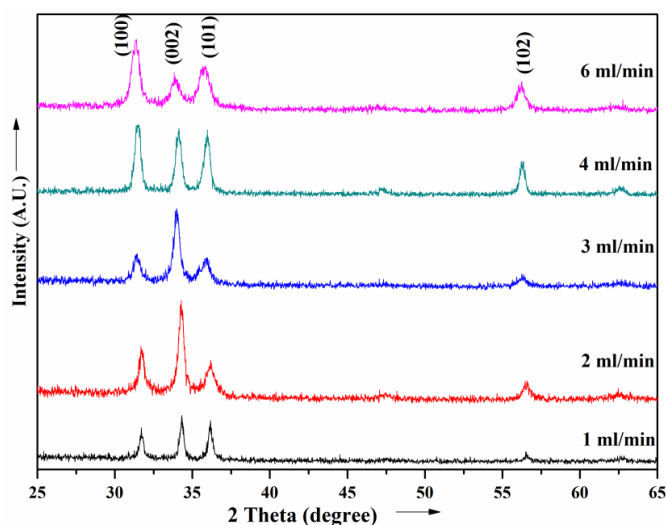


Figure 3.4: XRD pattern of ZnO thin films deposited at different spray rate.

The grain size of thin films were found to increase initially as the spray rate increased from 1 ml/min to 2 ml/min, further increase in the spray rate results in decreasing the grain size. It is found that strain is minimum when the spray rate is 2 ml/min after which it increases. This suggests that the spray rate plays a major role in the manner in which the crystal structure of ZnO thin films. The lattice parameter  $a$ , and  $c$  were calculated using the equation 2.3.2. The calculated value of ' $a$ ' and ' $c$ ' are

in agreement with the standard value [JCPDS file No. 080-0074,  $a= 3.25\text{\AA}$ ,  $c= 5.22\text{\AA}$ ].

Table 3.2: XRD data of ZnO thin films deposited at different spray rate.

Spray rate	Texture	D (nm)	a ( $\text{\AA}$ )	c ( $\text{\AA}$ )	Strain
1 ml/min	(002)	19.2	3.26	5.24	0.004
2 ml/min	(002)	22.3	3.27	5.24	0.004
3 ml/min	(002)	21.0	3.27	5.24	0.005
4 ml/min	(100)	18.5	3.27	5.25	0.006
6 ml/min	(100)	16.3	3.28	5.25	0.011

Transmittance spectra of the thin films prepared with different spray rates are presented in figure 3.5(a). It is found that, optical transmittance of these films initially increases i.e., as the spray rate increase from 1 ml/min to 2 ml/min; further increase in spray rate decreases the optical transmittance of the films. The films deposited at the spray rate of 2 ml/min show better optical transmittance in the visible region, which reveal that films has less defects and better crystallinity (Rusop et al. 2006). Further there are no interference effects in transmission spectra indicating the uniformity of surface and small grain size.

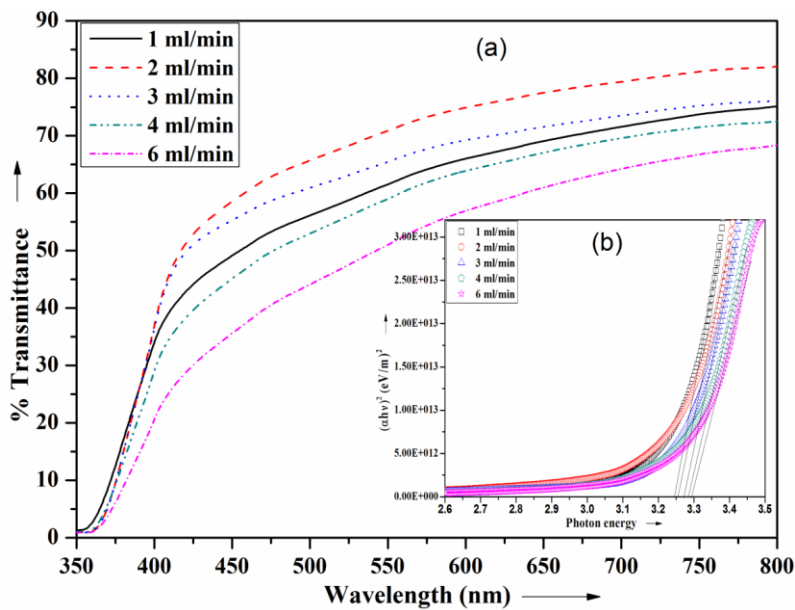


Figure 3.5: (a) Transmittance spectra and (b) Tauc's plot for ZnO thin films deposited at different spray rate.

For a direct allowed transition, the band gap of thin films can be determined using the equation 2.3.13. The variation of  $(\alpha h\nu)^2$  with  $h\nu$  of thin films deposited at different spray rate is shown in the figure 3.5(b). The energy band gap of ZnO thin films is found to be in the range  $3.26 \pm 0.03$  eV for the different spray rate used.

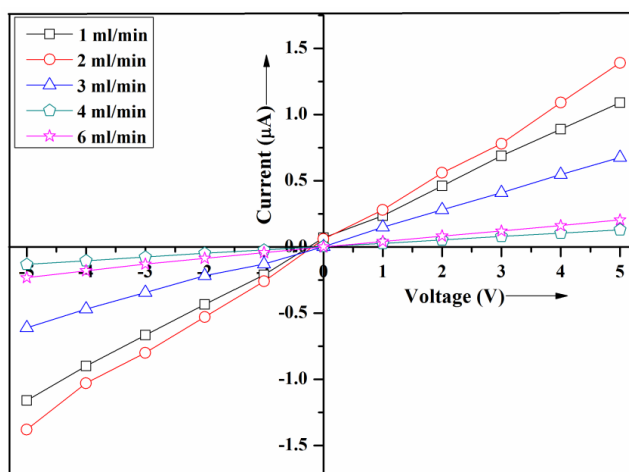


Figure 3.6: I-V characteristics of ZnO thin films deposited at different spray rate.

The variation in the electrical conductivity ( $\sigma$ ) of thin films deposited at different spray rate has been shown in figure 3.6. All the films show linear I-V characteristics satisfying Ohmic conduction mechanism. It is noted that the conductivity of the films deposited at  $450^\circ\text{C}$  with slow spray rate show lesser resistivity compared with films deposited at higher other spray rate.

### 3.2.3 Precursor molarity

ZnO films were deposited by varying only precursor concentration of spray solution from 0.05M to 0.2M, keeping substrate temperature  $450^\circ\text{C}$ , spray rate 2 ml/min and other deposition parameters constant as mentioned earlier. The structural, optical and electrical properties of the obtained films were studied.

It is observed from the XRD pattern of ZnO films shown in figure 3.7 that films deposited using different precursor molarities exhibit polycrystalline hexagonal wurtzite structure with (002) texture. The residual strain and average grain size of the wurtzite phase of ZnO thin films were calculated using the equation 2.3.3. The grain

size of ZnO films found to increase with increasing solution concentration from 0.05M to 0.2M indicating that improvement in the crystallinity of the films. The strain developed in the films were also evaluated and found that strain is minimum when the precursor molarity is 0.05M after which it increases (table 3.3). This suggests that the precursor molarity plays a major role in the crystal structure of ZnO thin films.

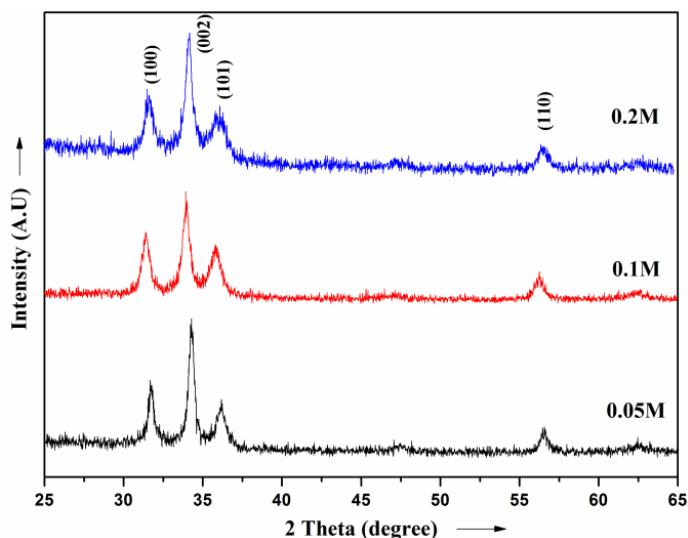


Figure 3.7: XRD pattern of ZnO thin films deposited at different precursor molarity.

Table 3.3: XRD data of ZnO films deposited with different precursor molarity.

Molarity (M)	Texture	D (nm)	a (Å)	c (Å)	Strain
0.05	(002)	22.3	3.27	5.24	0.004
0.1	(002)	17.1	3.27	5.24	0.007
0.2	(002)	16.4	3.26	5.25	0.011

Transmittance spectra of ZnO films deposited at different precursor molarities are shown in the figure 3.8(a). The films prepared using 0.05M precursor molarity show better transmittance in the visible region. At higher precursor molarity, optical transmittance of the thin films found to decrease. The optical band gap of thin films prepared by varying precursor molarity was calculated from optical absorption studies using the equation 2.3.13. The Tauc's plot for ZnO thin films deposited at different precursor molarities are presented in the figure 3.8(b). Optical band gap of ZnO film deposited at 0.05M is 3.24 eV which is found to increase with increase in precursor molarity.



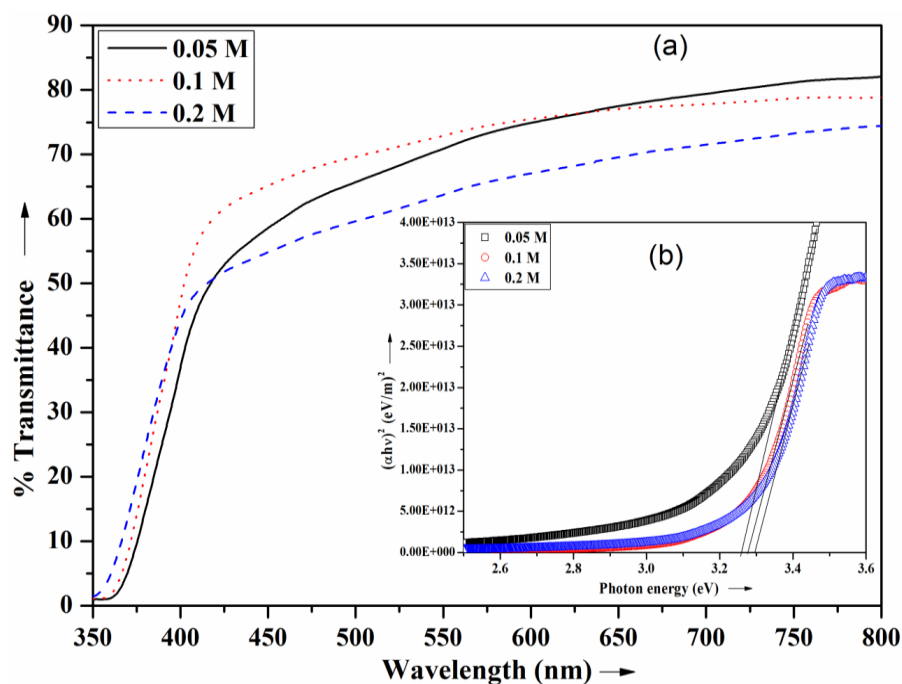


Figure 3.8: (a) Transmittance spectra and (b) Tauc's plot for ZnO thin films deposited at different precursor molarity.

The electrical resistivity measurements of thin films prepared from different molarities were carried out using two-probe method. All the films show linear I-V characteristics. It is found that from the electrical measurements, the resistivity of thin films increases slightly with increasing the precursor molarity. Hence the optimum spray parameters for obtaining good optical and electrical properties of ZnO thin films prepared using zinc acetate precursor is shown in the table 3.4.

Table 3.4: The optimum deposition parameters to prepare ZnO thin films.

Deposition parameter	Optimum condition
Substrate temperature	450°C
solvent	Methanol
Nozzle to substrate distance	26 cms
Precursor molarity	0.05 M
Spray rate	2 ml/min
Compressed air pressure	2 bar
Carrier gas	air

### 3.3 EFFECT OF FILM THICKNESS

The ZnO thin films were prepared using zinc acetate precursor and optimised deposition parameters (table 3.4) were used for the film deposition. The films of different thickness were prepared and all these films were annealed at 450°C in air. The structural, optical and electrical properties of these thin films were studied and the results are discussed in this section.

The XRD pattern of ZnO films with different thickness are shown in the figure 3.9. From the figure it is observed that all the films exhibit hexagonal wurtzite structure with (002) texture. The 450 nm thin films show broad and less intensity peaks indicating low level of crystallinity of films. As the films thickness increases the intensity of (100), (002) and (101) peaks are also increases indicating improvement in the crystallinity of the films.

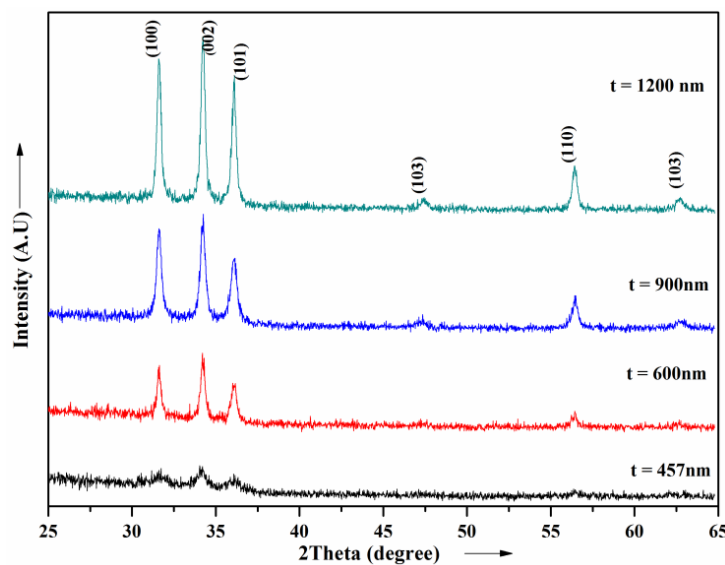


Figure 3.9: XRD pattern of ZnO films of different thickness.

The average grain size and strain in the ZnO films with different thickness were calculated using the equation 2.3.3 and the results are summarized in the table 3.5. Grain size of the ZnO thin films found to increase with increasing film thickness, indicating improvement in crystallinity of the films. The lattice parameter a and c of the films with different thickness were calculated using the equation 2.3.2. The significant change in the lattice parameter was not observed.

Table 3.5: XRD data of ZnO films with different thickness.

Film thickness (nm)	Texture	D (nm)	Strain
450	(002)	14.4	0.002
600	(002)	23.2	0.004
870	(002)	28.6	0.0008
1200	(002)	39.4	0.0006

The morphology of thin film (600 nm) shows smooth and uniform distribution of grains on the film surface [fig. 3.10 (a)], whereas the morphology of thick (1.2  $\mu\text{m}$ ) films show fiber like structures with rough surface [fig. 3.10(b)]. This suggests that the surface roughness increases with increasing film thickness. The percentage composition of zinc and oxygen in ZnO films is investigated by EDAX analysis.

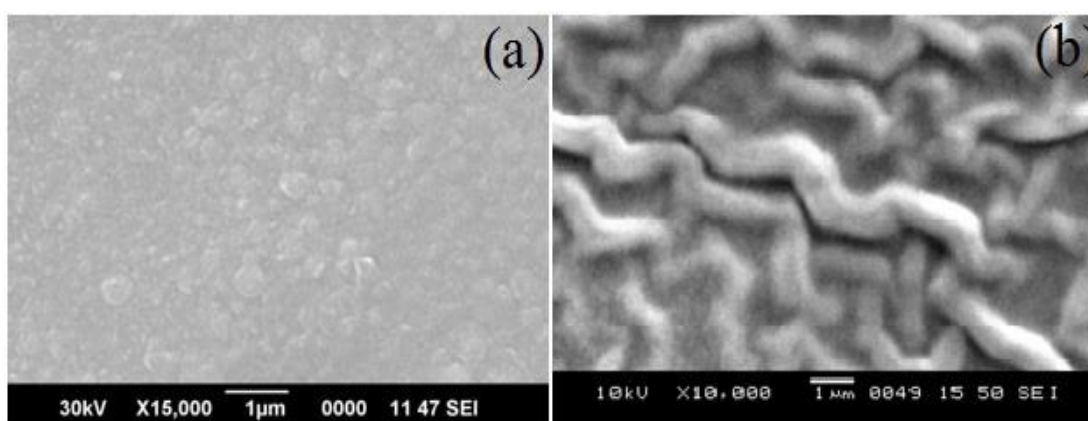


Figure 3.10: SEM image of ZnO films with thickness (a) 600 nm and (b) 1.2  $\mu\text{m}$ .

Transmittance spectra of thin films with different thickness are shown in figure 3.11(a). The sharp absorption edge is observed in the UV range for all films. The average transmittance of thin films is found to decrease from 85% to 70% with increase in film thickness from 450 nm to 1.2  $\mu\text{m}$  respectively. The decrease in the optical transparency of ZnO films may be due to increase in the film thickness and hence the surface roughness. This result was expected as more and more photons are adsorbed in a material when the thickness is increased (Prasada and Santhosh 2009). Seo et al. (2014) reported the decrease in the transmittance with increasing film thickness due to the free carrier absorption in their AGZO films.

The variations of  $(\alpha h\nu)^2$  with  $h\nu$  for ZnO films with different thickness are shown in the figure 3.11(b). The optical band gap of ZnO thin films found to increase from 3.24 eV to 3.29 eV with increase in film thickness from 450 nm to 1.2  $\mu\text{m}$  respectively. This increase in optical band gap of ZnO films with thickness is consistent with reduced strain in the film. According to the reports strain changes the inter atomic spacing of semiconductors which affects the energy gap (Pankove 1971) and band gap increases for increase in compressive strain along c-axis but decreases for increase in tensile strain (Prasada and Santhosh 2009). This explains the increase in band gap with the decrease of tensile strain as the thickness increases.

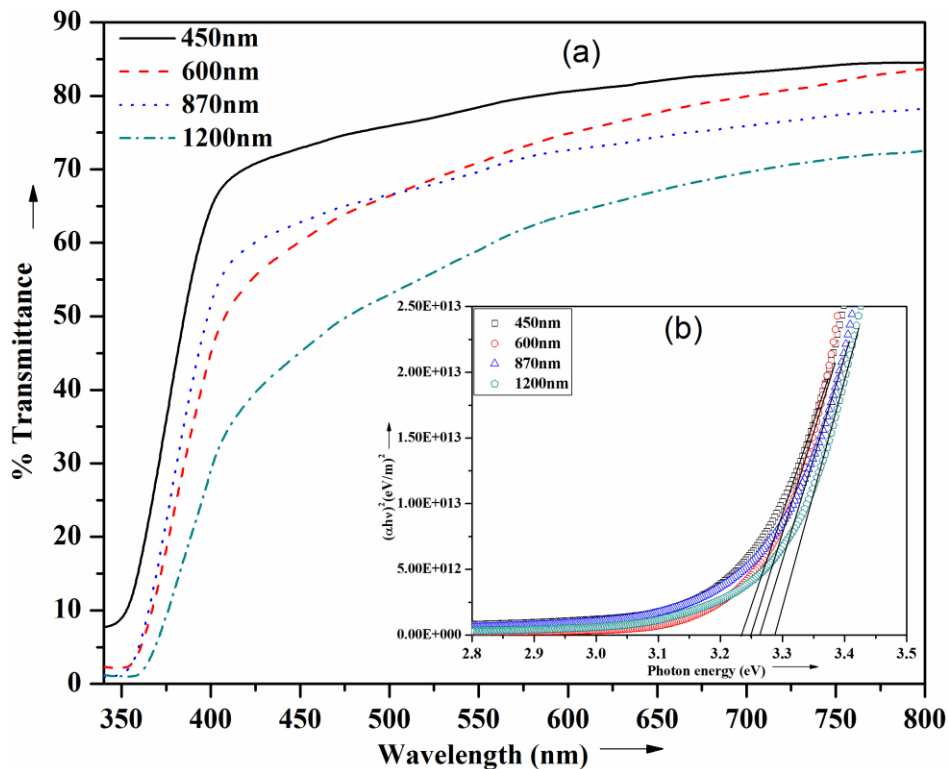


Figure 3.11: (a) Transmittance spectra and (b) Tauc's plot for ZnO films with different thickness.

The electrical conductivity of the ZnO film was determined using the equation 2.3.16. The linear I-V characteristics of thin films with different thickness are shown in the figure 3.12 which shows the stability of current over a range of voltage from -5 V to +5 V. The conductivity of ZnO thin films observed in the present case is found to increase with increase in the film thickness. Films with thickness 1.2  $\mu\text{m}$  show highest conductivity of 0.79 S/cm. In general increase in conductivity of ZnO films

with increase in film thickness is due to increased grain size and decreased grain boundary scattering by the reduction of the number of grain boundaries.

Table 3.6: Optical and electrical data of ZnO films with different thickness.

Film thickness (nm)	$E_g$ (eV)	$\sigma$ (S/cm)	$E_a$ (meV)
450	3.24	0.11	379
600	3.25	0.16	348
870	3.27	0.39	341
1200	3.29	0.80	241

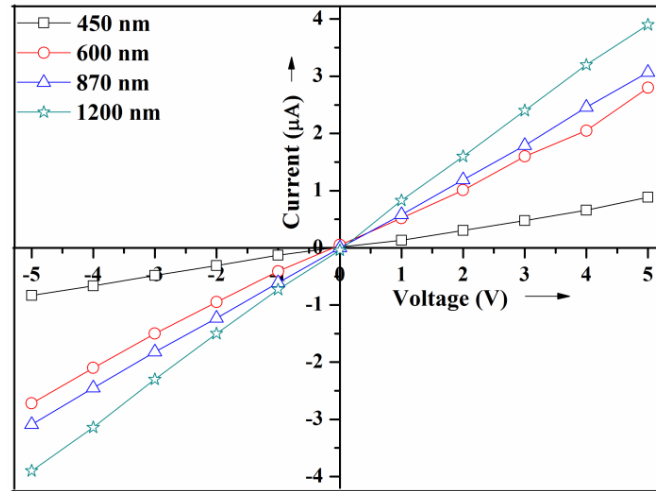


Figure 3.12 : I-V characteristics of ZnO films of different thickness.

The variation of  $\log R$  vs. reciprocal temperature ( $1/T$ ) of these films is shown in figure 3.13. From the logarithmic resistance profile with respect to reciprocal of temperature, the thermal activation energy of thin films is calculated using the equation 2.3.26. From the figure 3.13, it is observed that the ZnO films exhibit two linear parts in the graph indicating the presence of two activation energies at different region of temperature representing one shallow and deep donor level near the bottom of the conduction band. The estimated activation energy of thin films of different film thickness is shown in table 3.6. These activation energies depend on the film thickness. The activation energy increases with film thickness in the low temperature region [(0.0024 – 0.003) (1/K)] and decreases with thickness in the high temperature region [(0.0019–0.0024) (1/K)]. This is due to the low concentration of free atoms, in the low temperature range [(0.0024 – 0.003) (1/K)].

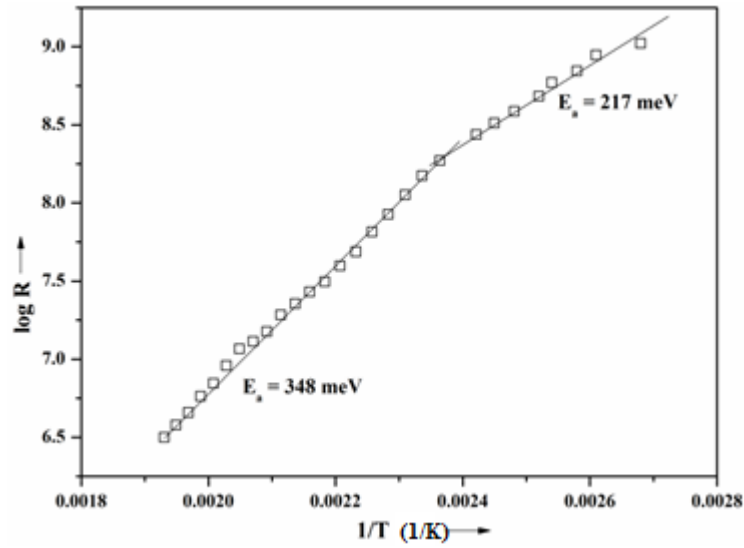


Figure 3.13: Plot of logR vs. 1/T of undoped ZnO thin film.

### 3.4 EFFECT OF ANNEALING TEMPERATURE

The *as-deposited* ZnO films were annealed at 450°C for different time durations. The annealing duration was varied from 0 to 6 h. It has been revealed that films annealed at 450°C for 4 h show better optical transmittance and electrical conductivity (Sadananda et al. 2014). The films annealed at 450°C for more than 4 h show a decrease in the transmittance. The increase in annealing duration increases the surface roughness of the films; hence light loss due to scattering is more. In order to study the effect of annealing temperature on the properties of ZnO thin films, the films were annealed at different temperatures in air. The results are discussed in the following section.

The XRD pattern of ZnO thin films annealed at different temperature are shown in the figure 3.14. On comparing with standard data, it is observed that all the films exhibit hexagonal wurtzite polycrystalline structure with (002) texture. The *as-deposited* films show broad and less intensity peaks indicating low level of crystallinity of thin films. As the annealing temperature increases the intensity of (100), (002) and (101) peaks are also found to increase indicating improvement in the crystallinity of the films.

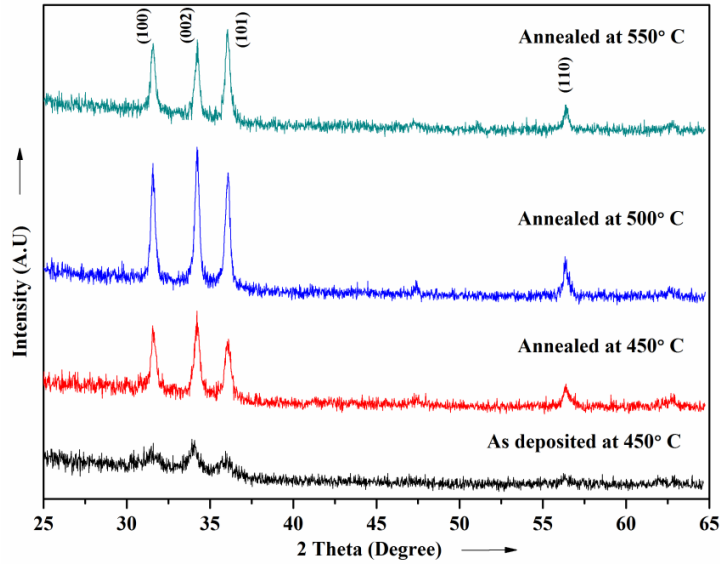


Figure 3.14: XRD pattern of ZnO thin films annealed at different temperatures.

The strain and average grain size of *as-deposited* and annealed ZnO were estimated from the equation 2.3.3. The figure 3.15 shows the variation of  $\beta\cos\theta/\lambda$  vs.  $4\sin\theta/\lambda$  for *as-deposited* and annealed ZnO films. The reciprocal of intercept on the y-axis gives the average grain size, and the slope of the plot gives the amount of residual strain. The grain size in the films found to increase with increase in annealing temperature (table 3.7), this is due to the annealing temperature provides thermal energy to activate atom diffusion and hence, facilitate to repairing the dislocated atomic occupancies and even promote the coalescence of adjacent particles (Wang et al. 2011). It is noted that strain is more in the *as-deposited* films and found to reduce (table 3.7) as the annealing temperature increased which indicates improvement in the crystallinity of thin films. The calculated lattice parameter remains unaffected with increase in annealing temperature up to 550°C.

Table 3.7: XRD data of ZnO films annealed at different temperatures for 4 h.

Annealing temp. (°C)	Texture	D (nm)	Strain
As-deposited at 450	(002)	8.9	0.028
450	(002)	22.3	0.004
500	(002)	34.4	0.0005
550	(101)	35.6	0.0006

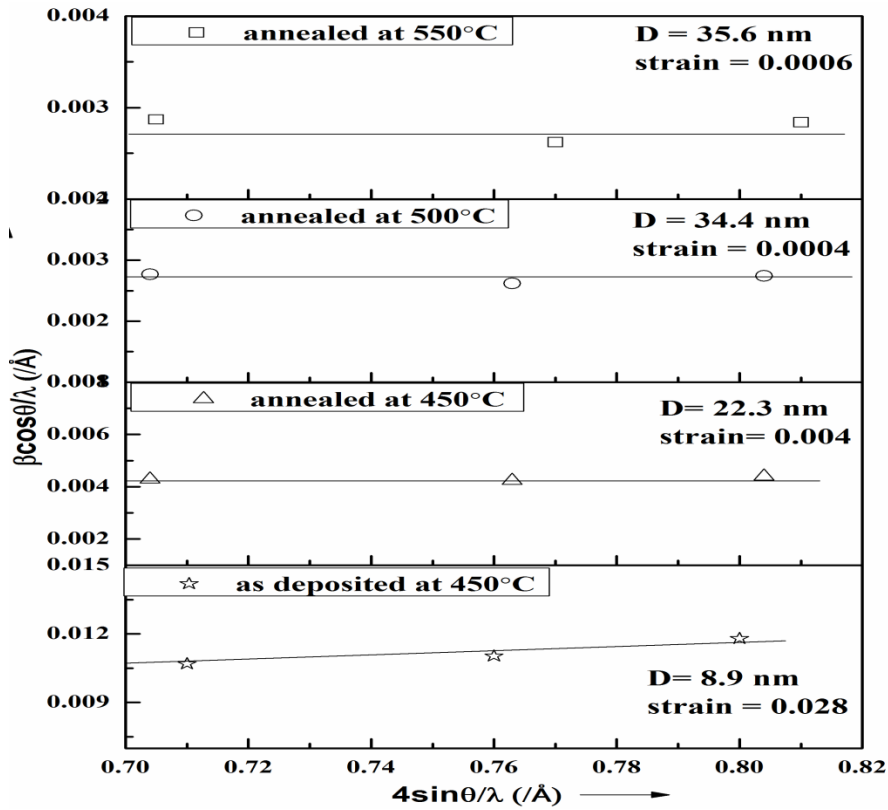


Figure 3.15: Strain and grain size evaluation of *as-deposited* and annealed ZnO films.

The scanning electron micrographs of ZnO thin films are shown in the figure 3.16. It shows that the *as-deposited* films (a) have non-uniformly distributed grains on the film surface. The morphology of the annealed film shows smooth and uniform distribution of grains on the film surface. It is observed that the grain size of the annealed ZnO films is increased with annealing. The film surface is almost uniform, continuous and without pinholes.

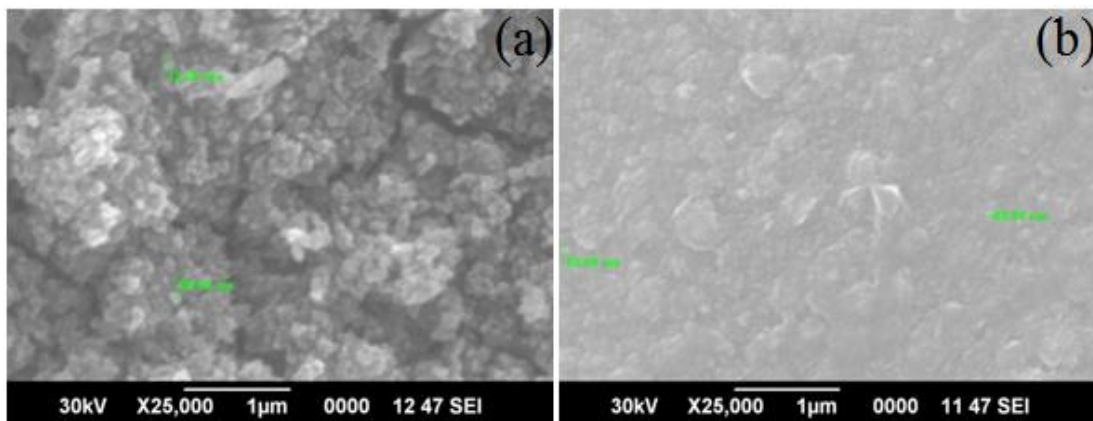


Figure 3.16: SEM image of ZnO films (a) *as-deposited* and (b) annealed at 450°C.



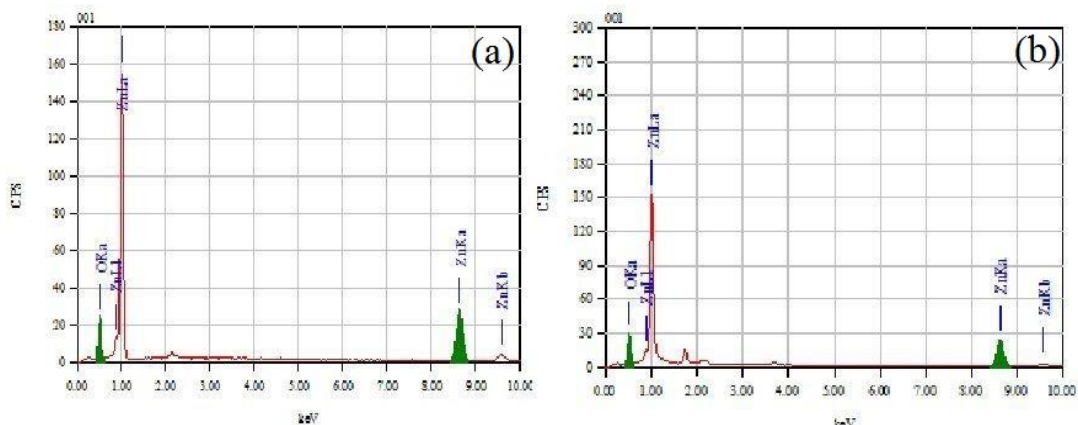


Figure 3.17: EDAX analysis of (a) *as-deposited* and (b) annealed ZnO thin films.

The composition analysis of ZnO films prepared by zinc acetate precursor is studied using EDAX technique. The EDAX spectrum of *as-deposited* and annealed ZnO thin films are shown in the figure 3.17 (a) and (b) respectively. The spectrum shows the presence of zinc and oxygen in the films. It is noted that the elements which are lighter than Na atom cannot be detected by EDAX technique. Hence technique is not so accurate in detecting the quantity of oxygen present in the film. The analysis showed that *as-deposited* films are oxygen deficient whereas the annealed films are found to almost stoichiometric. The percentage compositions of Zn and O in the *as-deposited* and annealed thin films are shown in the table 3.8.

Table 3.8 : Composition analysis of ZnO films using EDAX technique.

ZnO Sample	elements	
	Zn (at. %)	O (at. %)
<i>As-deposited</i>	52.09	47.91
annealed at 450° C for 4 h	49.34	50.66

In the present study, using XPS spectra, atomic percentage and chemical states of zinc and oxygen in the *as-deposited* and annealed ZnO films were investigated. The XPS survey spectra of thin films are first produced before the high resolution scan of oxygen and zinc. The survey spectra of *as-deposited* and annealed ZnO films acquired at pass energy 75 eV are shown in the figure 3.18 (a) & (b) respectively. It is observed from the survey scan that *as-deposited* thin films found to have 52.72 at. % of zinc

and 47.28 at. % of oxygen and in the annealed thin films found to have 36.46 at. % of Zn and 63.54 %

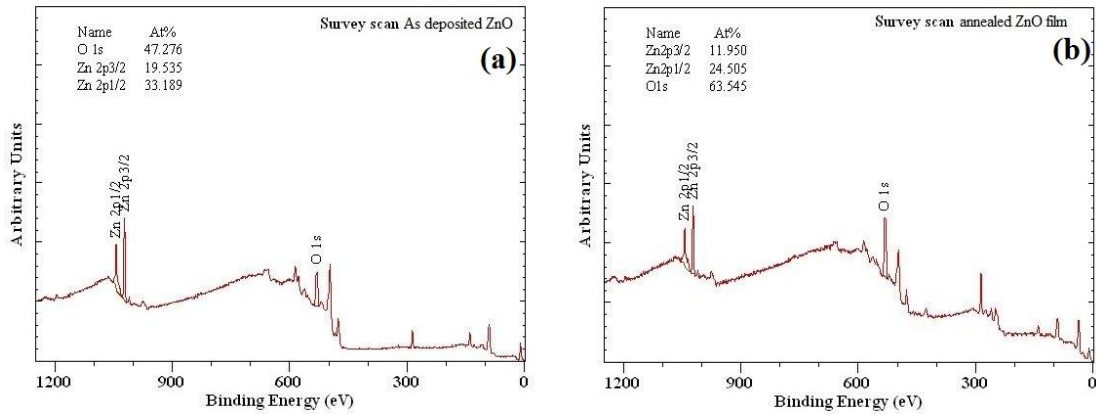


Figure 3.18: Survey scan of ZnO thin films (a) *as-deposited* and (b) annealed at 450°C for 4h.

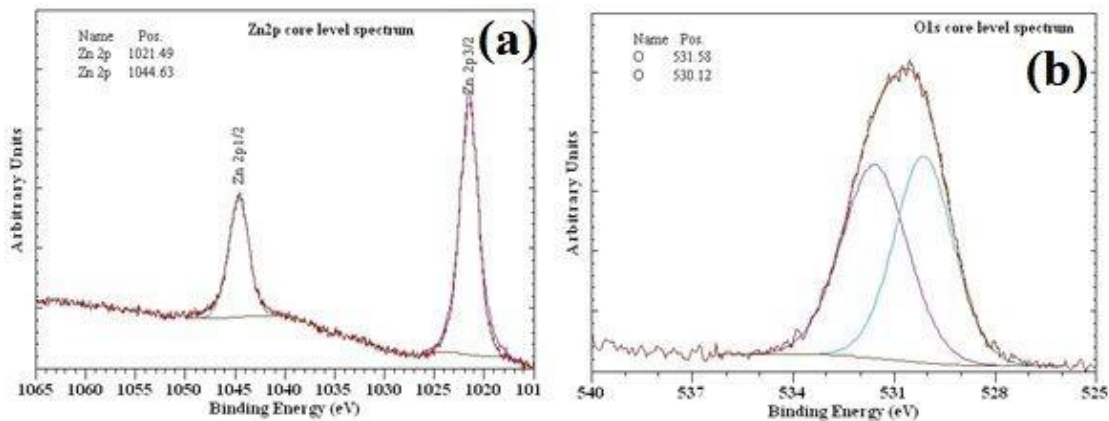


Figure 3.19: XPS spectra of *as-deposited* ZnO films (a) Zn2p and (b) O1s spectrum.

The Zn2p and O1s spectra of *as-deposited* thin films acquired at pass energy of 25 eV is shown in the figure 3.19 (a) and (b) respectively. From Zn2p spectra, it is noticed that Zn2p<sub>3/2</sub> peak appeared at binding energy of 1021.50 eV and 1021.60 eV for *as-deposited* and annealed films respectively. These peaks are attributed to Zn-O bond rather than metallic Zn-Zn bond since the binding energy of Zn-O bond (1021.90 eV) is higher than Zn-Zn binding energy (1021.45 eV). Similarly Zn2p<sub>1/2</sub> peak of *as-deposited* and annealed films appeared at 1044.63 eV and 1044.90eV respectively, can also be attributed to binding energy of Zn-O bond (1044.78) (Aksoy et al. 2012).

In the O1s spectra of *as-deposited* film, peak could be divided in to two Gaussian components one with low binding energy and other with high binding energy, these peaks located at 530.12 eV and 531.58 eV. The peak position on the low binding energy side of O1s spectra at 530.12 eV corresponds to  $O^{2-}$  ions on wurtzite structure of hexagonal  $Zn^{2+}$  ion array, surrounded by Zn atoms with their full complement of nearest neighbour  $O^{2-}$  ions (Chen et al. 2001). The other component located at higher binding energy at 531.58 eV is arised either due to the loosely bound oxygen or due to the presence of hydrated oxides in the film. The atomic percentage of zinc and oxygen in the ZnO films were estimated and are found to 52.17 at.% and 47.83 at.% respectively. From the O1s spectrum it is confirmed that, among the total 47.83 at.% of oxygen present in the film, 48.8 at.% of oxygen are strongly bonded to zinc and rest 51.2 at. % of oxygen is loosely bonded to the surface.

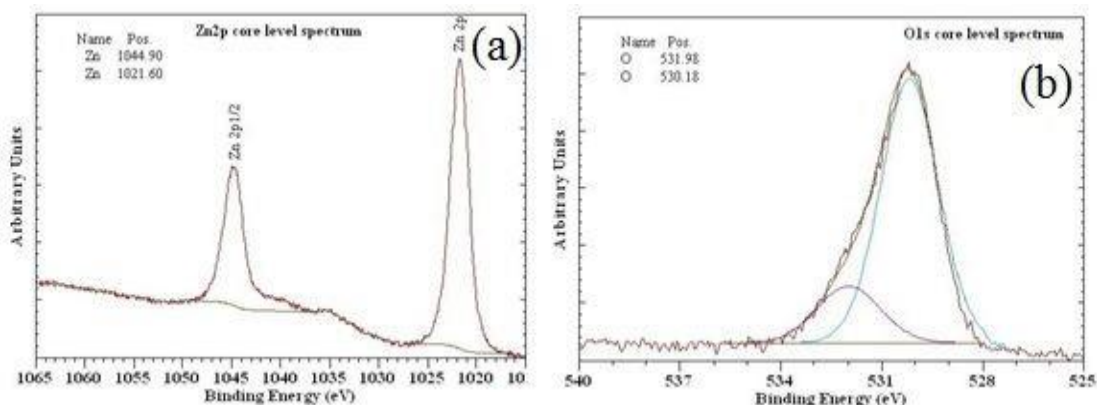


Figure 3.20: XPS spectra of annealed ZnO thin films (a) Zn2p spectra and (b) O1s spectra.

The Zn2p and O1s spectra of the annealed films acquired at pass energy 25 eV is shown in the figure 3.20 (a) and (b) respectively. In the O1s spectra of annealed ZnO films, two peaks are positioned at 530.18 eV and 531.98 eV. The peak position on the low binding energy side of the O1s spectra at 530.18 eV corresponds to  $O^{2-}$  ions on wurtzite structure of hexagonal  $Zn^{2+}$  ion array, surrounded by Zn atoms with their full complement of nearest neighbour  $O^{2-}$  ions [Chen et al. 2001]. The atomic percentage of zinc and oxygen in the ZnO films were estimated and are found to 36.46 at. % and 63.54 at. % respectively. From the O1s spectrum it is confirmed that, among the total

63.54 at. % of oxygen present in the film, 70.7 at. % of oxygen are bonded to zinc and rest 29.3 at. % of oxygen is loosely bonded to the surface.

Transmittance spectra of ZnO thin films annealed at different temperatures are shown in the figure 3.21. From the fig. it is seen that films annealed at 450°C exhibit better optical transmittance in the visible region, further increase in annealing temperature results reduction in the optical transmittance of the films. The increase in optical transmittance of ZnO films with annealing is may be due to the increase in grain sizes, structural homogeneity, and crystallinity (Kalyani et al. 2013). The decrease in the optical transmittance at higher annealing temperature may be due increase in surface roughness which leads to more light loss due to optical scattering.

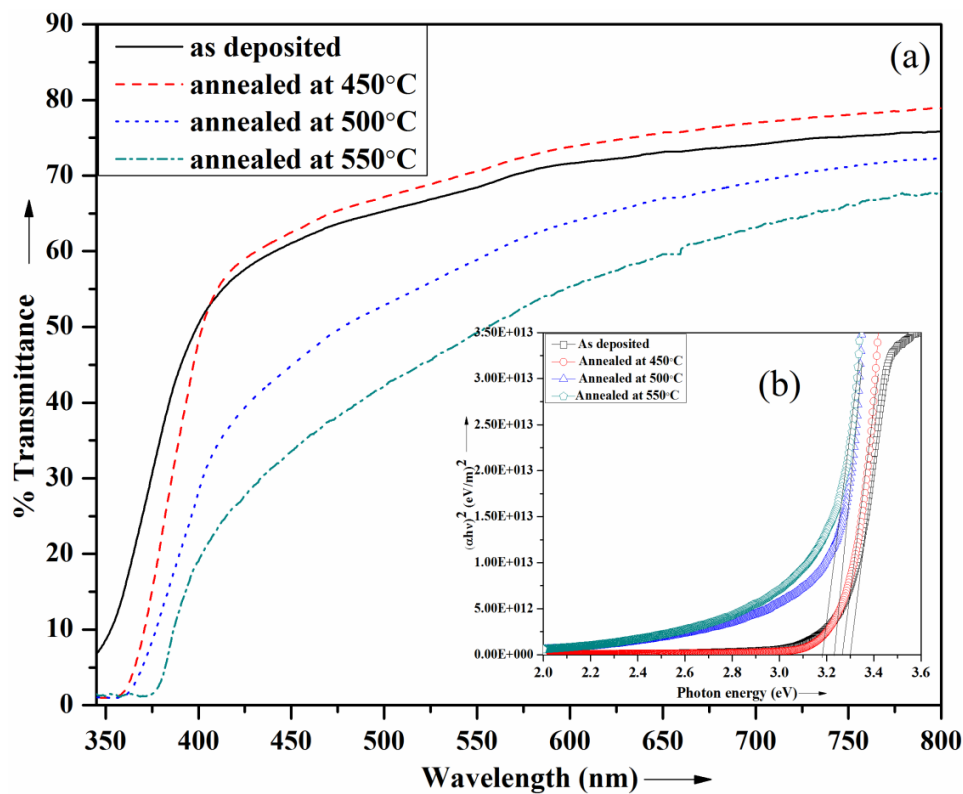


Figure 3.21: (a) Transmittance spectra and (b) Tauc's plot for ZnO thin films annealed at different temperatures for 4 h.

The variations of  $(\alpha h\nu)^2$  with  $h\nu$  for the *as-deposited* and annealed films are shown in the figure 3.21 (b). The band gap of *as-deposited* ZnO film is found to be 3.30 eV, which reduces to 3.19 eV as the annealing temperature increases up to 550°C. According to reports, decrease in the band gap occurs due to the appearance of

band tail resulting from defects associated with the presence of cavities and surface roughness (Regragui et al. 2001).

The linear I-V characteristics of ZnO films are shown in the figure 3.22. In the present study the electrical conductivity of *as-deposited* ZnO film is found to be very low of the order of 0.004 S/cm. The poor conductivity of *as-deposited* films may be due to grain boundary effects and also, due to adsorption oxygen since air is used as carrier gas. There is a possibility of chemisorptions of large number of oxygen molecules on the surface and grain boundaries of the film, which will create the potential barrier that affects the electrical transport causing a reduction in conductivity (Joseph et al. 1999).

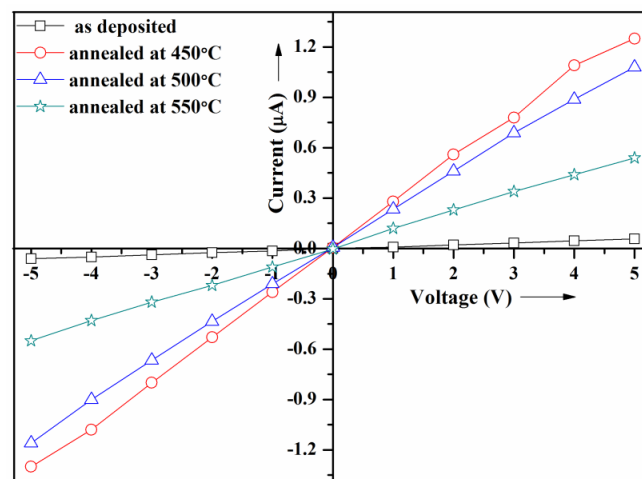


Figure 3.22: I-V characteristics of ZnO films annealed at different temperatures.

The *as-deposited* thin films are annealed at different temperatures in air for 4 h and the conductivity data is presented in table 3.9. It is noted that the conductivity of the thin films increased by two orders of magnitude after annealing the sample. The conductivity of thin films found to increase when annealed at 450°C and decreased slowly with further increasing annealing temperature. This might be due to either an increase in the carrier concentration and/or increase of the mobility. The increase of annealing temperature provides energy to repair the atomic dislocations and also promotes the coalescence of smaller grains to grow large grains. The increase in grain size, thus leads to the increase of mobility change that has been reported in the literature (Rusop et al. 2006).

Table 3.9: Optical and electrical data of ZnO films annealed at different temperatures for 4 h.

Annealing temp.(°C)	$E_g$ (eV)	$\sigma$ (S/cm)	$E_a$ (meV)		$n$ (1/cm <sup>3</sup> )	$\mu$ (cm <sup>2</sup> V <sup>-1</sup> s <sup>-1</sup> )
As-deposited at 450	3.30	0.004	---		---	---
450	3.24	0.16	348	217	$9.92 \times 10^{16}$	9.38
500	3.23	0.11	355	226	$9.54 \times 10^{16}$	7.86
550	3.18	0.08	406	239	$9.22 \times 10^{16}$	4.22

In order to understand the nature of charge carriers in ZnO thin film, hot probe technique is used. The experiment is done by attaching a cold probe and a hot probe to a semiconductor surface. Both probes are wired to a sensitive electrometer. In the present study cold probe is connected to the negative terminal and hot probe is connected to the positive terminal of the meter, Keithley multimeter reads positive voltage. This confirms n-type nature of charge carriers in ZnO thin film.

The variation of  $\log R$  with reciprocal of temperature ( $1/T$ ) of ZnO thin films is shown in figure 3.13. From the logarithmic resistance profile with respect to reciprocal of temperature, the thermal activation energy was calculated using equation 2.3.26 and the results are shown in table 3.9. The graph shows a linear behavior in two regions indicating the presence of two donor levels below the conduction band. The first one from (0.0019-0.0024) 1/K and the other from (0.0024-0.003) 1/K. In these two ranges the activation energy is proportional to the slope according to equation 2.3.26. ZnO thin film presents first donor level with activation energy of 217 meV in the ( $1/T$ ) range (0.0024-0.003) 1/K and another donor level with activation energy of 348 meV in the ( $1/T$ ) range (0.0019-0.0024)1/K.

The *as-deposited* ZnO films show high resistivity due to chemisorptions of oxygen (Chang 1980) at grain boundaries is possible since air was used as carrier gas during deposition. During deposition it is quite likely that large number of oxygen molecules chemisorbed in the film both at the surface and grain boundaries. At the end of deposition, due to the rapid cooling effect these molecules do not get sufficient time to leave the sample. These samples are subjected to a post-deposition heat treatment. As the temperature increases from room temperature to 280°C, the chemisorbed molecules begin to leave the sample rapidly and the conductivity

increases (Prasada and Santhosh 2009). The adsorbed oxygen may produce potential barrier which hinders the electrical transport. The principal chemisorptions species in ZnO is  $O_2^{1-}$  at low temperature and as the temperature of the sample rises, the chemisorbed  $O_2^{1-}$ , desorbed from the sample surface donating an electron to ZnO ( $O_2^{1-} \rightarrow O_2 + e$ ) (Chang 1980), and hence the conductivity rises rapidly.

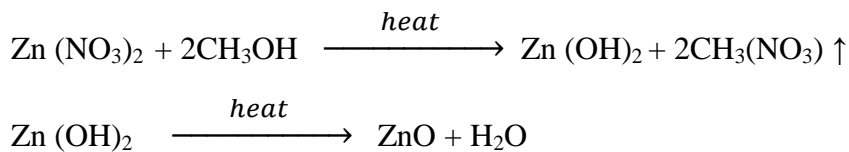
Hall measurements of ZnO films annealed at different temperatures were carried out at room temperature in a magnetic field of 0.5T. The present study used Van der Paw setup shown in figure 2.10(c). The symmetrical shape of samples, as shown in figure 2.10(b), was prepared by using an appropriate mask during deposition. These symmetrical shape helps in simplifying the measurements, as mentioned earlier. The resistivity of the samples measured in the absence of the magnetic field. For Hall measurements require a uniform magnetic field, which was setup by the help of an electromagnet. The measurements were made by following the Van der Paw procedure explained as earlier. The carrier concentration and mobility of the carriers are calculated using the equation 2.3.24 and 2.3.25 respectively.

The carrier concentration and mobility of thin films annealed at different temperatures were determined and the results are summarized in the table 3.9. The low electrical conductivity of *as-deposited* films is due to the presence of small crystallite sizes. It is observed from the XRD results that, annealing improved crystallite size of the films. At higher annealing temperatures, the conductivity is found to be reduced. This decrease in the conductivity is due to decrease in the mobility of the carriers, confirmed by the Hall measurements.

### 3.5 PREPARATION OF ZNO THIN FILMS USING ZINC NITRATE PRECURSOR

#### 3.5.1 Experimental details

The ZnO thin films were prepared on to glass substrate using a starting solution of 0.05M concentration of zinc nitrate  $[Zn(NO_3)_2 \cdot 6H_2O]$  in methanol  $[CH_3OH]$ . This solution was sprayed on to the heated glass substrate by means of spray nozzle at the constant pressure of 2bar. The deposition temperature was maintained at  $450 \pm 5^\circ C$ . Air was used as carrier gas. The separation between the substrate and nozzle was optimized to get the uniform film deposition. The deposited ZnO films were annealed at different temperatures for 4 h in air. During the deposition the possible pyrolytic reaction can takes place.



#### 3.5.2 Results & Discussion

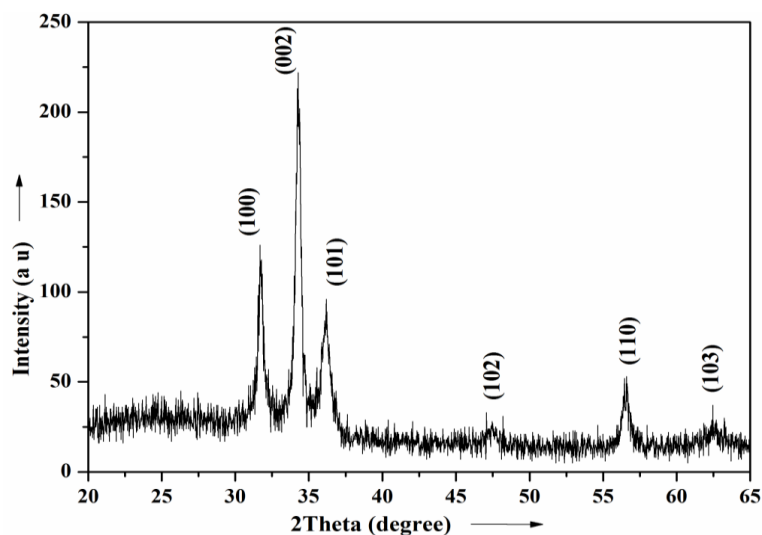


Figure 3.23: XRD pattern of ZnO film annealed at  $450^\circ C$  for 4 h.

The XRD pattern of ZnO thin films annealed at  $450^\circ C$  is shown in the figure 3.23. The strain and average grain size of the wurtzite phase was estimated using the



equation 2.3.3. The calculated average grain size is 24.6 nm. The lattice parameter  $a$  and  $c$  were calculated using the equation 2.3.3. The estimated lattice parameter  $a = 3.234 \text{ \AA}$  and  $c = 5.233 \text{ \AA}$ , are in agreement with the JCPDS data. Structurally not many changes were observed on comparing the ZnO thin films prepared using zinc acetate and nitrate precursors. In both the cases films exhibit hexagonal wurtzite structure with (002) texture.

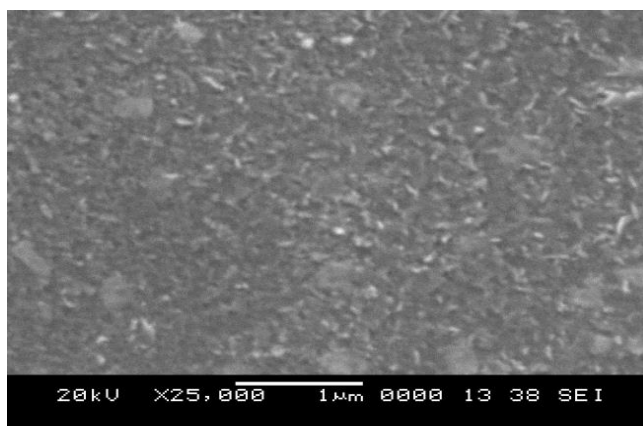


Figure 3.24: SEM image of ZnO films annealed at 450°C for 4 h.

The morphology of ZnO thin films prepared from zinc nitrate precursor show plane and smooth surface (fig. 3.24). Morphology of the thin films prepared using zinc acetate precursor is smoother than the films prepared using zinc nitrate precursor. The presence of zinc and oxygen in the ZnO thin films are confirmed by EDAX analysis and it shows that *as-deposited* films are oxygen deficient whereas films annealed at 450°C show slightly excess of oxygen.

The composition analysis of ZnO thin films prepared using zinc nitrate precursor is also confirmed by XPS technique. The Zn2p and O1s spectra of annealed ZnO films acquired at pass energy of 25 eV is shown in the figure 3.25(a) and (b) respectively. From Zn2p spectra, it is noticed that Zn2p<sub>3/2</sub> peak appeared at binding energy 1021.64 eV. This peak is attributed to Zn-O bond rather than metallic Zn-Zn bond since the binding energy of Zn-O bond (1021.90 eV) is higher than Zn-Zn binding energy (1021.45 eV).

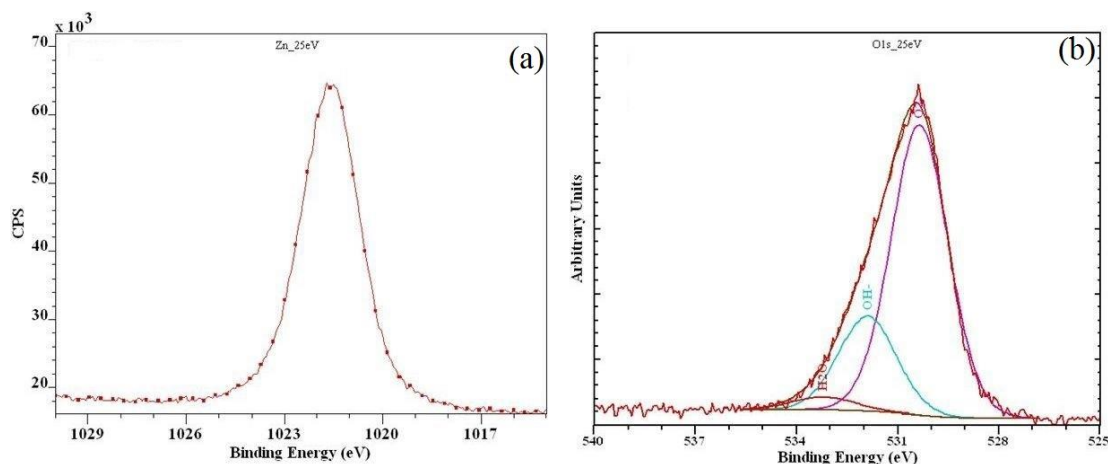


Figure 3.25: (a) Zn2p spectra and (b) O1s spectra of annealed ZnO films.

In the O1s spectra of ZnO film, peak could be divided into two Gaussian components one with low binding energy and other with high binding energy peaks positioned at 530.36 eV and 531.90 eV. The peak position on the low binding energy side of the O1s spectrum at 530.36 eV corresponds to  $O^{2-}$  ions on wurtzite structure of hexagonal  $Zn^{2+}$  ion array, surrounded by Zn atoms with their full complement of nearest neighbour  $O^{2-}$  ions (Chen et al. 2001). The other component located at higher binding energy at 531.90 eV is arised either due to the loosely bound oxygen or due to the presence of hydrated oxides in the film. The atomic percentage of zinc and oxygen in the ZnO films are estimated and are found to 40.7 at. % and 59.3 at. % respectively. From the O1s spectrum it is confirmed that, among the total 59.3 at. % of oxygen present in the film, 70.26 at. % of oxygen are strongly bonded to zinc and rest 29.74 at. % of oxygen is loosely bonded to the surface.

Optical transmittance spectra of ZnO films annealed at different temperatures are shown in the figure 3.26(a). The *as-deposited* films show average transparency of above 80 % in the visible region. The optical transmittance of thin films found to decrease with increasing annealing temperature. The decrease in optical transmittance at higher annealing temperatures may be due increase in surface roughness which leads to more light loss due to optical scattering. The optical transmittance of ZnO films prepared using zinc nitrate precursor is almost same as that of ZnO films prepared using zinc acetate precursor.

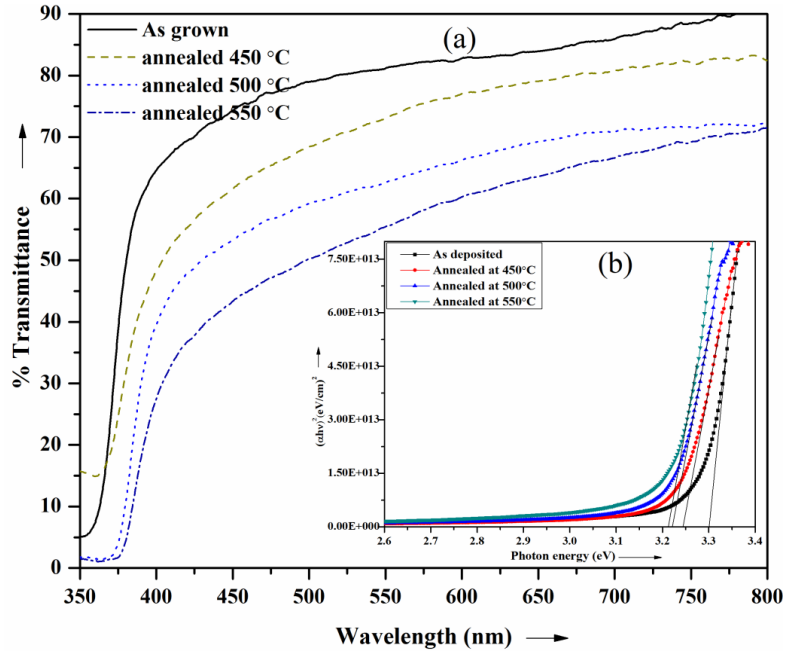


Figure 3.26: (a) Optical transmittance spectra and (b) Tauc's plot for ZnO films annealed at different temperatures.

The variation of  $(\alpha h\nu)^2$  with  $h\nu$  for the *as-deposited* and annealed films is shown in the figure 3.26(b). The band gap of *as-deposited* ZnO film is 3.30 eV, which reduces to 3.22 eV as the annealing temperature increases up to 550°C.

Table 3.10: Optical and electrical data of ZnO films annealed at different temperatures for 4h.

Annealing temp. (°C)	$E_g$ (eV)	$\sigma$ (S/cm)	$E_a$ (meV)	$n$ ( $1/\text{cm}^3$ )	$\mu$ ( $\text{cm}^2 \text{v}^{-1} \text{s}^{-1}$ )
As-deposited at 450	3.30	0.05	478	243	--
450	3.24	0.34	335	185	$1.81 \times 10^{17}$
500	3.22	0.27	385	196	$1.89 \times 10^{17}$
550	3.21	0.21	423	214	$1.56 \times 10^{17}$

The *as-deposited* and annealed ZnO films prepared using zinc nitrate precursor exhibit linear I-V characteristics, shown in the figure 3.27. The conductivity of *as-deposited* thin films is found to be very low of the order of 0.05 S/cm. The poor conductivity of *as-deposited* ZnO films may be due to grain boundary effects and also, due to adsorption oxygen since air is used as carrier gas. There is a possibility of chemisorptions of large number of oxygen molecules on the surface and grain

boundaries of the film, which will create the potential barrier that affects the electrical transport causing a reduction in conductivity (Joseph et al. 1999).

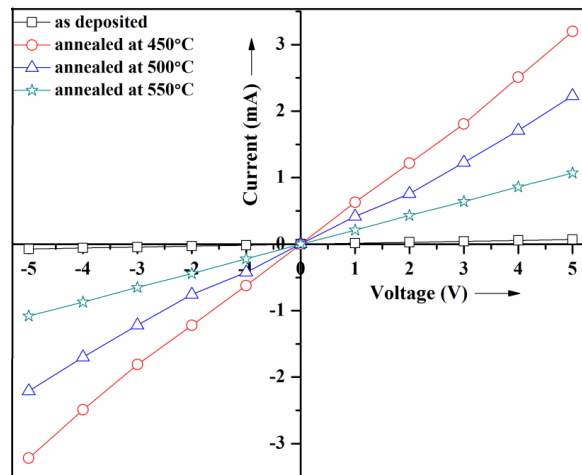


Figure 3.27: I-V characterization of ZnO films annealed at different temperatures.

It is observed that the conductivity of ZnO thin films increased by an order of magnitude after annealing the sample at 450°C. The conductivity data of ZnO films annealed at different temperatures are presented in the table 3.10. It is found that the conductivity of ZnO films increases to 0.34 S/cm, when annealed at 450°C and decreases slowly on further increasing annealing temperature. This might be due to either an increase in the carrier concentration and/or increase of the mobility.

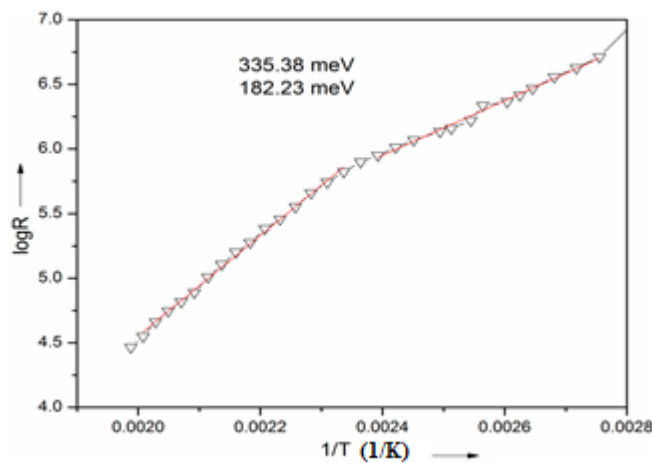


Figure 3.28: Variation of logR with 1/T of ZnO films annealed at 450°C.

The activation energy for thin films prepared from zinc nitrate precursor was determined using the equation 2.3.26 and measured data are shown in table 3.10. The variation of  $\log R$  with reciprocal of temperature ( $1/T$ ) plot is shown in the figure 3.28. The graph shows two distinct regions, low temperature region corresponds to extrinsic conduction whereas high temperature region corresponds to intrinsic conduction in the film.

In the present study, logarithmic resistance curve with variation in the reciprocal temperature of ZnO film shows a linear behavior in two regions. This shows the presence of two donor levels below the conduction band. The first one from (0.0019-0.0023)  $1/K$  and the other from (0.0023-0.003)  $1/K$ . In these two ranges the activation energy is proportional to the slope according to equation 2.3.26. Undoped thin film presents first donor level with activation energy of 182 meV in the ( $1/T$ ) range (0.0023-0.003)  $1/K$  and another donor level with activation energy of 335 meV in the ( $1/T$ ) range (0.0019 - 0.0023)  $1/K$ .

Hall measurements of these films were made at room temperature in a magnetic field strength of 0.5 T by using Van der Pauw method. The carrier concentration and mobility of the carriers are calculated using the equation 2.3.24 and 2.3.25 respectively. The results are summarized in the table 3.10.

The electrical properties of ZnO films deposited using zinc nitrate precursor are comparable with the films prepared using zinc acetate precursor. In both the cases *as-deposited* films show low conductivity which is found to increase after annealing the films at 450°C. Though there is improvement in the conductivity of the ZnO films, the order of magnitude is more in films prepared from zinc acetate precursor; hence for the further study zinc acetate precursor was used.

## **CHAPTER 4**

# **ZnO THIN FILMS DOPED WITH GROUP V ELEMENTS**

### **4.1 INTRODUCTION**

Thin films, deposited by most of the well-known deposition techniques, usually have low electrical conductivity. The optical and electrical properties of undoped ZnO do not reach the requirements of high performance semiconductor devices. In order to enhance the electrical properties, ZnO should be doped with suitable dopants. The selection of suitable dopant is the primary requirement of doping. However mere inclusion of impurities will not be enough to increase the electrical conductivity. To obtain good electrical conductivity, the following requirements have to be satisfied.

- An adequate concentration of dopant atoms has to be incorporated into the material.
- The incorporated dopants must produce shallow levels in the forbidden bandgap region of the material, i.e., the energy levels of these dopants have to be close enough to the corresponding band edge (conduction band edge for donors and valence band edge for acceptors). Only then the dopants will get easily ionized at the device working temperature (usually room temperature) providing desired quantity of free carriers in the respective bands.

The incorporation of dopants must not provoke spontaneous formation of some oppositely charged defects which would de-activate them, either directly, by pairing with dopants or by compensating their electrical activity from the distance. This is not a rare possibility. In fact this problem has been impeding the progress of thin film semiconductor research, especially in that of II-VI semiconductors (Desnica 1998).

Doping of semiconductor still suffers from considerable short comings. The mechanisms that limit the doping of semiconductors are explained as follows.

#### a. Self compensation of native defects

Native defects (also referred as intrinsic defects) commonly occur in semiconductors. The three basic types of point defects are vacancies (a point missing from the lattice site), self-interstitials (additional atom in the lattice) and antisites (in a compound semiconductor, when for example a cation is sitting in an anion site). For each of these types, the defects can occur either on cation site or on anion site. Because formation of native defects often requires breaking or rearranging of bonds, deep levels in semiconductor bands are typically introduced. The occupation of levels determines the charge state of the defect. Depending on the location of levels in the gap and charge states they can assume, native defects can have donor character or acceptor character or even be amphoteric.

#### b. Compensation by other configurations of impurity

Suppose an impurity is incorporated in to the crystal with the goal of introducing shallow acceptor level it is necessary for impurity to be located in substitutional lattice site. But if the growth condition is such that a large number of impurity atoms are incorporated to the interstitial sites as opposed to the substitutional site significant compensation will occur.

#### c. Solubility limit

In order to dope a material, impurities that act as dopants may be introduced in to the semiconductor. In p-type material, the concentration of acceptor impurities incorporated in the lattice limits the hole concentration. If this hole concentration is limited it can lead to limitation in the achievable doping level (Walle 1997).

#### d. Formation of complexes

In the process of doping a semiconductor there is a possibility of formation of complexes between dopant impurities and native defects. Indeed if the binding energy between native defect and dopant is large enough the formation energy of resulting complex may be lower than that of the individual defect.

Zinc oxide is a typical semiconductor which can be made conductive both by intrinsic dopants (defects) as well as by extrinsic ones (foreign atoms). The low resistivity at room temperature that is degenerate doping which is acquired for the application of ZnO as transparent electrodes can be achieved in two different ways.

- Creation of intrinsic donors by lattice defects (for instance oxygen vacancies or zinc atoms on interstitial lattice sites).
- Introduction to extrinsic dopants (either metal with oxidation number three on substitutional metal lattice sites or halogens with oxidation number minus one on oxygen lattice sites).

It was believed that the oxygen vacancy is a dominant donor in the zinc oxide films. The annealing process of ZnO single crystals or thin films under reduced condition increased the carrier concentration, while oxidation process decreased the carrier concentration. But recently comprehensive studies reported that the zinc vacancy and oxygen interstitials acts as acceptors whereas zinc interstitials and oxygen vacancies have shallow energetic donor positions in the band gap. During deposition, different defects are most likely to form depending on the growth atmosphere. The zinc vacancy and oxygen interstitials are most likely defects for oxygen rich atmosphere, while oxygen vacancy dominates under zinc rich condition (Elmer 2010).

Achieving p-type doping in wide-band-gap semiconductors, such as ZnO, GaN and ZnSe are quite difficult. The realization of p-type in ZnO for applications has been proven difficult and thought to be the bottleneck in the development of ZnO based devices due to the asymmetric doping limitations. The difficulties can arise from a variety of causes.

- Attempted dopant may be compensated by low-energy native defects, such as  $Zn_i$  or  $V_O$  or the presence of hydrogen background impurities.
- High activation energy and low solubility of the dopant in the host material is another possibility. Deep impurity level can also be a source of doping problem, causing significant resistance to the formation of shallow acceptor level.



- In spite of achieving p-type ZnO, with the ageing there is a slow transition from p-type conductivity to n-type conductivity. It is probably assigned to the acceptor migration from the substitutional sites to interstitial sites. (Rajeswari and Chandra 2013).

Even with all the above difficulties, p-type conductivity is achieved by incorporating group-I elements (Li, Na, and K) for Zn sites or group-V elements (N, P, Sb and As) for O sites, often with apparently very high hole concentrations but with low mobility. It has been believed that the most promising dopants for p-type ZnO are the group-V elements, although theory suggests some difficulties in achieving shallow acceptor level (Yuan et al. 2008; Miao et al. 2006; Aoki et al. 2002). Generally a known n-type dopant to produce p-type levels in ZnO is Nitrogen, which is known to provide the shallowest acceptor states. However, N has low solubility making it imperative to decrease the background donor concentration and increase solubility by co-doping (Morkoc and Ozgur 2007).

Generally if it is difficult to make p-type ZnO by N doping, then it should be equally difficult to do so by P, As, Sb doping. However, the exact opposite is true; that is, good p-type material has been made using all three dopants (Limpijumnong et al. 2004; Chen and Hung 2014). The conventional wisdom is based on acceptor energy and solubility, which are functions of ionic size. Of the group V elements,  $N_O$  should have the smallest acceptor transition energy and highest solubility, and  $P_O$ ,  $As_O$ , and  $Sb_O$ , should be deeper and more difficult to incorporate. To explain the experimental disagreement with this scenario, Limpijumnong et al. (2004) examined what would happen if As actually went on the Zn site, where it would fit better, rather than the O site. Using DFT, they indeed found that a complex,  $As_{Zn}-2V_{Zn}$ , has a rather low formation energy (high solubility), and a relatively shallow acceptor transition energy. Two recent studies are consistent with this finding: (1) dopant As tends mainly to go on the Zn site and (2) As-doped ZnO contains high quantities of Zn vacancies (Jagadish and Pearton, 2006).

The possible acceptors in ZnO include group I elements, such as Li, Na, and K, Ag, Cu, and Zn vacancies, and group V elements such as N, P, As, and Sb. However,

many of these form deep acceptors and do not contribute sufficiently to p-type conduction. Zn vacancies have low formation energy in n-ZnO and can be created by high-energy (2 MeV) electrons. They were shown to be dominant acceptors in *as-deposited* n-type ZnO using positron annihilation spectroscopy (Tuomisto et al. 2003). It is believed that the most promising dopants for p-type ZnO are the group V elements, although theory suggests some difficulty in achieving shallow acceptor level (Park et al. 2002). Plasma sources are used for N doping, whereas conventional effusion cells can be employed for As, Sb, and P. The activation energy of P was reported to be 127 meV (Hwang et al. 2005). Among these candidates, N would make a good acceptor dopant, because it has an electronic core structure and ionic radius similar to that of O and hence should readily substitute for O. But as mentioned above, its solubility is low (Jagadish and Pearton, 2006).

Though there are difficulties in achieving p-type doping, different group of researchers have expended a good effort to realize p-type ZnO using different dopants. Ye et al. (2003) used NH<sub>3</sub> as the nitrogen source for dc reactive magnetron sputtering of p-type ZnO. Results show a hole concentration of  $3.2 \times 10^{17} \text{ cm}^{-3}$  and a resistivity of 35  $\Omega$ -cm.

Miao et al. (2006) reported the realization of phosphorus-doped p-type ZnO thin films by MOCVD. Phosphorous doped films were prepared at different substrate temperature. Study also reported that the conduction type of thin films is greatly dependent on the growth temperature and all the films exhibited p-type conduction after annealing. The lowest resistivity of 11.3  $\Omega$ -cm and the highest hole concentration of  $8.84 \times 10^{18} \text{ cm}^{-3}$  at 420°C.

Kumar et al. (2010) prepared As doped thin films using ZnO: Zn<sub>3</sub>As<sub>2</sub> target on sapphire substrate by R F sputtering. XPS analysis suggested the formation of As<sub>Zn</sub>-2V<sub>Zn</sub> complex. Hall measurement showed p-type conductivity in As doped thin films.

Pan et al. (2007) obtained the Sb doped p-type thin films on quartz substrate by PLD method. The high purity ZnO-Sb<sub>2</sub>O<sub>3</sub> ceramic disk with 2% Sb was used as target. XPS analysis confirmed the incorporation of Sb in the film as Sb<sub>Zn</sub> rather than

Sb<sub>2</sub>O<sub>3</sub>. The p-type conduction in Sb doped films is achieved at the growth temperature of 550 °C with a resistivity of 3 Ω-cm.

Minhong et al. (2009) studied the effect of argon pressure on the structural, optical, and electrical properties of the Bi doped films using RF magnetron sputtering. Hirotaka et al. (2008) reported the superconducting properties of ZnO-doped (Bi, Pb)-2223 thick film on Ni and NiO substrates prepared by spray deposition technique and Mista et al. (2004) studied the varistor performance of nanocrystalline Zn–Bi–O thin films prepared by reactive RF magnetron sputtering at room temperature.

There were few reports on the Sb and Bi doped ZnO thin films prepared using physical methods such as PLD and sputtering techniques, hence present study selects antimony and bismuth as dopant. The Sb and Bi doped ZnO thin films were prepared separately using simple and inexpensive spray pyrolysis technique. The structural, optical and electrical properties of these films were studied.

## **4.2 ANTIMONY (Sb) DOPED ZnO THIN FILMS**

In the present investigation antimony (Sb) doped ZnO thin films were prepared by spraying precursor solution of zinc acetate anhydrous [Zn(CH<sub>3</sub>COO)<sub>2</sub>] (Alfa Aesar 99.99%) and antimony acetate [Sb(CH<sub>3</sub>COO)<sub>3</sub>] (Alfa Aesar 99%), in methanol. The deposition parameters were maintained almost identical to that for the deposition of undoped ZnO thin films (table 3.4).

### **4.2.1 Effect of doping concentration**

Sb doped thin films were prepared by spray pyrolysis technique. The Sb dopant concentration is varied from 0 to 5% in the precursor solution. The obtained films of thickness 600 nm were annealed at 450°C and their structural, optical and electrical properties were studied.

XRD pattern of Sb doped thin films were compared with that of undoped thin film as shown in figure 4.1. The Sb doped films exhibit hexagonal wurtzite polycrystalline structure. Undoped thin films have preferred orientation along (002) direction. Sb doped thin films show a preferred orientation along (101) direction. Further, it is observed that with increase in the concentration of dopant, the intensity corresponding to the (101) set of planes decreases. There is no peak for free antimony or related compound detected in the XRD pattern.

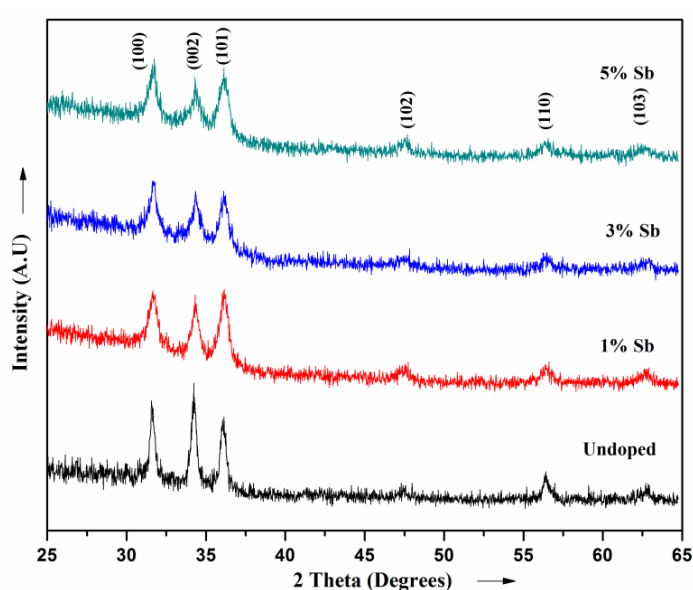


Figure 4.1: XRD pattern of Sb doped ZnO thin films.

The crystal quality of the thin films is estimated from the grain size. The average grain size (D) and strain in the Sb doped films were determined using equation 2.3.3. The grain size is found to decrease marginally for films doped with Sb (table 4.1). The lattice parameters ‘a’ and ‘c’ of Sb doped thin films were calculated using equation 2.3.2. The doping does not result many changes in lattice parameter indicating no lattice distortion.

Table 4.1: XRD data of Sb doped ZnO thin films.

Sb (at. %)	Texture	D (nm)	Strain
1	(101)	19.7	0.002
3	(101)	16.3	0.019
5	(101)	13.9	0.031

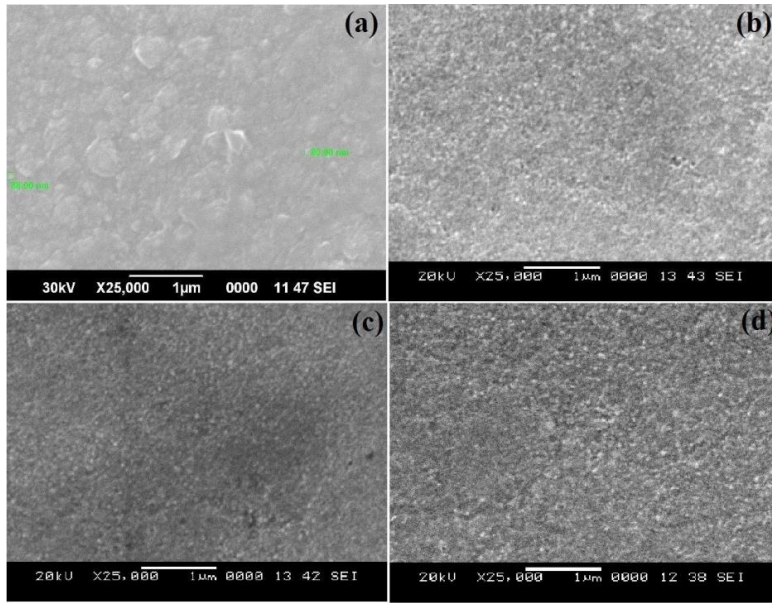


Figure 4.2: SEM image of (a) undoped film and (b) 1% Sb, (b) 3% Sb, (c) 5% Sb doped ZnO films.

The scanning electron micrographs of Sb doped ZnO films were compared with those of undoped thin film and are shown in the figure 4.2. The morphology of the thin films remains almost unaffected with Sb doping. It appears that the surface roughness of thin films decreased with increasing dopant concentration. The presence of Sb in the ZnO films was confirmed by EDAX analysis as presented in the figure 4.3.

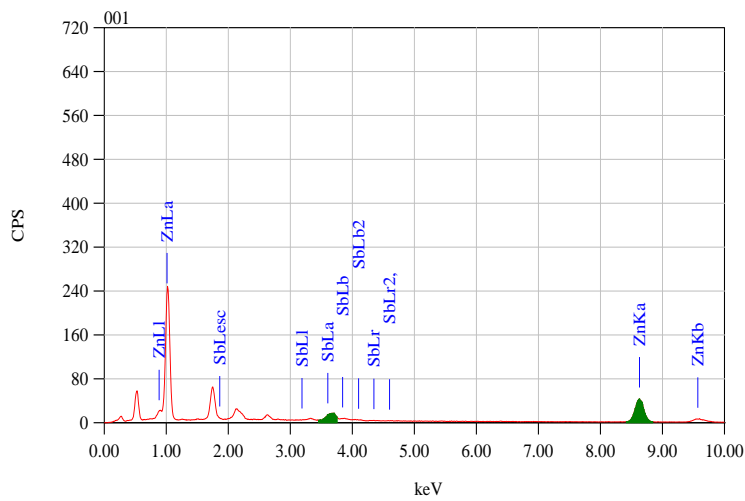


Figure 4.3: EDAX spectrum of Sb doped ZnO thin films.

The composition analysis of Sb doped ZnO thin films were investigated using X-ray photoelectron spectroscopy (XPS). The XPS spectrum of 3% Sb doped thin films is shown in the figure 4.4. Figure 4.4(a) and (b) shows the survey scan and Zn2p spectrum respectively. In Zn2p spectrum two binding energy peaks located at 1021.00 eV and 1044.0 eV corresponding to Zn2p<sub>3/2</sub> and Zn2p<sub>1/2</sub> core levels respectively. Figure 4.4(c) shows the O1s and Sb3d core level spectrum.

Figure 4.4(c) shows the O1s XPS spectra of Sb doped thin films. There are two asymmetric O1s peaks are located at the binding energies 530.44 eV and 532.7 eV. The peak corresponding to the lower binding energy is due to Zn-O bond and the other peak located at the higher binding energy accords with the chemisorbed oxygen (Liqiang et al. 2002). It is seen from the figure 4.4(c) that an O1s peak is moved slightly to the higher binding energy direction compared with undoped O1s peak. This slight shift in binding energy with Sb doping is attributed to minor lattice distortion, which is not reflected in the lattice parameters.

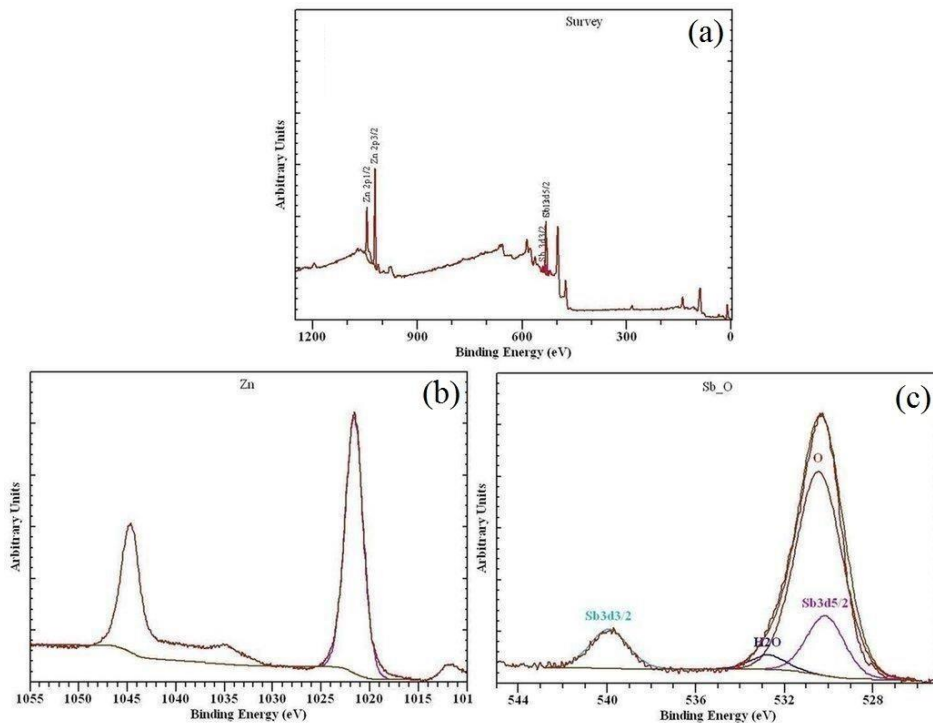


Figure 4.4: XPS spectra of ZnO: 3% Sb thin films annealed at 450°C. (a) Survey scan, (b) Zn2p spectrum and (c) Sb3d, O1s spectrum.

The figure 4.4(c) shows Sb3d core level XPS spectrum of 3% Sb doped thin film, which show two asymmetric peaks located at 530.13 eV and 539.92 eV and these peaks are assigned to Sb3d<sub>5/2</sub> and Sb3d<sub>3/2</sub> region, respectively. The Sb3d<sub>5/2</sub> and Sb3d<sub>3/2</sub> peaks are ascribed to Sb-O bonding, further these peaks suggests that the Sb has been incorporated into the ZnO film and exists in the form of Sb<sub>Zn</sub> rather than Sb<sub>O</sub> (Chu et al. 2011; Izquierdo et al 1989). Also note that, no Sb<sub>2</sub>O<sub>3</sub> phase was observed in the XRD patterns. Isolated Sb<sub>Zn</sub> acts as a donor, which cannot result in p-type conductivity. However, Hall measurements show p-type conduction in 3% Sb doped films, suggesting Sb-related acceptor state present in the films. According to the model for large-sized-mismatched group-V dopant in ZnO, the Sb<sub>Zn</sub>-2V<sub>Zn</sub> complex was believed to be the most likely candidate to form a shallow acceptor level among the complexes. The atomic percentage of zinc, antimony and oxygen in the Sb doped films are estimated and are found to be 48.7%, 3.0 % and 48.3% respectively.

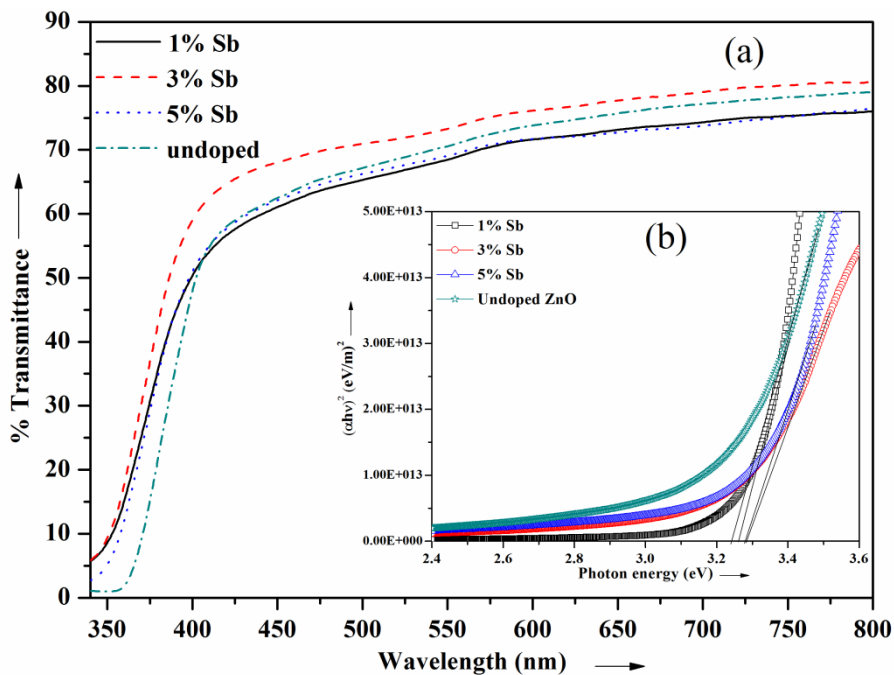


Figure 4.5: (a) Transmittance spectra and (b) Tauc's plot for Sb doped ZnO thin films.

Transmittance spectra of Sb doped thin films are presented in the figure 4.5(a). It is found that, all the films show transmittance above 75% in the visible region. This indicates that the Sb dopant does not affect the transmittance of the film. It is observed that the absorption edge in Sb doped thin films is in the UV region which

shifts to lower wavelength region when compared with undoped thin films. The Sb doped thin films have a direct band gap. For the direct allowed transition, the band gap of thin films can be determined using the equation 2.3.13.

Figure 4.5(b) shows the variation of  $(ahv)^2$  with  $h\nu$  for Sb doped thin films. It is found that band gap slightly changed from 3.24 eV to 3.28 eV as the concentration of dopant increased from 0 to 5% respectively. This shows that no significant change in the optical band gap of ZnO films with Sb doping.

The variation in the electrical conductivity ( $\sigma$ ) of ZnO thin films with the concentration of Sb dopant is shown in figure 4.6. It is noted that the conductivity of thin films increases up to 3% addition of Sb. This may be due to replacement of  $Zn^{2+}$  by  $Sb^{3+}$ , contributing additional charge carriers to the electrical conduction. Thus increase in the electrical conductivity may be attributed to the presence of number of charge carriers introduced by the dopant (Caglar et al. 2007). Decrease in the conductivity of 5% Sb doped thin films may be due to disorder produced in the ZnO film, which leads to ionized impurity scattering or phonon scattering. The high conductivity of 5.4 S/cm was obtained for 3% Sb doped thin films.

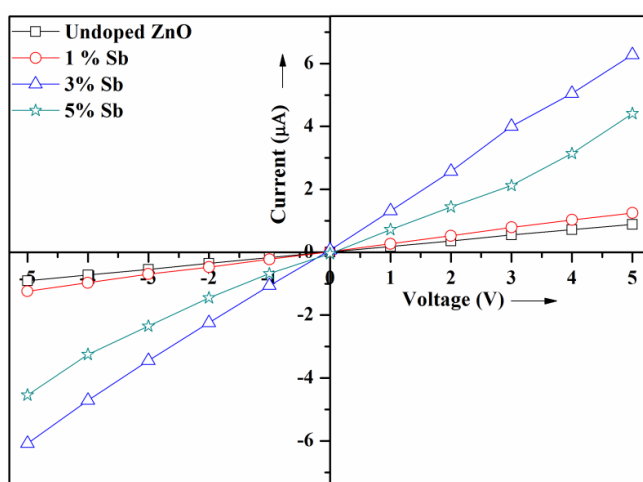


Figure 4.6: I-V characteristics of Sb doped ZnO thin films.

Figure 4.7 shows a plot of  $\log R$  vs. reciprocal temperature for 3% Sb doped thin film. Thus activation energy ( $E_a$ ) was calculated from the slope of the plot using the equation 2.3.26 and the results are presented in the table 4.2. The plot shows two



activation energies at the two region of temperature. These activation energies represent shallow and deep acceptor levels in the films. Thus the charge carriers in the films increases by antimony doping and trapping levels with activation energy less than 55 meV contribute to the electrical conductivity with very low energy loss (Gonzales et al. 1998).

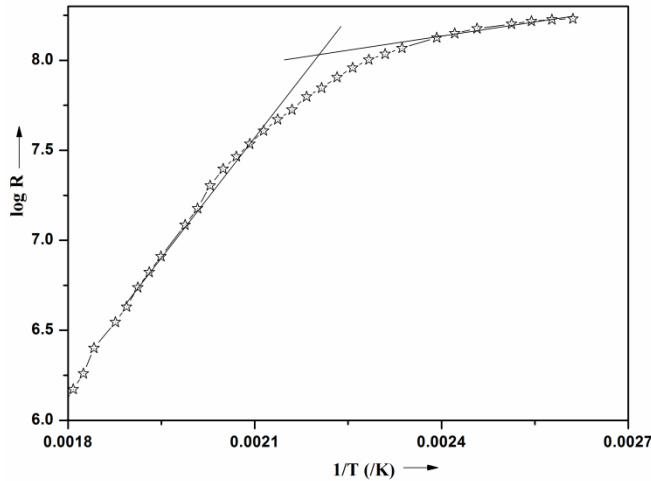


Figure 4.7: Variation of logR as a function of 1/T of 3% Sb doped films.

Table 4.2: Optical and electrical data of Sb doped ZnO thin films.

Sb %	$E_g$ (eV)	$\sigma$ (S/cm)	$E_a$ (meV)	C.C ( $1/cm^3$ )	$\mu$ ( $cm^2 V^{-1} s^{-1}$ )	conduction type	
0	3.24	0.16	348	217	$9.92 \times 10^{16}$	9.38	n
1	3.26	0.53	441	56.0	$3.57 \times 10^{17}$	9.30	n
3	3.28	5.41	444	49.9	$6.25 \times 10^{17}$	34.05	p
5	3.28	4.67	449	67.7	$6.51 \times 10^{17}$	32.72	p

The nature of charge carriers in Sb doped thin films was determined by hot probe technique. The experiment is done by attaching a cold probe and a hot probe to a semiconductor surface. Both probes are wired to a sensitive multimeter. The cold probe is connected to the negative terminal and hot probe is connected to the positive terminal of the meter, Keithley multimeter reads positive voltage for 1% Sb doped films showing n-type conductivity. Multimeter shows negative voltage reading for 3% and 5% Sb doped films. This shows p-type nature of charge carriers in thin film. According to Limpijumng et al (2004),  $Sb_{Zn}-2V_{Zn}$  complex was most likely candidate to form a shallow acceptor level in large-sized mismatched group-V-doped

ZnO. The n-type conductivity is observed in the 1% Sb doped thin films is due to low concentration of dopant which is not enough to change the conductivity from n-type to p-type. Although  $\text{Sb}_{\text{Zn}}$  is produced in the film, the concentration of  $\text{Sb}_{\text{Zn}}-2\text{V}_{\text{Zn}}$  complex is too small to show p-type conductivity. On increasing the doping concentration to 3% and above, the formation of  $\text{Sb}_{\text{Zn}}-2\text{V}_{\text{Zn}}$  complex is sufficient to flip the conductivity from n-type to p-type.

Further the p-type conductivity of 3% Sb doped films was confirmed by Hall measurements. Hall measurement data of undoped and Sb-doped thin films are shown in table 4.2. It is observed that p-type conduction can be achieved by the addition of 3% Sb and above. It is worth noting that the films prepared with 3% Sb show the low resistivity of  $0.185 \Omega\text{-cm}$  with a mobility of  $34.05 \text{ cm}^2 \text{ V}^{-1} \text{ s}^{-1}$ , and a hole concentration of  $6.25 \times 10^{17} / \text{cm}^3$ .

#### 4.2.2 Effect of annealing temperature

Since 3% Sb doped films have better combination of optical and electrical properties. The 3% Sb doped films were annealed at different temperatures to study the effect of annealing on the structural, morphological and optical and electrical properties.

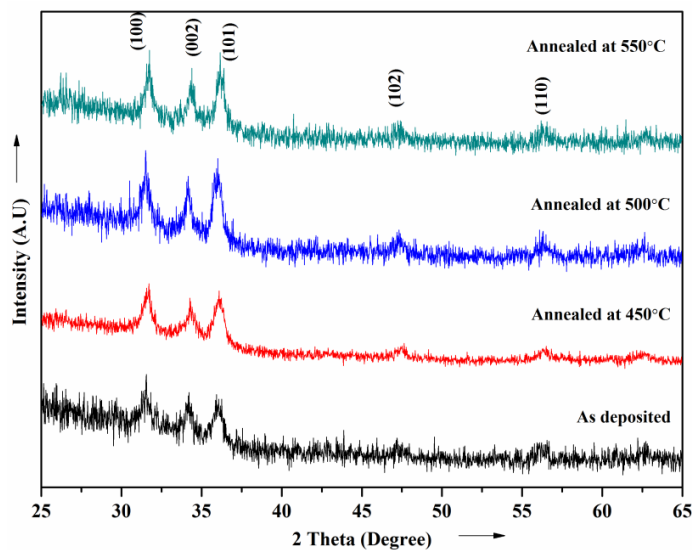


Figure 4.8: XRD pattern of *as-deposited* and annealed ZnO: 3% Sb films.

Figure 4.8 shows the XRD pattern of *as-deposited* and annealed 3% Sb doped thin films. All the films exhibit polycrystalline hexagonal wurtzite structure with (101) texture. The crystal quality of the annealed films was decided by the grain size calculated from the peaks in the diffraction pattern. The grain size (D) and strain in the annealed Sb doped films were estimated and the results are summarized in the table 4.3. The grain size is found to increase marginally with annealing temperature whereas strain is found to decrease with increase in annealing temperature. The lattice parameters of 3% Sb doped films remain unaltered with annealing.

Table 4.3: XRD data of ZnO: 3% Sb films annealed at different temperatures for 4 h.

Annealing temp.(°C)	Texture	D (nm)	Strain
As-deposited at 450	(101)	8.69	0.009
450	(101)	16.3	0.0019
500	(101)	17.4	0.0016
550	(101)	23.3	0.0011

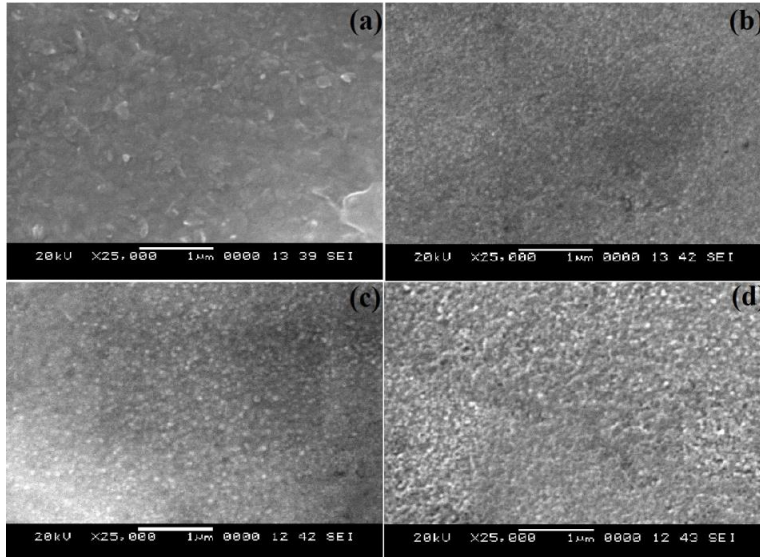


Figure 4.9: SEM image of ZnO: 3% Sb thin films (a) *as-deposited* and annealed at (b) 450°C, (c) 500°C, (d) 550°C.

SEM image of *as-deposited* and annealed Sb doped thin films are shown in the figure 4.9. The morphology of *as-deposited* film shows plane and smooth surface [fig. 4.9 (a)]. After annealing the films at 450°C, randomly oriented fine grains on the film surface is seen from the micrograph [fig. 4.9(b)]. The films annealed at 500°C and

550°C, show uniform distribution grains with slight increase in size [fig. 4.9(c) & (d)].

Optical transmittance spectra of Sb doped thin films annealed at different temperatures are shown in figure 4.10(a). The *as-deposited* films show average transmittance of 80 % in the visible region. The films annealed at 450°C show the transparency nearly same as that of *as-deposited* films. The transmittance of films reduces to 70% when annealed at 550°C. This reduction in the transmittance of the films may be due to shrinkage of pores between the grains and increase in separation between the grains. This results the increase in grain boundaries. Increase in grain boundary increases the light scattering in the films. Thus, as thin film annealing temperature was increased, the pores between nanoparticles shrunk resulting in a decrease in film transmittance (Hidayat et al. 2008).

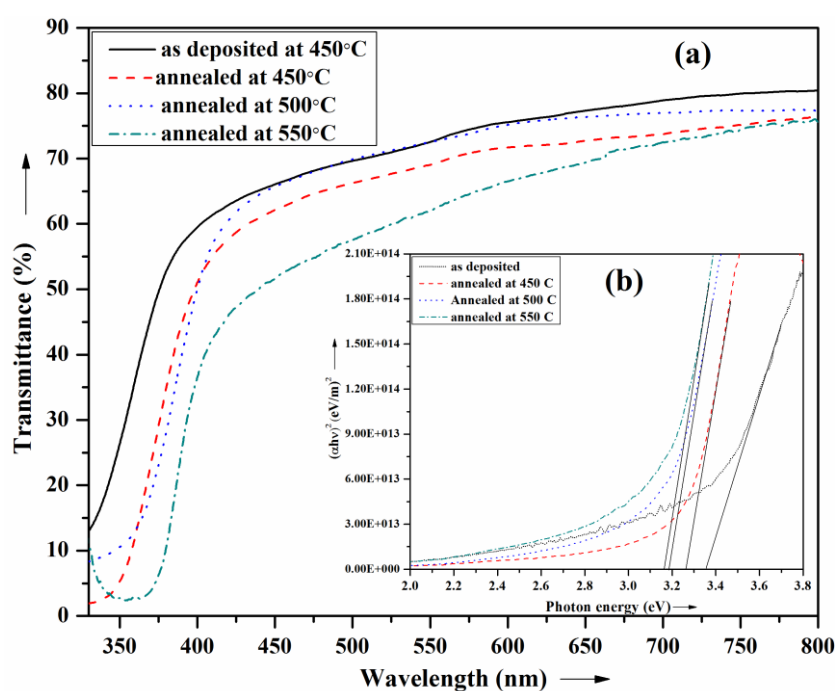


Figure 4.10: (a) Transmittance spectra and (b) Tauc's plot for ZnO: 3% Sb films annealed at different temperatures.

The variations of  $(\alpha h\nu)^2$  with photon energy of Sb doped thin films annealed at different temperatures are shown in the figure 4.10(b). The estimated band gap values are shown in the table 4.4. It is observed that the energy band gap of Sb doped thin

films decrease with increase in annealing temperature. According to reports, decrease in the band gap occurs due to appearance of band tail resulting from defects associated with the presence of cavities and surface roughness (Regragui et al. 2001).

Current -voltage characteristics of *as-deposited* and annealed 3% Sb doped thin films are shown in the figure 4.11. The *as-deposited* 3% Sb doped films show low conductivity of 0.13 S/cm, which may be due to grain boundary effects and also, due to adsorption of air was used as carrier gas.

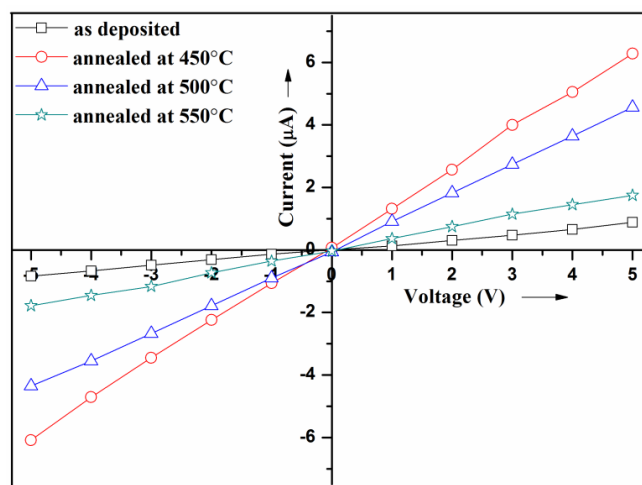


Figure 4.11: I-V characteristics of annealed ZnO: 3% Sb thin films.

The electrical conductivity of Sb doped films found to be increased on annealing at 450°C and then decreased with a further increase in annealing temperature. The increase in conductivity may be due to the decrease in the grain boundary and crystal lattice deficiencies of the film, which is due to the defects like oxygen at interstitials, are decreased with annealing. This in turn causes a rise in the concentration of charge carriers (Lin et al. 2008). The observed increase in conductivity may be due to the enhancement of film crystallinity and increase in mobility whereas low conductivity of the films at 500°C and above is due to the chemisorptions of oxygen on the film surface (Mohamod 2007) and hence decrease in mobility of charge carriers.

Table 4.4: Optical and electrical data of ZnO: 3% Sb films annealed at different temperatures for 4 h.

Annealing temp.(°C)	$E_g$ (eV)	$\sigma$ (S/cm)	$E_a$ (meV)		C.C. ( $1/\text{cm}^3$ )	$\mu$ ( $\text{cm}^2 \text{V}^{-1} \text{s}^{-1}$ )	type
as-deposited at 450	3.36	0.13	524	153	---	--	n
450	3.28	5.41	444	44.9	$6.25 \times 10^{17}$	34.05	p
500	3.19	3.23	497	89.6	$8.74 \times 10^{17}$	23.07	p
550	3.16	0.74	539	129	$8.97 \times 10^{17}$	15.16	n

As the annealing temperature increased to 500°C and above the conductivity of the 3% Sb doped films were found to be decreased. The decrease in electrical conductivity of annealed films is due to decrease in mobility of the films shown by Hall measurements. The study show an increase in the activation energy for films annealed at temperature above 450°C (table 4.4). The activation energy is least for films annealed at 450°C; hence it contributes more to the electrical conductivity. The conductivity type of 3% Sb doped thin films annealed at different temperatures was studied by hot probe technique. The films annealed at 500°C show p-type conductivity, whereas the films annealed at 550°C show n-type conductivity.

The conductivity type of Sb doped films was confirmed by Hall measurements. Since insulating glass is used as substrate which ensures that the electrical signal originates from the ZnO thin films rather than the substrate. Sb doped films annealed at 450°C show a maximum conductivity of 5.41 S/cm, with a carrier concentration of  $6.25 \times 10^{17} \text{cm}^{-3}$  and Hall mobility of  $34.05 \text{ cm}^2 \text{V}^{-1} \text{s}^{-1}$  at room temperature. The film annealed at 550°C exhibits n-type conductivity, may be due to concentration of donors is higher than the concentration of acceptors. This is because when the annealing temperature increases from 450°C to 500°C, more acceptors related to Sb are activated in the film, when the annealing temperature further increases and reaches 550°C, the annealing temperature is high to be in favour of the existence of  $\text{Sb}_{\text{Zn}}-2\text{V}_{\text{Zn}}$  in the film (Zhao et al. 2011).

### 4.3 BISMUTH (Bi) DOPED ZnO THIN FILMS

In the present study bismuth (Bi) doped ZnO thin films were prepared by spraying precursor solution of zinc acetate anhydrous  $[\text{Zn}(\text{CH}_3\text{COO})_2]$  (Alfa Aesar 99.99%) and Bismuth nitrate  $[\text{Bi}(\text{NO}_2)_3]$  (Alfa Aesar 99.99%), in methanol. The deposition parameters were maintained almost identical to that for the deposition of undoped ZnO thin films (table 3.4).

#### 4.3.1 Effect of doping concentration

Bi doped ZnO thin films were prepared by spray pyrolysis technique. The Bi dopant concentration is varied from 0 to 5% in the precursor solution. The obtained films of thickness 600 nm were annealed at  $450^\circ\text{C}$  and their structural, optical and electrical properties were studied.

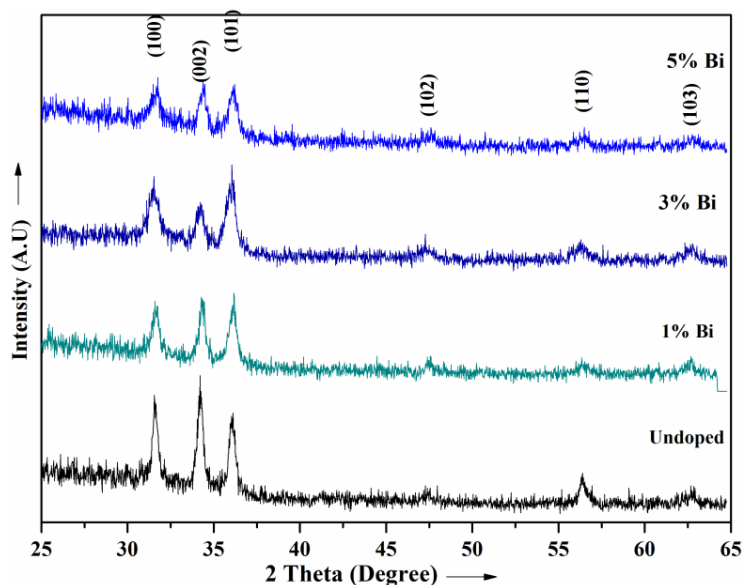


Figure 4.12: XRD pattern of Bi doped ZnO thin films.

Figure 4.12 shows the XRD pattern of Bi doped thin films deposited at  $450^\circ\text{C}$ . Bi doped thin films exhibit polycrystalline hexagonal wurtzite structure indexed according to the JCPDS 36-1451. It is seen from the XRD pattern that doping of Bi alters the orientation of the grains. XRD pattern of undoped ZnO exhibits a preferential orientation along (002) plane, whereas Bi doped films show reduced peak intensity along (002) plane and slightly increased peak intensity along (101) plane.

This indicates that loss of preferential orientation of the films with Bi doping. There is no peak corresponding to Bi or related phases found in the XRD pattern. The grain sizes (D) and strain in the Bi doped ZnO films were estimated from the X- ray diffraction pattern using equation 2.3.3 and the results are shown in table 4.5.

It is noted that grain size slightly decreased from 22.3 nm to 13.0 nm as the concentration of Bi increased from 0 to 5 %. The nucleation steps may change during film growth, the reduction in the nucleation centre may occur in the presence of Bi ions, this reduces the grain size. Acharya et al. (2012), Srinivasan and Kumar, (2008) were also reported the decrease in grain size in the Cd and Mn doped thin films respectively. Even after the Bi doping, ZnO retains its hexagonal structure which confirms the stability of the film. The residual strain in the film is found to increase in increase in doping concentration (table 4.5). The lattice parameter a and c of Bi doped thin films were calculated using the equation 2.3.2 and are almost unaffected by doping indicates no distortion in the lattice.

Table 4.5: XRD data of Bi doped ZnO thin films.

Bi (%)	Texture	D (nm)	Strain
1	(101)	20.4	0.0026
3	(101)	15.9	0.0039
5	(101)	13.0	0.0055

The scanning electron micrographs of Bi doped thin films are shown in the figure 4.13. The surface morphology of the thin films show marked changes on Bi doping. The granular morphology is seen in the each micrograph. The size of the granules increased as the dopant concentration increased from 1 % to 5 %. The incorporation of Bi in the ZnO lattice was confirmed by EDAX analysis as shown in the figure 4.14.



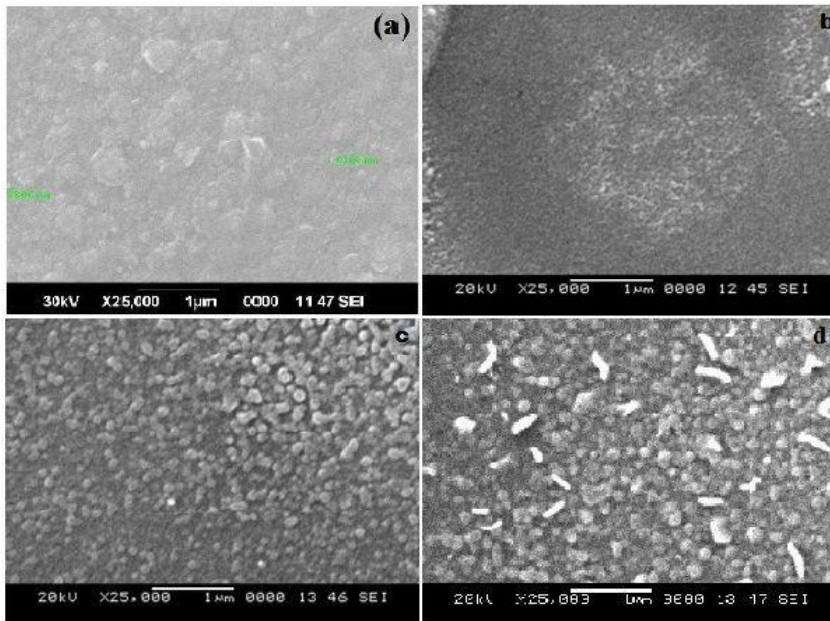


Figure 4.13: SEM image of (a) undoped, (b) 1%, (b) 3% and (c) 5% Bi doped ZnO thin films.

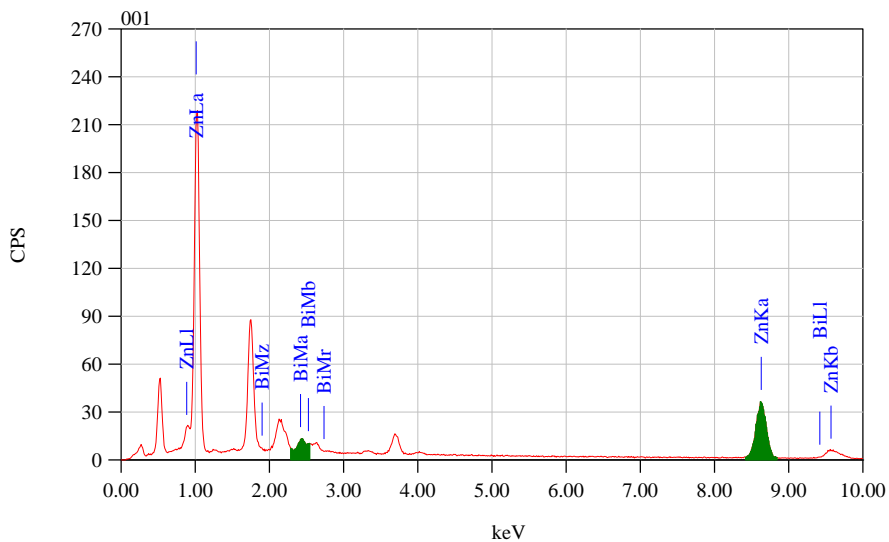


Figure 4.14: EDAX spectrum of Bi doped ZnO thin film.

The composition analysis of bismuth doped thin films was investigated using X-ray photoelectron spectroscopy (XPS). The XPS spectra of Bi doped thin films are shown in the figure 4.15. Figure 4.15(a) shows the Zn2p spectrum. The Zn2p spectrum shows two binding energy peaks at 1021.19 eV and 1044.63 eV corresponding to Zn2p<sub>3/2</sub> and Zn2p<sub>1/2</sub> respectively. Figure 4.15(b) shows the asymmetric two O1s peak.

Figure 4.15(b) shows the O1s spectra of Bi doped thin films. There are two asymmetric O1s peaks are located at the binding energies 530.3 eV and 532 eV. The peak corresponding to the lower binding energy is due to Zn-O bond and the other peak located at the higher binding energy accords with the chemisorbed oxygen (Liqiang et al. 2002). The O1s peak is moved slightly to the higher binding energy direction with Bi doping. This may be attributed to minor lattice distortion.

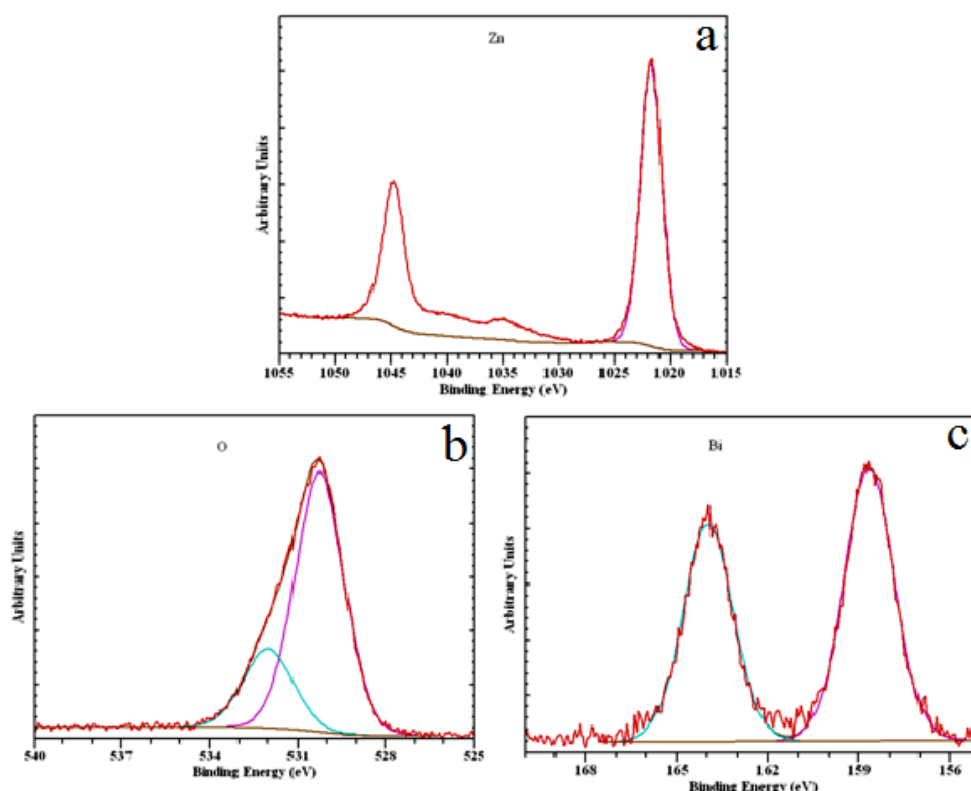


Figure 4.15: XPS spectra of annealed ZnO: 3% Bi films; (a) Zn2p spectra, (b) O1s spectra and (c) Bi4f spectra.

The figure 4.15(c) represents Bi4f core level spectra of Bi doped film which show two asymmetric peaks located at 158.7 eV and 163.9 eV calculated using Gaussian peak fitting. The peaks located at 163.9 eV and 158.7 eV are assigned to Bi 4f<sub>5/2</sub> and Bi 4f<sub>7/2</sub> region, respectively. The peak located at 163.9 eV confirms the presence of Bi<sup>3+</sup> in the ZnO lattice (Jingjing et al. 2011). The peak located at about 158.7 eV, which is attributed to the Bi-O bonding rather than Zn-Bi bonding in the Bi doped thin films. This is because no peaks located below 157.0 eV attributed to Zn-Bi bonding in the Bi doped films; the contents of Bi<sub>2</sub>O<sub>3</sub> may be very small in the Bi doped

films. Otherwise no peaks will be located at about 157 eV attributed to isolate Bi in Bi doped thin films (Xiaofeng et al. 2010). The atomic percentage of zinc, bismuth and oxygen in the Bi doped thin films is estimated and are found to be 50.25%, 2.58% and 47.17% respectively.

The optical transmittance of Bi doped thin films was measured in the visible region. The transmittance spectra of Bi doped films was compared with that of undoped thin films and shown in the figure 4.16(a). From the spectra it is observed that all films show the average transmittance above 75% in the visible region, which means incorporation of Bi into ZnO film doesn't affects the transmittance of the films.

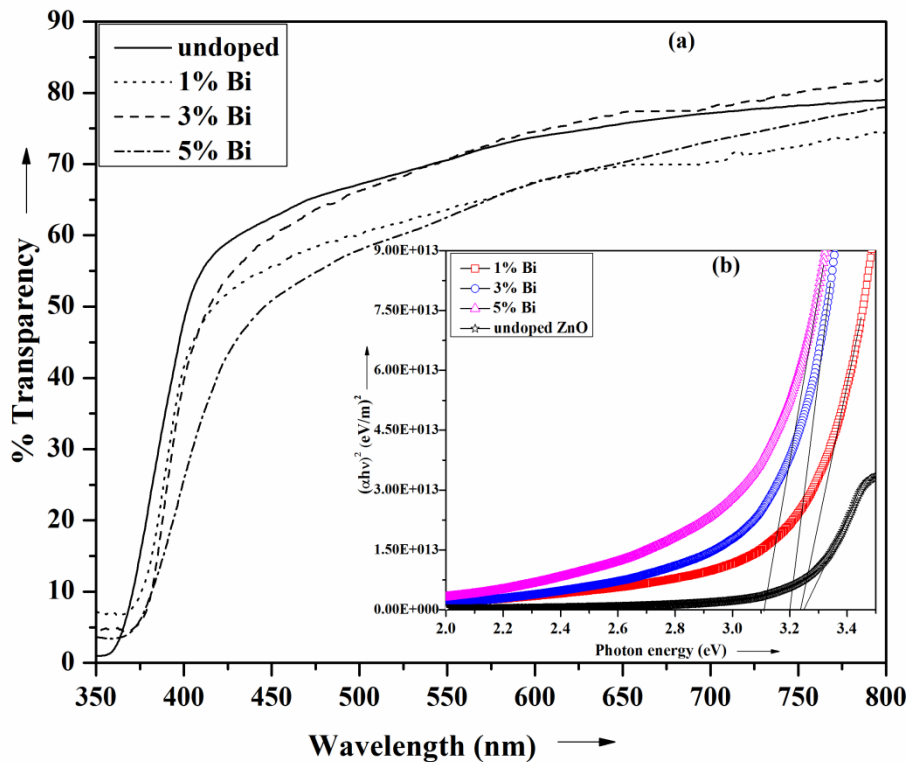


Figure 4.16: (a) Transmittance spectra and (b) Tauc's plot for Bi doped ZnO thin films.

The optical band gap of Bi doped thin films compared with that of undoped thin films as shown in the figure 4.16(b). The optical band gap decreases from 3.24 eV to 3.12 eV; optical absorption edge shows red shift with increase in Bi doping concentration from 0 to 5%. The reduction in the band gap of Bi doped thin films is also reported by Minhong et al. (2009). This systematic reduction in the band gap

with increasing Bi concentration might arise from the doping effect. Reduction in the band gap is due to more disorder produced in the film by doping. This rise in the disorder leads to a redistribution of states band to tail, allowing more number of transitions of band to tail and tail to tail (ÓLeary et al. 1997). Thus reduction in the band gap and widening of Urbach tail occurred.

The incorporation of Bi into ZnO lattice affects the electrical properties of the films. It is noted that the electrical conductivity of the thin films increased with increased Bi concentration up to 5%. The calculated conductivity values are shown in table 4.6. The increase in the conductivity may be due to substitution of  $\text{Bi}^{3+}$  to  $\text{Zn}^{2+}$  in ZnO lattice, contributing additional charge carriers for electrical conduction. Thus increase in the electrical conductivity may be attributed to the presence of extra charge carriers introduced by the dopant (Zhu et al. 2006). I-V characteristics of Bi doped thin films are presented in figure 4.17.

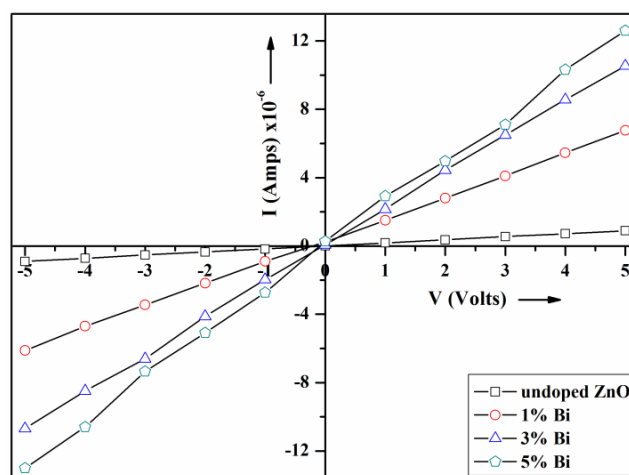


Figure 4.17 : I-V characteristics of Bi doped ZnO thin films.

The figure 4.18 represents  $\log R$  versus  $1/T$  plot for 3% Bi doped ZnO films. The plot shows a linear behavior in two regions indicating double activation energies. In these two regions the activation energy is proportional to the slope; hence activation energy can be calculated using equation 2.3.26. The increase in electrical conductivity of the Bi doped films was explained by the observed activation energy. The measured activation energies are found to be decreased with increased Bi dopant concentration (table 4.6). The observed least value of activation energy is 97.1 meV for 5% Bi

doped thin films. This will contribute to the electrical conductivity of Bi doped films with very low energy loss hence conductivity is maximum (Gonzales et al. 1998).

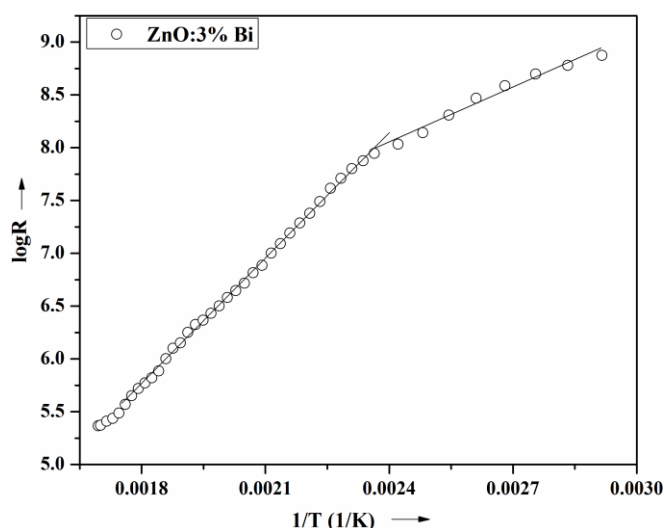


Figure 4.18: Variation of logR vs. reciprocal temperature of 3% Bi doped thin films.

Condition type of carriers in Bi doped thin films was also studied by hot probe technique. These films show positive voltage on the multimeter indicating n-type conductivity. Further the n-type conductivity of Bi doped ZnO films are confirmed by Hall measurements. The calculated data of mobility and carrier concentration of Bi doped thin films with different dopant concentrations are shown in the table 4.6.

Table 4.6: Optical and electrical data of Bi doped ZnO thin films.

Bi %	$E_g$ (eV)	$\sigma$ (S cm <sup>-1</sup> )	$E_a$ (meV)		$n$ (cm <sup>-3</sup> )	$\mu$ (cm <sup>2</sup> V <sup>-1</sup> sec <sup>-1</sup> )
1	3.23	2.76	341	115	$1.49 \times 10^{18}$	11.7
3	3.20	4.22	338	105	$2.00 \times 10^{18}$	13.2
5	3.12	6.04	285	97.1	$2.63 \times 10^{18}$	14.4

### 4.3.2 Effect of annealing temperature

The 3% Bi doped ZnO thin were prepared and these films were annealed at different temperatures to study the effect of annealing on the structural, morphological and optical and electrical properties.

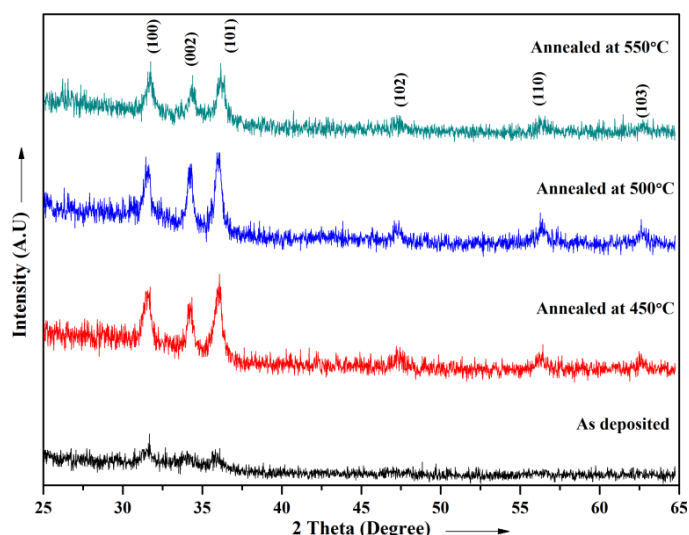


Figure 4.19: XRD spectra of ZnO:3% Bi films annealed at different temperatures for 4 h.

XRD pattern of *as-deposited* and annealed 3% Bi doped thin films is presented in figure 4.19. The *as-deposited* and annealed films show polycrystalline hexagonal wurtzite structure with (101) preferential orientation. The *as-deposited* films have more stress, which is developed during the deposition due to the accumulation of crystallographic defects. Annealing of the films reduces the stress. The peak intensity of (101) plane increased with increase in annealing temperature. The estimated grain size of the films found to increase with increase in annealing temperature (table 4.7). This suggests that annealing improve the crystallinity of the films.

Table 4.7: XRD data of annealed 3% Bi doped ZnO films.

Annealing temp.(°C)	Texture	D (nm)	Strain
As-deposited at 450	(101)	7.58	0.0112
450	(101)	15.9	0.0039
500	(101)	17.2	0.0078
550	(101)	24.6	0.0041

Scanning electron micrographs of *as-deposited* and annealed 3% Bi doped thin films are shown in the figure 4.20. The morphology of *as-deposited* film appears a patched grain clusters [fig. 4.20(a)]. The uniformly distributed grains are seen from the micrograph when the films are annealed 450°C [fig. 4.20(b)]. Further increase in the annealing temperature to 500°C and 550°C show increase in the grain size [fig. 4.20(c) & (d)] respectively.

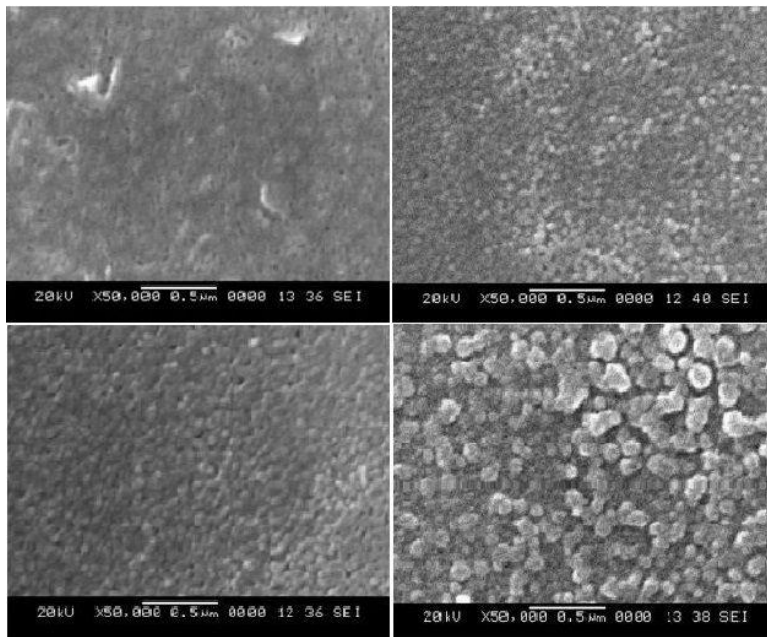


Figure 4.20: SEM image of ZnO: 3% Bi films (a) as-deposited and annealed at (b) 450°C, (c) 500°C, (d) 550°C.

Optical transmittance spectra of *as-deposited* and annealed ZnO: 3% Bi films are shown in figure 4.21(a). *As-deposited* films show transparency of 75% in the visible region. On increasing annealing temperature transparency of Bi doped films remains same suggesting that transmittance is unaffected by annealing.

The optical band gap of *as-deposited* and annealed ZnO: 3% Bi thin films are shown in the figure 4.21(b). The optical band gap of *as-deposited* Bi doped thin films is 3.30 eV which reduces to 3.05 eV, as the annealing temperature increases to 550°C (table 4.8). According to reports, decrease in the band gap occurs due to appearance of band tail resulting from defects associated with the presence of cavities and surface roughness (Regragui et al. 2001).

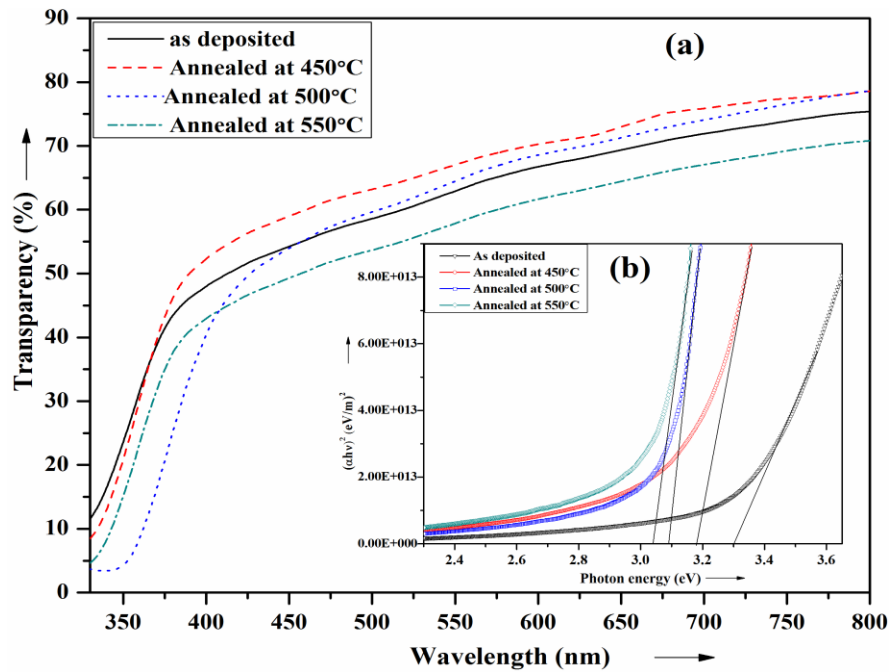


Figure 4.21: (a) Transmittance spectra and (b) Tauc's plot for ZnO: 3% Bi films annealed at different temperatures.

Figure 4.22 shows the I-V characteristics of ZnO: 3% Bi thin film annealed at different temperatures. The films annealed at 500°C show maximum conductivity; further increase in the annealing temperature resulting decrease in conductivity of the films. The improvement in electrical conductivity of the ZnO: 3% Bi films were observed after annealing at 450°C. The observed increase in mobility and hence conductivity may be due to the enhancement of films crystallinity and grain growth. On the other hand the low values of conductivity observed for films annealed at 550°C is due to the chemisorptions process of oxygen taking place on the films surface which acts as an acceptor of electrons from occupied conduction band states (Mohamed 2007).



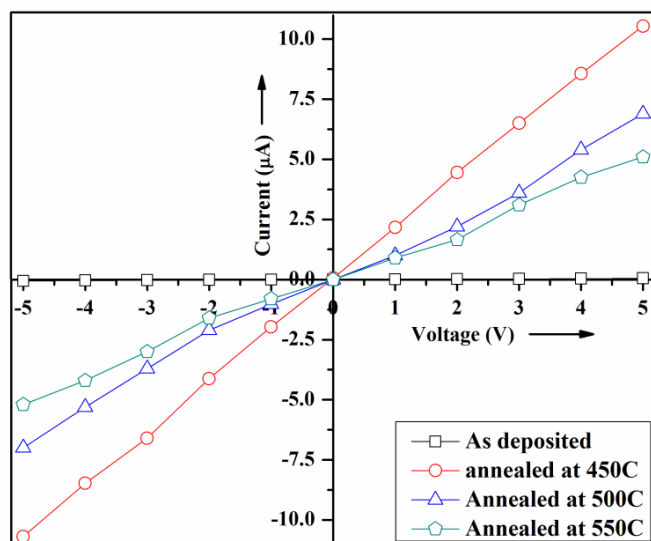


Figure 4.22: I-V characteristics of annealed ZnO: 3% Bi thin films.

The estimated activation energy of annealed ZnO: 3% Bi films are shown in the table 4.8. The increase in electrical conductivity of the Bi doped films with annealing is explained by the observed activation energy. The least value of activation energy contributes more for conductivity. Hence the conductivity is high for films annealed at 500°C. The condition type of annealed ZnO: 3% Bi films were also studied by hot probe technique. All the annealed Bi doped films show positive voltage on the multimeter indicating n-type conductivity. Further the n-type conductivity of these films was confirmed by Hall measurements. The estimated data of mobility and carrier concentration of annealed Bi doped films are shown in the table 4.8. It is noted that the 3% Bi doped films annealed at 500°C show a conductivity of 4.95 S/cm with a mobility of  $16.6 \text{ cm}^2 \text{ V}^{-1} \text{ sec}^{-1}$  and a carrier concentration of  $1.86 \times 10^{18} / \text{cm}^3$ .

Table 4.8: Optical and electrical data of ZnO: 3% Bi films annealed at different temperatures for 4 h.

Annealing temp.(°C)	$E_g$ (eV)	$\sigma$ (S/cm)	$E_a$ (meV)	$n$ ( $1/\text{cm}^3$ )	$\mu$ ( $\text{cm}^2 \text{ V}^{-1} \text{ sec}^{-1}$ )
As-deposited at 450	3.30	0.052	---	---	---
450	3.20	4.22	338	105	$2.00 \times 10^{18}$
500	3.09	4.95	280	94.8	$1.86 \times 10^{18}$
550	3.05	1.75	329	122	$2.10 \times 10^{18}$

## CHAPTER 5

# ZnO THIN FILMS DOPED WITH GROUP III ELEMENTS

### 5.1 INTRODUCTION

ZnO with a wurtzite structure is naturally an n-type semiconductor because of a deviation from stoichiometry due to the presence of intrinsic defects such as oxygen vacancies “V<sub>o</sub>” and Zn interstitials “Zn<sub>i</sub>”. Undoped ZnO shows intrinsic n-type conductivity with very high electron densities of about 10<sup>21</sup>cm<sup>-3</sup>. Although it is experimentally known that unintentionally doped ZnO is n-type, whether the donors are Zn<sub>i</sub> and V<sub>o</sub> is still controversial. The density of impurities in semiconductors is one of the major parameter that can control position of Fermi level. The first-principles suggest that none of the native defects show high concentration shallow donor characteristics. First principle calculations have also suggested that the unintentionally incorporated hydrogen acts as source of conductivity and behaves as shallow donor in ZnO (Walle 2000).

Achievement of intentional n-type doping is relatively easy compared to p-type doping. When the zinc oxide is doped with group III elements such as B (Rajendra et al. 2012), Al (Vrushali et al. 2013), Ga (Thirunavukkarasu 2013), In (Auttasit et al. 2012) it substitutes zinc site and group VII elements such as Cl (Ramin and Farid 2012), F (Yoon et al. 2008) substitute oxygen site, resulting in n-type conductivity. As n-type dopants, rare earth metals (group III B) Sc and Y (Minami et al. 2000), group IV elements Si (Clatot et al. 2011), Ge (Jiang et al. 2009), and Sn (Mejda et al. 2013) can be used. Various deposition methods such as MBE, sputtering, PLD, and chemical vapor deposition (CVD) have been used to produce highly conductive n-type films (Miyamoto et al. 2004; Fortunato et al. 2008; Matsubara et al. 2003; Martin et al. 2002).

Morkoc and Ozgur (2007) reported that the group III elements such as Al, Ga, In are substitutional elements for Zn, which are probably more suitable for n-type doping of ZnO due to their lower vapor pressures compared to group VII elements such as Cl, Br, and I substituting for O. Oxidation of Al source during MBE growth may also become a problem because of its high reactivity with O. Ga and In are less reactive than Al.

The importance of n-type doping in ZnO comes from the need for transparent electrodes with high conductivity. The resistivities below  $10^{-4}$   $\Omega$ -cm with carrier concentrations above  $10^{21}$   $\text{cm}^{-3}$  have been obtained for n-type thin films. Al-doped films prepared by photo assisted metal-organic vapor-phase epitaxy (MOVPE) were shown to exhibit a minimum resistivity of  $6.2 \times 10^{-4}$   $\Omega$ -cm (Myong et al. 1997). Resistivities as low as  $1.2 \times 10^{-4}$   $\Omega$ -cm have been reported for Ga-doped thin films grown by chemical vapor deposition (Atev et al. 1995). It should be noted that the dopant concentrations in these films, which were meant to be used for transparent conductive electrodes, are relatively high. Thus, n-type doped thin films are developed very well. Such films are successfully used for applications in transparent ohmic contacts as well as light-emitting diodes as n-type layers.

In the present work the optical and electrical properties of spray deposited ZnO thin films have been studied by doping with third group metals namely aluminium (Al), indium (In), and gallium (Ga). The doping concentration is varied from 0 to 5%. The effects of annealing on the optical and electrical properties of these films were also studied.

## **5.2 ALUMINIUM (Al) DOPED ZnO THIN FILMS**

In the present study aluminium (Al) doped ZnO thin films were prepared by spraying precursor solution of zinc acetate anhydrous  $[\text{Zn}(\text{CH}_3\text{COO})_2]$  (Alfa Aesar 99.99%) and aluminium chloride  $[\text{AlCl}_3]$  (Alfa Aesar 99.99%), in methanol. The deposition parameters were maintained almost identical to that for the deposition of undoped ZnO thin films (table 3.4).

### 5.2.1 Effect of doping concentration

The Al doped ZnO thin films were prepared on glass substrate by varying the aluminium doping concentration from 0 to 5%. The structural, morphological, optical and electrical properties of these films were studied in detail. The thickness of Al doped ZnO films were maintained around 600 nm throughout the study.

XRD pattern of Al doped ZnO thin films are shown in the figure 5.1. The estimated values of  $d_{hkl}$  were compared with the standard data which confirmed that Al doped thin films exhibit polycrystalline hexagonal wurtzite structure. The films doped with 3% Al show (002) texture which changes to (101) for further increase in doping concentration. From the figure 5.1 it is seen that increase in doping concentration decrease the (002) peak intensity. However there is no peak corresponding to aluminium or aluminium related phase detected in the XRD pattern.

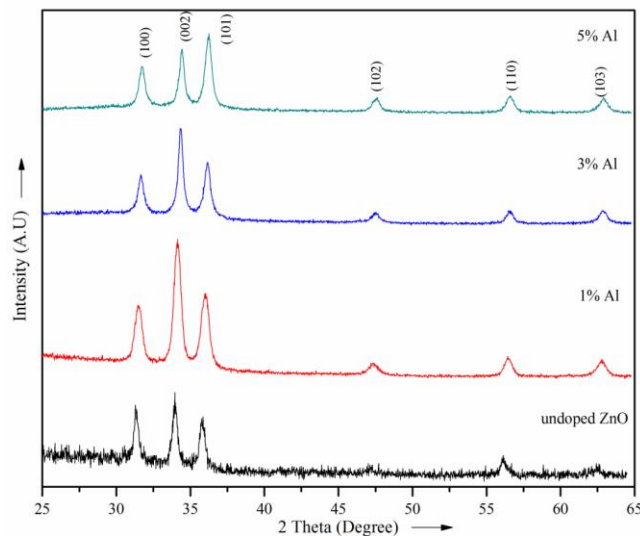


Figure 5.1: XRD spectra of undoped and Al doped ZnO films.

The residual strain and grain size of Al doped thin films were estimated from the XRD pattern using equation 2.3.3 and the results are shown in the table 5.1. The strain is found to increase with increasing Al concentration. The lattice parameters  $a$  and  $c$  of Al doped thin films were calculated using equation 2.3.2. The lattice parameters were found to be constant up to 5% Al doping.

Table 5.1: XRD data Al doped ZnO thin films.

at.% Al	Texture	D (nm)	Strain
1	(002)	20.5	0.0016
3	(002)	25.8	0.0036
5	(101)	18.9	0.0057

The SEM image of Al doped thin films are shown in the figure 5.2. It is observed that the undoped thin films show smooth and plane surface. The morphology of 1% Al [fig. 5.2(b)] doped thin films show uniform distribution of tiny grains. An increase in the Al concentration increases the grain size without affecting the uniform distribution of grains up to 3% [fig 5.2(c)]. The presence of aluminium in ZnO films is confirmed by EDAX analysis [fig 5.3]. The SEM image of Al doped ZnO films show uniform distribution of grains and these grains have same composition as background confirmed by EDAX analysis.

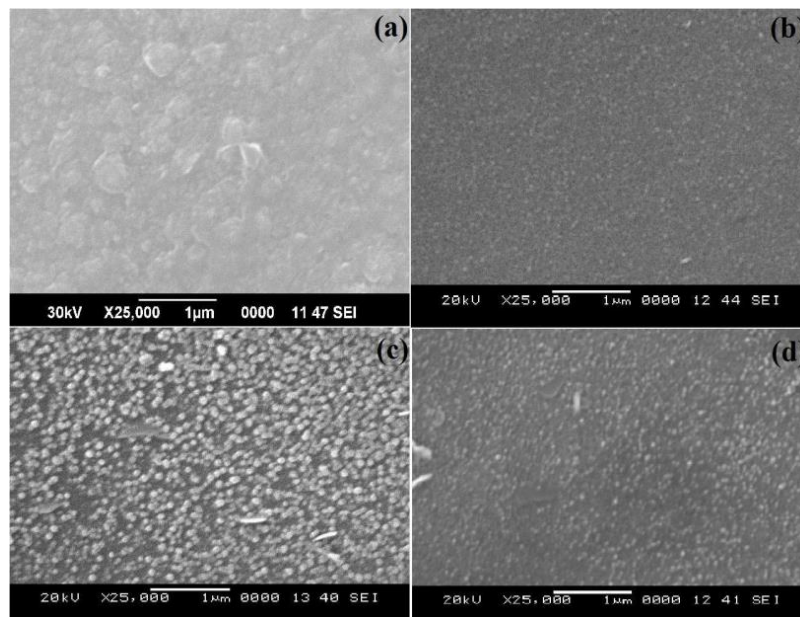


Figure 5.2: SEM image of (a) undoped, (b) 1% Al, (c) 3% Al & (d) 5% Al doped ZnO films.

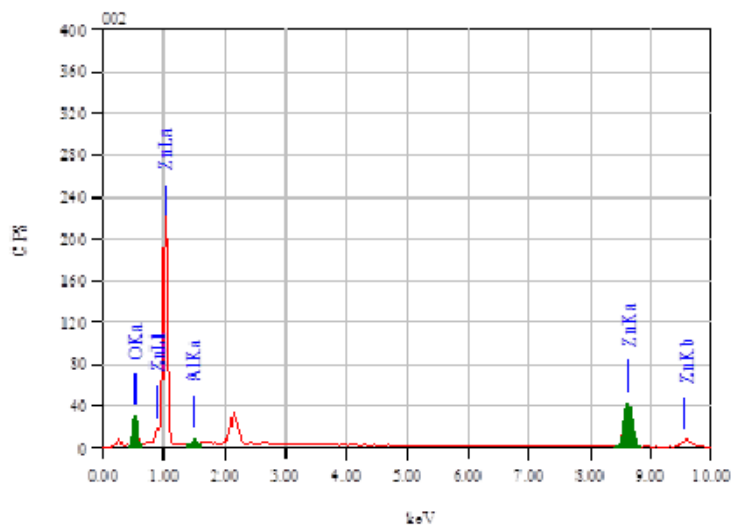


Figure 5.3: EDAX spectrum of 3% Al doped ZnO films.

The transmittance spectra of Al doped thin films are shown in the figure 5.4(a). Undoped films show the transparency above 77% in the visible region. The high transparency of 83% for wavelengths over 550 nm is recorded for 1% Al doped thin films. An increase in transmittance may be due to the fact that doped films provides more voids than the undoped films, which may reduce the optical scattering (Hong et al. 2007). It is also observed from the figure 5.4(a) that sharp absorption edge is slightly shifted to lower wavelength region for Al doped films, which confirms the incorporation of Al into the ZnO films.

Figure 5.4 (b) show the band gap evaluation of Al doped thin films. According to practical and theoretical results, ZnO exhibits direct band to band transitions (Centinorgu and Goldsmith 2007) and the variation of absorption coefficient with photon energy for direct allowed transitions between bands should obey the equation 2.3.13. The estimated energy band gap of Al doped films are shown in table 5.2.

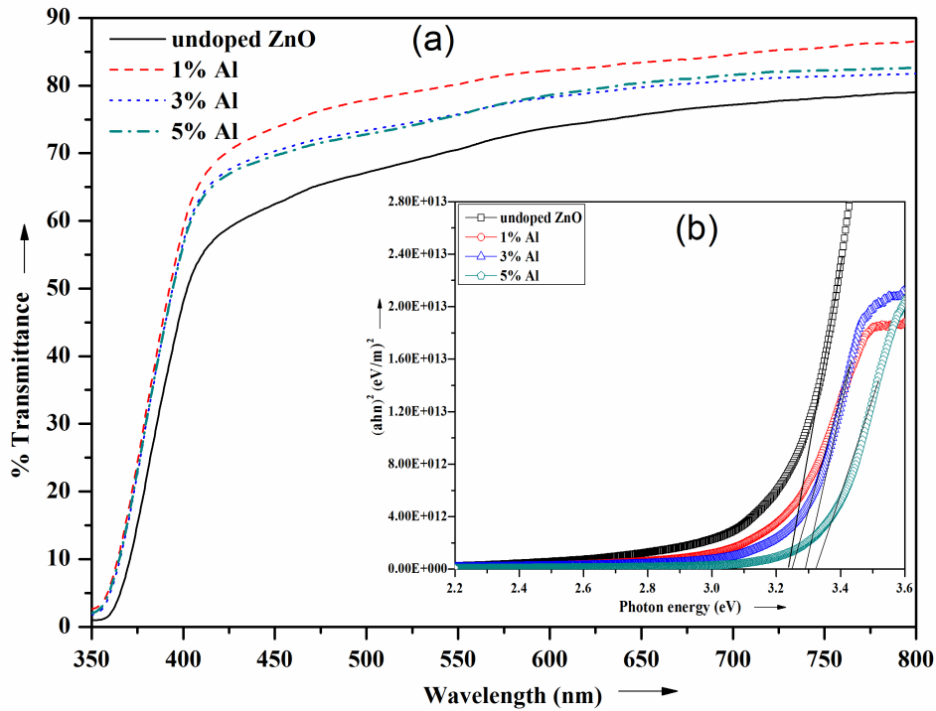


Figure 5.4: (a) Transmittance spectra and (b) Tauc's plot for Al doped ZnO thin films.

The optical band gap of the ZnO thin films found to increase from 3.24 eV to 3.33 eV with increasing Al concentration from 0 to 5 % respectively. The increase in optical band gap is due to the Burstein-Moss effect (Sernelius et al. 1988). This indicates the rise in Fermi level in the conduction band due to increased charge carriers, which leads to broadening of the optical band-gap. According to the reports, energy band gap of single crystal ZnO is about 3.37 eV (Pankove 1975), which is greater than estimated band gap. The observed low value of band gap may be due to the presence of native point defects like zinc interstitials and oxygen vacancies. These point defects create intrinsic defect levels leading to n-type doping. The defect levels exists approximately 0.01-0.05 eV below the conduction band (Pearnton et al, 2005).

I-V characteristics of Al doped thin films are shown in the figure 5.5. The conductivity of undoped thin film was 0.16 S/cm which was increased by three orders of magnitude when doped with aluminium. Films doped with 3% Al show high conductivity of 106 S/cm. The improved conductivity in Al doped thin films due to the replacement of  $\text{Zn}^{2+}$  ions by  $\text{Al}^{3+}$  ions substitutionally (Xu et al. 2006). Addition of small quantity of aluminium contributes more number of free charge carriers in the

doped films and hence results increase in the conductivity. Further increase in Al concentration (5%) reduces the conductivity of the films. This decrease in conductivity may be due to the segregation of excess aluminium in grain boundary and these aluminium ions acts as inactive donors hence reduce the conductivity of the films. Also the estimated activation energy for 5% Al doped films more (table 5.2) hence it contributes least to the conductivity.

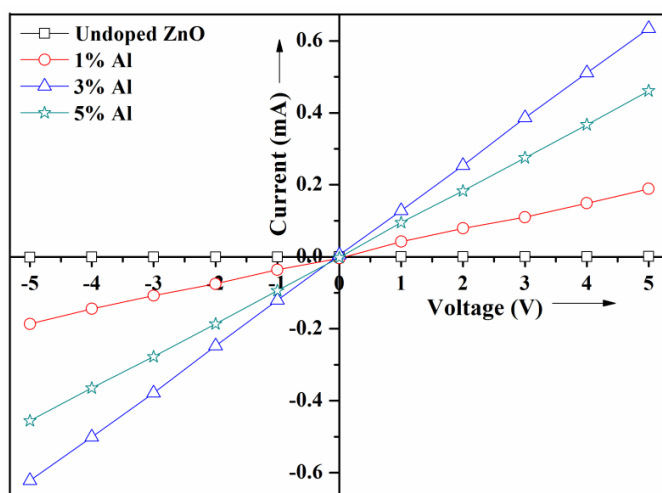


Figure 5.5: I-V characteristics of Al doped ZnO films.

Table 5.2: Optical and electrical data of Al doped ZnO thin films.

at.% Al	$E_g$ (eV)	$\sigma$ (S/cm)	$E_a$ (meV)		$n$ ( $1/\text{cm}^3$ )	$\mu$ ( $\text{cm}^2 \text{V}^{-1} \text{s}^{-1}$ )
0	3.24	0.16	348	217	$9.92 \times 10^{16}$	9.38
1	3.25	23.3	182	38.8	$5.45 \times 10^{18}$	26.7
3	3.29	106	125	44.0	$1.95 \times 10^{19}$	34.1
5	3.33	78.6	230	63.8	$1.62 \times 10^{19}$	30.4

The variation of  $\log R$  with  $1/T$  for 3% Al doped film is shown in the figure 5.6 and results are shown in table 5.2. There are two linear parts having different slopes are observed for all Al doped thin films. This indicates that there are two mechanisms for electrical conduction. According to reports the electron concentration in the films increase by Al doping and the trapping levels with activation energy less than 55 meV contribute to the electrical conductivity with a very low energy loss (Gonzales et al. 1998).



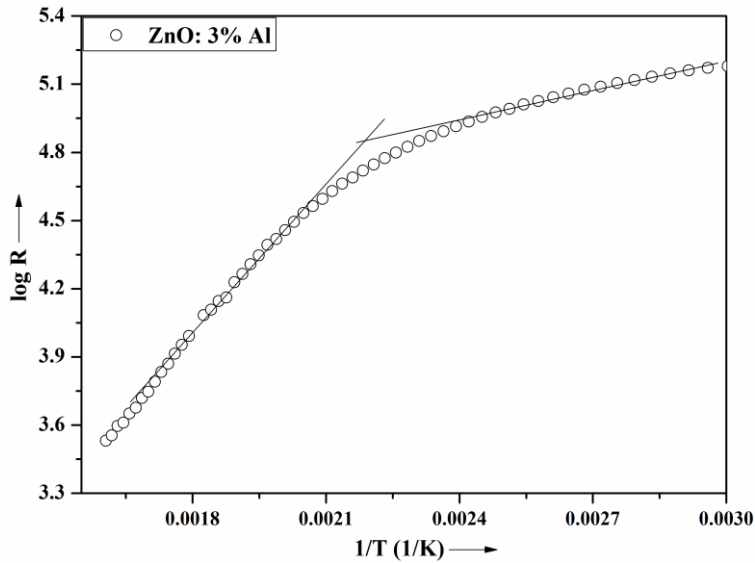


Figure 5.6: Variation of logR vs. 1/T for 3% Al doped ZnO thin films.

Hall measurements of Al doped ZnO thin films were carried out in a magnetic field strength of 0.5T and the results are summarized in the table 5.2. The study shows an increase in the carrier concentration ( $n$ ) and mobility ( $\mu$ ) of thin films after doping with the aluminium which indicates that divalent zinc ion being replaced by trivalent aluminium ions leading to the formation of zinc interstitials. The thin films prepared with 3% Al show the highest conductivity of 106 S/cm with a electron concentration of  $19.5 \times 10^{18} / \text{cm}^3$  and a Hall mobility of  $34.1 \text{ cm}^2 \text{ V}^{-1} \text{ s}^{-1}$ . The reduction in the mobility at higher (5%) Al doping concentration indicates that it is a grain boundary scattering mechanism rather than ionized impurity scattering (Gil and Myoung 2009) since the grain size decreased for 5% Al doped films. The reduced mobility explains the decrease in conductivity of the films at higher doping level (5% Al).

### 5.2.2 Effect of annealing temperature

The spray deposited 3% Al doped ZnO films show better optical and electrical properties, hence these films were further annealed at different temperatures and their structural, morphological, optical and electrical properties were studied.

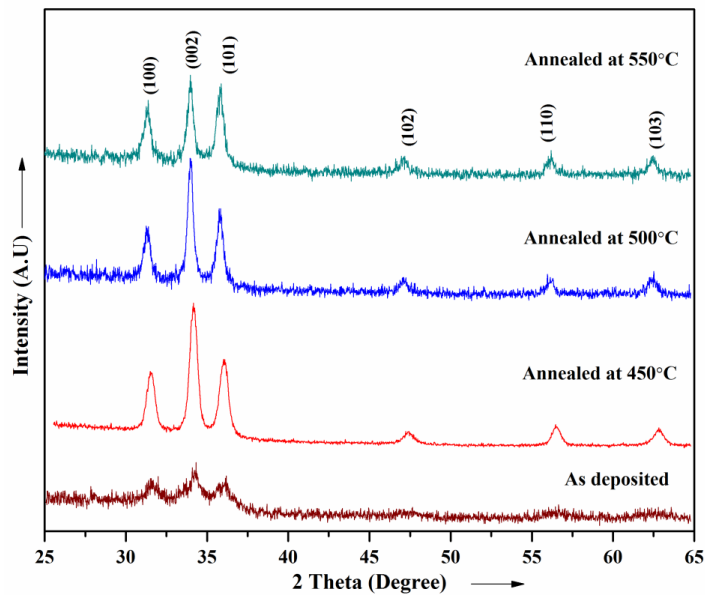


Figure 5.7: XRD pattern of ZnO: 3% Al thin films.

XRD pattern *as-deposited* and annealed Al doped ZnO thin films are shown in figure 5.7. All the films exhibit polycrystalline hexagonal wurtzite structure with (002) texture. The (002) peak intensity increased with an increase in the annealing temperature indicating improvement in crystallinity of the films. The strain and grain size of the annealed Al doped ZnO films were estimated and the results are summarized in table 5.3. The increase in grain size and decrease in residual strain of Al doped films with annealing temperature indicates improvement in crystallinity of the films.

Table 5.3: XRD data of ZnO: 3% Al film annealed at different temperatures for 4 h.

Annealing Temp ( ° C)	Texture	D (nm)	Strain
As-deposited at 450	(002)	10.5	0.0048
450	(002)	25.8	0.0036
500	(002)	27.2	0.0031
550	(002)	29.3	0.0029

The SEM image of *as-deposited* and annealed 3% Al doped thin films are shown in the figure 5.8. The *as-deposited* films show a smooth surface morphology whereas considerable transformations have been observed in the morphology of Al doped films on annealing. The films annealed at 450°C show a fine grains and the estimated

average grain size is 30 nm. The average grain size of the films annealed at 500°C and 550°C are 34 nm and 38.6 nm respectively.

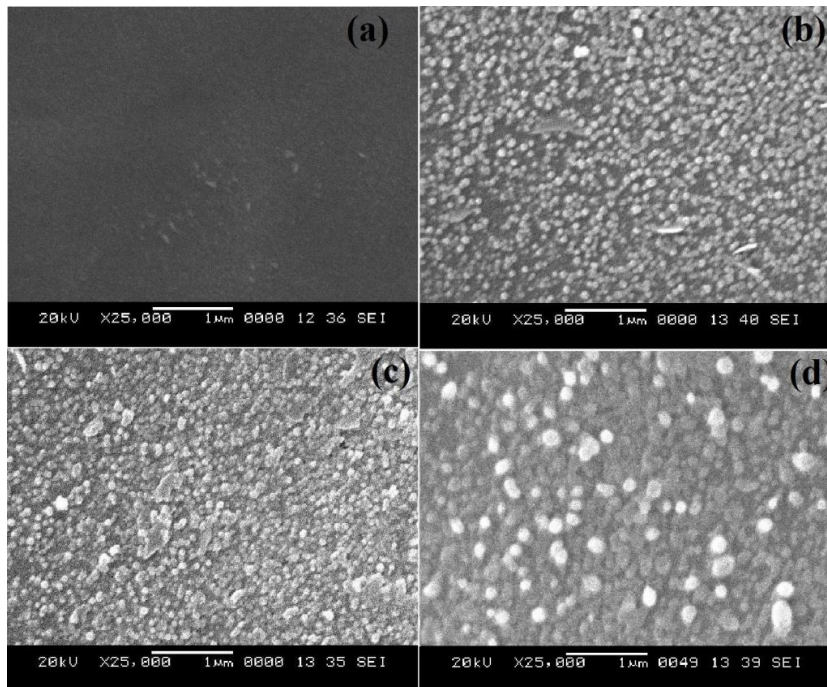


Figure 5.8: SEM image of ZnO: 3% Al thin films (a) *as-deposited*, (b) annealed at 450°C, (c) annealed at 500°C and (d) annealed at 550°C.

Transmittance spectra of *as-deposited* and annealed Al doped ZnO films are shown in the figure 5.9(a). The *as-deposited* film show less transmittance than the annealed films. The films annealed at 450°C attained a maximum transmittance of 80% in the visible region. Figure 5.9(b) represents the Tauc's plot for *as-deposited* and annealed 3% Al doped thin films. The band gap of *as-deposited* Al doped thin films is 3.37 eV which is found to decrease with an increase in annealing temperature. This decrease is may be due to decrease in the carrier concentration.

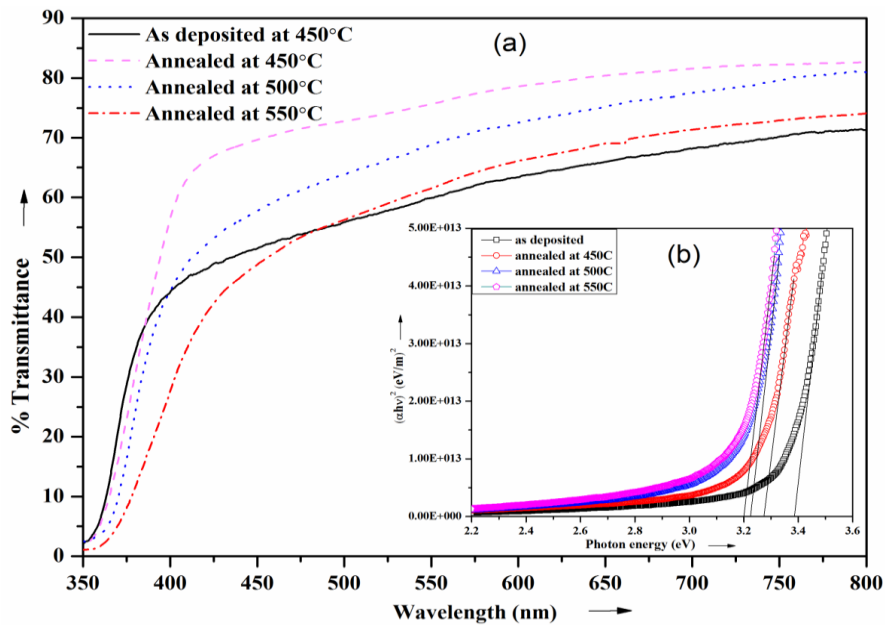


Figure 5.9: (a) Transmittance spectra and (b) Tauc's plot for *as-deposited* and annealed ZnO: 3% Al thin films.

The variation of current with voltage of *as-deposited* and annealed ZnO: 3% Al films are shown in figure 5.10. It reveals that the *as-deposited* film have low conductivity of 5.5 S/cm. On annealing, an increase in the grain size is observed. The increase in grain size decreases the grain boundary scattering, thus increases the Hall mobility and carrier concentration results in improvement in the conductivity (Lin et al. 2013).

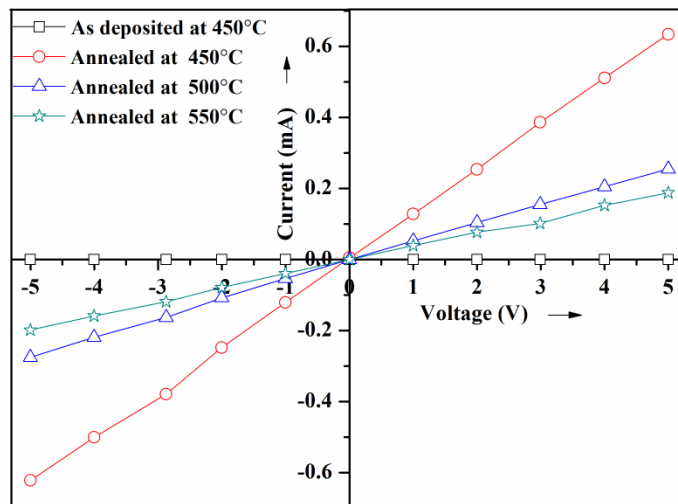


Figure 5.10: I-V characteristics of ZnO: 3% Al thin films.

The films annealed at 500°C and 550°C show decrease in conductivity which is due to the decrease in carrier concentration. The possible reason for decrease of carrier concentration is that after annealing treatment Al interstitials diffuse into ZnO matrix, which decreases the amount of donors. The other possibility is that evaporation of zinc during annealing possibly decreases the intrinsic donors inside the film, these results in decrease of carrier concentration (Kim et al. 2005). In general, an increase in the annealing temperature reduces the conductivity of Al doped films by increasing grain boundaries and crystal deficiencies of the film (Ohyama et al. 1998). The activation energy of the annealed films was estimated using equation 2.3.26 and the data are shown in the table 5.4. The films annealed at 450°C show least activation energy and high carrier concentration leading to maximum conductivity of the films.

Table 5.4: Optical and electrical data of ZnO: 3% Al films annealed at different temperatures for 4 h.

Annealing temp. (°C)	$E_g$ (eV)	$\sigma$ (S/cm)	$E_a$ (meV)		$n$ (1/cm <sup>3</sup> )	$\mu$ (cm <sup>2</sup> V <sup>-1</sup> s <sup>-1</sup> )
As-deposited at 450	3.37	5.50	326	134	---	---
450	3.29	106	125	44.0	$1.95 \times 10^{19}$	34.05
500	3.22	81.9	285	58.5	$1.36 \times 10^{19}$	37.7
550	3.16	59.8	312	86.5	$9.61 \times 10^{18}$	38.92

### 5.3 INDIUM (In) DOPED ZnO THIN FILMS

In the present investigation indium (In) doped ZnO thin films were prepared by spraying precursor solution of zinc acetate anhydrous  $[\text{Zn}(\text{CH}_3\text{COO})_2]$  (Alfa Aesar 99.99%) and indium chloride  $[\text{InCl}_3]$  (Alfa Aesar 99.99%), in methanol. The deposition parameters were maintained almost identical to that for the deposition of undoped ZnO thin films (table 3.4). The obtained film thickness of 600 nm was used for the study.

#### 5.3.1 Effect of doping concentration

In doped ZnO thin films were prepared on glass substrate by spray pyrolysis technique. The indium concentration is varied from 0 to 5% in the precursor solution. The films were annealed at 450°C and their structural, optical and electrical properties were studied in detail.

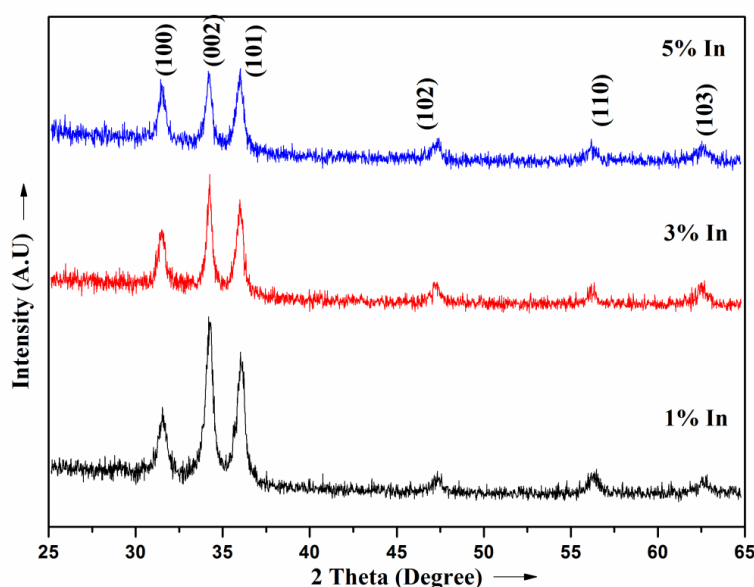


Figure 5.11: XRD pattern of In doped ZnO films.

XRD pattern of In doped ZnO films is shown in the figure 5.11. All the films exhibit hexagonal wurtzite structure with (002) texture. The strain and averaged grain size of In doped ZnO films were calculated using Williamson-Hall equation (2.3.3).

The estimated grain size and strain values are shown in table 5.5. The estimated lattice parameter remains almost same as that of undoped films.

Table 5.5: XRD data of indium doped ZnO thin films.

In at.%	Texture	D (nm)	Strain
1	(002)	25.0	0.0027
3	(002)	27.2	0.0030
5	(101)	23.4	0.0042

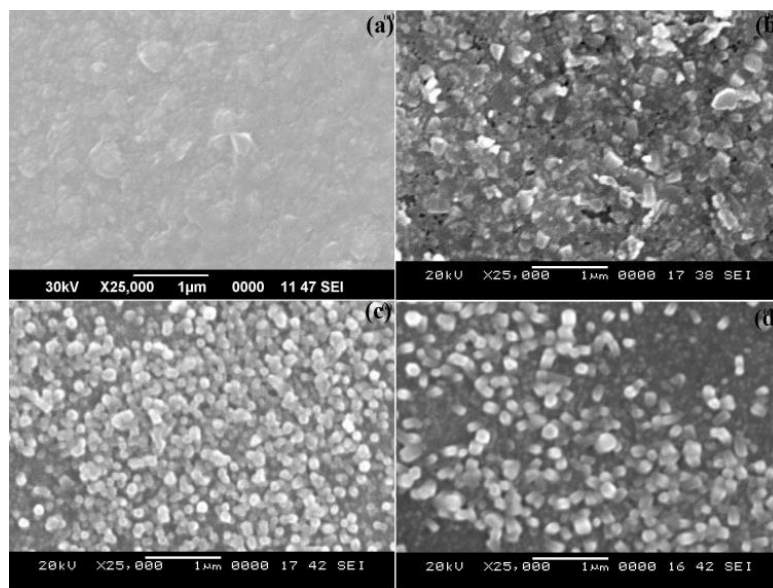


Figure 5.12: SEM image of (a) undoped (b) 1% In, (c) 3% In and (d) 5% In doped ZnO thin films.

The SEM images of indium doped films and undoped films are shown in the figure 5.12. The undoped thin film shows plane and smooth surface. The indium doped films exhibit grain like structure on the surface. The morphology of In doped films appears uniform distribution of grains on the surface. The inclusion of indium improves the grain growth of thin films. The surface morphology of thin film becomes rough with increasing In concentration. The inclusion of indium into ZnO film was confirmed by EDAX analysis [fig. 5.13]. The SEM image of In doped ZnO films show grains with increasing size and they are not rich in indium but have same composition as background confirmed by EDAX analysis.

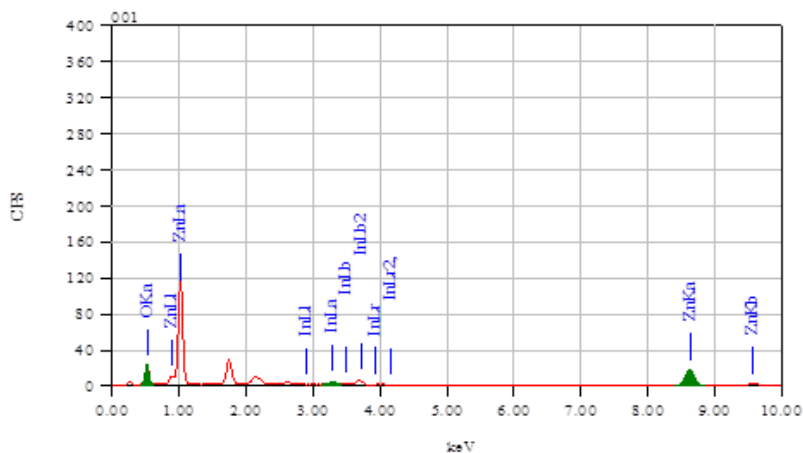


Figure 5.13: EDAX spectrum of 3% In doped ZnO thin films.

The composition analysis of indium doped ZnO thin films were investigated using X-ray photoelectron spectroscopy (XPS). The XPS spectrum of 3% In doped thin films is shown in the figure 5.14. Figure 5.14(a) and (b) shows the survey scan and Zn2p spectrum respectively. In Zn2p spectrum binding energy peak located at 1020.6 eV corresponding to Zn2p<sub>3/2</sub> core level. Figure 5.14 (c) and (d) shows the O1s and In3d core level spectrum respectively.

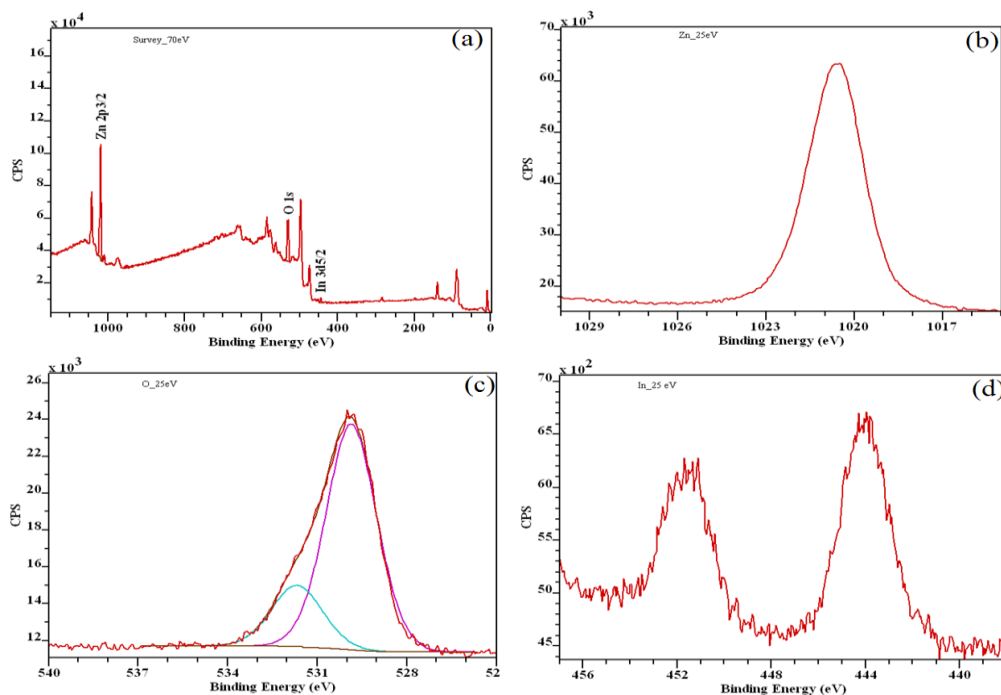


Figure 5.14: XPS spectra of ZnO: 3% In thin films annealed at 450°C (a) Survey scan, (b) Zn2p spectra, (c) O1s spectra and (d) In3d spectra.



Figure 5.14(c) shows the O1s XPS spectra of In doped thin films. There are two O1s peaks are located at the binding energies 529.8 eV and 531.6 eV. The peak corresponding to the lower binding energy is due to Zn-O bond and the other peak located at the higher binding energy accords with the chemisorbed oxygen caused by surface hydroxyl group corresponding to O–H bonds (Liqiang et al. 2002).

Figure 5.14(d) shows In3d core level XPS spectrum of 3% In doped thin film, which shows two asymmetric peaks located at 444.05 eV and 451.8 eV and these peaks are corresponding to In3d<sub>3/2</sub> and In3d<sub>5/2</sub> region, respectively (Satish and Mulla 2009). The In3d<sub>5/2</sub> and In3d<sub>3/2</sub> peaks are ascribed to In-O bonding, further these peaks suggest that In has been incorporated into the ZnO film and exists in the form of In<sub>Zn</sub> rather than In<sub>O</sub>. The atomic percentage of zinc, indium and oxygen in the In doped ZnO films is estimated and are found to 49.6%, 2.8% and 47.6% respectively.

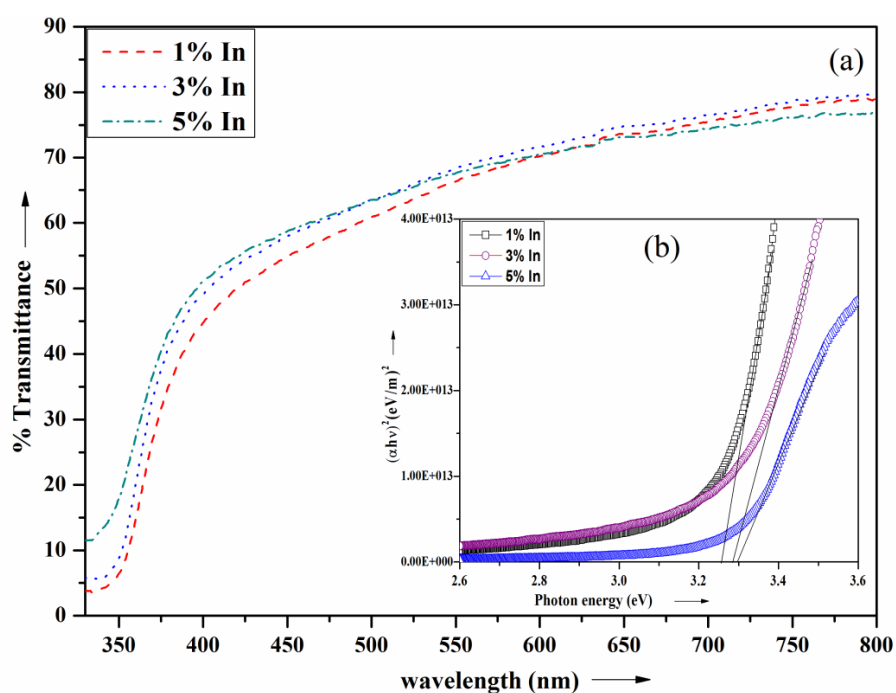


Figure 5.15: (a) Transmittance spectra and (b) Tauc's plot for In doped ZnO thin films.

The transmittance spectra of In doped thin film deposited on glass substrate at 450°C is shown in figure 5.15(a). All the films show the average transmittance above the 75 % in the visible region, which means incorporation of In into ZnO lattice does

not affects the transmittance of the films. Tauc's plot for In doped thin films are shown in figure 5.15(b). It is found that optical band gap of ZnO films increase from 3.24 eV to 3.31 eV; optical absorption edge shows blue shift with increasing In concentration from 0 to 5%. The broadening of energy band gap of the ZnO films may be explained on the basis of Moss-Burstein theory (Sernelius et al. 1988).

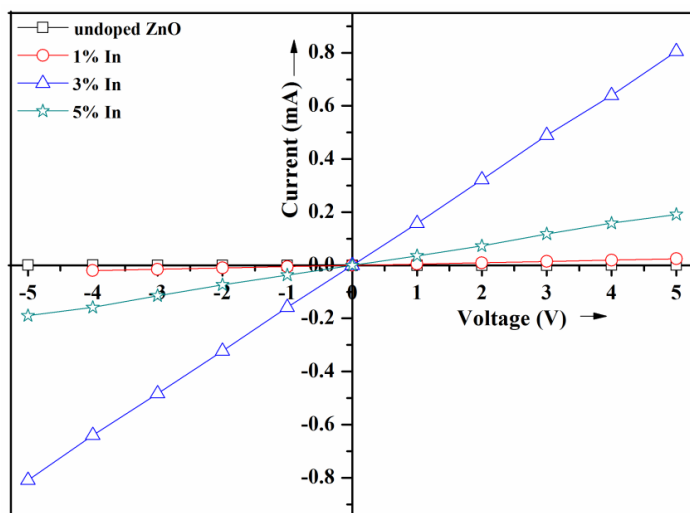


Figure 5.16: I-V characteristics of In doped ZnO thin films.

The estimated band gap, conductivity and activation energies of In doped films are shown in table 5.6. Figure 5.16 shows the linear I-V characteristics of In doped ZnO thin films. The electrical conductivity of the ZnO films increases sharply with an increase in indium concentration up to 3%. This increase in conductivity may be due to substitution of  $\text{In}^{3+}$  to  $\text{Zn}^{2+}$  in ZnO lattice, contributing extra charge carriers to the electrical conduction. Thus increase in the electrical conductivity may be attributed to the presence of large number of charge carriers introduced by the dopant (Yasemin et al. 2011). Addition of small quantity of indium contributes more number of free charge carriers in the doped films, therefore conductivity increases. It is noted that at higher doping concentration (5%), conductivity of the thin films decreases. This decrease in conductivity is may be due to the segregation of excess indium in grain boundary which reduces the conductivity of the films (Samanta et al. 2012).

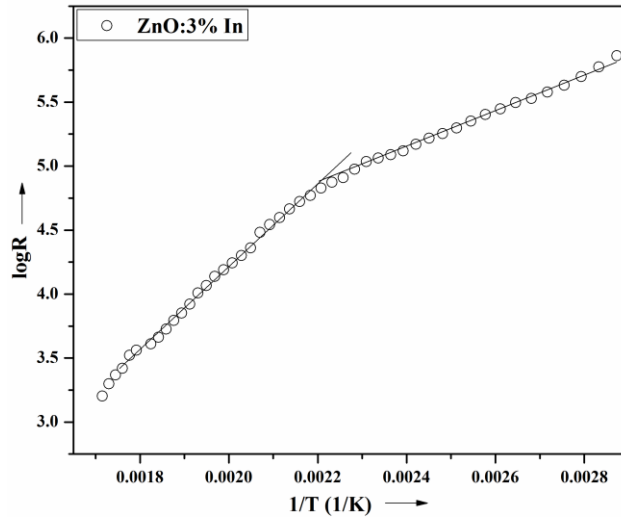


Figure 5.17: Variation of  $\log R$  vs.  $1/T$  of 3% In doped ZnO thin film.

Figure 5.17 shows the variation of  $\log R$  with reciprocal temperature for the 3% In doped thin film. The activation energies of In doped thin films were calculated using the equation 2.3.26 and the results are shown in table 5.6. It is noted that the shallow donor levels with least activation energy of 68.2 meV is observed for 3% In doped films, hence it contributes more to the electrical conductivity with very low energy loss. On the other hand, conductivity of 5% In doped films decreases which is in agreement with the observed high activation energy of shallow donor levels of 5% In doped films.

Table 5.6: Optical and electrical data of In doped ZnO thin films.

In (%)	$E_g$ (eV)	$\sigma$ (S/cm)	$E_a$ (meV)		$n$ ( $1/\text{cm}^3$ )	$\mu$ ( $\text{cm}^2 \text{V}^{-1} \text{sec}^{-1}$ )
0	3.24	0.16	348	217	$9.92 \times 10^{16}$	9.38
1	3.27	35.2	170	83.1	$7.2 \times 10^{18}$	31.1
3	3.29	253	126	68.2	$3.7 \times 10^{19}$	43.6
5	3.31	147	196	129	$2.5 \times 10^{19}$	36.8

Hall measurements of In doped ZnO films were carried out in a magnetic field of 0.5T at room temperature and the results are summarized in table 5.6. The films prepared with 3% In show high conductivity of 253 S/cm with a electron concentration of  $3.68 \times 10^{19} \text{ cm}^{-3}$  and a Hall mobility of  $43.6 \text{ cm}^2 \text{ V}^{-1} \text{ s}^{-1}$ . The carrier concentration is found to decrease in 5% In doped films. The reduction in mobility of 5% In doped films may be due to grain boundary scattering mechanism rather than

ionized impurity scattering (Pan et al. 2007) since the grain size decreased for 5% In doped films. The reduced carrier concentration and mobility explains the decrease in conductivity of thin films at higher doping concentrations. The n-type conductivity in indium doped films is confirmed by Hall measurements.

### 5.3.2 Effect of annealing temperature

The spray deposited 3% In doped ZnO films show better optical and electrical properties, hence these films were annealed at different temperatures and their structural, morphological, optical and electrical properties were studied.

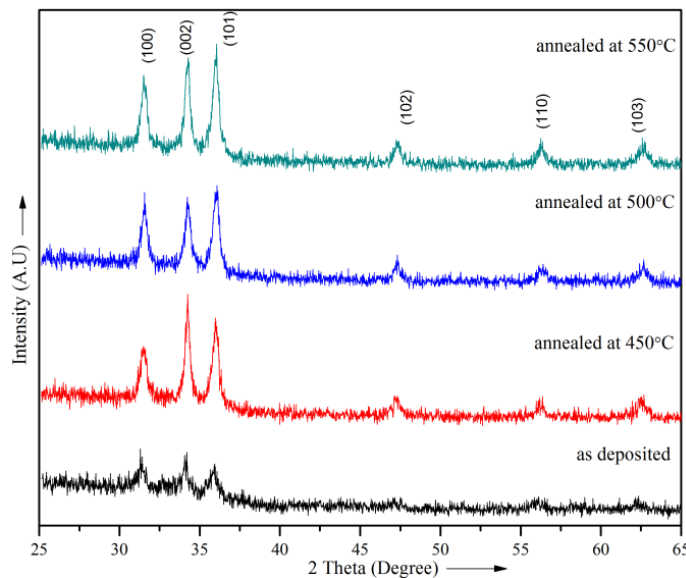


Figure 5.18: XRD pattern of ZnO: 3% In thin films.

The films doped with 3% indium were annealed at different temperatures for 4 h. The XRD patterns of *as-deposited* and annealed films are shown in the figure 5.18. All the films exhibit hexagonal wurtzite structure. The (002) peak intensity of In doped thin films decreased, whereas (101) peak intensity is increased for films annealed above 450°C, hence change in the texture from (002) to (101) is observed. The estimated grain size of In doped thin films found to increase with an increase in annealing temperature, indicating an improvement in crystallinity of the films. The residual strain is found to decrease with increase in annealing temperature. Table 5.7

summarizes the results of estimated strain and grain size of the *as-deposited* and annealed In doped films.

Table 5.7: XRD data of ZnO: 3% In films annealed at different temperatures for 4 h.

Annealing temp. (°C)	Texture	D (nm)	Strain
As-deposited at 450	(002)	13.6	0.0111
450	(002)	25.1	0.0030
500	(101)	26.4	0.0023
550	(101)	29.5	0.0014

SEM images of the 3% In doped ZnO films annealed at different temperatures are shown in the figure 5.19. The as grown films show smooth and uniform surface. On annealing marked changes in surface morphology of In doped films are observed. The films annealed at 450°C show an increase in grain size, with grains of equal size are uniformly distributed on the surface. On further annealing at high temperatures, films show further grain growth. It is seen that the roughness of 3% In doped films increase with annealing temperature.

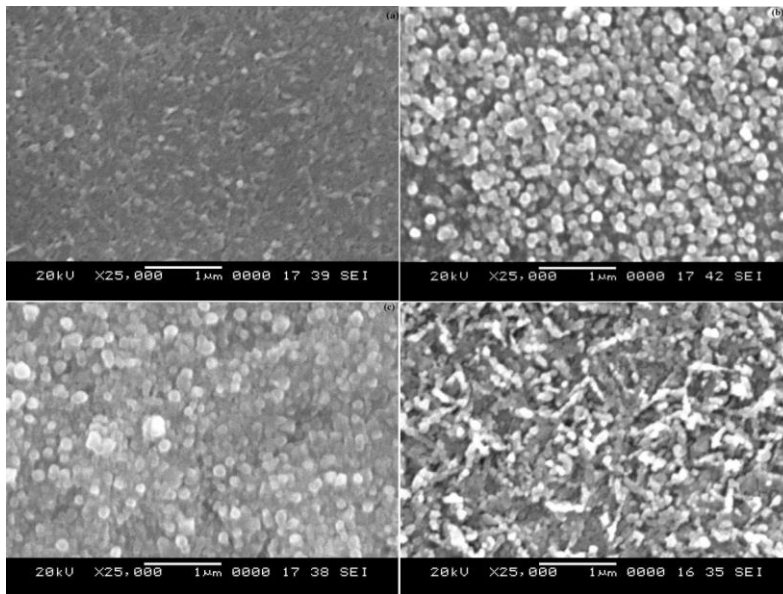


Figure 5.19: SEM image of ZnO: 3% In films (a) *as-deposited*, (b) annealed at 450°C, (c) annealed at 500°C, (d) annealed at 550°C.

The transmittance spectra of 3% In doped ZnO films are shown in the figure 5.20(a). The *as-deposited* In doped films show high transmittance in the visible

region. The transmittance of In doped films slightly decreased when annealing at 550°C. The Tauc's plot for 3% In doped thin films annealed at different temperatures are shown in the figure 5.20(b). The optical band gap of *as-deposited* film is 3.36 eV which is slowly decreased with increased annealing temperature (table 5.8).

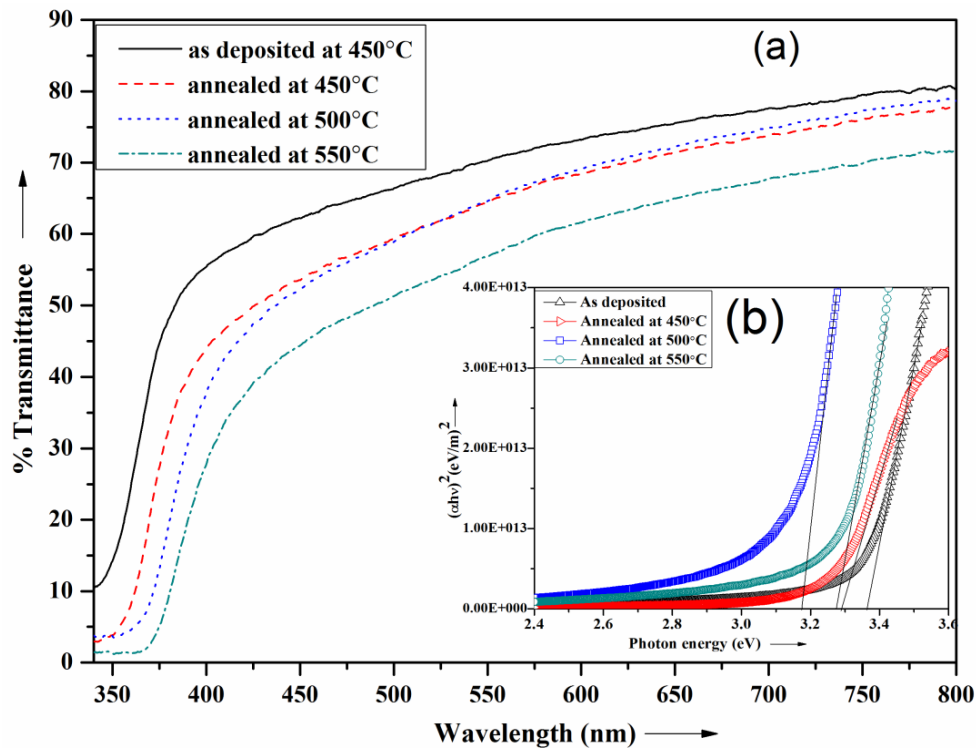


Figure 5.20: (a) Transmittance spectra and (b) Tauc's plot for *as-deposited* and annealed ZnO: 3% In thin films.

I-V characteristics of 3% In doped thin films annealed at different temperatures has been shown on the figure 5.21. It is observed that the *as-deposited* films have low conductivity. The drastic improvement in conductivity of films is observed with annealing. The films annealed at temperature 500°C found to have higher electrical conductivity than the films annealed at other temperatures (table 5.8). The increase in conductivity is due to the increase in carrier concentration.

The calculated activation energies are quite large for *as-deposited* In doped films which contributes least to the conductivity hence low conductivity of the films. High conductivity of the films annealed at 500°C is explained by the observed activation energies (table 5.8). The least activation energy of shallow donor of In doped films

annealed at 500°C is observed, which contributes more to the conductivity with very low energy loss.

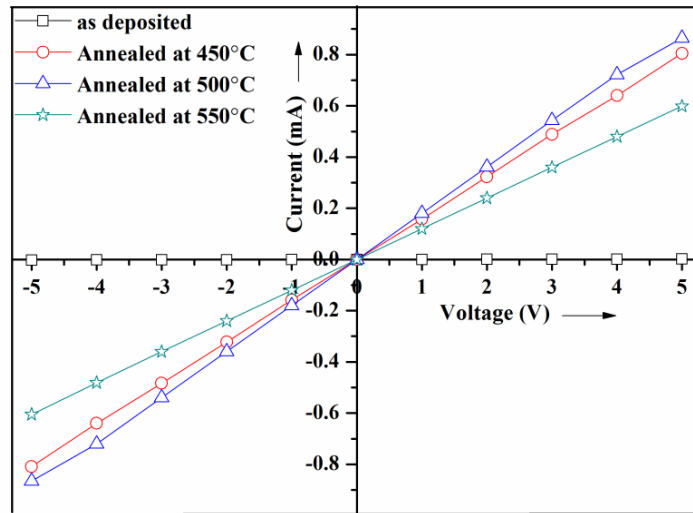


Figure 5.21: I-V characteristics of ZnO: 3% In thin films.

The carrier concentration and mobility of annealed In doped films were determined from the Hall measurements and the results are shown in table 5.8. Hall measurements confirmed the high conductivity of the films annealed at 500°C by showing an increase in carrier concentration. Further the n-type conductivity of In doped films are confirmed by Hall measurements.

Table 5.8: Optical and electrical data of ZnO: 3% In films annealed at different temperatures for 4 h.

Annealing temp (°C)	$E_g$ (eV)	$\sigma$ (S/cm)	$E_a$ (meV)	$n$ ( $1/\text{cm}^3$ )	$\mu$ ( $\text{cm}^2\text{V}^{-1}\text{s}^{-1}$ )
As-deposited at 450	3.36	0.88	297	129	----
450	3.29	253	126	68.2	$3.7 \times 10^{19}$
500	3.22	297	116	64.9	$5.2 \times 10^{19}$
550	3.16	224	189	87.8	$9.4 \times 10^{18}$

## 5.4 GALLIUM (Ga) DOPED ZnO THIN FILMS

In the present investigation gallium (Ga) doped ZnO thin films were prepared by spraying precursor solution of zinc acetate anhydrous  $[\text{Zn}(\text{CH}_3\text{COO})_2]$  (Alfa Aesar 99.99%) and gallium chloride  $[\text{GaCl}_3]$  (Alfa Aesar 99.99%), in methanol. The deposition parameters were maintained almost identical to that for the deposition of undoped ZnO thin films (table 3.4).

### 5.4.1 Effect of doping concentration

The Ga doped ZnO thin films were prepared by spray pyrolysis technique. The Ga concentration in the precursor solution is varied from 0 to 5%. The obtained films of thickness 600 nm were annealed at growth temperature for 4 h and their structural, optical and electrical properties were studied.

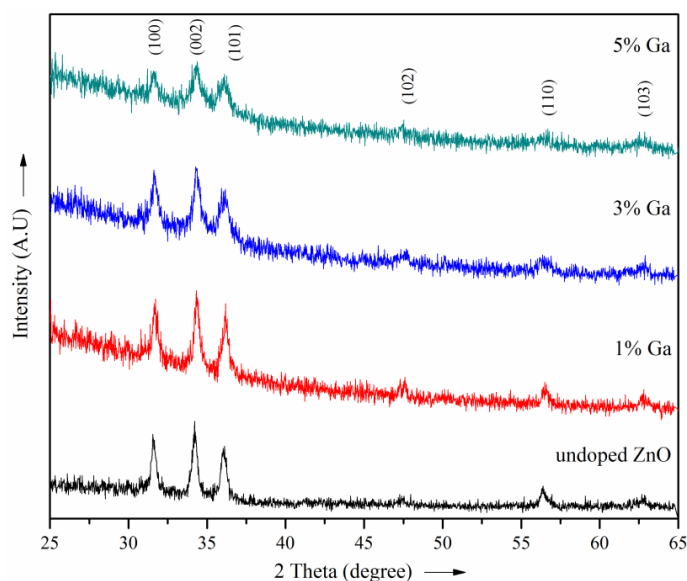


Figure 5.22: XRD pattern of Ga doped ZnO thin films.

XRD pattern of gallium doped ZnO thin films are shown in the figure 5.22. XRD pattern of these films provides information about the crystal structure and crystallinity of the films. The Ga doped thin films exhibit hexagonal wurtzite structure with (002) texture. It is observed that the (002) peak intensity of films drastically reduced with increased Ga dopant concentration. This indicates that the deterioration of



crystallinity of ZnO films at higher dopant concentrations. The average grain size and residual strain in Ga doped thin films were calculated using equation 2.3.3 and results are shown in table 5.9. The grain size of ZnO films found to decrease with an increase in the Ga concentration. Further the lattice parameter of Ga doped thin films were calculated using equation 2.3.2. It was found that the lattice parameter remains constant with Ga doping.

Table 5.9: XRD data of Ga doped ZnO thin films.

at. % Ga	Texture	D (nm)	Strain
1	(002)	21.7	0.0075
3	(002)	18.6	0.0060
5	(002)	15.9	0.0109

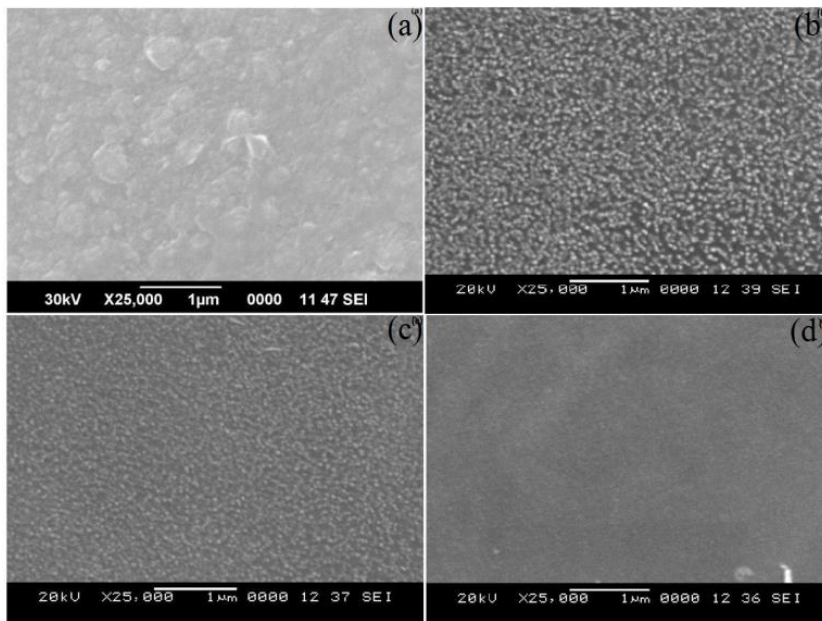


Figure 5.23: SEM image of (a) undoped, (b) 1% Ga, (c) 3% Ga and (d) 5% Ga doped ZnO films.

The scanning electron micrograph of undoped and Ga doped thin films has been shown in the figure 5.23. The morphology of undoped sample shows plane and smooth surface. It is observed that the increase in Ga concentration causes the reduction in the grain size and smoothness of the film surface. The XRD result shows an incorporation of Ga into ZnO film reduces the grain size; the decrease in the grain

size can reduce the roughness of the film surface. SEM results are in consistent with XRD results. The presence of gallium in ZnO films is confirmed by EDAX analysis. The EDAX spectrum of 3% Ga doped thin films is shown in the figure 5.24.

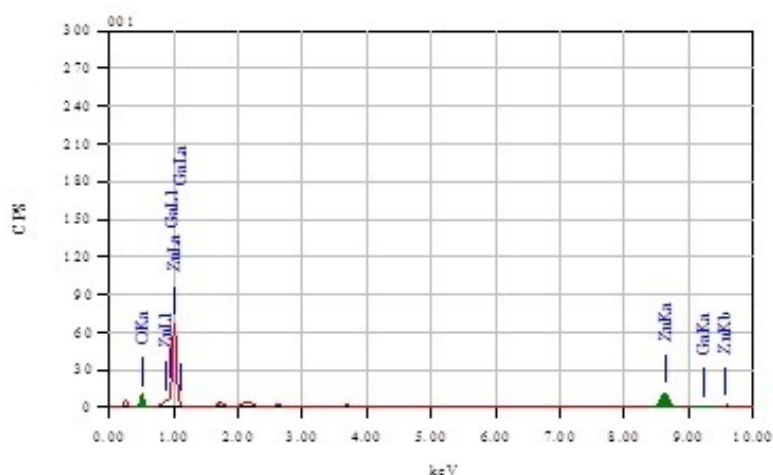


Figure 5.24: EDAX spectrum of 3% Ga doped ZnO thin films.

The composition analysis of 3% Ga doped ZnO thin films were investigated using X-ray photoelectron spectroscopy (XPS). The XPS spectra of Ga doped thin films are shown in the figure 5.25. Figure 5.25(a) shows the survey scan spectra and figure 5.25(b) shows the Zn2p spectra. The Zn2p peak located at binding energy 1020.5 eV corresponding to Zn2p<sub>3/2</sub> core level.

Figure 5.25(c) shows the O1s spectra of Ga doped ZnO thin films. There are two asymmetric O1s peaks are located at the binding energies 529.9 eV and 531.6 eV. The peak corresponding to the lower binding energy is due to Zn-O bond and the other peak located at the higher binding energy accords with the chemisorbed oxygen (Liqiang et al. 2002). The O1s peak is moved slightly to the higher binding energy direction with Ga doping.

The figure 5.25(c) represents Ga2p core level spectra of Ga doped film which show a peak located at 1116.5 eV. The peak located at 1116.5 eV is assigned to Ga 2p<sub>3/2</sub> which confirms the presence of Ga<sup>3+</sup> in the ZnO lattice. This peak located at 1116.5 eV is attributed to the Ga-O bonding rather than Zn-Ga bonding in Ga doped

thin films. The estimated atomic percentage of zinc, gallium and oxygen in Ga doped films are 48.56, 2.65% and 48.75% respectively.

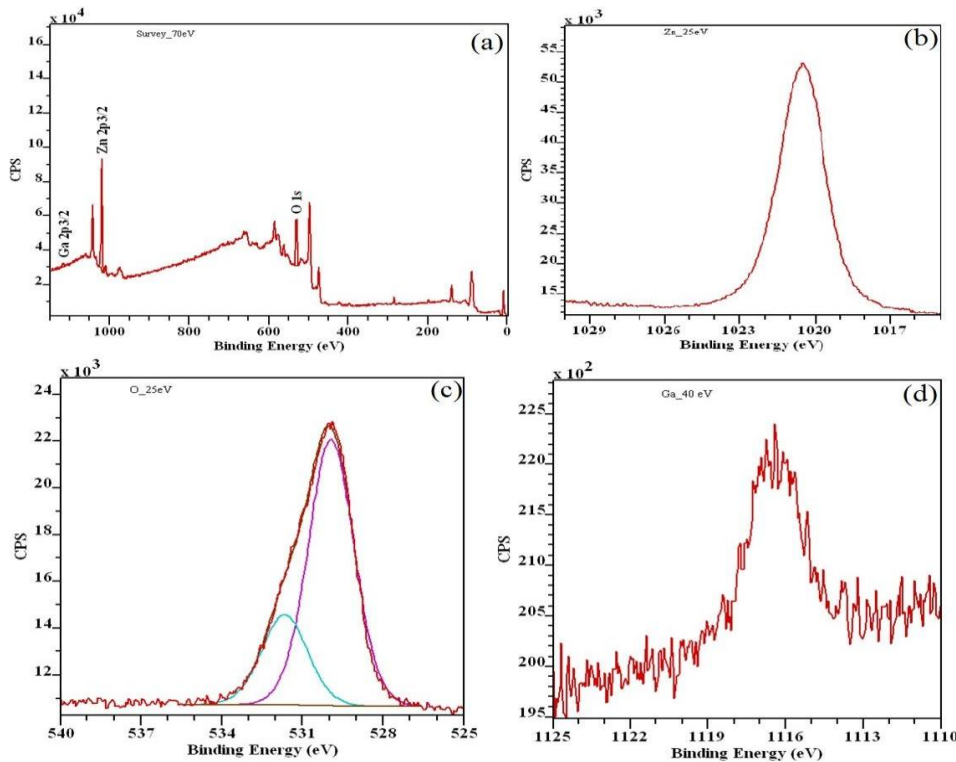


Figure 5.25: XPS spectra of ZnO: 3%Ga thin films annealed at 450°C (a) Survey scan (b) Zn<sub>2p</sub> spectra, (c) O1s spectra and (d) Ga<sub>2p</sub> spectra.

The transmittance spectra of Ga doped thin films in the wavelength range of 300 nm to 800 nm are shown in the figure 5.26(a). The Ga doped films have better transmittance than the undoped films. It is also observed from the figure 5.26(a) that sharp absorption edge is slightly shifted to lower wavelength region for Ga doped films, which also confirms the incorporation of Ga into the ZnO film.

Figure 5.26(b) shows the Tauc's plot for Ga doped thin films. It is found that the energy band gap of ZnO thin films slightly increased from 3.24 eV to 3.29 eV, with increased Ga dopant concentration 0 to 5% respectively (table 5.10). An increase in the optical band gap is due to the Burstein-Moss effect (Sernelius et al. 1988). This indicates the rise in Fermi level in the conduction band due to increased charge carriers, which leads to broadening of the optical band-gap.

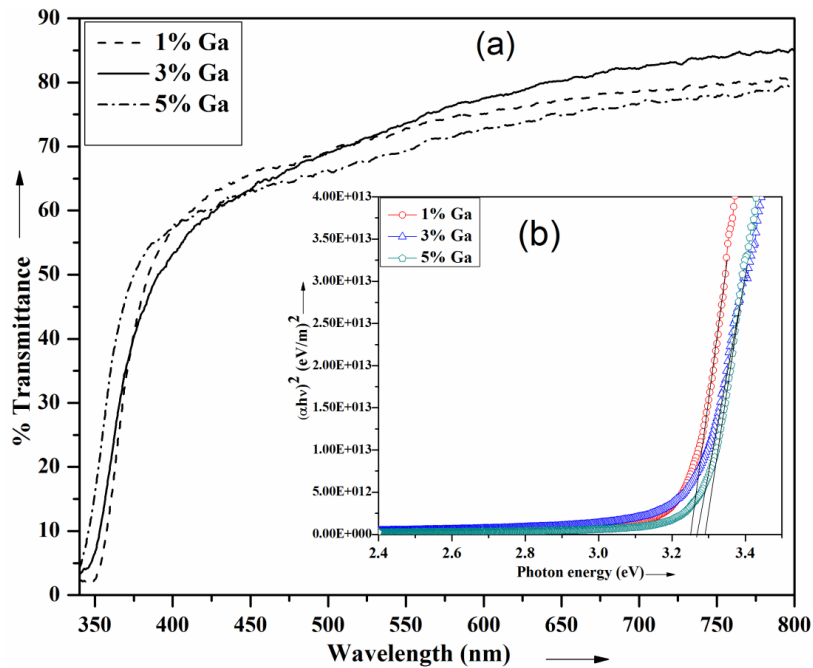


Figure 5.26: (a) Transmittance spectra and (b) Tauc's plot for Ga doped ZnO thin films.

I-V characteristics of Ga doped thin films are shown in the figure 5.27. All the Ga doped films show linear characteristics, satisfying Ohmic conduction mechanism. The electrical conductivity of the ZnO thin films has been improved with gallium doping. The sharp increase in conductivity of thin films is observed with an increase in the Ga concentration up to 3%. Further increase in dopant concentration (5%) results decrease in conductivity of the films. The increase in the conductivity is due to the replacement of divalent Zn ions by trivalent Ga ions, contributing an extra charge carrier. At higher doping concentrations the excess Ga ions may be segregates at the grain boundaries, which in turn decrease the film conductivity due to scattering of the free carriers in these regions. However, since the concentration of Ga is small, peaks were not detected in XRD pattern (Gomez and Olvera 2006).

Table 5.10: Optical and electrical data Ga doped ZnO thin films.

% Ga	$E_g$ (eV)	$\sigma$ (S/cm)	$E_a$ (meV)	$n$ ( $1/\text{cm}^3$ )	$\mu$ ( $\text{cm}^2 \text{V}^{-1} \text{s}^{-1}$ )	
0	3.24	0.16	348	217	$9.92 \times 10^{16}$	9.38
1	3.25	166	146	87.2	$1.94 \times 10^{19}$	53.6
3	3.26	308	167	54.9	$2.74 \times 10^{19}$	70.2
5	3.29	8.21	244	123	$3.32 \times 10^{18}$	36.8

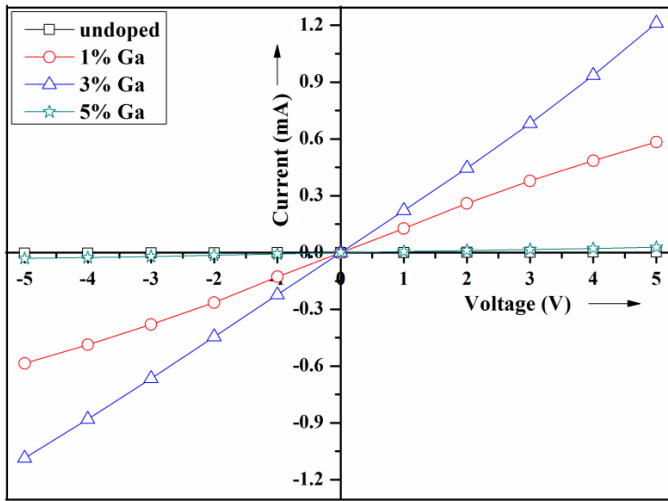


Figure 5.27: I-V characteristics of Ga doped ZnO thin films.

Figure 5.28 shows the variation of  $\log R$  with reciprocal temperature of 3% Ga doped thin film. Ga doped films show two linear parts having different slopes, indicating that there are two mechanisms for electrical conduction. The 3% Ga doped films found to have shallow donor levels with activation energy of 54.9 meV which contributes more to the electrical conductivity with very low energy loss, whereas films doped with 5% Ga show decrease in conductivity. This decrease in conductivity is explained by the observed high activation energy of shallow donor levels. The hot probe technique and Hall measurements indicate n-type conductivity of Ga doped films.

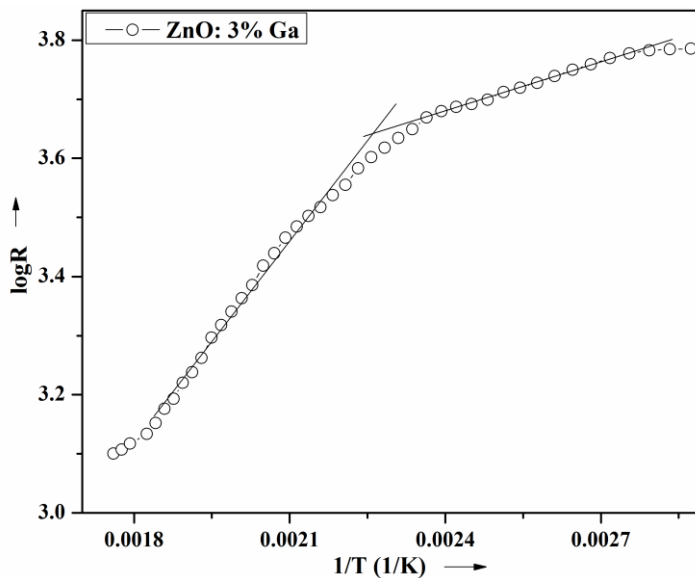


Figure 5.28: Variation of  $\log R$  vs. reciprocal temperature of ZnO: 3% Ga thin film.

### 5.4.2 Effect of annealing temperature

The 3% Ga doped ZnO films show high transmittance and electrical conductivity. These films were annealed at different temperatures for 4 h and their structural, optical and electrical properties were studied.

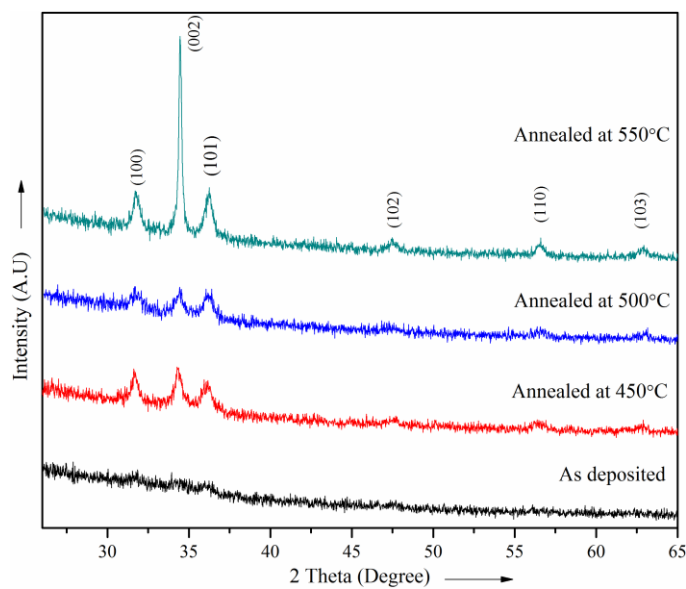


Figure 5.29 :XRD pattern of ZnO: 3% Ga thin films.

XRD pattern of 3% Ga doped thin films annealed at different temperatures are shown in the figure 5.29. It is observed from XRD pattern that the *as-deposited* films have low level of crystallinity. On increasing annealing temperature, the improvement in peak intensity indicates increase in the crystallinity of Ga doped films. The 3% Ga doped films annealed at 550°C show better crystallinity. The strain and average grain size of 3% Ga doped thin films were estimated and the results are shown in table 5.11. The grain size of Ga doped films is found to increase with an increase in annealing temperature.

Table 5.11: XRD data of ZnO: 3% Ga films annealed at different temperature for 4 h.

Annealing temp. (°C)	Texture	D (nm)	Strain
As-deposited at 450	(002)	8.5	0.0141
450	(002)	21.9	0.0060
500	(002)	19.2	0.0042
550	(002)	33.3	0.0037

The scanning electron micrographs of *as-deposited* and annealed 3% Ga doped thin films were shown in the figure 5.30. The *as-deposited* film presents plane, smooth and homogeneous surface. The films annealed at different temperatures show increase in grain size. It is seen that the surface roughness of the annealed Ga doped ZnO films found to increase with an increase in annealing temperature, which may be due to increased grain size.

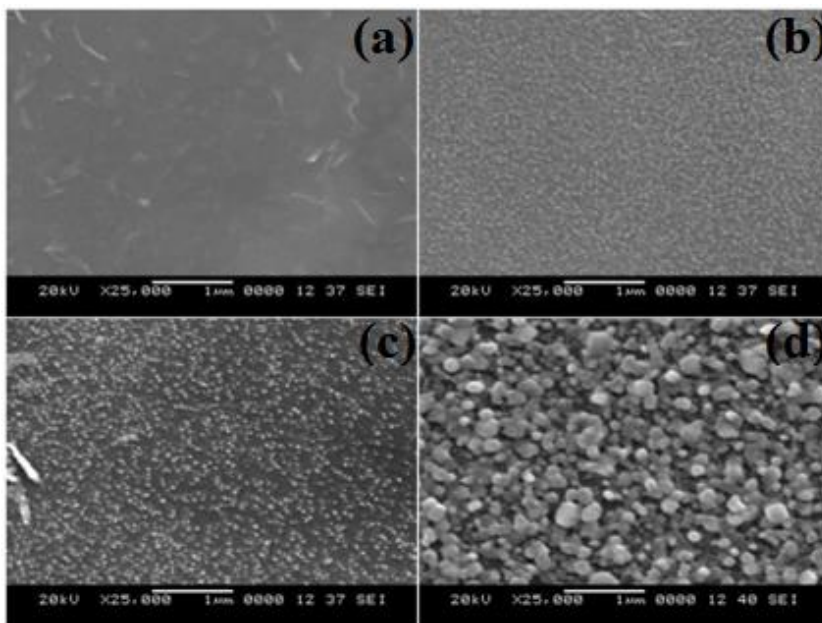


Figure 5.30: SEM image of ZnO: 3% Ga films (a) *as-deposited*, (b) annealed at 450°C, (c) annealed at 500°C and (d) annealed at 550°C.

The transmittance spectra of 3% Ga doped thin films annealed at different temperatures are shown in the figure 5.31(a). The *as-deposited* Ga doped films show optical transmittance approximately 80% in visible region. The transmittance of the Ga doped films unaffected even after annealing at 450°C. Further increase in the annealing temperature reduces the transmittance of the films. This decrease in the transmittance is may be due to more optical scattering. The increase in annealing temperature shifted the absorption edge of Ga doped films towards longer wavelength side [figure 5.31(b)], indicating that the reduction in the optical band gap of the Ga doped thin films. This reduction in  $E_g$  is due to decrease in the carrier concentration with increasing annealing temperature.

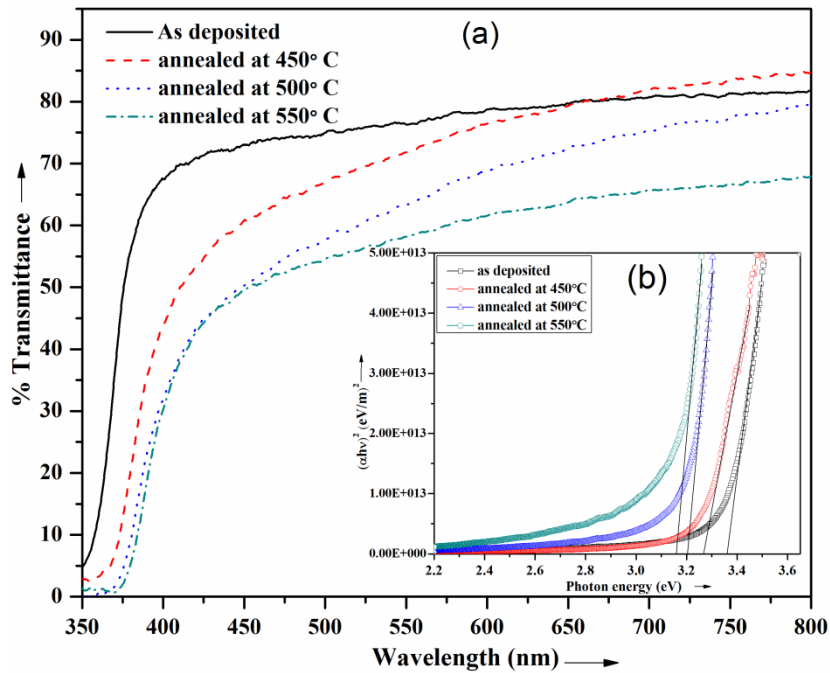


Figure 5.31: (a) Transmittance spectra and (b) Tauc's plot for ZnO: 3% Ga thin films.

Figure 5.32 depicts the I-V characteristics 3% Ga doped films annealed at different temperatures. The *as-deposited* Ga doped films show conductivity of 3.49 S/cm. The drastic improvement in the conductivity of Ga doped films is observed with annealing. The high conductivity of 308 S/cm is achieved for 3% Ga doped films when annealed at 450°C.

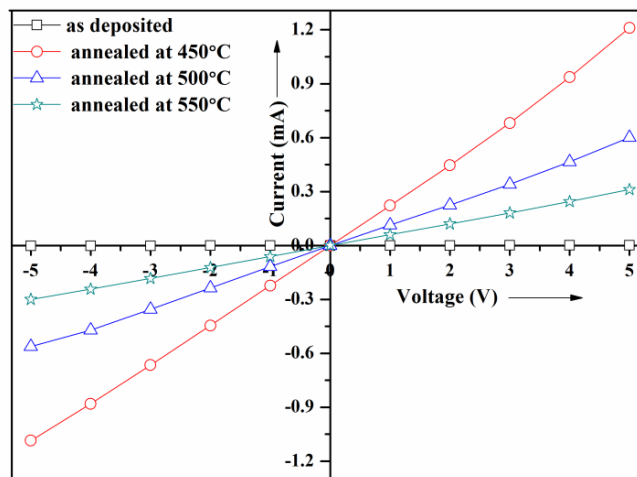


Figure 5.32: I-V characteristics of ZnO: 3% Ga thin films.



It is observed that the conductivity of Ga doped films is continuously decreased with further increase in the annealing temperature. The reduction in the conductivity has been attributed to the incorporation of oxygen atoms during the annealing process (Won 2005). It results in the decrease of the electron concentration in the Ga doped ZnO films (table 5.12). According to the scattering mechanism of transparent conducting oxides described by Pei et al. (2001) at low temperatures, ionized impurity scattering is dominant and at the higher temperatures the grain boundary scattering introduces the decrease in the conductivity and thereby reduces the mobility of the charge carriers. For the temperature range between 450°C to 550°C, the conductivity decreased from 308 S/cm to 82.6 S/cm respectively.

Table 5.12: Optical and electrical data of ZnO: 3% Ga films annealed at different temperatures for 4 h.

Annealing temp. (°C)	$E_g$ (eV)	$\sigma$ (S/cm)	$E_a$ (meV)		$n$ ( $1/\text{cm}^3$ )	$\mu$ ( $\text{cm}^2 \text{V}^{-1} \text{s}^{-1}$ )
As-deposited at 450	3.36	3.49	344	178	$1.94 \times 10^{17}$	2.82
450	3.26	308	167	54.9	$2.74 \times 10^{19}$	70.2
500	3.20	158	166	102	$1.45 \times 10^{19}$	67.9
550	3.16	82.6	147	133	$8.14 \times 10^{18}$	63.5

The estimated activation energies are quite high for *as-deposited* Ga doped films, which contributes least to the conductivity hence low conductivity of the films. High conductivity of the films annealed at 450°C is explained by the observed activation energies. The least activation energy is observed for Ga doped films annealed at 450°C which is one of the reasons for higher conductivity. The Hall measurements data of annealed Ga doped films were shown in table 5.12. The high conductivity of Ga doped films annealed at 450°C is confirmed by an increase in carrier concentration and mobility. Both carrier concentration and mobility of the Ga doped films decreased above the annealing temperature 450°C.

## **CHAPTER 6**

### **SUMMARY AND CONCLUSIONS**

Chapter 6 outlines the summary of the work presented in the thesis along with the conclusions pertaining to the research work. Scope for the future work also has been included in the chapter.

#### **6.1 SUMMARY OF THE PRESENT WORK**

The work presented in this thesis is broadly classified as six chapters with several sections in each chapter. The first chapter titled Introduction covers introduction to zinc oxide, literature survey, scope and objectives of the work. The second chapter titled Experimental techniques deals with the materials and methods employed in the present work. The third chapter describes detailed study of undoped ZnO thin film. The fourth chapter titled doping of ZnO films with group V elements covers the results and discussion of Sb and Bi doped ZnO films. The chapter five titled doping of ZnO films with group III elements deals with the results and their interpretations. The chapter six describes the summary and conclusions of the work.

The undoped, Sb, Bi, Al, In and Ga doped ZnO thin films have been prepared using zinc acetate precursor by spray pyrolysis technique. The obtained thin films were characterised using XRD, SEM, EDAX, XPS, UV-Visible spectroscopy and Keithley instruments. The effects of doping concentration and annealing temperature on the structural, morphological, optical and electrical properties of the films have been studied. The findings have been briefed below.

The ZnO thin films were prepared using zinc acetate and zinc nitrate precursor solution by simple and inexpensive spray pyrolysis technique. The effect of film thickness on the structural, optical and electrical properties spray deposited ZnO thin films were studied. The films with thickness 600 nm show stable optical and electrical property; hence the film thickness of 600 nm is maintained throughout the study. The influence of annealing temperature on the optical and electrical properties of ZnO thin

films was studied. The films annealed at 450°C for 4 hrs show better combination of transmittance and conductivity. The properties of ZnO thin films prepared using zinc nitrate precursor by spray pyrolysis technique were investigated. Effect of annealing temperature on the optical and electrical properties of ZnO films was also studied. The transmittance and conductivity of ZnO films prepared using zinc nitrate precursor is almost same as that of films prepared using zinc acetate precursor. Hence zinc acetate precursor is used for doping study. The undoped ZnO thin films exhibit polycrystalline hexagonal wurtzite structure with (002) texture. The grain size of ZnO thin films found to increase with increasing film thickness and annealing temperature. EDAX technique was employed to study the composition analysis of undoped and doped ZnO thin films, which confirmed the incorporation of dopant into the ZnO film. The X-ray photoelectron spectroscopy was used to estimate the oxygen percentage in the undoped and doped ZnO films. The presence of dopants in the ZnO film is also confirmed by XPS analysis. XPS analysis shows that *as-deposited* ZnO thin films have oxygen vacancy with 52.17 at. % of zinc, 38.64 at. % of oxygen strongly bonded to the zinc and 9.19 at. % oxygen loosely bonded to the surface of the films. The films annealed at 450°C for 4hr found to have oxygen with 36.46 at. % zinc, 31at. % of oxygen strongly bonded with zinc and 32.54 at. % of oxygen loosely bonded to the film surface.

The Sb & Bi doped ZnO films were prepared separately using zinc acetate precursor by spray pyrolysis technique. The influences of Sb and Bi doping concentration on the structural, optical and electrical properties of ZnO films were studied. The effect of annealing temperature on the optical and electrical properties of ZnO: Sb and ZnO: Bi thin films were studied independently. Sb / Bi, doped ZnO thin films exhibit polycrystalline hexagonal wurtzite structure with (101) texture. The grain size of Sb and Bi doped ZnO thin films found to be decreased with increasing doping concentration whereas annealing temperature increases the grain size of 3% Sb and 3% Bi doped ZnO films. Surface morphology of Sb and Bi doped ZnO films were studied by scanning electron microscopy. SEM image show smooth surface morphology for Sb doped films and rough surface morphology for Bi doped films when compared with surface morphology of undoped films. The optical transmittance

of ZnO films in visible region remains unaltered with Sb and Bi doping. The optical transmittance of Sb and Bi doped films found to decrease at higher annealing temperatures. The activation energy of Sb and Bi doped ZnO films were estimated from the  $\log R$  vs.  $1/T$  plot. The doped ZnO thin films are found to have two donor levels with different activation energies. The donor level having low activation energy will contribute to conductivity of the films with very low energy loss. Hall measurements for all the Sb, Bi doped ZnO thin films were made at room temperature in a magnetic field strength of 0.5T, which can identify conduction type, carrier concentration and mobility of the doped ZnO films.

The group III elements (Al, In & Ga) doped ZnO films were prepared using zinc acetate precursor by spray pyrolysis technique. The influences of Al, In and Ga doping concentration on the structural, optical and electrical properties of ZnO films were studied. The effect of annealing temperature on the optical and electrical properties of ZnO: 3%Al, ZnO: 3%In and ZnO:3% Ga doped films were investigated. Al, Ga and In doped ZnO films exhibit polycrystalline hexagonal wurtzite structure with (002) texture. The grain size of Al and In doped ZnO thin films found to be increased with increasing doping concentration up to 3%, whereas grain size of Ga doped films found to decrease with increasing doping concentration. The increase in annealing temperature increases the grain size of 3% Al, 3% In and 3% Ga doped ZnO films. Surface morphology of Al, In and Ga doped ZnO films were studied by scanning electron microscopy. SEM image show smooth surface for Al and Ga doped films and rough surface for In doped films when compared with surface morphology of undoped films. The optical transmittance of ZnO films found to increase with Al and Ga doping whereas transmittance remains unaltered with In doping. The optical transmittance of Al, Ga, and In doped films found to decrease at higher annealing temperatures. The activation energy of Al, In and Ga doped ZnO films were estimated from the  $\log R$  vs.  $1/T$  plot. All the doped ZnO thin films are found to have two donor levels with different activation energies. Hall measurements for Al, In and Ga doped ZnO thin films were made at room temperature in a magnetic field strength of 0.5T. From the study carrier concentration and mobility of the doped ZnO films have been evaluated.

## 6.2 CONCLUSIONS OF THE PRESENT WORK

The spray deposited undoped ZnO thin films found to have a combination of transmittance above 75% in the visible region and electrical conductivity of 0.16 S/cm with carrier concentration  $9.92 \times 10^{16} /\text{cm}^3$  and mobility  $9.38 \text{ cm}^2/\text{Vs}$ . The 3% Sb and 3% Bi doped ZnO films have better combination of optical and electrical properties. Hall measurements confirmed the p-type conductivity of ZnO thin films doped with 3% Sb and above. The 3% Al, 3% Ga and 3% In doped ZnO films found to have highly transparent and conducting properties. Among these dopants The Ga doped films show better optical and electrical property. The 3% Ga doped ZnO films found to have a combination of transmittance 80% and electrical conductivity of 308 S/cm with a carrier concentration  $2.74 \times 10^{19} /\text{cm}^3$  and a mobility  $70.2 \text{ cm}^2 \text{ V}^{-1} \text{ s}^{-1}$ . Sb and Bi doped ZnO thin films are found to be suitable for transparent electrode applications. Sb doped ZnO thin films found to have p-type conductivity hence it can be used for device applications needing p-type conductivity electrodes. Polycrystalline Al, Ga, In doped ZnO films with highly transparent and conducting properties makes suitable for transparent electrode applications.

## 6.3 SCOPE FOR THE FUTURE WORK

The optical and electrical property of the doped ZnO films was studied in the present investigation. The other properties such as mechanical and thermoelectric property of the Sb and Bi doped ZnO films can be studied. Gas sensing properties of Sb, Bi doped ZnO thin films can be studied. Device application of the Al, In and Ga doped ZnO films can be studied.

## REFERENCES

Acharya, A.D., Moghe, S., Panda, R. Shrivastava, S.B., Gangrade, M., Shripathi, T., Phase, D.M. and Ganesan, V. (2012). "Effect of Cd dopant on electrical and optical properties of ZnO thin films prepared by spray pyrolysis route." *Thin Solid Films*, 525, 49-55.

Aida, M.S., Tomasella, E., Cellier, J., Jacquet, M., Bouhssira, N., Abed, S. and Mosbah, A. (2006). "Annealing and oxidation mechanism of evaporated zinc thin films from zinc oxide powder." *Thin Solid Films*, 515(4), 1494-1499.

Aksoy, S., Caglar, Y., Ilican, S. and Caglar, M. (2012). "Sol-gel derived Li-Mg co doped ZnO films: Preparation and characterization via XRD, XPS, FESEM." *J. Alloys. Compd.*, 512(1), 171-178.

Alver, U., Kılınç T., Bacaksız, E., Küçükömeroğlu, T., Nezir, S., Mutlu, İ.H. and Aslan, F. (2007). "Synthesis and characterization of spray pyrolysis zinc oxide microrods" *Thin Solid Films*, 515(7-8), 3448-3451.

Anubha, J., Sagar, P. and Mehra, R.M. (2006). "Band gap widening and narrowing in moderately and heavily doped n-ZnO films." *Solid State Electron.*, 50(7-8), 1420-1424.

Aoki, T., Shimizu, Y., Miyake, A., Nakamura, A., Nakanishi, Y. and Hatanaka, Y. (2002). "p-type ZnO layer formation by excimer laser doping." *Phys. Status Solidi B*, 229(2), 911-914.

Ataev, B.M., Bagamadova, A.M., Djabrailov, A.M., Mamedov, V.V. and Rabadanov, R.A. (1995). "Highly conductive and transparent Ga-doped epitaxial ZnO films on sapphire by CVD." *Thin Solid Films*, 260(1), 19-20.

Auttasit, T., and Lee, M.-W. (2012). "ZnO nanorods on undoped and indium-doped ZnO thin films as a TCO layer on nonconductive glass for dye-sensitized solar cells." *Superlattices Microstruct.*, 52(5), 987-996.

- Bachari, E.M., Baud, G., Amor, S.B. and Jacquet, M. (1999). "Structural and optical properties of sputtered ZnO films." *Thin Solid Films*, 348(1), 165-172.
- Bagnall, D.M., Chen, Y.F., Zhu, Z., Yao, T., Koyama, S., Shen, M.Y. and Goto, T. (1997). "Optically pumped lasing of ZnO at room temperature." *Appl. Phys. Lett.*, 70(17), 2230-2232.
- Bouderbala, M., Hamzaoui, S., Amrani, B., Reshak, M., Adnane, T. and Zerdali, M. (2008). "Thickness dependence of structural, electrical and optical behaviour of undoped ZnO thin films." *Physica B*, 403(18), 3326 -3330.
- Calnan, S. and Tiwari, A.N. (2010). "High mobility transparent conducting oxides for thin film solar cells." *Thin Solid films*, 518(7), 1839-1849.
- Cao, H. and Zhao, Y.G. (1999). "Random Laser Action in Semiconductor Powder." *Phys. Rev. Lett.*, 82(11), 2278-2281.
- Centinorgu, E. and Goldsmith, S. (2007). "Chemical and thermal stability of the characteristics of filtered vacuum arc deposited ZnO, SnO<sub>2</sub> and zinc stannate thin films." *J. Phys. D: Appl. Phys.*, 40(17), 5220-5236.
- Chang, S-C. (1980). "Oxygen chemisorptions of tin oxide correlation between electrical conductivity and EPR measurements." *J. Vac. Sci. Technol. A*, 17(1) 366-369.
- Chen, H.-G. and Hung, S.-P. (2014). "Epitaxial growth of Sb-doped nonpolar a-plane ZnO thin films on r-plane sapphire substrates by RF magnetron sputtering." *J. Alloys Compd.*, 586(1), S339-S342.
- Chen, M., Pei, Z.L., Wang, X., Sun, C. and Wen, L.S. (2001). "Structural, electrical, and optical properties of transparent conductive oxide ZnO:Al films prepared by dc magnetron reactive sputtering." *J. Vac. Sci. Technol. A*, 19, 963.

Christian, P., Abdelkader, N., George, B. and Burak, A. (2012). "MOCVD-growth of thin ZnO films from zinc acetylacetonate and air." *J. Cryst. Growth*, 348(1), 5-9.

Chu, S., Wang, G.P., Zhou, W.H., Lin, Y.Q., Chernyak, L., Zhao, J.Z., Kong, J.Y., Li, L., Ren, J.J. and Liu, J.L. (2011). "Electrically pumped waveguide lasing from ZnO nanowires." *Nat. Nanotechnol.*, 6(8), 506.

Clatot, J., Campet, G., Zeinert, A., Labrugere, C., Nistor, M. and Rougier, A. (2011). "Low temperature Si doped ZnO thin films for transparent conducting oxides." *Sol. Energy Mater. Sol. Cells*, 95(8), 2357-2362.

Cortes, A., Gomez, H., Mariotti, E.R., Riveros, G. and Dalchiale, E.A. (2004). "Grain size dependence of the bandgap in chemical bath deposited CdS thin films." *Sol. Energy Mater. Sol. Cells*, 82(1-2), 21-34.

Craciun, V., Elders, J., Gardeniers, J.G.E. and Boyd, I.W. (1994). "Characteristics of high quality ZnO thin films deposited by pulsed laser deposition." *Appl. Phys. Lett.*, 65(23), 2963-2965.

Cullity, B.D. (1956). *Elements of X-ray Diffraction*, Addison Wesley Publishing Company, Massachusetts.

Dedova, T., Krunk, M., Grossberg, M. Volobujeva, O. and Oja, A.I. (2007). "A novel deposition method to grow ZnO nanorods: Spray pyrolysis." *Superlattices Microstruct.*, 42(1-6), 444-450.

Desnica, U.V. (1998). "Doping limits in II-VI compounds-challenges, problems and solutions", *Prog. Cryst. Growth and Charact.*, 36(4), 291-357.

Dhara, S. and Giri, P.K. (2010). "Stable *p*-type conductivity and enhanced photoconductivity from nitrogen-doped annealed ZnO thin film." *Thin Solid Films*, 520(15), 5000-5006.



Elmer, K. (2010). *Hand Book of Transparent Conducting Oxides*, 1<sup>st</sup> edn, Springer, New York, chapter: Transparent conducting zinc oxide and its derivatives, pp. 193-265.

Ergin, B., Ketenci, E. and Atay, F. (2009). "Characterization of ZnO films obtained by ultrasonic spray pyrolysis technique." *Int. J. Hydrogen Energy*, 34(5), 5249-5254.

Exarhos, G.J. and Zhou, X.D. (2007). "Discovery-based design of transparent conducting oxide films." *Thin Solid Films*, 515(18), 7025-7052.

Fang, T.-H. and Kang, S.-H. (2010). "Optical and physical characteristics of In-doped ZnO nanorods." *Curr. Appl. Phy.*, 10(4), 1076-1086.

Fay, S., Feitknecht, L. Schluchter, R., Kroll, U. Vallat-S. and Shah, E.A. (2006). "Rough ZnO layers by LP-CVD process and their effect in improving performances of amorphous and microcrystalline silicon solar cells." *Sol. Energy Mater. Sol. Cells*, 90(18-19), 2960-2967.

Florescu, D.I., Mourokh, L.G., Pollak, F.H., Look, D.C., Cantwell, G. and Li, X. (2002). "High spatial resolution thermal conductivity of bulk ZnO (0001)." *J. Appl. Phys.*, 91(2-3), 890-892.

Fortunato, E., Raniero, L., Silva, L., Goncalves, A., Pimentel, A., Barquinha, P., A´guas, H., Pereira, L., Goncalves, G., Ferreira, I., Elangovan, E. and Martins, R. (2008). "Highly stable transparent and conducting gallium-doped zinc oxide thin films for photovoltaic applications." *Sol. Energy Mater. Sol. Cells*, 92(12), 1605-1610.

Fouad, O.A., Ismail, A.A., Zaki, Z.I. and Mohamed, R.M. (2006). "Zinc oxide thin films prepared by thermal evaporation deposition and its photocatalytic activity." *Appl. Catal., B.*, 62(1-2), 144-149.

Funakubo, H., Mizutani, N., Yangetsu, M., Saiki, A. and Shinozaki, K. (1999). "Orientation control of ZnO thin film prepared by CVD." *J. Electron.*, 4(S1), 25-32.

- Gil, M.N. and Myoung, S.K. (2009). "Al-doped ZnO via sol-gel spin-coating as a transparent conducting thin film." *J. Inform. Display*, 10(1), 24-27.
- Gomez, H. and Olvera, M.L. (2006). "Ga-doped ZnO thin films: Effect of deposition temperature, dopant concentration, and vacuum-thermal treatment on the electrical, optical, structural and morphological properties." *Mater. Sci. Eng., B*, 134(1), 20-26.
- Gong, H., Wang, Y., Yan, Z. and Yang, Y. (2002). "The effect of deposition conditions on structure properties of radio frequency reactive sputtered polycrystalline ZnO films." *Mater. Sci. Semicond. Process.*, 515(1), 31-34.
- Gong, J., Zhang, X., Pei, Z., Sun, C. and Wen, L. (2011). "Effect of enhanced plasma density on the properties of aluminium doped zinc oxide thin films produced by DC magnetron sputtering." *J. Mater. Sci. Technol.*, 27(5), 393-397.
- Gonzales, A. E. J., Urueta, J. A. S. and Parra, R. (1998). "Optical and electrical characteristics of aluminium doped zinc oxide thin films prepared by sol-gel method." *J. Cryst. Growth*, 192(3-4), 430-438.
- Heerden, V.J.L, and Swanepoel, R. (1997). "XRD analysis of ZnO thin films prepared by spray pyrolysis." *Thin Solid Films*, 299 (1-2), 72-77.
- Hidayat, D., Ogi, T., Iskandar, F. and Okuyama, K., (2008). "Single crystal ZnO: Al nanoparticles directly synthesized using low-pressure spray pyrolysis." *Mater. Sci. Eng. B*, 151(3), 231-237.
- Hirota, O., Akinori, K. and Makoto, O. (2008). "Superconducting properties of ZnO-doped (Bi, Pb)-2223 thick film on Ni and NiO substrates prepared by spray deposition technique." *Physica C*, 468(6), 447-452.
- Hong, M.Z., Dan, Q.Y., Zhi, M.Y., Lai, R.X. and Jian, L. (2007). "Preparation of aluminum doped zinc oxide films and the study of their microstructure, electrical and optical properties." *Thin Solid Films*, 515(17), 6909-6914.

Huang, M.H., Mao, S., Feick, H., Yan, H., Wu, Y., Kind, H., Weber, E., Russo, R. and Yang, P. (2001). "Room-Temperature Ultraviolet Nanowire Nanolasers." *Sci.*, 292(5523), 1897-1899.

Hwang, D.-K., Kim, H.-S., Lim, J.-H., Oh, J.-Y., Yang, J.-H., Park, S.-J., Kim, K.-K., Look, D.C. and Park, Y.S. (2005). "Study of the photoluminescence of phosphorus-doped p-type ZnO thin films grown by radio-frequency magnetron sputtering." *Appl. Phys. Lett.*, 86(15), 151917.

Ilican, S., Caglar, Y., and Caglar, M. (2008). "Preparation and characterization of ZnO thin films deposited by sol-gel spin coating method." *J. Optoelectron. Adv. Mater.*, 10 (10), 2578 -2583.

Izquierdo, R., Sacher, E. and Yelon, A. (1989). "X-ray photoelectron spectra of antimony oxides." *Appl. Surf. Sci.*, 40(1-2), 175-177.

Jagdish, C. and Pearton, S.J. (2006). *Zinc Oxide-Bulk, Thin Films and Nanostructures*, 1<sup>st</sup> edn, Elsevier, Amsterdam, Netherlands, chapter 2, pp. 34.

Janotti, A. and Vandewalle, C.G. (2009). "Fundamentals of zinc oxide as a semiconductor." *Rep. Prog. Phys.*, 72(126501), 1-29.

Jiang, M., Liu, X. and Wang, H. (2009). "Conductive and transparent Bi-doped ZnO films prepared by rf magnetron sputtering." *Surf. Coat. Technol.*, 203(24), 3750-3753.

Jiang, M., Wang, Z. and Ning, Z. (2009). "Study of structural and optical properties of Ge doped ZnO films." *Thin Solid Films*, 517(24), 6717-6720.

Jingjing, X., Mindong, C. and Fu, D. (2011). "Study on highly visible light active Bi-doped TiO<sub>2</sub> composite hollow sphere." *Appl. Surf. Sci.*, 257(17), 7381-7386.

Joseph, B., Gopchandran, K.G., Manoj, P.K., Koshy, P. and Vaidyan, V.K. (1999). "Optical and electrical properties of zinc oxide films prepared by spray pyrolysis." *Bull. Mater. Sci.*, 22(5), 921-926.

Joseph, B., Manoj, P.K. and Vaidyan, V.K. (2005). "Studies on preparation and characterization of indium doped zinc oxide films by chemical spray deposition." *Bull. Mater. Sci.*, 28(5), 487- 493.

Kalyani, N., Ching, Y.C., and Chou, Y.T., (2013). "Influence of annealing on properties of spray deposited ZnO thin films." *Journal of Nanomaterials*, 2013, 8.

Kang, S.J. and Joung, Y.H. (2007). "Influence of substrate temperature on the optical and piezoelectric properties of ZnO thin films deposited by RF magnetron sputtering." *Appl. Surf. Sci.*, 253(17), 7330-7335.

Kim, K.K., Kim, H.S., Hwang, D.K., Lim, J.H. and Park, S.J. (2003). "Realization of p -type ZnO thin films via phosphorus doping and thermal activation of the dopant." *Appl. Phys. Lett.*, 83(1), 63-65.

Kim, K.K., Niki, S., Oh, J.Y., Song, J.O., Seong, T.Y., Park, S.J., Fujita, S. and Kim S.W. (2005). "High electron concentration and mobility in Al doped n-ZnO epilayer achieved via dopant activation using rapid-thermal annealing." *J. Appl. Phys.*, 97(6), 066103- 066105.

Kim, M.S., Yim, K.G., Kim, S., Nam, G., Lee, D.-Y., Kim, J.S., Kim, J.S. and Leem, J.-Y. (2012). "Growth and characterization of indium doped zinc oxide thin films prepared by sol-gel method." *Acta Phys. Pol. A*, 121(1), 217-220.

Kittel, C. (1996). "*Introduction to Solid State Physics*." Wiley, New Jersey.

Kondo, T., Sawada, Y., Akiyama, K., Funakubo, H., Kiguchi, T., Seki, S., Wang, M.H. and Uchida, T. (2008). "Step coverage study of indium-tin-oxide thin films by spray CVD on non-flat substrates at different temperatures." *Thin Solid Films*, 516(17), 5864–5867.

Kumar, A., Kumar, M. and Singh, B.P. (2010). "Fabrication and characterization of magnetron sputtered arsenic doped p-type ZnO epitaxial thin films." *Appl. Surf. Sci.*, 256(23), 7200-7203.

Labeau, M., Rey, P., Deschanvres, J.L., Joubert, J.C. and Delabouglise, G. (1992). "Thin films of high-resistivity zinc oxide produced by a modified CVD method." *Thin Solid Films*, 213(1), 94-98.

Liang, H.W., Lu, Y.M., Shen, D.Z., Yan, J.F., Li, J.F., Zhang, J.Y. Liu, Y.C. and Fan, X.W. (2005). "Investigation of growth mode in ZnO thin films prepared at different temperature by plasma-molecular beam epitaxy." *J. Cryst. Growth*, 278(1-4), 305-310.

Lim, W., Wang, Y.-L., Ren, F., Nortona, D.P., Kravchenko, I.I., Zavada, J.M. and Pearton, S.J. (2008). "Indium zinc oxide thin films deposited by sputtering at room temperature." *Appl. Surf. Sci.*, 254(9), 2878-2881.

Limpijumnong, S., Zhang, S.B., Wei, S.-H. and Park, C.H. (2004). "Doping by large-size-mismatched impurities: the microscopic origin of arsenic- or antimony-doped p-type zinc oxide." *Phys. Rev. Lett.*, 92(15), 155504-4.

Lin, J.-P. and Wu, J.-M. (2008). "The effect of annealing processes on electronic properties of sol-gel derived Al-doped ZnO films." *Appl. Phys. Lett.*, 92, 134103.

Lin, Y.C., Hsu, C.Y., Hung, S.K. and Wen, D.C. (2013). "Influence of TiO<sub>2</sub> buffer layer and post-annealing on the quality of Ti-doped ZnO thin films." *Ceram. Int.*, 39(5), 5795-5803.

Liqiang, J., Zili, X., Jing, S., Xiaojun S., Weimin, C. and Haichen, G. (2002). "The preparation and characterization of ZnO ultrafine particles." *Mater. Sci. Eng. A*, 332(1-2), 356-361.

Liu, H., Pan, X., Ding, P., Ye, Z., He, H. and Huang, J. (2012). "Effects of diffusion temperature and diffusion time on fabrication of Na-diffused p-type ZnO thin films." *Mater. Lett.*, 80, 175-177.

Liu, Z.W., Sun, C.W., Zhang, Q.Y., Wang, Y.N., Wu, B. and Jin, Z.X. (2007). "Morphology and interface characteristics of ZnO films deposited at room temperature and 750°C." *Surf. Coat. Technol.*, 201(9-11), 5422-5426.

Lokhande, B.J. Patil, P.S. and Uplane, M.D. (2002). "Deposition of highly oriented ZnO films by spray pyrolysis and their structural, optical and electrical characterization." *Mater. Lett.*, 57(3), 573-579.

Look, D.C. (2001). "Recent advances in ZnO materials and devices." *Mat. Sci. Eng. B.*, 80(1-3), 383-387.

Ma, Q.-B., Ye, Z.-Z., He, H.-P., Zhu, L.-P. and Zhao, B.-H. (2007). "Effects of deposition pressure on the properties of transparent conductive ZnO: Ga films prepared by DC reactive magnetron sputtering." *Mater. Sci. Semicond. Process.*, 10(4-5), 167-172.

Maity, A.B., Bhattacharyya, D., Sharma, S.K., Chaudhuri, S. and Pal, A.K. (1995). "Electrical conductivity of nanostructured ZnTe films." *Nanostruct. Mater.*, 5(6), 717-726.

Martin, A., Espinos, J.P., Justo, A., Holgado, J.P., Yubero, F. and Gonzalez, E.A.R. (2002). "Preparation of transparent and conductive Al-doped ZnO thin films by ECR plasma enhanced CVD." *Surf. Coat. Technol.*, 151-152, 289-293.

Matsubara, K., Fons, P., Iwata, K., Yamada, A., Sakurai, K., Tampo, H. and Niki, S. (2003). "ZnO transparent conducting films deposited by pulsed laser deposition for solar cell applications." *Thin Solid Films*, 431- 432, 369-372.

Mejda, A., Michel, C. and Najoua, K.T. (2013). "Study on the doping effect of Sn-doped ZnO thin films." *Superlattices Microstruct.*, 53, 213-222.

Miao, Y., Ye, Z., Xu, W., Chen, F., Zhou, X., Zhao, B. and Zhu, L. (2006). "p-type conduction in phosphorous-doped ZnO thin films by MOCVD and thermal activation of the dopant." *Appl. Surf. Sci.*, 252(22), 7953-7956.

Minami, T., Yamamoto, T. and Miyata, T. (2000). "Highly transparent and conductive rare earth-doped ZnO thin films prepared by magnetron sputtering." *Thin Solid Films*, 366(1-2), 63-68.

Minhong, J., Xinyu, L. and Hua, W. (2009). "Conductive and transparent Bi-doped ZnO thin films prepared by rf magnetron sputtering." *Surf. Coat. Technol.*, 203(24), 3750- 3753.

Mishra, U.K. and Singh, J. (2008). "*Semiconductor Device Physics and Design.*" Springer, Netherlands.

Mista, W., Ziajab, J. and Gubanski, A. (2004). "Varistor performance of nano-crystalline Zn-Bi-O thin films prepared by reactive RF magnetron sputtering at room temperature." *Vacuum*, 74 (2), 293-296.

Miyamoto, K., Sano, M., Kato, H. and Yao, T. (2004). "High-electron-mobility ZnO epilayers grown by plasma-assisted molecular beam epitaxy." *J. Cryst. Growth*, 265(1-2), 34-40.

Mohamed, H.A. (2007). "The effect of annealing and ZnO dopant on the optoelectronic properties of ITO thin films." *J. Phys. D: Appl. Phys.*, 40, 4234-4240.

Morkoc, H. and Ozgur, U. (2007). *Zinc Oxide: fundamentals, materials and device Technology*, 1<sup>st</sup> edn, WILEY-VCH Verlag, Weinheim, chapter 4, pp. 245-268.

Mosbah, A., Moustaghfir A., Abed, S., Bouhssira, N., Aida, M.S., Tomasella, E. and Jacquet M. (2005). "Comparison of the structural and optical properties of zinc oxide thin films deposited by d.c. and r.f. sputtering and spray pyrolysis." *Surf. Coat. Technol.*, 200(2), 293-296.

Myong, S.Y., Baik, S.J., Lee, C.H., Cho, W.Y. and Lim, K.S. (1997). "Extremely transparent and conductive ZnO:Al thin films prepared by photo-assisted metalorganic chemical vapor deposition (photo-MOCVD) using AlCl<sub>3</sub>(6H<sub>2</sub>O) as new doping material." *Jpn. J. Appl. Phys. Part 2: Letters* 366(8B), L1078-L1081.

Nakao, S., Saitosh, K., Ikeyama, M., Niwa, H., Tanemura, S., Miyagamaand, Y. and Miyagama, S. (1996). "Microstructure of germanium films crystallized by high energy ion irradiation." *Thin Solid Films*, 281, 10.

Nam, E., Kang, Y.-H., Jung, D. and Kim, Y.S. (2010). "Anode material properties of Ga-doped ZnO thin films by pulsed DC magnetron sputtering method for organic light emitting diodes." *Thin Solid Films*, 518(22), 6245-6248.

Nese and Sertap (2008). "Admittance spectroscopy of spray-pyrolysed ZnO film." *Physica B*, 403(18), 3159-3163.

Ohyama, M., Kozuka, H. and Yoko, T. (1998). "Sol-Gel preparation of transparent and conductive aluminum-doped zinc oxide films with highly preferential crystal orientation." *J. Am. Ceram. Soc.*, 81(6), 1622-1632.

ÓLeary, S.K., Zukotynski, S. and Perz, J.M., (1997). "Disorder and optical absorption in amorphous silicon and amorphous germanium." *J. Non-Cryst. Solids*, 210(2-3), 249-253.

Ozgur, U., Alivov, Y. I., Liu, C., Teke, A., Reshchikov, M.A., Dogan, S., Avrutin, V., Cho, S.-J. and Morkoc, H. (2005). "A comprehensive review of ZnO materials and devices." *J. Appl. Phys.*, 98(041301), 1-103.

Pamplin, B.R. (1979). "Spray pyrolysis of ternary and quaternary solar cell materials." *Prog. Cryst. Growth Charact.*, 1(4), 395-403.

Pan, X., Ding, P., He, H., Huang, J. Lu, B., Zhang, H. and Ye, Z. (2012). "Optical properties and structural characteristics of ZnO thin films grown on a-plane sapphire substrates by plasma-assisted molecular beam epitaxy." *Opt. Commun.*, 285(21-22), 4431-4434.

Pan, X., Ye, Z., Li, J., Gu, X., Zeng, Y., He, H., Zhu, L. and Che, Y. (2007). "Fabrication of Sb-doped p-type ZnO thin films by pulsed laser deposition." *Appl. Surf. Sci.*, 253(11), 5067-5069.



Pankove, J.I. *Optical Processes in Semiconductors*, Dover Publication, New York, 1971, p. 22 (Chapter 2).

Park, C.H., Zhang, S.B. and Wei, S.-H. (2002). "Origin of p-type doping difficulty in ZnO: The impurity perspective." *Phys. Rev. B*, 66(7), 073202-073204.

Park, N-K., Lee, Y.J., Yoon, S.H., Han, G.B., Ryu, S.O., Lee, T.J., Lee, W.G. and Bae, Y.J. (2008). "The epitaxial growth of ZnO nanowires for optical devices by a modified thermal evaporation method." *Scr. Mater.*, 59(3), 328-331.

Pearnton, S.J., Norton, D.P., Ip, K., Heo, Y.W. and Steiner, T. (2005). "Recent progress in processing and properties of ZnO." *Prog. Mater. Sci.*, 50(3), 293-340.

Polley, T.A., Carter, W.B., and Poker D.B. (1999). "Deposition of zinc oxide thin films by combustion CVD." *Thin Solid Films*, 357(2), 132-136.

Prasada, R. and Santhoshkumar, M.C. (2009). "Effect of thickness on structural, optical and electrical properties of nanostructured ZnO thin films by spray pyrolysis." *Appl. Surf. Sci.*, 255(8), 4579-4584.

Prasada, R.T., Santhoshkumar, M.C., Safarulla, A., Ganesan, V., Barman, S.R. and Sanjeeviraj, C. (2010). "Physical properties of ZnO thin films deposited at various substrate temperatures using spray pyrolysis." *Physica B*, 405(9), 2226-2231.

Rajendra, S.G., Sambhaji, S.B., Rajaram, S.M., Bhagwat, N.P., Sanjay, L.G., Han, S.-H. and Joo, O.-S. (2012). "Roughness-based monitoring of transparency and conductivity in boron-doped ZnO thin films prepared by spray pyrolysis." *Mater. Res. Bull.*, 47(12), 4257-4262.

Rajeswari, Y.N. and Chandra, B.A. (2013). "Synthesis, dopant study and device fabrication of Zinc Oxide nanostructures: mini review." *Prog. Nanotech. Nanomater.*, 2(1), 1-20.

Ramin, Y. and Farid, J.-S. (2012). "Effect of chlorine ion concentration on morphology and optical properties of Cl-doped ZnO nanostructures." *Ceram. Int.*, 38(7), 5821-5825.

Ratheesh, K.P.M., Vijayakumar, K.P. and Sudha, K.C. (2007). "On the origin of blue-green luminescence in spray pyrolysed ZnO films." *J. Mater Sci.*, 42(8), 2598-2602.

Regragui, M., Addou, M., Idrissi, B.E., Bernède, J.C., Outzourhit, A. and Chamikh, E. (2001). "Effect of the annealing time on the physico-chemical properties of WO<sub>3</sub> thin films prepared by spray pyrolysis." *Mater. Chem. Phys.*, 70(1), 84-89.

Reynolds, D., Look, D. and Jogai, B. (1996). "Optically pumped ultraviolet lasing from ZnO." *Solid State Commun.*, 99(126501), 873-875.

Rozati, S.M. and Akesteh, S. (2007). "Characterization of ZnO: Al thin films obtained by spray pyrolysis technique." *Mater. Charact.*, 58(4), 319-322.

Rusop, M., Uma, K., Soga, T. and Jimbo, T. (2006). "Post-growth annealing of zinc oxide thin films pulsed laser deposited under enhanced oxygen pressure on quartz and silicon substrates." *Mat. Sci. & Eng. B*, 127(2-3), 150-153.

Sadananda, K.N., Kasturi, V.B. and Shivakumar, G.K. (2014). "Effect of annealing on the properties of zinc oxide nanofiber thin films grown by spray pyrolysis technique." *Appl. Nanosci.*, 4(2), 209-216.

Satish, S.B., and Mulla, I.S. (2009) "H<sub>2</sub>S gas sensitive indium-doped ZnO thin films: Preparation and characterization." *Sens. Actuators, B*, 143, 164-170.

Schroder, D.K. (2005). "*Semiconductor Material and Device characterization.*" Wiley Inter Science, New Jersey.

Senthilkumar, V. and Vickraman P. (2010). "Annealing temperature dependent on structural, optical and electrical properties of indium oxide thin films deposited by electron beam evaporation method." *Curr. Appl. Phys.*, 10(3), 880-885.

Seo, K-W., Shin, H-S., Lee, J-H., Chung, K-B, and Kim, H-K. (2014). “The effects of thickness on the electrical, optical and morphological properties of Al and Ga co-doped ZnO films grown by linear facing target sputtering.” *Vacuum*, 101, 250-256.

Sernelius, B.E., Berggren, K.F., Jin, Z.C., Hamberg, I. and Granqvist, C.G. (1988). “Band-gap tailoring of ZnO by means of heavy Al doping.” *Phys. Rev. B*, 37(17), 10244 -10248.

Shibata, T., Unno, K., Makino, E., Ito, Y. and Shimada, S. (2002). “Characterization of sputtered ZnO thin film as sensor and actuator for diamond AFM probe.” *Sens. Actuators A*, 102(1-2), 106-113.

Shin, J.-H., Shin, D.-K., Lee, H.-Y. and Lee, J.-Y. (2011). “Properties of multilayer gallium and aluminum doped ZnO transparent thin films deposited by pulsed laser deposition process.” *Trans. nonferrous Met. Soc. China*, 21, 96-99.

Song, Y.S., Park, J.K., Kim, T.W. and Chung, C.W. (2004). “Influence of process parameters on the characteristics of indium zinc oxide thin films deposited by DC magnetron sputtering.” *Thin solid films*, 467(1-2), 117–120.

Srinivasan, G. and Kumar, J. (2008). “Effect of Mn doping on the microstructures and optical properties of sol-gel derived ZnO thin films.” *J. Cryst. Growth*, 310(7-9), 1841-1846.

Sun, Y.W. and Tsui, Y.Y. (2007). “Production of porous nanostructured zinc oxide thin films by pulsed laser deposition.” *Opt. Mater.*, 29(8), 1111-1114.

Sze, S.M. (2006). “Physics of Semiconductor Devices.” Wiley, New York.

Szu, K.W., Ting, C.L., Sheng, R.J., Jenh, Y.J., Jason S.C.J. and Jiun, Y.T. (2011). “Effects of post-annealing on the structural and nanomechanical properties of Ga-doped ZnO thin films deposited on glass substrate by rf-magnetron sputtering.” *Appl. Surf. Sci.*, 258(3), 1261-1266.

Tellier, J., Kuscer, D., Malic, B., Cilensek, J., Skarabot, M., Kovac, J., Goncalves, G., Musevic, I. and Kosec, M. (2010). "Transparent, amorphous and organics-free ZnO thin films produced by chemical solution deposition at 150° C." *Thin Solid Films*, 518(18), 5134-5139.

Thirunavukkarasu, K. and Jothiramalingam, R. (2013). "Synthesis and structural characterization of Ga-ZnO nanodisk/nanorods formation by polymer assisted hydrothermal process." *Powder Technol.*, 239, 308-313.

Tiburcio, S.A., Sanchez, J.A. and Avila, G.A. (1998). "Properties of gallium-doped ZnO deposited onto glass by spray pyrolysis." *Sol. Energy Mater. Sol. Cells*, 55(1-2), 3-10.

Tolansky, S. (1950). "Interferometric evaluation of thicknesses of thin films." *Le Journal De Physique*, 11, 373-374.

Tsay, C.-Y., Fan, K.-S., Chen, S.-H. and Tsai, C.-H. (2010). "Preparation and characterisation of ZnO transparent semiconductor thin films by sol-gel method." *J. Alloys. Compd.*, 495(1), 126-130.

Tsay, C.-Y., Fan, K.-S., Lei C.-M. (2012). "Synthesis and characterization of sol-gel derived gallium-doped zinc oxide thin films." *J. Alloys Compd.*, 512(1), 216-222.

Tsoutsouva, M.G., Panagopoulos, C.N., Papadimitriou, D., Fasaki, I. and Kompitsas, M. (2011). "ZnO thin films prepared by pulsed laser deposition." *Mat. Sci. & Eng. B*, 176(6), 480-483.

Tuomisto, F., Ranki, V. and Saarinen, K. (2003). "Evidence of the Zn vacancy acting as the dominant acceptor in n-type ZnO." *Phys. Rev. Lett.*, 91(20), 205502-205505.

Tvarozek, V., Shtereva, K., Novotny, I., Kovac, J., Sutta, P., Srnanek, R., and Vincze, A. (2008). "RF diode reactive sputtering of n- and p-type zinc oxide thin films." *Vacuum*, 82(2), 166-169.

Van, D.P.L.J. (1958). "A method of measuring the resistivity and Hall coefficient on lamellae of arbitrary shape." *Philips Technical Review*, 20, 220-224.

Varnamkhasti, M.G., Fallah, H.R. and Zadsar, M. (2012). "Effect of heat treatment on characteristics of nanocrystalline ZnO films by electron beam evaporation." *Vacuum*, 86(7), 871-875.

Venkatachalam, S. and Kanno, Y. (2009). "Preparation and characterization of nano and microcrystalline ZnO thin films by PLD." *Curr. Appl. Phys.*, 9(6), 1232-1236.

Venkatachalam, S., Iida, Y. and Kanno, Y. (2008). "Preparation and characterization of Al doped ZnO thin films by PLD." *Superlattices Microstruct.*, 44(1), 127-135.

Vossen, J. L. (1977) *Physics of Thin films*, 9, 1. Academic Press, Inc., Orlando.

Vrushali, S., Bhole, M.P. and Patil, D.S. (2013). "Effect of open air annealing on spin coated aluminum doped ZnO nanostructure." *Mater. Chem. Phys.*, 141(1), 81-88.

Walle, V.D.C.G. (1997). *Doping of wide band gap II- VI compounds: Theory*, Academic Press, Massachusetts, U. S. A.

Wang, C., Chen, Z. Hu, H. and Zhang, D. (2009). "Effect of the oxygen pressure on the microstructure and optical properties of ZnO films prepared by laser molecular beam epitaxy." *Physica B: Condensed Matter.*, 404(21), 4075-4082.

Wang, S-K., Ting, C.L., Sheng, R.J., Jenh, Y.J., Jason, S.C.J. and Jiun, Y.T. (2011). "Effects of post- annealing on the structural and nanomechanical properties of Ga-doped ZnO thin films deposited on glass substrate by rf-magnetron sputtering." *Appl. Surf. Sci.*, 258(3), 1261-1266.

Williamson, G.K. and Hall, W.H. (1953). "X-ray line broadening from fided Aluminium and Wolfram." *Acta Metall.*, 1(1), 22-31.

Won, J.L., Chae, R.C., Kyung, M.C., and Se Y.J. (2005). "Rapid thermal annealing effect of Al-doped ZnO thin films." *J. Korean Phys. Soc.*, 47, S296 -S299.

Xiaofeng, X., Shen, Y., Ning, X., Wei, H., Lai, J., Ying, Z. and Jiada, W. (2010). "Large-sized-mismatched group-V element doped ZnO films fabricated on silicon substrates by pulsed laser deposition." *Vacuum*, 84(11), 1306-1309.

Xu, Z.Q., Deng, H., Li, Y., Guo, Q.H. and Li, Y.R. (2006). "Characteristics of Al-doped c-axis orientation of ZnO thin films by the sol-gel method." *Mater. Res. Bull.*, 41(2), 354-358.

Yacobi, B.G. (2004). "*Semiconductor Materials: An Introduction to Basic Principles*." Kluwer Academic Publishers, New York.

Yang, Z., Lim, J.-H., Chu, S., Zuo, Z. and Liu, J.L. (2008). "Study of the effect of plasma power on ZnO thin films growth using electron cyclotron resonance plasma-assisted molecular beam epitaxy." *Appl. Surf. Sci.*, 255(5), 3375-3380.

Yasemin, C., Ilican, S., Caglar, M., and Yakuphanoglu, F. (2007). "Effects of In, Al and Sn dopants on the structural and optical properties of ZnO thin films." *Spectrochim. Acta Part A*, 67, 1113-1119.

Yasemin, C., Saliha, I., Mujdat, C. and Fahrettin, Y. (2011). "Boron doped nanostructure ZnO films on to ITO substrate." *J. Alloys Compd.*, 509(6), 3177-3182.

Yasemin, C., Seval, A., Saliha, I. and Mujdat, C. (2009). "Crystalline structure and morphological properties of undoped and Sn doped ZnO thin films." *Superlattices Microstruct.*, 46(3), 469.

Ye, Z.Z., Lu, J.G., Chen, H.H., Zhang, Y.Z., Wang, L., Zhao, B.H. and Huang, J.Y. (2003). "Preparation and characteristics of p-type ZnO films by DC reactive magnetron sputtering." *J. Cryst. Growth*, 253(1-4), 258-264.

Yolanda, Y.V., Daren, L. and Pei, T.C. (2006). "Pulsed laser deposition of zinc oxide." *Thin Solid Films*, 501(1-2), 366-369.

Yoon, H.S., Lee, K.S., Lee, T.S., Cheong, B., Choi, D.K., Kim, D.H., and Kim, W.M. (2008). "Properties of fluorine doped ZnO thin films deposited by magnetron sputtering." *Sol. Energy Mater. Sol. Cells*, 92(11), 1366-1372.

You, H.-C. (2013). "Indium doping concentration effects in the fabrication of zinc oxide thin film transistors." *Int. J. Electrochem. Sci.*, 8, 9773-9784.

Yuan, G.D., Zhang, W.J., Jie, J.S., Fan, X., Zapein, J.A., Leung, Y.H., Luo, L.B., Wang, P.F., Lee, C.S. and Lee, S.T. (2008). "P-type ZnO nanowire arrays." *Nano Lett.*, 8(8), 2591-2597.

Zhang, Z., Bao, C., Yao, W., Ma, S., Zhang, L. and Hou, S. (2011). "Influence of deposition temperature on the crystallinity of Al-doped ZnO thin films at glass substrates prepared by RF magnetron sputtering method." *Superlattices Microstruct.*, 49(6), 644-653.

Zhao, Z., Hu, L., Zhang, H., Sun, J., Bian, J. and Zhao, J. (2011). "Effect of different annealing temperature on Sb-doped ZnO thin films prepared by pulsed laser deposition on sapphire substrates." *Appl. Surf. Sci.*, 257(11), 5121-5124.

Zhong, W.W., Liu, F.M., Cai, L.G., Zhou, C.C., Ding, P. and Zhang, H. (2010). "Annealing effects of co-doping with Al and Sb on structure and optical-electrical properties of the ZnO thin films." *J. Alloys Compd.*, 499(2), 265-268.

Zhu, B.L., Xie, C.S., Wu, J., Zeng, D.W., Wang, A.H. and Zhao, X.Z. (2006). "Influence of Sb, In and Bi dopants on the response of ZnO thick films to VOCs." *Mater. Chem. Phys.*, 96(2-3), 459-465.

## **LIST OF PUBLICATIONS:**

### **International Journal Publications**

1. **Sadananda Kumar N.,** Kasturi V. Bangera, Anandan C., G.K. Shivakumar  
“Properties of ZnO: Bi thin films prepared by spray pyrolysis technique”  
**Journal of Alloys and Compounds**, 578 (2013) 613-619.
2. **Sadananda Kumar N.,** Kasturi V. Bangera, G.K. Shivakumar  
“Effect of annealing on the properties of zinc oxide nanofiber thin films grown by spray pyrolysis technique”  
**Applied Nanoscience**, 4 (2014) 209–216.
3. **Sadananda Kumar N.,** Kasturi V. Bangera, G.K. Shivakumar  
“Properties of nanostructured Al-doped ZnO thin films prepared by spray pyrolysis technique”  
**Semiconductors**, 48 (2014) 1023-1027.
4. **Sadananda Kumar N.,** Kasturi V. Bangera, G.K. Shivakumar  
Effect of annealing on the properties of Bi doped ZnO thin films grown by spray pyrolysis technique  
**Superlattices & Microstructures**, 75 (2014) 303-310.
5. **Sadananda Kumar N.,** Kasturi V. Bangera, G.K. Shivakumar  
“Effect of annealing on the properties of Sb doped zinc oxide thin films grown by spray pyrolysis”  
**AIP Conference Proceedings**, 1576 (2014) 52-54
6. **Sadananda Kumar N.,** Kasturi V. Bangera, G.K. Shivakumar  
“Properties of antimony doped zinc oxide thin films prepared by spray pyrolysis technique”; **Semiconductors** (To appear)



## Conference Presentations

1. **Sadananda Kumar N., Kasturi V. Bangera, G.K. Shivakumar**  
Properties of the zinc oxide nanofiber thin films grown by spray pyrolysis technique. **International Conference on “Materials Science, Metal & Manufacturing” (M3 2011)** held at Hotel Fort Canning, **Singapore** Dec. 12-13, 2011.
2. **Sadananda Kumar N., Kasturi V. Bangera, G.K. Shivakumar**  
“Properties of undoped and Bi doped ZnO thin films prepared by Spray Pyrolysis technique”  
**International Conference on “Recent advances in materials science;**  
Hotel Atria, Bangalore Nov. 6-8, 2012.
3. **Sadananda Kumar N., Kasturi V. Bangera, G.K. Shivakumar**  
“Nanostructured Al doped zinc oxide thin films prepared by spray pyrolysis technique”  
**International symposium for research scholars (ISRS) on “Metallurgy, Materials science and Engineering;** IIT Madras, Chennai, Dec. 13-15, 2012.
4. **Sadananda Kumar N., Kasturi V. Bangera, G.K. Shivakumar**  
“Effect of annealing on the properties of Sb doped zinc oxide thin films grown by spray pyrolysis”  
**International conference on Optoelectronic materials and thin film Applications Technology (OMTAT 2013);** Hotel Riviera Suites, **Cochin** Jan. 3-5, 2013.

## BIO DATA

NAME : SADANANDA KUMAR N.  
PERMANENT ADDRESS : 2-48(1), ANTHARA HOUSE  
NARICOMBU POST & VILLEGE  
BANTWAL TALUK  
D. K. 574231  
Email address : [sadananda.kumar@gmail.com](mailto:sadananda.kumar@gmail.com)

## EDUCATIONAL QUALIFICATIONS

M. Sc. in Materials Science : 60.6%  
Passing Year : 2003  
University : Mangalore University  
B. Sc. (Physics, Chemistry, maths) : 63.3%  
Passing Year : 2001  
University : Mangalore University

## **Journal Publications**

1. Sadananda Kumar N., Kasturi V. Bangera, Anandan C., G.K. Shivakumar, "Properties of ZnO:Bi thin films prepared by spray pyrolysis technique" *J. Alloys compd.*, 578 (2013) 613-619
2. Sadananda Kumar N., Kasturi V. Bangera, G.K. Shivakumar, "Effect of annealing on the properties of zinc oxide nanofiber thin films grown by spray pyrolysis technique" *Appl. Nanosci.*, 4 (2014) 209 -216.
3. Sadananda Kumar N., Kasturi V. Bangera, G.K. Shivakumar, "Effect of annealing on the properties of Sb doped zinc oxide thin films grown by spray pyrolysis" *AIP Conference Proceedings*, 1576, (2014) 52-54.

4. Sadananda Kumar N., Kasturi V. Bangera, G.K. Shivakumar “Properties of antimony doped zinc oxide thin films prepared by spray pyrolysis technique” *Semiconductors*, 48 (2014) 1023-1027.
5. Sadananda Kumar N., Kasturi V. Bangera, G.K. Shivakumar “Effect of annealing on the properties of Bi doped ZnO thin films grown by spray pyrolysis technique” *Superlattices & Microstructures*, 75 (2014) 303-310.
6. Sadananda Kumar N., Kasturi V. Bangera, G.K. Shivakumar, “Properties of nanostructured Al-doped ZnO thin films prepared by spray pyrolysis technique” Accepted for publication in *Semiconductors*.

### Conference Presentations

1. Sadananda Kumar N., Kasturi V. Bangera, G.K. Shivakumar, “Properties of the zinc oxide nanofiber thin films grown by spray pyrolysis technique” Presented in Annual International Conference on **Materials Science, Metal & Manufacturing**” Hotel Fort Canning, Singapore, Dec. 12-13, 2011.
2. Sadananda Kumar N., Kasturi V. Bangera, G.K. Shivakumar, “Properties of undoped and Bi doped ZnO thin films prepared by Spray Pyrolysis technique” Presented in International Conference on **Recent advances in materials science** ; Hotel Atria, Bangalore, Nov. 6-8, 2012.
3. Sadananda Kumar N., Kasturi V. Bangera, G.K. Shivakumar, “Nanostructured Al doped zinc oxide thin films prepared by spray pyrolysis technique” Presented in International symposium for research scholars (ISRS) on **Metallurgy, materials science and Engineering** ; IIT Madras, Chennai, Dec. 13-15, 2012.
4. Sadananda Kumar N., Kasturi V. Bangera, G.K. Shivakumar, “Effect of annealing on the properties of Sb doped zinc oxide thin films grown by spray pyrolysis” Presented in International conference on **Optoelectronic materials and thin film Applications Technology**; Hotel Riviera Suites, Cochin Jan. 3-5, 2013.